Universidade de Aveiro
2004

Departamento de Química

António José Queimada

Propriedades e Comportamento de Soluções de Hidrocarbonetos Pesados a Baixas Temperaturas: Medição e Modelação

Properties and Low Temperature Behaviour of Heavy Hydrocarbon Mixtures: Measurement and Modeling

DOCUMENTO PROVISÓRIO

Universidade de Aveiro
2004

Departamento de Química

António José Queimada

Propriedades e Comportamento de Soluções de Hidrocarbonetos Pesados a Baixas Temperaturas: Medição e Modelação

Properties and Low Temperature Behaviour of Heavy Hydrocarbon Mixtures: Measurement and Modeling

Dissertação apresentada à Universidade de Aveiro para cumprimento dos requisitos necessários à obtenção do grau de Doutor em Engenharia Química, realizada sob a orientação científica do Doutor. João A. P. Coutinho e da Doutora. Isabel M. D. J. Marrucho – Ferreira ambos Professores Auxiliares do Departamento de Química da Universidade de Aveiro e do Doutor Erling H. Stenby, Professor do Institut for Kemiteknik, Danmarks Tekniske Universitet, Dinamarca.

o júri

presidente

Prof. Doutor João Manuel Torrão
professor catedrático do Departamento de Línguas e Culturas da Universidade de Aveiro

Profª. Doutora Christelle Miqueu
Maitre de Conferences, Université de Pau et des Pays de l'Adour, França

Prof. Doutor Manuel M. Piñeiro
Professor titular do Departamento de Física Aplicada da Universidade de Vigo, Espanha

Prof. Doutor José J. C. Cruz Pinto
Professor catedrático do Departamento de Química da Universidade de Aveiro

Prof. Doutor Erling Halfdan Stenby
Professor do Institut for Kemiteknik, Danmarks Tekniske Universitet, Dinamarca

Prof. Doutor. João A. P. Coutinho
Professor auxiliar do Departamento de Química da Universidade de Aveiro

Prof. Doutora. Isabel M. D. J. Marrucho-Ferreira
Professora auxiliar do Departamento de Química da Universidade de Aveiro

agradecimentos O doutorando agradece o apoio financeiro da FCT e do FSE no âmbito do III Quadro Comunitário de Apoio.

resumo

Fruto da constante evolução da ciência e da tecnologia, referências ao uso de novos fluídos surgem a um ritmo cada vez maior. Novos refrigerantes, mais “amigos” do ambiente, líquidos iónicos, uma nova classe de solventes ou perfluorocarbonetos, moléculas capazes de dissolver suficiente oxigénio para poderem ser utilizadas como substitutas do sangue ou como fonte de oxigénio em processos biotecnológicos ou ainda como surfactantes em processos de extracção supercrítica com dióxido de carbono, são apenas alguns dos novos exemplos.

Para o design correcto de produtos e processos envolvendo estes novos fluídos, o conhecimento de algumas das suas propriedades termofísicas é fundamental. Embora a medição experimental seja o procedimento mais rigoroso para a determinação de qualquer propriedade termofísica, muitas das vezes, estas medições são morosas e caras. As gamas de temperatura, pressão e composição de interesse podem ainda ser tais que tornam as medições experimentais inexequíveis sendo a solução mais conveniente a utilização de um modelo teórico, empírico ou misto que devolve o valor da propriedade termofísica nas condições desejadas com uma razoável exactidão.

O contributo desta dissertação de doutoramento é maioritariamente para o estudo de moléculas lineares de diferentes tamanhos de cadeia, com um especial ênfase para misturas assimétricas. A família dos n-alcanos por apresentar um imenso interesse industrial a nível da indústria petrolífera e petroquímica, quer porque as suas propriedades permitem a sua utilização como materiais termoactivos em isolamento ou armazenamento de energia, quer ainda por ser uma família modelo para tantas outras moléculas, como surfactantes, ácidos gordos ou polímeros, foi seleccionada para esse efeito.

Várias medições foram realizadas em sistemas cuja escassez ou inexistência de dados experimentais foi verificada. Tensões superficiais, tensões interfaciais, densidades e viscosidades da fase líquida foram determinadas para um conjunto significativo de fluídos em gamas alargadas de temperatura e composição, tendo sido dada especial atenção a sistemas assimétricos de n-alcanos e a algumas fracções de petróleo, representativas de sistemas reais.

Diferentes metodologias foram adoptadas para a modelação dos resultados obtidos, com o cuidado de avaliar alguns dos modelos termodinâmicos que constituem o estado-da-arte, tendo sido demonstrado que um novo modelo baseado no Princípio dos Estados Correspondentes introduz melhorias consideráveis na modelação quando comparado com modelos convencionais.

abstract

As a result of the continuous scientific and technological developments, several new fluids of interest are showing up every day. New refrigerants, more environmentally friendly, ionic liquids, a new class of solvents or perfluoroalkanes, molecules able to dissolve enough oxygen in order to be used as blood substitutes or oxygen carrier agents in biotechnological processes or as surfactants in supercritical carbon dioxide extraction, are a few examples.

For the correct product and process design of these new fluids, knowledge of some thermophysical properties are required. Although the experimental measurement is the most rigorous procedure for evaluating any thermophysical property, frequently these are expensive and time-consuming. The temperature, pressure and composition ranges of interest may also be so broad that the measurements may be unfeasible, with a common solution being the use of a theoretical, empirical or semi-empirical model that returns the thermophysical property at the desired conditions with a considerable accuracy.

This thesis contributes to the study of various thermophysical properties of nonpolar molecules of different chain lengths, with a special emphasis on asymmetric mixtures. The n-alkane family was chosen for that purpose since it has a vast industrial interest, starting from the petrochemical industry to termoactive phase change materials, for energy storage and release. It can also be regarded as a reference family for studying other molecules such as surfactants, fatty acids or polymers.

A number of experimental measurements were performed in systems were data deficiency was found. Properties such as vapor-liquid and liquid-liquid interfacial tensions and liquid phase densities and viscosities were measured for a significant number of fluids in broad ranges of temperature and composition. A special emphasis was put on asymmetric n-alkane mixtures and some petroleum fractions, representative of real systems.

Several methodologies were adopted for modeling the obtained results, and for that purpose some state-of-the-art thermodynamic models were evaluated. As will be demonstrated an improved Corresponding States model enhanced considerably model accuracy.

Contents

LIST OF SYMBOLS XIII
LIST OF FIGURES XV
LIST OF TABLES XXI
GENERAL INTRODUCTION XXIII
PART I: EXPERIMENTAL 1
I.1. Introduction 3
I.2. Experimental Methods, Results and Discussion 7
I.2.1. Interfacial Tension 7
I.2.2. Viscosity 27
I.2.3. Liquid Density 37
I.2.4. Characterization of the Distillation Cuts 46
I.3. Conclusions 53
PART II: DATA CORRELATION 55
II.1 Introduction 57
II.2 Critical Properties and Acentric Factors 59
II.3 Surface Tension - Viscosity Relations 67
II.4. Conclusions 79
PART III: MODELING 81
III.1 Introduction 83
III.2. The Corresponding States Principle 87
III.2.1. Pure Fluids 87
III.2.2. Simple Mixtures 110
III.3. Gradient Theory of Fluid Interfaces 119
III.4. Friction Theory 135
III.5. Solid – Liquid Equilibrium in Hydrocarbon Fluids 147
III.6. Conclusions 155
FINAL CONCLUSIONS 157
PERSPECTIVES FOR FUTURE WORK 161
REFERENCES 165
PUBLICATION LIST 175

List of Symbols

% AAD	percent average absolute deviation
A - F	correlation parameters
a	energy parameter of a cubic equation of state
a_0	correlation parameter
b	co-volume of a cubic equation of state
c	influence parameter
c_1	correlation parameter
f	equivalent substance reducing ratio for temperature
f_0	Helmholtz free energy density
g	radial distribution function
h	equivalent substance reducing ratio for volume
MW	molecular weight
m	number of data points
n	chain length of n-alkane, C_nH_{2n+2}
n	mole number
N	mixture reference component
P	pressure
R	gas constant
T	absolute temperature/K
V	molar volume
x	mole fraction
X	thermophysical property
X_{Ai}	mole fraction of component *i* not bonded at site *A*
Z	compressibility factor
Z_{ra}	*Rackett* compressibility factor

Greek Letters

β	association volume
Δ	association strength
ε	association energy
η	viscosity
η	reduced fluid density
Ω	grand thermodynamic potential
μ	chemical potential
γ	surface tension
σ	surface tension
ϕ	volume shape factor
ρ	density
λ_i	characterization parameters for extending the simple two-parameter CST
θ	energy shape factor
ω	Pitzer acentric factor

Subscripts

0	spherical reference fluid
1,2,3	non-spherical reference fluids
a	accepted value
c	critical property
exp	experimental value
fus	melting point
i, j, k	pure component indexes.
j	target or working fluid in corresponding states models
l	liquid
m	mixture property
N	homogeneous nucleation
r	reduced property
v	vapor

Superscripts

B	correlation parameter
sat.	saturation property
assoc.	association
phys.	physical

List of Figures

Figure I. 1: NIMA DST 9005 tensiometer (up). Wilhelmy plate (middle) and Du Noüy ring (bottom). *10*

*Figure I. 2: Surface tension of n-C_7H_{16}: ●, this work, +, Grigoryev et al., 1992; x, Jasper, 1972; ◊ Jasper et al., 1955; △, Koefoed et al., 1958; * McLure et al., 1982.* *14*

Figure I. 3: Interfacial tension of n-C_7H_{16} (1) + n-$C_{16}H_{34}$ (2). Squares, 293.15 K; triangles, 303.15 K; lozenges 333.15 K; Filled symbols, this work; open symbols Koefoed et al., 1958, 1979; grey symbols, Pugachevich et al., 1979. ..... *20*

Figure I. 4: Interfacial tension of n-$C_{10}H_{22}$ (1) + n-$C_{16}H_{34}$ (2). Squares, 293.15 K; Triangles, 303.15 K; Circles, 313.15 K; Lozenges, 323.15 K; Asterisks, 333.15 K; Filled symbols, this work; Δ, 333.15 K from Pandey et al., 1982. ..... *20*

Figure I. 5: Surface tension of n-$C_{16}H_{34}$ (1) + n-$C_{20}H_{42}$ (2). Lozenges, 323.15 K; circles, 333.15 K; squares, 343.15 K. Filled symbols, this work. Open symbols, Águila-Hernandez, 1987. ..... *21*

Figure I. 6: Surface tension of n-C_7H_{16} + n-$C_{22}H_{46}$ (filled symbols) and n-C_7H_{16} + n-$C_{20}H_{42}$ + n-$C_{24}H_{50}$ (open symbols). Circles, 343.15 K; triangles, 333.15 K; lozenges 323.15 K; squares, 313.15 K. *22*

Figure I. 7: Surface tension of n-$C_{10}H_{22}$ + n-$C_{22}H_{46}$ (filled symbols) and n-$C_{10}H_{22}$ + n-$C_{20}H_{42}$ + n-$C_{24}H_{50}$.(open symbols). Circles, 343.15 K; triangles, 333.15 K; lozenges 323.15 K; squares, 313.15 K. *24*

Figure I. 8: H_2O + n-C_7H_{16} (circles) and H_2O + n-$C_{10}H_{22}$ (squares) liquid-liquid interfacial tensions. Filled symbols, this work; Open symbols, Zeppieri et al., 2001. ..... *26*

Figure I. 9: AMV 200 Anton Paar automated microviscometer. Right: detail of the working principle (Dandekar et. al., 1998) *27*

Figure I. 10: Viscosity of n-$C_{16}H_{34}$: ● this work, □ DIPPR, 1998, Δ, Vargaftik, 1975. ..... *29*

Figure I. 11: Viscosity of n-C_7H_{16} + n-$C_{22}H_{46}$ (filled symbols) and n-C_7H_{16} + n-$C_{20}H_{42}$ + n-$C_{24}H_{50}$.(open symbols). Circles, 343.15 K; squares, 333.15 K, triangles, 323.15 K, lozenges, 313.15 K. *30*

Figure I. 12: Viscosity of n-$C_{10}H_{22}$ + n-$C_{22}H_{46}$ (filled symbols) and n-$C_{10}H_{22}$ + n-$C_{20}H_{42}$ + n-$C_{24}H_{50}$.(open symbols). Circles, 343.15 K; squares, 333.15 K, triangles 323.15 K, lozenges, 313.15 K. *36*

Figure I. 13: Anton Paar DMA 58 densimeter *37*

Figure I. 14: Liquid density of n-$C_{10}H_{22}$: ● this work, □ DIPPR, 1998; Δ, Vargaftik, 1975. ..... *38*

Figure I. 15: Comparison of the binary n-C_7H_{16} + n-$C_{22}H_{46}$ (filled symbols) and ternary n-C_7H_{16} + n-$C_{20}H_{42}$ + n-$C_{24}H_{50}$ (open symbols) liquid density results. Circles, 343.13 K; squares, 333.15 K, lozenges, 323.15 K; triangles, 313.15 K. *44*

Figure I. 16: Comparison of the binary n-$C_{10}H_{22}$ + n-$C_{22}H_{46}$ (filled symbols) and ternary n-$C_{10}H_{22}$ + n-$C_{20}H_{42}$ + n-$C_{24}H_{50}$ (open symbols) liquid density results. Circles, 343.13 K; squares, 333.15 K, lozenges, 323.15 K; triangles, 313.15 K. *45*

Figure I. 17: Gas chromatography analysis of the distillation cut obtained from Oso condensate. The higher peaks are the n-alkanes. 47

Figure I. 18: DSC measurements for distillation cuts from Brent a), Oso Condensate b), Troll c), DUC d), and Sahara Blend e). 49

Figure II. 1: n-alkane critical temperatures. Experimental and correlation results with the Tsonopoulos (1987) correlation. 61

Figure II. 2 n-alkane critical pressure. Experimental and correlation results with the Magoulas et al. (1990) correlation. 62

Figure II. 3 n-alkane critical density. Experimental and correlation results with the Marano et al (1997a) correlation. 63

Figure II. 4 n-alkane acentric factors. Experimental and correlation results with the Han et al. (1993) correlation. 65

Figure II. 5: Plots of ln σ as a function of reciprocal viscosity, $1/\eta$ for several pure n-alkanes: ◆, n-C_6H_{14}, □, n-C_7H_{16}, ▲ n-C_8H_{18}, x, n-C_9H_{20}, ●, n-$C_{10}H_{22}$, ◊, n-$C_{11}H_{24}$, +, n-$C_{12}H_{26}$, Δ, n-$C_{13}H_{28}$, -, n-$C_{15}H_{32}$, x, n-$C_{16}H_{34}$, *, n-$C_{18}H_{38}$, ○, n-$C_{20}H_{42}$. 69

Figure II. 6: Plots of A as a function of chain length of the n-alkane. 71

Figure II. 7: Plots of B as a function of MW. 72

Figure II. 8: ln σ as a function of $1/\eta$ for n-$C_{10}H_{22}$ (1) + n-$C_{20}H_{42}$ (2): ●, x(2)=0.2, □, x(2)=0.4, ▲, x(2)=0.5, ○, x(2)=0.6, *, x(2)=0.8. 73

Figure II. 9: Plots of A for n-alkane mixtures as a function of average chain length. 75

Figure II. 10: Plots of B for n-alkane mixtures as a function of average molecular weight. 76

Figure II. 11: ln σ as a function of $1/\eta$ for petroleum distillation cuts: ×, Troll, ■, Brent, ▲, Sahara Blend. 78

Figure III. 1: Reduced vapor pressure (P_r) as a function of the acentric factor (ω) at Tr = 0.5. ○, experimental, (–) Eq. III.6, (--), Eq. III.5 92

Figure III. 2: Reduced liquid density (ρ_r) as a function of the acentric factor (ω) at T_r=0.5. ○, experimental, (–) Eq. III.6, (--), Eq. III.5 92

Figure III. 3: Reduced surface tension for n-alkanes as a function of acentric factor at Tr=0.5. ○, experimental, (–) Eq. III.6, (--), Eq. III.5 93

Figure III. 4: Reduced viscosity (η_r) as a function of the acentric factor (ω) at T_r=0.5. ○, experimental, (–) Eq. III.6, (--), Eq. III.5 93

Figure III. 5: Reduced thermal conductivity as a function of the acentric factor (ω) at T_r=0.5. 94

Figure III. 6: Reduced speed of sound as a function of the acentric factor (ω) at T_r=0.5. 94

Figure III. 7: Average deviation of the reduced vapor pressure predicted with the linear perturbation model as a function of the chain length of the n-alkane. 101

Figure III. 8: Average deviation of the reduced vapor pressure predicted with the 2nd order perturbation model as a function of the chain length of the n-alkane. 101

Figure III. 9: Average deviation of the reduced liquid density predicted with the linear perturbation model as a function of the chain length of the n-alkane. 102

Figure III. 10: Average deviation of the reduced liquid density predicted with the second-order perturbation model as a function of the chain length of the n-alkane. 102

Figure III. 11: Average deviation of the reduced viscosity predicted with the linear perturbation model as a function of the chain length of the n-alkane. 103

Figure III. 12: Average deviation of the reduced viscosity predicted with the 2nd order perturbation model as a function of the chain length of the n-alkane. 103

Figure III. 13: Comparison of experimental and predicted surface tension for n-alkanes-2nd order perturbation model. 105

Figure III. 14: Comparison of experimental and predicted surface tension for n-alkanes- ECST model. 109

Figure III. 15: Graphical presentation of experimental and predicted values of surface tension of n-heptane using the new predictions. 109

*Figure III. 16: Surface tension of n-C_7H_{16} (1) + n-$C_{10}H_{22}$ (2). ■, 293.15 K; ▲, 303.15 K; ●, 313.15 K; ∪ , 323.15 K; *, 333.15 K; –, model. 115*

*Figure III. 17: Surface tension of n- $C_{10}H_{22}$ (1) + n-$C_{16}H_{34}$ (2). ■, 293.15 K; ▲, 303.15 K; ●, 313.15 K; ∪ , 323.15 K; *, 333.15 K; Δ, Pandey et al., 1982, 303.16 K; –, model. 115*

*Figure III. 18: Surface tension of n- C_7H_{16} (1) + n-$C_{16}H_{34}$ (2). ■, 293.15 K; ▲, 303.15 K; ●, 313.15 K; ∪ , 323.15 K; *, 333.15 K; □, 293.15 K - Koefoed et al., 1958; Δ, 303.15 K - Koefoed et al., 1958; ○, 303.15 K - Pugachevich et al., 1979; ◊, 333.15 K - Pugachevich et al., 1979; –, model. 116*

*Figure III. 19: Surface tension of n- $C_{16}H_{34}$ (1) + n-$C_{20}H_{42}$ (2). ▲, 303.15 K; ●, 313.15 K; ∪ , 323.15 K; *, 333.15 K; ■, 343.15 K; ◊, 323.15 K – Águila-Hernandez, 1987; ○, 333.15 K - Águila-Hernandez, 1987; □, 343.15 K - Águila-Hernandez, 1987; –, model. 116*

Figure III. 20: Surface tension of (*), n- C_7H_{16} (1) + n-$C_{24}H_{50}$ (2), (o), n- C_7H_{16} (1) + n-$C_{20}H_{42}$ (2) + n-$C_{24}H_{50}$ (3). –, model. 117

Figure III. 21: Liquid density of the binary mixture n-$C_{10}H_{22}$ + n-$C_{20}H_{42}$. Experimental results and model predictions. 117

Figure III. 22: Viscosity of the binary mixture n-$C_{10}H_{22}$ + n-$C_{20}H_{42}$. Experimental results and model predictions. 118

Figure III. 23: n-alkane vapor pressures. Experimental (o, n-C_4H_{10}, Δ, n-C_5H_{12}, ◊, n-C_6H_{14}, x, n-C_7H_{16}) and CPA results (—). 126

Figure III. 24: n-heptane saturation densities. Experimental (o, liquid, Δ, vapor), CPA (—), SRK (- -) and PR (– —) estimates. 127

Figure III. 25: Water vapor pressure: experimental (o) and CPA results (—). 127

Figure III. 26: Water density. Experimental (o, liquid, Δ, vapor) and CPA (—) estimates. 128

Figure III. 27: Ethanol vapor pressure. experimental (o) and CPA results (—). 129

Figure III. 28: Ethanol density. Experimental (o, liquid, Δ, vapor) and CPA (—) estimates. 129

Figure III. 29: n-heptane influence parameters. CPA (□), SRK (o) and PR (Δ) estimates. 130

Figure III. 30: Water influence parameters. CPA estimates (•) and correlation (—). 131

Figure III. 31: Ethanol influence parameters. CPA estimates (•) and correlation (—). 131

Figure III. 32: n-alkane surface tension. Experimental (o, n-C_4H_{10}, Δ, n-C_5H_{12}, ◊, n-C_6H_{14}, +, n-C_7H_{16}) and gradient theory results (—). 132

Figure III. 33: Water surface tension. Experimental (o) and gradient theory results (—). 133

Figure III. 34: Ethanol surface tension. Experimental (o) and gradient theory results (—). 133

Figure III. 35: Viscosity of the binary mixture n-C_7H_{16} + n-$C_{20}H_{42}$; experimental results and model predictions. 140

Figure III. 36: Viscosity of the binary mixture n-C_7H_{16} + n-$C_{22}H_{46}$; experimental results and model predictions. 140

Figure III. 37: Viscosity of the binary mixture n-$C_{10}H_{22}$ + n-$C_{20}H_{42}$. Experimental results and model predictions. 141

Figure III. 38: Viscosity of the binary mixture n-$C_{16}H_{34}$ + n-$C_{20}H_{42}$; experimental results and model predictions. 141

Figure III. 39: Viscosity of the ternary mixture n-C_7H_{16} + n-$C_{20}H_{42}$ + n-$C_{24}H_{50}$; experimental results and model predictions. 142

Figure III. 40: Liquid density of the binary mixture n-C_7H_{16} + n-$C_{20}H_{42}$; experimental results and model predictions. 142

Figure III. 41: Liquid density of the binary mixture n-C_7H_{16} + n-$C_{22}H_{46}$; experimental results and model predictions. 143

Figure III. 42: Liquid density of the binary mixture n-$C_{10}H_{22}$ + n-$C_{20}H_{42}$. Experimental results and model predictions. 143

Figure III. 43: Liquid density of the binary mixture n-$C_{16}H_{34}$ + n-$C_{20}H_{42}$; experimental results and model predictions. 144

Figure III. 44: Liquid density of the ternary mixture n-C_7H_{16} + n-$C_{20}H_{42}$ + n-$C_{24}H_{50}$; experimental results and model predictions. 144

Figure III. 45: Comparison between the experimental and calculated percentage of crystallized paraffins in a n-$C_{10}H_{22}$+n-$C_{24}H_{50}$+n-$C_{25}H_{52}$+n-$C_{26}H_{54}$ mixture (mol%, respectively, 80%, 7.71% 6.62% and 5.67%) (Pauly et al., 2004) 150

Figure III. 46: Measured and predicted precipitation curves for distillation cuts from Brent a), Oso Condensate b), Troll c), DUC d), and Sahara Blend e). 151

Figure III. 47: Relation between total n-alkane content and wax appearance temperatures for the studied cuts. 153

List of Tables

Table I. 1: Pure n-alkane interfacial tension and comparison with literature 15

Table I. 2: Interfacial tension of binary n-alkane mixtures 18

Table I. 3: Interfacial tension of ternary n-alkane mixtures 23

Table I. 4: Liquid-liquid interfacial tension of water + n-alkane systems 25

Table I. 5: Interfacial tension of some petroleum distillation cuts 25

Table I. 6: Pure n-alkane viscosity and comparison with literature 31

Table I. 7: Viscosity of binary n-alkane mixtures 33

Table I. 8: Viscosity of ternary n-alkane mixtures 35

Table I. 9: Viscosity of the petroleum distillation cuts 36

Table I. 10: Pure n-alkane liquid density and comparison with literature 39

Table I. 11: Liquid density of binary n-alkane mixtures 41

Table I. 12: Liquid density of ternary n-alkane mixtures 43

Table I. 13: Liquid density of the petroleum distillation cuts 44

Table I. 14: n-alkane composition (wt %) and average molecular weight (g/mol) of the distillation cuts studied 48

Table I. 15: measured wax appearance temperatures (WAT) 48

Table II. 1: n-alkane selected experimental critical properties and acentric factors 60

Table II. 2: Least squares fit for n-alkanes, and corresponding σ_N and T_N values 70

Table II. 3: Least-squares fit for some n-alkane mixtures 74

Table II. 4: Estimation of mixture surface tension or viscosity from Eq. 1 using ln A=3.41 and Eq. 8 for B. 77

Table II. 5: Least-squares fit for petroleum distillation cuts 77

Table III. 1: Studied n-alkanes 96

Table III. 2: Selected reference systems 98

Table III. 3 Correlating coefficients of the reference fluids to be used with Eqs. III.8- III.11 98

Table III. 4: Percent average absolute deviation of the linear and 2nd order models as a function of reduced temperature 99

Table III. 5: Evaluation of the 2º order perturbation model for surface tension 104

Table III. 6: Evaluation of the new predictive ECST model for surface tension 108

Table III. 7: Estimation of the surface tension of n-alkane mixtures for different values of n (Eq. III.32) with the corresponding states model 113

Table III. 8: Modeling results with the new CS model..... 114

Table III. 9: CPA parameters for the pure components selected for this work (SI units)..... 125

Table III. 10: Modeling results in the reduced pressure range $0.45 < T_r < 0.80$ 126

Table III. 11: Correlation coefficients for calculating the influence parameters (Eq. III.60)..... 132

Table III. 12: Modeling results with pure component properties for the f-theory and the PR EOS reported on table III.10. 139

Table III. 13: Pure component properties used within the f-theory and the PR EOS..... 139

Table III. 14: Comparison between measured and predicted wax appearance temperature (WAT)..... 150

"No flying machine will ever fly from New York to Paris...[because] no known motor can run at the requisite speed for four days without stopping."

Orville Wright (1871-1948), co-inventor of the first successful airplane.

General Introduction

As a result of the systematic demand for new products, the nature and number of different chemicals in which we may be interested in is increasing considerably. In fact, in a short period of time, the chemical industry has changed from the production of a tiny number of small molecules to the large-scale production of a huge number of chemicals with broad compositional, structural and size differences.

Thermophysical properties are frequently required both for product and process design, and in many cases these are scarce or unavailable. During process design, knowledge of thermophysical properties is essential for determining the optimum process conditions, concerning steps as different as distillation, extraction, adsorption, reaction, heat and mass transfer and fluid transport. From the viewpoint of product design, various properties may determine the selection of a specific fluid for a particular purpose, for example viscosity for lubricants, surface tension for detergents, vapor pressure for perfumes or thermal conductivity for insulating materials. To develop products with improved performance, we thus need a good knowledge of the function-determining thermophysical properties.

One of the most well documented families of chemicals is that of n-alkanes. Many of the measurements available so far were done due to the importance that alkanes have for the petroleum industry. In the past, the focus has been on light oils and for this reason data

for compounds above n-hexadecane (n-$C_{16}H_{34}$) are scarce with the available data covering only a narrow temperature range.

Advances in oil extraction technology, founded on the progressive reservoir depletion, are enabling the additional recovery of heavier oils, rising oil lifetime (Ali, 2003; Babadagli, 2003). The mixture of heavier and lighter components makes the new oils heavier and more asymmetric, and thus, the increasing interest in heavier and asymmetric n-alkane mixtures.

Mixtures containing lighter and heavier compounds, can also be found at another industries such as those producing paints and polymers.

Another recent interest on the use of heavy n-alkanes, in the form of the cheap paraffin wax, is related to energy management (storage and release) provided by phase change materials (Farid *et al*., 2004). In these materials, a broad melting temperature range is used to store or release latent heat by means of the solid-liquid phase change. Typically these materials should have a large melting latent heat, high thermal conductivity, a melting temperature in the desired working range, melt congruently with no subcooling, be low in cost, chemically stable, non-toxic and non-corrosive. Some difficulties are now being addressed, particularly those related to low thermal conductivity, density change, stability of properties under cycling, flammability and, less frequently, subcooling (Farid *et al.*, 2004). Some of the applications of paraffin wax as a phase change material are solar energy storage, temperature controlled clothing for athletes and campers and household heating and insulation.

As the industrial interest in most of the heavier components was small till recently, the available experimental data is particularly reduced. Because the experimental measurement of thermophysical properties is an expensive and time-consuming procedure, the alternative is to select models from which the desired properties can be obtained within the required accuracy. Although several models have been proposed, it is still essential to carry out some experimental measurements on new systems of interest in order to assess their limitations and provide a basis for the development of improved models.

During the work conducted for this thesis a particular attention was devoted to two somewhat neglected thermophysical properties: interfacial tension and viscosity. Some liquid density measurements were performed and vapor pressures, thermal conductivities

and speeds of sounds were addressed on the modeling part. Thermal analysis of some petroleum distillation cuts by Differential Scanning Calorimetry (DSC) were also performed.

The importance of interfacial tension for the petroleum industry extends far beyond the extraction process, when oil has to travel through capillary channels and where this type of flow is strongly dominated by surface tension effects. In fact, it is not unusual in the extraction of crudes to add surfactants to modify the interfacial properties between crude oil and the geological reservoir (Farid *et al.*, 2004). Other operations such as multiphase transport in pipelines, adsorption, distillation or extraction also rely on this property. Outside the refinery, the environmental concerns about oil spills, both on sea and fresh waters, are a field where the study of the oil-water interface can provide important information, since it can determine the path, transport mechanisms and fate of organic pollutants in the environment. Other industries were interfacial tensions arising from long alkyl chains are important are those producing coatings, paints, detergents, cosmetics and agrochemicals.

Other valuable properties to model oil extraction from reservoirs are viscosity and liquid density. The importance of viscosity is well known. All equations expressing the flow of fluids contain this property, and several product characteristics can be largely determined by its magnitude. Lubricants and paints are examples of products for which the viscosity is one of the key properties. Generally, it is much easier to find open literature studies of phase equilibria rather than studies on non-equilibrium properties such as viscosity. Although literature data have been substantially increased over the last few decades, information about asymmetric or heavy systems is still scarce.

This thesis is organized in three parts, that deal separately with the experimental details, results and discussion (Part I), data correlation (Part II) and modeling of experimental data using some state-of-the-art and new thermodynamic models (Part III). This separation allows the reader to select one or more chapters without having to go through the entire text.

Part I details the experimental apparatuses used to measure vapor-liquid and liquid-liquid interfacial tensions, viscosities and liquid densities on a group of pure and mixed n-alkanes, with a special attention devoted to asymmetric mixtures. Measurements were

performed in broad temperature and composition ranges and results are reported on tables together with their estimated uncertainties. Some chain length effects on the results will be discussed in this chapter. Finally some measurements on petroleum distillation cuts, representative of real fluids will also be presented.

Part II deals with data correlation. An overview of critical properties and an assessment of correlations to extend the available data for those n-alkanes for which there is no experimental evidence is first presented and discussed, since these are fundamental for modeling purposes. Afterwards, correlating relations among some of the measured properties are presented. Some interesting results relating surface tension to viscosity will be presented at this point showing that its possible to relate equilibrium properties with transport properties.

Part III addresses various thermodynamic models for the estimation of thermophysical properties, with a special attention devoted to the properties measured on Part I: interfacial tensions, viscosities and liquid densities. Some emphasis was put on corresponding states models (section III.2) since these are the most versatile (the same formalism can be applied for different properties), require a small amount of experimental information, and are, in spite of their simplicity, surprisingly accurate. It will be shown that with a simple, theoretically sound extension, these models can be selected for the prediction of several properties of pure and mixed, lighter and heavier n-alkanes with average deviations comparable to the experimental uncertainties.

On section III.3 preliminary results on the coupling of the gradient theory of fluid interfaces with an association equation of state, the Cubic-Plus-Association (CPA) equation of state for the simultaneous modeling of the equilibrium pressures and densities, and interfacial tensions will be presented. The advantage of this combination is the possibility of modeling the important aqueous-hydrocarbon liquid-liquid (and vapor-liquid) interfaces for more complex systems, were phase equilibrium needs to be considered.

Results will also be presented from the friction theory for viscosity modeling, a new state-of the-art model based on the attractive and repulsive pressures calculated from a cubic equation of state. During this section (III.4) the liquid density estimates obtained from a cubic equation of state will also be presented and discussed.

Finally, taking advantage of the thermal behavior of the distillation cuts determined on Part I, modeling of these results will be presented on section III.5 using a simple model that has demonstrated to be able to correctly describe solid-liquid equilibrium of petroleum fluids (Coutinho, 1998; Coutinho *et al.*, 2002; Mirante *et al.*, 2001; Dauphin *et al.*, 1999; Daridon *et al.*, 2001).

PART I: EXPERIMENTAL

"The true worth of an experimenter consists in pursuing not only what he seeks in his experiment, but also what he did not seek."

Claude Bernard (1813-1878), Physiologist.

" Science is a wonderful thing if one does not have to earn one's living at it."

Albert Einstein (1879-1955), Physicist.

I.1. Introduction

Since most of the available experimental data on thermophysical properties appeared due to industry needs, there is still a huge amount of molecules to study. Of course, it is impossible (both expensive and time consuming) to carry out all the required experimental measurements on all interesting molecules and their mixtures in broad temperature, pressure and composition conditions. And the uncertainty required for the desired property may not always be small. For this reason, models are regularly used, but, since models always introduce some simplifications, one should first check their performance for the estimation of a small amount of experimental data, representative of the system(s) under study.

In the particular case of asymmetric n-alkane mixtures, surface tension and viscosity are among the most important thermophysical properties, those that present the smallest amount of experimental information. Liquid densities can easily be found for some mixtures of lighter components, but when one of the components involved is heavier than n-eicosane, the amount of experimental data is again, scarce.

Pure, binary and ternary mixtures as well as some petroleum distillation cuts from different origins were measured. Compositions and thermal behavior of the later were determined using Gas Chromatography (*Hewlett Packard 6890*) and Differential Scanning Calorimetry (*Setaram DSC 141*).

Lighter pure n-alkanes were chosen to evaluate the accuracy of the measuring methods, while heavier n-alkanes were measured since data for most of these fluids are still lacking. Some mixtures, especially asymmetric n-alkane mixtures were selected. For 6 binary and 2 ternary mixtures all of the referred properties were measured at the same compositions and temperatures in order to examine the effect of chain length and asymmetry. Ternary mixtures, consisting of n-heptane (or n-decane) + n-eicosane + n-tetracosane were prepared with equal mole fractions of n-eicosane and n-tetracosane in order to compare the results with the binary mixture n-heptane (or n-decane) + n-docosane. Crude oil fractions were chosen to represent real fluids. The results obtained will serve as a basis to the extrapolation, of the selected models to systems of practical interest.

A viscometer and a densimeter from *Anton Paar* and a *Nima* tensiometer were chosen for the measurements reported in this chapter. Although other measuring techniques with higher precisions can be selected for the measurement of these thermophysical properties (Rusanov, 1996; Wakeham *et al*., 1991), these equipment have shown to present the right balance between accuracy, precision, measuring time and amount of sample. One big disadvantage of these apparatuses is that measurements can only be performed at a set of different temperatures, without any pressure control, with the system pressure being roughly the atmospheric pressure. So, the reported results that will follow are not saturation-line properties. Still, as the dependence of the selected properties on pressure is small in the considered temperature range (283.15 K – 343.15 K), results can also be compared with saturation results as will be latter shown.

Measurements were performed from 283.15 K (or slightly above the fluid melting point) up to 343.15 K in temperature intervals of 10 K. This temperature range, although superiorly limited by the working range of the *Anton Paar* densimeter, shall present enough experimental information for describing the temperature influence on the selected thermophysical properties. It also permits to gather important information about the low-temperature behavior of the selected fluids.

For the considered binary mixtures, the full composition range was studied, allowing some insights about the composition effects on the measured properties.

All the results will be presented according to the *International System of Units* (Taylor, 1995), together with their estimated uncertainties, by the use of the law of the

propagation of uncertainty (Taylor *et al.*, 1994), considering the individual uncertainties of the variables involved on the measurements. These calculations, together with a comparison with available literature data will give a good overview on the precision and accuracy of the reported results.

"If your experiment needs statistics, then you ought to have done a better experiment"

Ernest Rutherford (1871 - 1937), Physicist

Vapor–liquid and liquid-liquid interfacial tensions, liquid densities and viscosities are reported for some pure, binary and ternary n-alkane mixtures, and some petroleum distillation cuts representative of real systems. Interfacial tensions were measured using a NIMA DST 9005 Dynamic Surface Tensiometer based on the Wilhelmy plate method (vapor-liquid interfaces) and the Du Noüy ring method (liquid-liquid interfaces). Liquid densities were determined using an Anton Paar DMA 58 vibrating U-tube densimeter and viscosities from an Anton Paar AMV8 rolling ball viscometer.

Thermal analysis from Differential Scanning Calorimetry using a Setaram DSC 141 calorimeter and compositions from gas chromatography using an Hewlett Packard 6890 chromatograph of the reported petroleum distillation cuts are also presented and discussed.

Results are reported on tables together with their estimated uncertainties.

I.2. Experimental Methods, Results and Discussion

I.2.1. Interfacial Tension

A *NIMA DST 9005* tensiometer from *NIMA Technology, Ltd*. was used for these measurements. It incorporates a microbalance (Peterson, 1997) able to read force within 10^{-6} mN, which was operated on the *Wilhelmy plate* method (Rusanov *et al*., 1996) for the

liquid-vapor interfacial tensions and on the *Du Noüy* ring method (Rusanov *et al.*, 1996; Harkins *et al.*, 1930; Freud *et al.*, 1930; Huh et al., 1975) for the liquid-liquid interfacial tensions (Figure I. 1).

The plate (or ring) is connected to the microbalance and afterwards immersed and detached from the evaluating interface, resulting on a total force (F) which, when the contact angle (θ) is zero (Figure I. 1), can be separated into the following three components:

$$F = weight - up\ thrust + int\,erfacial\ tension \times wetted\ lenght \qquad \text{(I. 1)}$$

Before making any measurements the balance is zeroed, thereby eliminating the weight term.

At the interface, the up thrust is zero and so, the force measured by the balance is only due to the interfacial tension:

$$F_{int\,erface} = int\,erfacial\ tension \times wetted\ lenght \qquad \text{(I. 2)}$$

Generally, the interfacial tension is thus given by:

$$\sigma = \frac{F_{int\,erface}}{wetted\ lenght} \qquad \text{(I. 3)}$$

where σ is the interfacial tension, in $N.m^{-1}$.

When the contact angle between the ring (or plate) and the measuring interface is different from zero (Figure I. 1), the force measured by the balance has to be corrected:

$$\sigma = \frac{F_{interface}}{wetted\ lenght \times cos(\theta)} \qquad \text{(I. 4)}$$

In the *Wilhelmy* plate method, the wetted length is equal to the plate perimeter:

$$\sigma = \frac{F_{interface}}{2 \times (width + thickness)} \qquad \text{(I. 5)}$$

while for the *Du Noüy* ring, it is equal to the sum of the inner and outer ring diameters:

$$\sigma = \frac{F_{interface}}{(\pi d + \pi(d - 2t))} \qquad \text{(I. 6)}$$

where d is the ring outer diameter and t is the wire thickness.

The *Wilhelmy* plate method is an absolute method, since it does not require any hydrostatic correction. This would suggest using this method for all the measurements. Unfortunately, only with some liquid-vapor interfaces we can guarantee that the angle θ formed between the lower edge of the plate and the interface is zero.

Two reasons were thus involved in the selection of different measuring methods for liquid-liquid and liquid-vapor interfaces. The first is the need of density data required for the ring method, and not needed with the plate, making the last very convenient for vapor-liquid interfaces were complete wetting of the *Wilhelmy* plate can be obtained (θ = 0). On the other hand, for liquid –liquid interfaces, complete wetting is best assured by the use of the *Du Noüy* ring where, due to its circular shape and the largest wetting perimeter, can be withdrawn with a zero contact angle. However, with this method, an hydrostatic correction is required due to the pull up of measuring fluid on the inner side of the ring.

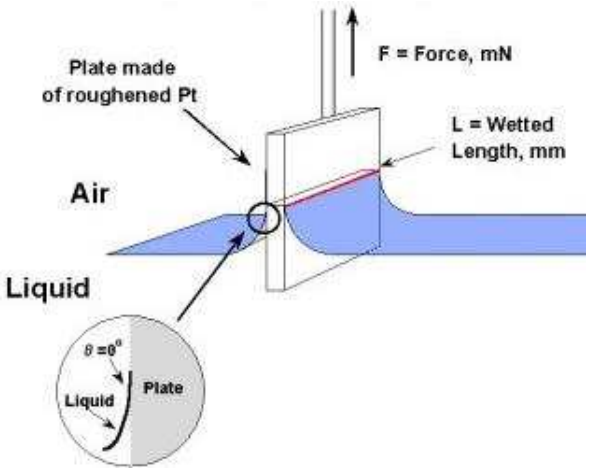

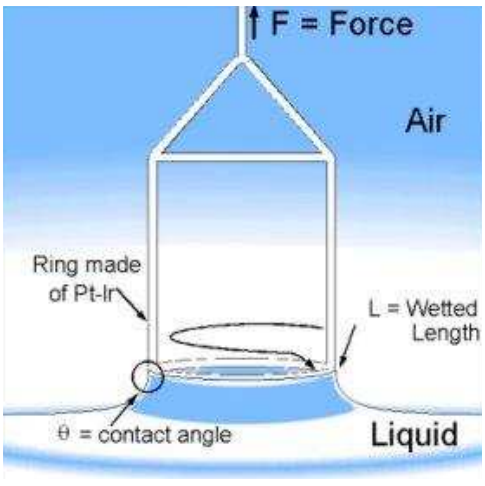

Figure I. 1: **NIMA DST 9005 tensiometer (up). *Wilhelmy* plate (middle) and *Du Noüy* ring (bottom).**

It was shown (Rusanov *et al.*, 1996, Huh *et al.*, 1975, Martin *et al.*, 1999) that this correction depends on the difference of mass densities between the involved phases, and it is automatically performed by the tensiometer acquisition software after inputting the density difference.

Plate perimeter and ring diameter and thickness were first measured within ±10 μm and are introduced in the acquisition software. Platinum plates and rings were used. Dimensions of the *Wilhelmy* plate were 20.20 mm width and 0.18 mm thickness and those of the *Du Noüy* ring 20.75 mm diameter and 500 μm wire thickness. From the force measurements and the plate (or ring) dimensions, this tensiometer automatically returns interfacial tension values.

This tensiometer can also be used to measure force, contact angles and dynamic interfacial tension. Several measurement parameters can be easily changed giving this equipment considerable versatility (Martin *et al*., 1999).

All of the used chemicals were commercial products with a stated purity of at least 98%: n-heptane (Riedel de Haën, ≥ 99 %), n-decane (Aldrich, ≥ 99 %), n-hexadecane (Sigma, ≥ 99 %), n-eicosane (Sigma, ≥ 99 %), n-docosane (Fluka, ≥ 98 %) and n-tetracosane (Fluka, ≥ 99 %). Liquid room-temperature n-alkanes (n-heptane, n-decane, and n-hexadecane) were dried over molecular sieves. For the vapor-liquid interfacial tensions no further purification was carried out, while for liquid-liquid (water + n-alkane) measurements, the n-alkanes were first purified by column chromatography with basic alumina, since it was earlier reported that trace contaminants in the n-alkanes could be enriched in the aqueous-n-alkane interface, reducing the interfacial tensions (Goebel *et al*., 1997; Gaonkar *et al.*, 1984). For the n-alkanes heavier than n-$C_{16}H_{34}$, no such effect was observed, while for the lower ones, results were considerably improved after column chromatography.

For the measurements, approximately 50 cm^3 of each liquid phase were introduced in a thermostated glass vessel. Temperature was controlled within 0.01 K by an external Pt100 probe directly immersed on the system and connected to an *HAAKE F6* circulator. The accuracy of this temperature measuring system was assured by calibration against a certified *Thermometrics S10 thermistor.* Average absolute deviation (Eq. I.7) was smaller than 0.04 K with a maximum deviation of -0.07 K at 319.72 K:

$$\% \; AAD = \frac{1}{m} \sum \left| \frac{X - X_a}{X_a} \right| \times 100 \qquad \text{(I. 7)}$$

where m is the number of data points, X is the measured temperature in K and subscript a stands for the accepted value from the thermistor.

Mixtures were carefully prepared by weighting the components in a *Mettler Toledo AB204* analytical balance (± 0.0001 g). Uncertainty in mole fraction was calculated to be less than 2×10^{-5}.

Balance and tensiometer were calibrated with masses provided by the manufacturers.

Before the measurements, the glass vessel was carefully cleaned with water and detergent to completely remove the previous sample. After that, the vessel was washed with plenty of distilled water and dried before use. The glass vessel was regularly soaked in 5M nitric acid in order to remove any extra contaminant. Surfactant-free paper was used for cleaning purposes.

Special precautions were taken to avoid evaporation of the more volatile components such as n-heptane and n-decane during the mixture measurements. For that purpose, the tensiometer was hermetically closed and a small portion of these components was introduced inside the tensiometer chamber in order to saturate the gas phase. Humidity was removed from the tensiometer chamber using dried silica gel.

Before each vapor-liquid measurement, the plate was flamed in a Bunsen burner in order to eliminate contaminants.

For the liquid-liquid interfacial tensions the *Du Noüy* ring was immersed in an acidic mixture (20% conc. HCl + 20% conc. HNO_3) for 15 minutes and after that washed with plenty of ultra-pure water, since it was reported previously that flame cleaning could promote the adsorption of non-polar species to the ring while measuring aqueous-hydrocarbon interfaces (Gaonkar *et al.*, 1984; Lunkenheimer, 1989).

The interface was cleaned by suction with a Pasteur pipette and discarded. This allows the removal of some surface-active contaminants and the formation of a new and clean interface.

During the measurements, the *Wilhelmy plate* or the *Du Noüy ring* were immersed and detached from the interface, after the liquid level was automatically determined by the tensiometer. Interfacial tension was obtained from the maximum value of the plot interfacial tension vs. immersion depth while the plate or ring was detached. For each system, at least 9 interfacial tension values were recorded, from which an average was taken.

For the water-n-alkane interfacial tensions, the first step was the introduction of ultra-pure water on the measuring vessel. After that, the ring was immersed to determine the liquid level and then it was totally immersed on the aqueous phase so that the measuring part of the *Du Noüy* ring never touched the n-alkane phase over it. The n-alkane was then carefully transferred to the measuring vessel, and after a period of time necessary to reach the desired thermal equilibrium at the target temperature, plus 15 minutes, the measurement started. Since with the *Du Noüy* ring the maximum force is obtained without breaking the interface, the ring was always wetted by the aqueous phase. If, somehow, the ring broke the interface during the measurement, all the procedure was repeated, since the contact with the organic phase makes the ring hydrophobic (Gaonkar *et al.*, 1984 ; Lunkenheimer, 1989).

An initial set of pure component measurements was carried out to evaluate the ability of the measuring system to reproduce literature data. Pure component interfacial tension was measured from 273.15 K (or above the melting point) up to 343.15 K.

Results are reported and compared with literature values (Jasper *et al*.,1953; McLure *et al*. 1982; Jasper, 1972; Koefoed *et al*. 1958; Águila-Hernandez, 1987; Jasper *et al*., 1955). in Table I. 1 and

Figure I. 2. The uncertainty reported in this table heading (± 0.03 $mN.m^{-1}$) is the maximum uncertainty found from all data. This was evaluated using the law of propagation of uncertainty in which force, plate dimensions and temperature were considered (Taylor *et al*., 1994). Details on these calculations can be found at Appendix I.

Deviations were calculated using *percent average absolute deviations* (% AAD, Eq. I.7), where *m* is the number of data points, *X* is the interfacial tension and the subscript *a* stands for the accepted (literature) values. An overall average absolute deviation of 1.2 % was obtained. No literature data was found for n-tetracosane. The

maximum deviation was 2.6 % for n-hexadecane at 293.15 K, compared with the data from Koefoed *et al.* (1958). In

Figure I. 2 n-heptane results are presented, where data from Grigoryev *et al.*, (1992) taken at different temperatures from our measurements, are also included. The measured data agrees with the data previously reported as much as the different sets of data agree between themselves.

It should be noted that for n-docosane and n-tetracosane, at the lowest temperatures, surface tension decreases with decreasing temperature, an opposite trend to what is generally found. This phenomenon is particular of some heavy n-alkanes with chain length $14 < n \leq 50$, some alcohols and liquid crystals and is ascribed to surface freezing, where the surface presents solid ordering before the bulk liquid does, around 3 K above the melting point (Penfold, 2001; Wu *et al.*, 1993; Earnshaw *et al.*, 1992).

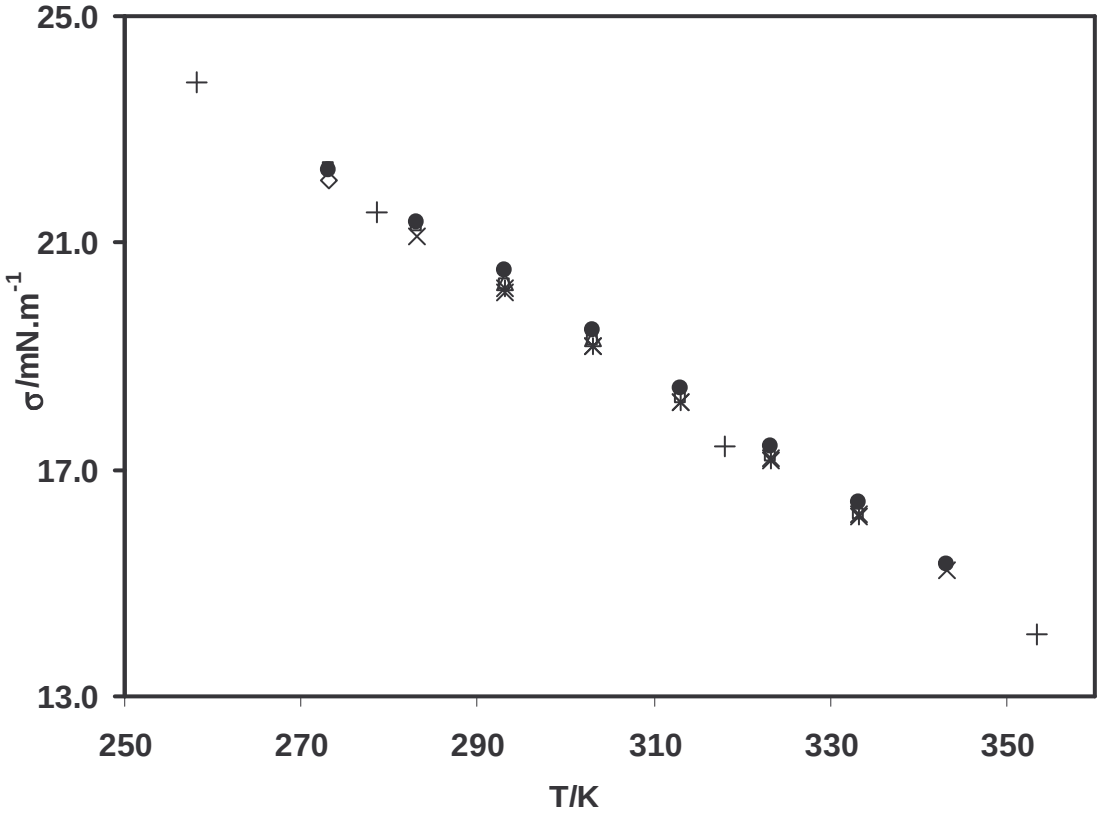

Figure I. 2: **Surface tension of n-C_7H_{16}: ●, this work, +, Grigoryev *et al.*, 1992; x, Jasper, 1972; ◊ Jasper *et al.*, 1955; △, Koefoed *et al.*, 1958; * McLure *et al.*, 1982.**

Table I. 1: Pure n-alkane interfacial tension and comparison with literature

n-alkane	T/K	σ/mN.m^{-1}							
		this work[a]	Jasper *et al.* (1953)	McLure *et al.* (1982)	Jasper (1972)	Koefoed *et al.* (1958)	Águila-Hernandez (1987)	Jasper *et al.* (1955)	% AAD[b]
n-C_7H_{16}	273.15	22.28	22.31					22.10	1.1
	283.15	21.37	21.30		21.12				
	293.15	20.50	20.28	20.21	20.14	20.30			
	303.15	19.47	19.27	19.17	19.17	19.31			
	313.15	18.42	18.25	18.19	18.18				
	323.15	17.41	17.24	17.18	17.20				
	333.15	16.42	16.22	16.19	16.22				
	343.15	15.32			15.24				
n-$C_{10}H_{22}$	293.15	24.09	23.89		23.83				1.5
	303.15	23.29	22.98		22.91				
	313.15	22.33	22.06		21.99				
	323.15	21.43	21.14		21.07				
	333.15	20.54	20.22		20.15				
	343.15	19.66			19.23				
n-$C_{16}H_{34}$	293.15	28.11	27.64		27.47	27.40			1.3
	303.15	27.02	26.79		26.62	26.63			
	313.15	26.23	25.95		25.76				
	323.15	25.29	25.11		24.91		25.08		
	333.15	24.40	24.27		24.06		24.25		
	343.15	23.51	23.42		23.20		23.38		
n-$C_{20}H_{42}$	313.15	27.58			27.21				1.1
	323.15	26.67			26.38		26.52		
	333.15	25.85			25.54		25.58		
	343.15	25.01			24.71		24.71		

n-alkane	T/K	σ/mN.m^{-1}							
		this work[a]	**Jasper *et al.* (1953)**	**McLure *et al.* (1982)**	**Jasper (1972)**	**Koefoed *et al.* (1958)**	**Águila-Hernandez (1987)**	**Jasper *et al.* (1955)**	**% AAD**[b]
n-$C_{22}H_{46}$	318.15	26.72[c]							
	323.15	27.42					27.15		1.1
	333.15	26.60					26.25		
	343.15	25.79					25.54		
n-$C_{24}H_{50}$	323.15	26.67[c]							
	333.15	27.05							
	343.15	26.22							

[a] maximum uncertainty: ± 0.03 mN·m^{-1}

[b] Eq. I.7.

[c] measured at temperatures were surface crystallization is known to occur.

Mixture data were measured above 293.15 K. and are presented on Tables I.2- I.3. Reported uncertainty corresponds, again, to the maximum uncertainty found from all the mixture points. The calculation procedure was the same used for the pure components, this time including also the uncertainty due to mixture preparation (Appendix I).

A comparison with mixture reported values from Koefoed *et al.* (1958), Águila-Hernandez (1987), Pugachevich *et al.*(1979) and Pandey *et al.* (1982) is presented on Figs. I.3 - I.5.

Pandey *et al*. (1982) reported 4 mixture data points ($0.05< x$ n-$C_{16}H_{34}$ <0.40) for the system n-decane + n-hexadecane at 303.16 K. Koefoed *et al*. (1958) and Pugachevich *et al* (1979) presented data for the mixture n-heptane + n-hexadecane at 293.15 K, 303.15 K, 333.15 K and 373.15 K. Águila-Hernandez (1987) presented full composition data for the mixture n-hexadecane + n-eicosane from 323.15 K up to 353.15 K. Visual inspection can be used to conclude that although our equipment seems to give systematically higher values than those reported on literature, small deviations are observed, which can guarantee that our measurements should have considerable accuracy.

Table I. 2: Interfacial tension of binary n-alkane mixtures

System	*x* (1)	*x* (2)	σ ± 0.07/mN·m^{-1}					
			293.15 K	303.15 K	313.15 K	323.15 K	333.15 K	343.15 K
n-C_7H_{16} (1)– n-$C_{10}H_{22}$ (2)	0.749	0.251	21.68	20.72	19.75	18.85	17.91	
	0.499	0.501	22.73	21.57	20.67	19.80	18.96	
	0.248	0.752	23.47	22.46	21.49	20.62	19.78	
n-C_7H_{16} (1)– n-$C_{16}H_{34}$ (2)	0.800	0.200	22.36	21.44	20.61	19.71	19.03	
	0.500	0.500	24.76	23.78	22.95	22.06	21.31	
	0.200	0.800	26.83	25.88	25.28	24.63	23.80	
n-C_7H_{16} (1)– n-$C_{20}H_{42}$ (2)	0.750	0.250			21.29	20.53	19.68	18.60
	0.500	0.500			23.76	22.87	22.19	21.57
	0.251	0.749			25.83	25.06	24.28	23.58
n-C_7H_{16} (1)– n-$C_{22}H_{46}$ (2)	0.750	0.250			21.55	20.81	20.03	19.15
	0.500	0.500			23.99	23.49	22.74	22.02
	0.250	0.750			25.93	25.54	24.92	24.27
n-C_7H_{16} (1)– n-$C_{24}H_{50}$ (2)	0.750	0.250			21.71	20.85	20.20	19.63
	0.500	0.500				23.76	23.17	22.66
	0.250	0.750				26.04	25.44	24.81
n-$C_{10}H_{22}$ (1) + n-$C_{16}H_{34}$ (2)	0.750	0.250	25.29	24.37	23.54	22.60	21.67	
	0.500	0.500	26.20	25.48	24.76	23.71	22.87	
	0.248	0.752	27.18	26.17	25.46	24.65	23.72	

System	*x* (1)	*x* (2)	σ ± 0.07/mN·m^{-1}					
			293.15 K	**303.15 K**	**313.15 K**	**323.15 K**	**333.15 K**	**343.15 K**
n-$C_{10}H_{22}$ (1) + n-$C_{20}H_{42}$ (2)	0.800	0.200	25.45	24.59	23.70	22.71	21.83	20.96
	0.600	0.400		25.77	24.86	24.04	23.11	22.18
	0.501	0.499		26.45	25.50	24.69	23.60	22.80
	0.400	0.600			26.00	25.25	24.34	23.60
	0.201	0.799			27.13	26.16	25.40	24.53
n-$C_{10}H_{22}$ (1) + n-$C_{22}H_{46}$ (2)	0.800	0.200			23.39	22.67	22.13	21.51
	0.600	0.400			25.36	24.29	23.49	22.87
	0.501	0.499			26.08	25.01	24.18	23.39
	0.400	0.600			26.67	25.55	24.78	23.94
	0.200	0.800				26.68	26.05	25.22
n-$C_{10}H_{22}$ (1) + n-$C_{24}H_{50}$ (2)	0.800	0.200			24.07	23.13	22.24	21.42
	0.599	0.401				24.64	23.84	22.96
	0.505	0.495				25.29	24.48	23.55
	0.400	0.600				25.99	25.04	24.10
	0.204	0.796				27.14	26.27	25.35
n-$C_{16}H_{34}$ (1)– n-$C_{20}H_{42}$ (2)	0.800	0.200		27.25	26.45	25.58	24.70	23.87
	0.600	0.400		27.63	26.89	25.94	25.11	24.25
	0.500	0.500			26.95	26.19	25.31	24.56
	0.400	0.600			27.15	26.32	25.41	24.64
	0.167	0.833			27.42	26.69	25.81	25.02

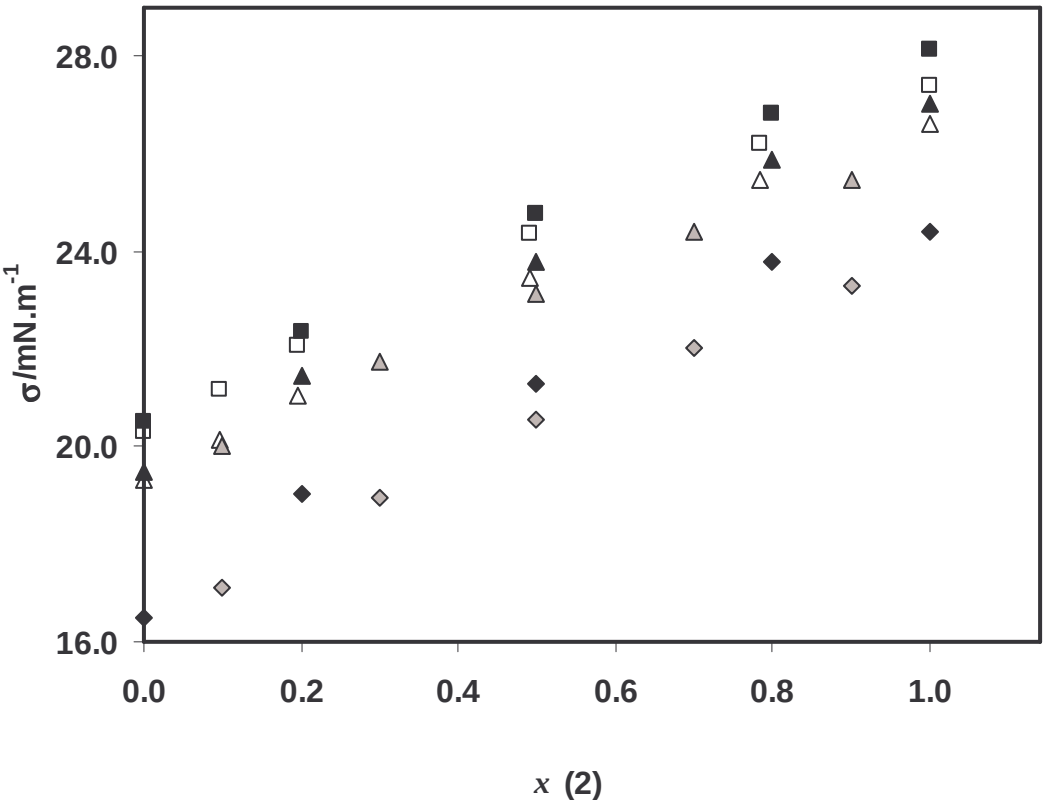

Figure I. 3: **Interfacial tension of n-C_7H_{16} (1) + n-$C_{16}H_{34}$ (2). Squares, 293.15 K; triangles, 303.15 K; lozenges 333.15 K; Filled symbols, this work; open symbols Koefoed *et al.*, 1958, 1979; grey symbols, Pugachevich *et al.*, 1979.**

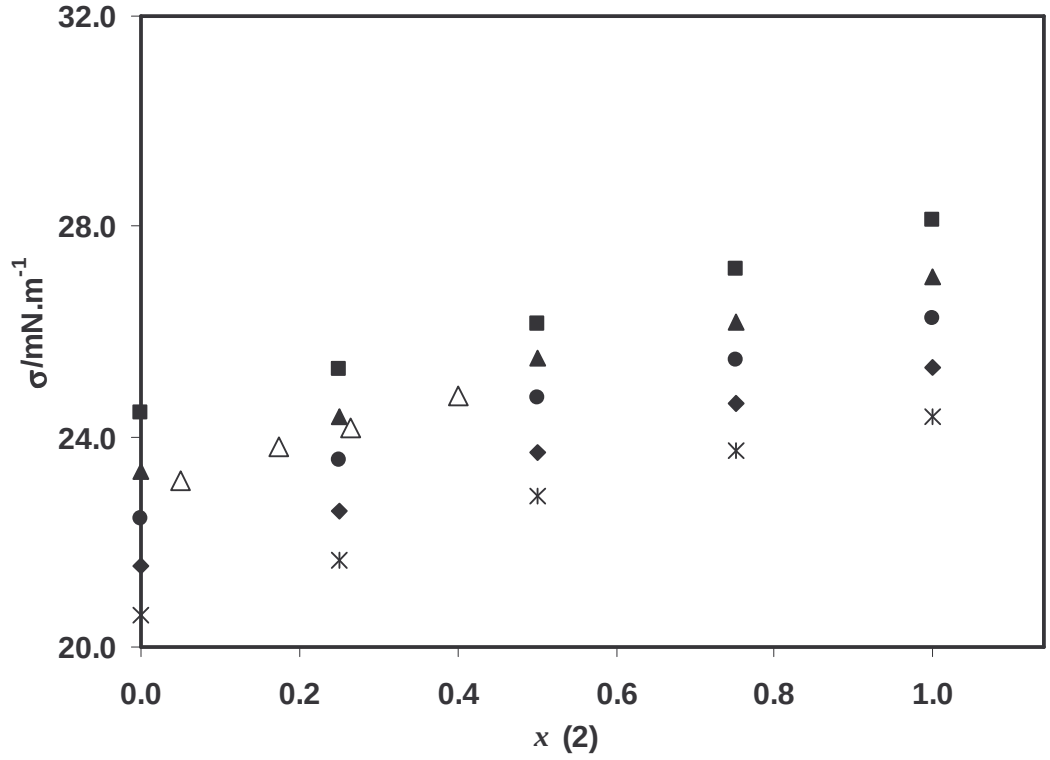

Figure I. 4: **Interfacial tension of n-$C_{10}H_{22}$ (1) + n-$C_{16}H_{34}$ (2). Squares, 293.15 K; Triangles, 303.15 K; Circles, 313.15 K; Lozenges, 323.15 K; Asterisks, 333.15 K; Filled symbols, this work; Δ, 333.15 K from Pandey *et al.*, 1982.**

It should also be noted that for the system n-heptane + n-hexadecane, data reported by Koefoed *et al*. (1958) for n-hexadecane presented the highest deviation from our data, as can be seen in Table I. 1. Mixture data from Pugachevich *et al.* (1979) are systematically lower than that reported either in this work or by Koefoed *et al.* (1958).

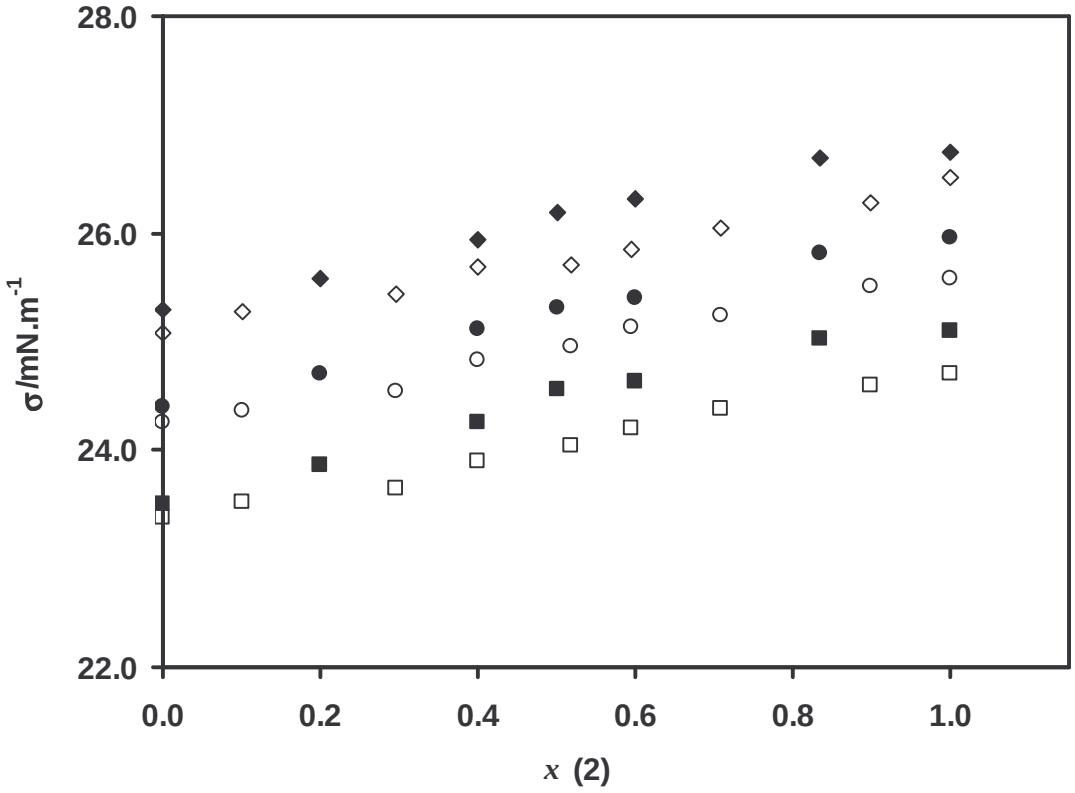

Figure I. 5: **Surface tension of n-$C_{16}H_{34}$ (1) + n-$C_{20}H_{42}$ (2). Lozenges, 323.15 K; circles, 333.15 K; squares, 343.15 K. Filled symbols, this work. Open symbols, Águila-Hernandez, 1987.**

For the mixture n-hexadecane + n-eicosane, our data is somewhat higher than that reported by Águila-Hernandez (1987), but small deviations are observed. Average absolute deviations (Eq. I.7) for the pure components are 0.7 % and 0.9%, respectively for n-hexadecane and n-eicosane. For the other mixtures, no data was previously available.

The curvature presented as a function of composition, where the mixture surface tension is higher than the corresponding mole fraction average, is typical of n-alkane mixtures. The opposite trend is commonly observed in mixtures containing other families of fluids. These differences are the consequence of the different surface compositions that will result in the minimum free energy of the system.

The ternary mixtures n-C_7H_{16} (or n-$C_{10}H_{22}$) + n-$C_{20}H_{42}$ + n-$C_{24}H_{50}$ were studied at equimolar compositions of n-$C_{20}H_{42}$ and n-$C_{24}H_{50}$ to allow for a comparison of this ternary data with those of the binaries n-C_7H_{16} (or n-$C_{10}H_{22}$) + n-$C_{22}H_{46}$. These systems are plotted on Figs. I.6-I.7 as a function of n-heptane and n-decane mole fractions, respectively. As can be seen from this figures and Tables I.2 and I.3, it seems that the binary data resembles that of the equivalent ternary. It is interesting to note that the equimolar (x = 0.5) mixture of n-eicosane and n-tetracosane presents surface tension values quite close to those of pure n-docosane, although systematically lower. A study on several other pure, binary and ternary data from different sources (Jasper *et al.*,1953; McLure *et al*. 1982; Jasper, 1972; Koefoed *et al*. 1958; Águila-Hernandez, 1987; Jasper *et al*., 1955; Grigoryev *et al*., 1992; Pandey *et al*., 1982; Pugachevich *et al*. 1980) showed that for n-alkanes with the same average chain length, surface tension slightly decreases with the increase on the number of components, as observed in this work.

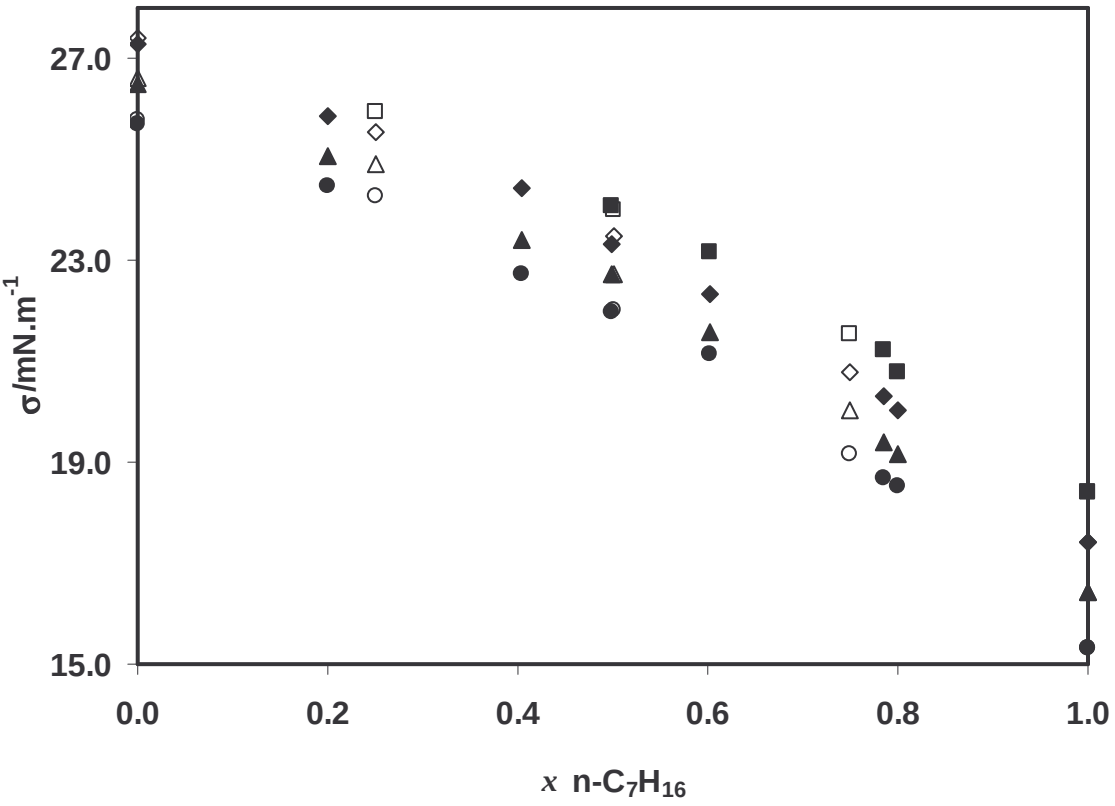

Figure I. 6: **Surface tension of n-C_7H_{16} + n-$C_{22}H_{46}$ (filled symbols) and n-C_7H_{16} + n-$C_{20}H_{42}$ + n-$C_{24}H_{50}$ (open symbols). Circles, 343.15 K; triangles, 333.15 K; lozenges 323.15 K; squares, 313.15 K.**

Table I. 3: Interfacial tension of ternary n-alkane mixtures

System	*x* (1)	*x* (2)	*x* (3)	σ ± 0.07/mN·m^{-1}			
				313.15 K	323.15 K	333.15 K	343.15 K
n-C_7H_{16} (1) + n-$C_{20}H_{42}$ (2) + n-$C_{24}H_{50}$ (3)	0.000	0.500	0.500		27.27	26.51	25.69
	0.200	0.401	0.399		25.87	25.08	24.46
	0.404	0.298	0.298		24.44	23.41	22.71
	0.499	0.250	0.251	24.07	23.34	22.73	21.99
	0.602	0.199	0.199	23.15	22.34	21.57	21.13
	0.785	0.107	0.108	21.22	20.33	19.40	18.70
n-$C_{10}H_{22}$ (1) + n-$C_{20}H_{42}$ (2) + n-$C_{24}H_{50}$ (3)	0.000	0.500	0.500		27.27	26.51	25.69
	0.201	0.400	0.399		26.26	25.56	24.77
	0.400	0.300	0.300	26.16	25.20	24.52	23.67
	0.500	0.250	0.250	25.33	24.65	23.85	23.16
	0.600	0.200	0.200	24.93	23.96	23.17	23.38
	0.800	0.100	0.100	23.56	22.86	21.92	21.02

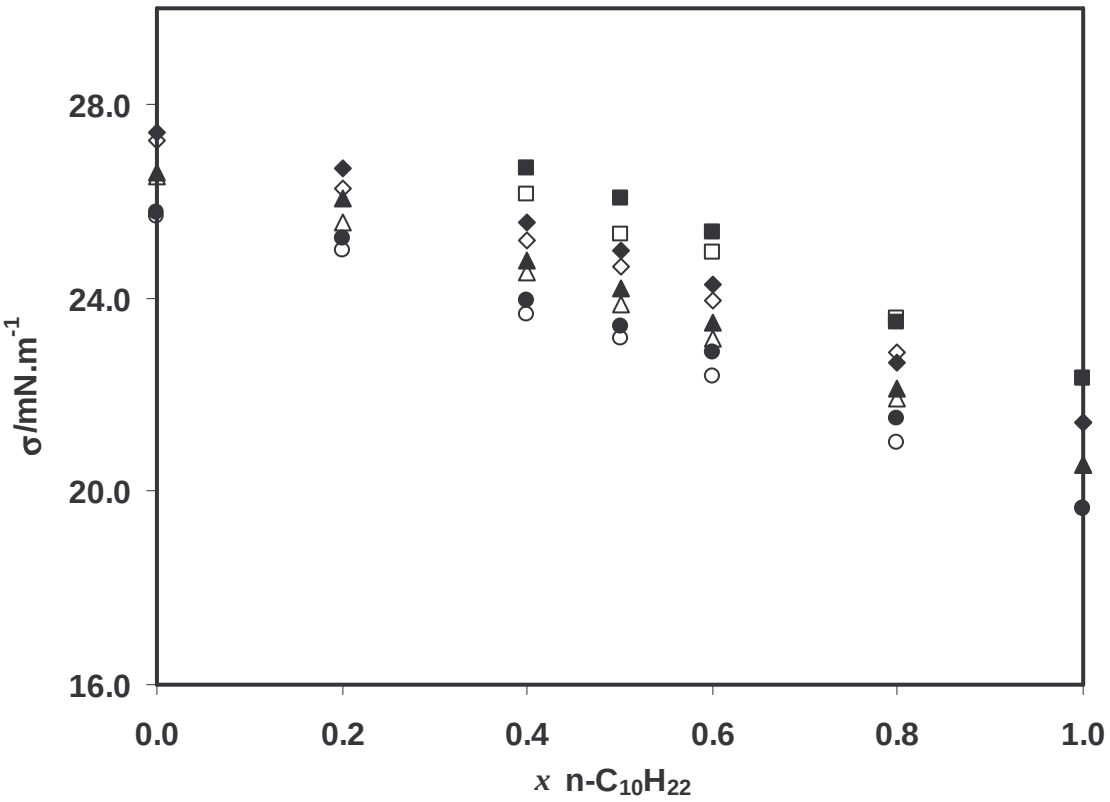

Figure I. 7: **Surface tension of $n\text{-}C_{10}H_{22}$ + $n\text{-}C_{22}H_{46}$ (filled symbols) and $n\text{-}C_{10}H_{22}$ + $n\text{-}C_{20}H_{42}$ + $n\text{-}C_{24}H_{50}$.(open symbols). Circles, 343.15 K; triangles, 333.15 K; lozenges 323.15 K; squares, 313.15 K.**

Liquid-liquid water – n-alkane interfacial tension data are presented in Table I. 4 and compared with literature values from Zeppieri *et al*. (2001) in Figure I. 8. As for the liquid-vapor interfacial tensions, small deviations are observed, with an average absolute deviation (Eq. I.7) for water-n-heptane and water-n-decane of 0.3 %. For the systems with n-eicosane, n-docosane and n-tetracosane no literature data was found.

In Table I. 5 some vapor-liquid interfacial tensions of petroleum distillation cuts (503.15 K – 648.15 K) from crudes of different sources (North Sea, Africa and Middle East) obtained from the Petrogal[1] refinery are presented. These were chosen since they are the basis for the diesels produced at the refinery and cover the range of n-alkane contents typically found there (3 to 30 wt %). The characterization of these fractions can be found at section I.2.4.

[1] Petrogal is the portuguese oil company.

Table I. 4: Liquid-liquid interfacial tension of water + n-alkane systems

System	σ ± 0.05/mN·m^{-1}									
	288.15 K	**293.15 K**	**298.15 K**	**303.15 K**	**308.15 K**	**313.15 K**	**318.15 K**	**323.15 K**	**333.15 K**	**343.15 K**
H_2O + n-C_7H_{16}	51.49	51.24	50.63	50.20	49.71	49.30	48.96	48.49		
H_2O + n-$C_{10}H_{22}$		52.06		51.22		50.28		49.46		
H_2O + n-$C_{16}H_{34}$				55.09		54.10		53.10	52.01	51.08
H_2O + n-$C_{20}H_{42}$						55.02		54.08	53.05	52.07
H_2O + n-$C_{22}H_{46}$								54.97	53.92	52.93
H_2O + n-$C_{24}H_{50}$								55.99	55.01	53.98

Table I. 5: Interfacial tension of some petroleum distillation cuts

Distillation cut	σ ± 0.03/mN.m^{-1}					
	293.15 K	**303.15 K**	**313.15 K**	**323.15 K**	**333.15 K**	**343.15 K**
Sahara	29.18	28.22	27.55	26.66	25.74	24.73
Duc	30.44	29.49	28.60	27.73	26.83	25.84
Troll	30.24	29.43	28.59	27.65	26.78	25.73
Brent	29.64	28.54	27.84	26.97	26.11	25.11
Oso	29.35	28.35	27.44	26.53	25.60	24.67

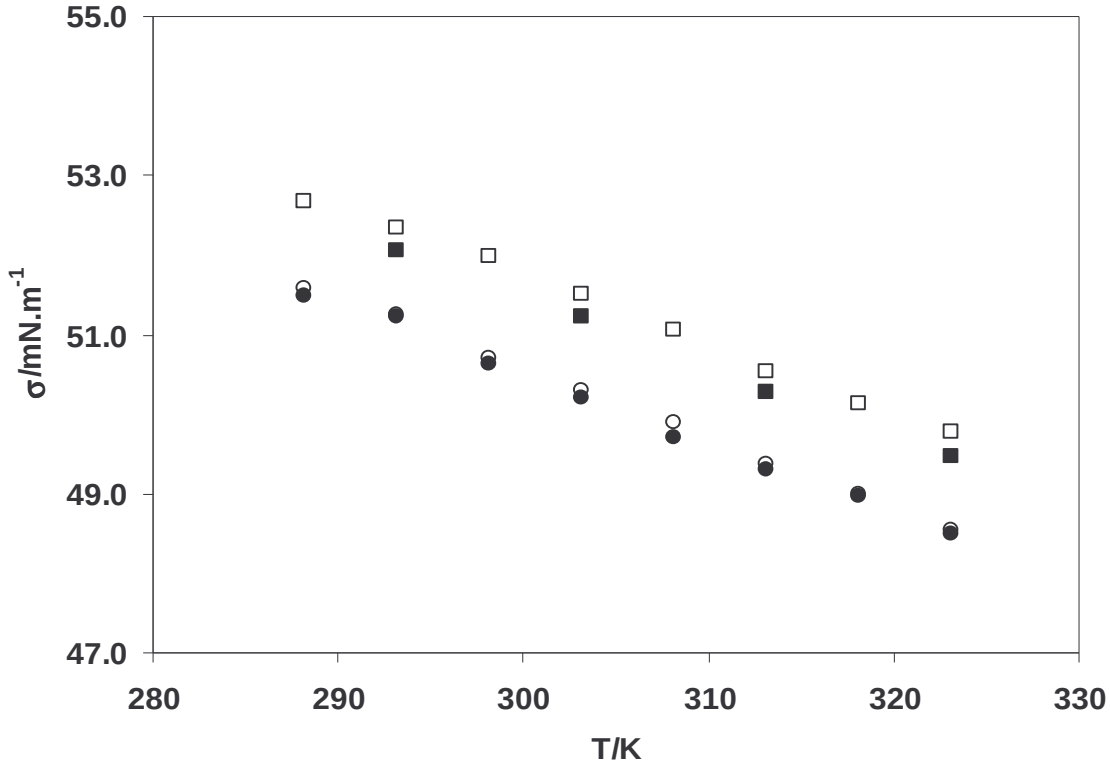

Figure I. 8: **H_2O + n-C_7H_{16} (circles) and H_2O + n-$C_{10}H_{22}$ (squares) liquid-liquid interfacial tensions. Filled symbols, this work; Open symbols, Zeppieri *et al.*, 2001.**

I.2.2. Viscosity

A rolling ball microviscometer from *Anton PAAR KG* (A*MV 200 Automated Microviscometer*) was used. This apparatus is based on the measurement of the time that a steel ball needs to roll down inside a glass capillary filled with sample, Figure I. 9.

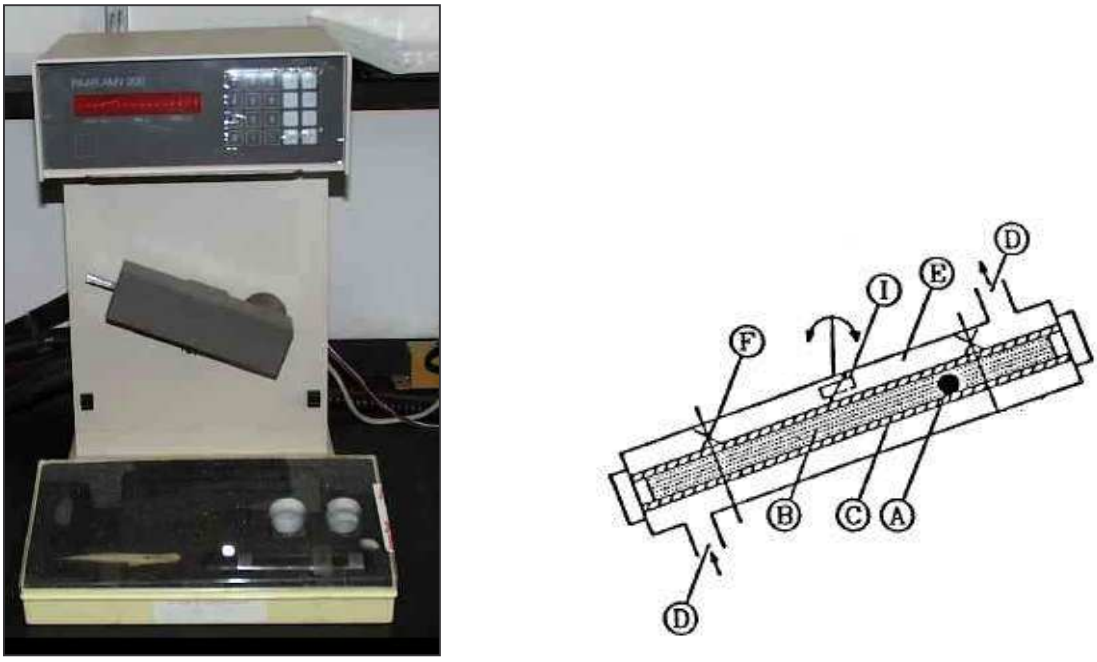

Figure I. 9: **AMV 200 *Anton Paar* automated microviscometer. Right: detail of the working principle (Dandekar *et. al.*, 1998)**

Several combinations of ball(A)/capillary(C) of different diameters can be selected, giving the possibility of measuring viscosities from 0.5 to 800 mPa·s. One of the advantages of this technique is that it requires very small amounts of sample (B). Depending on the capillary, only 0.12 to 2.5 cm^3 are used. For the measurements reported in this section, a glass capillary of 1.6 mm diameter and gold balls of 1.500 mm diameter were used. The measurement is fully automatic. Two magnetic sensors (F) are used to determine the rolling time which is reported within ± 0.01 s. Shear stress can be varied by selecting different rolling angles, and up to ten different rolling angles (both positive and negative) can be chosen from 15º to 90º. Up to six repetitions can be programmed for each angle.

The viscosity is calculated from the rolling times and the liquid density using the following equation:

$$\eta = \kappa(\alpha)\, t \left(\rho_{ball} - \rho_{liquid}\right) \qquad \text{(I. 8)}$$

where η is the viscosity, mPa·s, κ is a calibration constant which only depends on the angle α, t is the roll time, s, and ρ is the density, $Kg \cdot m^{-3}$. Density values to be used with Eq. I.8 are reported in section I.2.3.

The parameter κ is only angle-dependent and has to be determined, for each angle α, with liquids of known viscosity and density. Distilled water, Cannon Instruments Co. and HAAKE Medingen Gmbh viscosity standards were used for calibration. These standards were selected so that the entire measuring range was covered.

Temperature was controlled in the viscometer by the use of a *Heto* thermostatic circulator. A built-in temperature sensor (I), placed closed to the capillary surface, enclosed in a thermostatic capillary block (E) on whose walls the thermostatic water circulates (D), measured the temperature. The temperature working range for this instrument is 279.15 to 353.15 K with an uncertainty of ± 0.01 K.

The following chemicals were used in the measurements: n-heptane (Rathburn, ≥ 99 wt. %), n-decane (Aldrich, ≥99 wt. %), n-hexadecane (Aldrich, ≥ 99 wt. %), n-eicosane (Aldrich, ≥ 99 wt. %), n-docosane (Fluka, ≥ 98 wt. %) and n-tetracosane (Fluka, ≥ 99 wt %). Liquid room-temperature n-alkanes (n-heptane and n-decane) were dried over molecular sieves. No further purification was carried out.

Mixtures (total mass of 10 g) were carefully prepared by weighing the components on a *Sartorius* analytical balance (± 0.0001 g). After preparation, solutions were kept in the refrigerator between measurements.

Following the measurements, the viscometer capillary was carefully cleaned with toluene and ethanol and afterwards dried with vacuum.

Viscosity was measured, at atmospheric pressure, from 293.15 K (or above the melting point) up to 343.15 K in temperature intervals of 10 K. A new ball was used for each measurement.

The measured viscosities are reported in Tables I.6 – I.9. Each viscosity measurement was performed at 10 different rolling angles from 15.0º to 46.5º with four repetitions at each value. Each reported data point is thus an average of 40 different viscosity measurements.

It should be noted that, for n-heptane, viscosity is only reported up to 323.2 K, since at the highest temperatures, considerable deviations were found against literature data. These measurements would also correspond to a measuring range substantially below the lower limit suggested by the viscometer manufacturer.

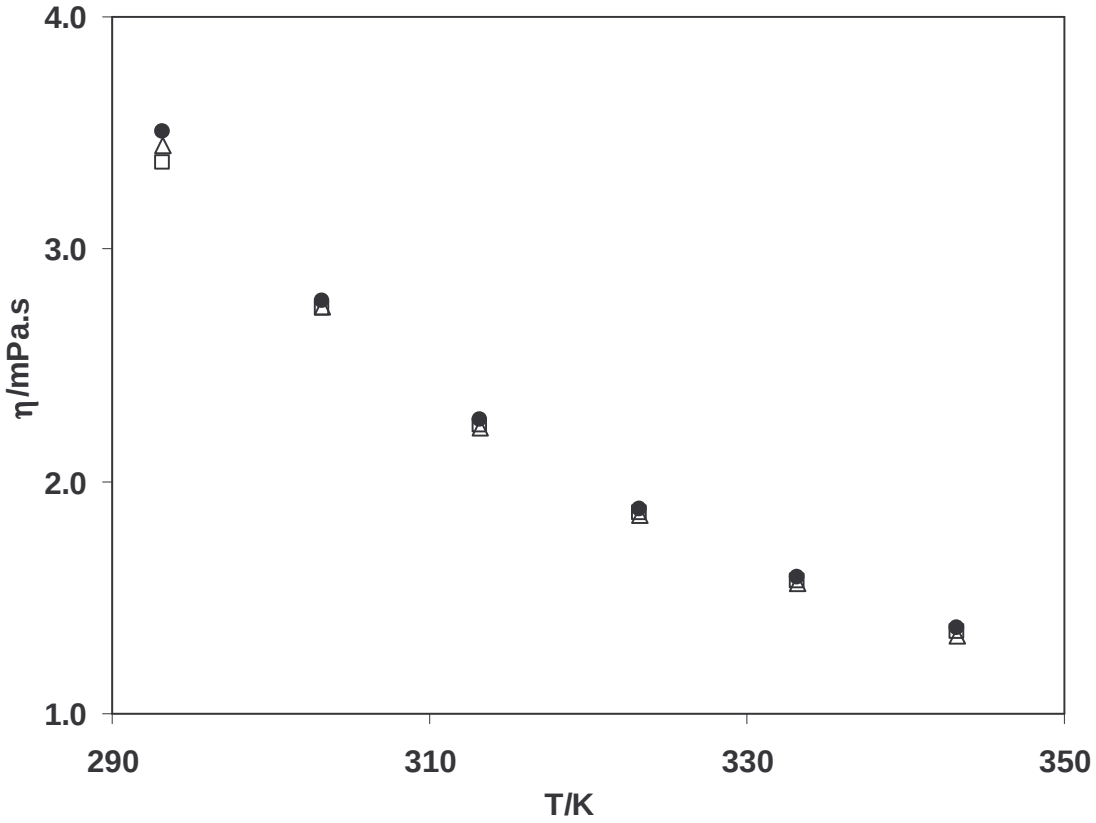

Figure I. 10: **Viscosity of n-$C_{16}H_{34}$: ● this work, □ DIPPR, 1998, Δ, Vargaftik, 1975.**

In Table I. 6 a comparison of the measured viscosities with literature pure component data is presented. Viscosity average absolute deviations (Eq. I.7) are below 5 % with the

maximum deviation found for n-tetracosane (4.7 %), for which only a small amount of experimental information is available (DIPPR, 1998; Wakefield *et al*., 1988). For the other n-alkanes deviations were the following: n-heptane, 1.7 %, n-decane, 3.2 %, n-hexadecane, 1.6 %, n-eicosane, 2.0 %, with the average of all deviations being 2.1 %, quite close to the values found by Dandekar *et al.* (1998) for the same equipment. No viscosity data was found for n-docosane. A graphical comparison of the deviations observed for n-hexadecane is presented in Figure I. 10.

Mixture results are reported on Tables I.7 – I.8. No literature data were found for any of the mixture points.

With these results, viscosities of the ternaries n-$C_{10}H_{22}$ + n-$C_{20}H_{42}$ + n-$C_{24}H_{50}$ and n-C_7H_{16} + n-$C_{20}H_{42}$ + n-$C_{24}H_{50}$ and those of the corresponding binaries (in terms of average chain length of the heavier components), n-$C_{10}H_{22}$ + n-$C_{22}H_{46}$ and C_7H_{16} + n-$C_{22}H_{46}$, can be compared, as already done for the measured interfacial tensions.

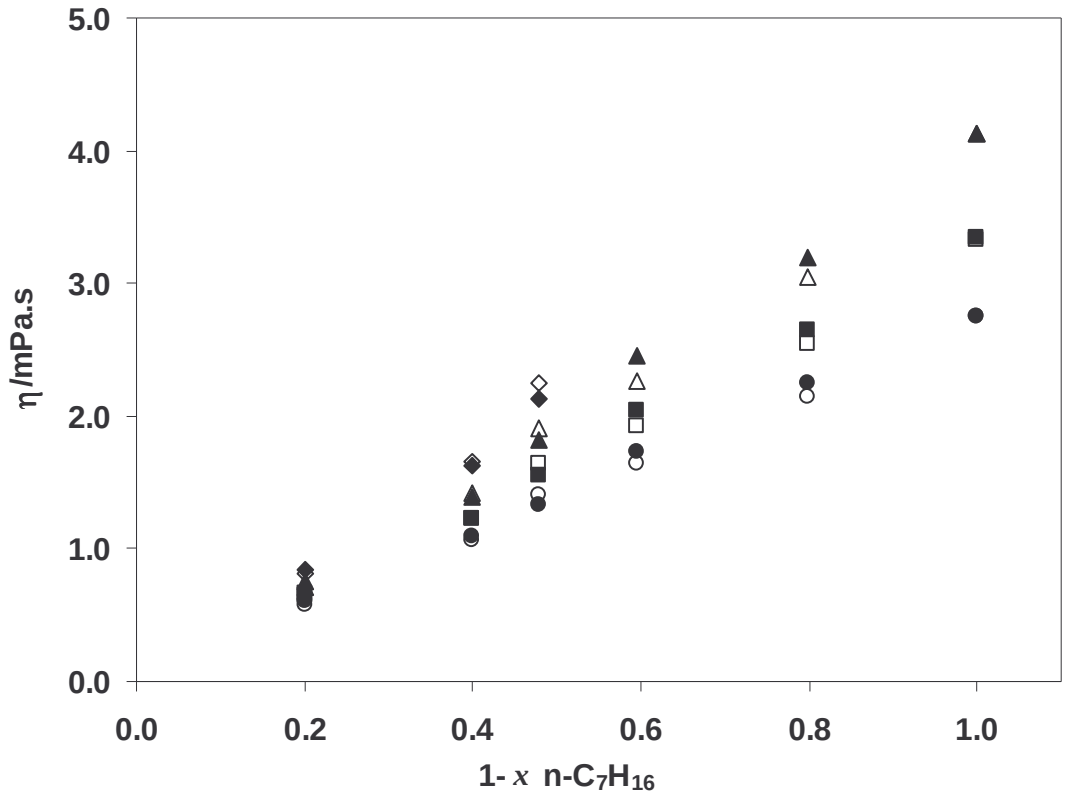

Figure I. 11: **Viscosity of n-C_7H_{16} + n-$C_{22}H_{46}$ (filled symbols) and n-C_7H_{16} + n-$C_{20}H_{42}$ + n-$C_{24}H_{50}$.(open symbols). Circles, 343.15 K; squares, 333.15 K, triangles, 323.15 K, lozenges, 313.15 K.**

Table I. 6: Pure n-alkane viscosity and comparison with literature

n-alkane	T/K	η/mPa·s									
		this work*	DIPPR, 1998 [1]	Wakefield *et al.*, 1988 [2]	Vargaftik, 1975	Ducoulombier *et al.*, 1986	Giller *et al.*, 1949	Knapstad *et al.*, 1989	Doolittle *et al.*, 1951	Assael *et al.*, 1992	Aminhabavi *et al.*, 1996	Aralaguppi *et al.*, 1999
$n\text{-}C_7H_{16}$	293.2	0.408	0.413		0.414	0.415	0.410	0.4101	0.4180			
	303.2	0.373	0.373		0.373	0.374				0.3675	0.368	0.372
	313.2	0.345	0.337		0.338	0.338						
	323.2	0.318	0.309		0.308	0.308			0.3100	0.3041		
$n\text{-}C_{10}H_{22}$	293.2	0.899	0.913		0.907	0.924	0.907					
	303.2	0.766	0.799									
	313.2	0.666	0.699			0.696						
	323.2	0.587	0.610									
	333.2	0.522	0.543			0.546						
	343.2	0.472	0.487									
$n\text{-}C_{16}H_{34}$	293.2	3.51	3.37		3.451							
	303.2	2.78	2.74		2.754							
	313.2	2.26	2.24		2.232	2.23						
	323.2	1.88	1.86		1.852							
	333.2	1.59	1.57		1.560	1.56						
	343.2	1.37	1.35		1.338							
$n\text{-}C_{20}H_{42}$	313.2	4.01	4.06		4.072							
	323.2	3.20	3.26		3.259							
	333.2	2.61	2.68		2.665							
	343.2	2.17	2.23		2.220							

n-alkane	T/K	η/mPa·s									
		this work*	**DIPPR, 1998** [1]	**Wakefield *et al*., 1988** [2]	**Vargaftik, 1975**	**Ducoulombier *et al*., 1986**	**Giller *et al*., 1949**	**Knapstad *et al*., 1989**	**Doolittle *et al*., 1951**	**Assael *et al*., 1992**	**Aminhabavi *et al*., 1996**	**Aralaguppi *et al*., 1999**
$n\text{-}C_{22}H_{46}$	323.2	4.13										
	333.2	3.34										
	343.2	2.75										
$n\text{-}C_{24}H_{50}$	333.2	4.48	4.21	4.32								
	343.2	3.67										

[1] average of reported experimental values.

[2] interpolation of reported values at 328.16 and 338.16 K.

Table I. 7: Viscosity of binary n-alkane mixtures

System	x (1)	x (2)	η/mPa·s					
			293.2 K	**303.2 K**	**313.2 K**	**323.2 K**	**333.2 K**	**343.2 K**
$n\text{-}C_7H_{16}$ (1)– $n\text{-}C_{20}H_{42}$ (2)	0.800	0.200	0.938	0.819	0.719	0.638	0.574	0.518
	0.600	0.400		1.57	1.33	1.14	0.989	0.869
	0.501	0.499		2.02	1.71	1.45	1.26	1.11
	0.403	0.597			2.15	1.81	1.54	1.34
	0.204	0.796			2.99	2.46	2.06	1.76
$n\text{-}C_7H_{16}$ (1)– $n\text{-}C_{22}H_{46}$ (2)	0.800	0.200		0.976	0.850	0.749	0.668	0.601
	0.600	0.400			1.62	1.39	1.23	1.10
	0.521	0.479			2.14	1.83	1.55	1.33
	0.404	0.596				2.45	2.04	1.73
	0.202	0.798				3.20	2.65	2.25
$n\text{-}C_7H_{16}$ (1)– $n\text{-}C_{24}H_{50}$ (2)	0.802	0.198			0.967	0.854	0.762	0.678
	0.602	0.398				1.68	1.44	1.26
	0.503	0.497				2.24	1.90	1.63
	0.404	0.596				2.60	2.20	1.86
	0.204	0.796					3.29	2.63
$n\text{-}C_{10}H_{22}$ (1) + $n\text{-}C_{20}H_{42}$ (2)	0.800	0.200	1.56	1.31	1.12	0.969	0.850	0.754
	0.600	0.400		2.01	1.68	1.42	1.23	1.07
	0.500	0.500		2.40	1.95	1.66	1.42	1.23
	0.400	0.600			2.38	1.96	1.68	1.44
	0.201	0.799			3.14	2.58	2.20	1.86

System	x (1)	x (2)	η/mPa·s					
			293.2 K	**303.2 K**	**313.2 K**	**323.2 K**	**333.2 K**	**343.2 K**
$n\text{-}C_{10}H_{22}$ (1) + $n\text{-}C_{22}H_{46}$ (2)	0.799	0.201		1.47	1.24	1.04	0.905	0.781
	0.600	0.400			2.05	1.71	1.45	1.26
	0.500	0.500			2.53	2.11	1.72	1.53
	0.400	0.600			2.93	2.43	2.04	1.74
	0.200	0.800				3.17	2.61	2.27
$n\text{-}C_{10}H_{22}$ (1) + $n\text{-}C_{24}H_{50}$ (2)	0.800	0.200			1.48	1.27	1.11	0.966
	0.601	0.399				2.09	1.78	1.53
	0.501	0.499				2.54	2.13	1.81
	0.400	0.600				3.11	2.59	2.18
	0.203	0.797				4.26	3.47	2.89
$n\text{-}C_{16}H_{34}$ (1) + $n\text{-}C_{20}H_{42}$ (2)	0.800	0.200	3.88	3.05	2.46	2.03	1.71	1.47
	0.600	0.400		3.48	2.79	2.30	1.91	1.62
	0.500	0.500		3.77	3.01	2.46	2.04	1.72
	0.401	0.599		4.07	3.22	2.62	2.19	1.84
	0.200	0.800			3.60	2.92	2.42	2.03

Table I. 8: Viscosity of ternary n-alkane mixtures

System	*x* (1)	*x* (2)	*x* (3)	η/mPa·s				
				303.2 K	**313.2 K**	**323.2 K**	**333.2 K**	**343.2 K**
$n\text{-}C_7H_{16}$ (1) + $n\text{-}C_{20}H_{42}$ (2) + $n\text{-}C_{24}H_{50}$ (3)	0.800	0.100	0.100	0.940	0.812	0.716	0.652	0.584
	0.600	0.200	0.200		1.66	1.42	1.23	1.07
	0.502	0.249	0.249		2.25	1.91	1.64	1.41
	0.400	0.300	0.300		2.74	2.27	1.93	1.64
	0.202	0.399	0.399			3.05	2.55	2.15
	0.000	0.500	0.500			4.13	3.33	2.75
$n\text{-}C_{10}H_{22}$ (1) + $n\text{-}C_{20}H_{42}$ (2) + $n\text{-}C_{24}H_{50}$ (3)	0.801	0.100	0.099	1.43	1.20	1.03	0.896	0.789
	0.600	0.200	0.200		1.98	1.66	1.41	1.22
	0.504	0.248	0.248		2.36	2.00	1.69	1.45
	0.401	0.300	0.299			2.40	2.01	1.71
	0.203	0.395	0.402			3.22		2.22
	0.000	0.500	0.500			4.13	3.33	2.75

As can be seen from Figs. I.11 and I.12, viscosities of the binary mixtures tend to be higher than the equivalent ternary mixture, as seen before for the interfacial tensions (see I.2.1). Similar conclusions from experimental studies of binary and quaternary n-alkane mixtures were reported by Wakefield *et al.* (1988).

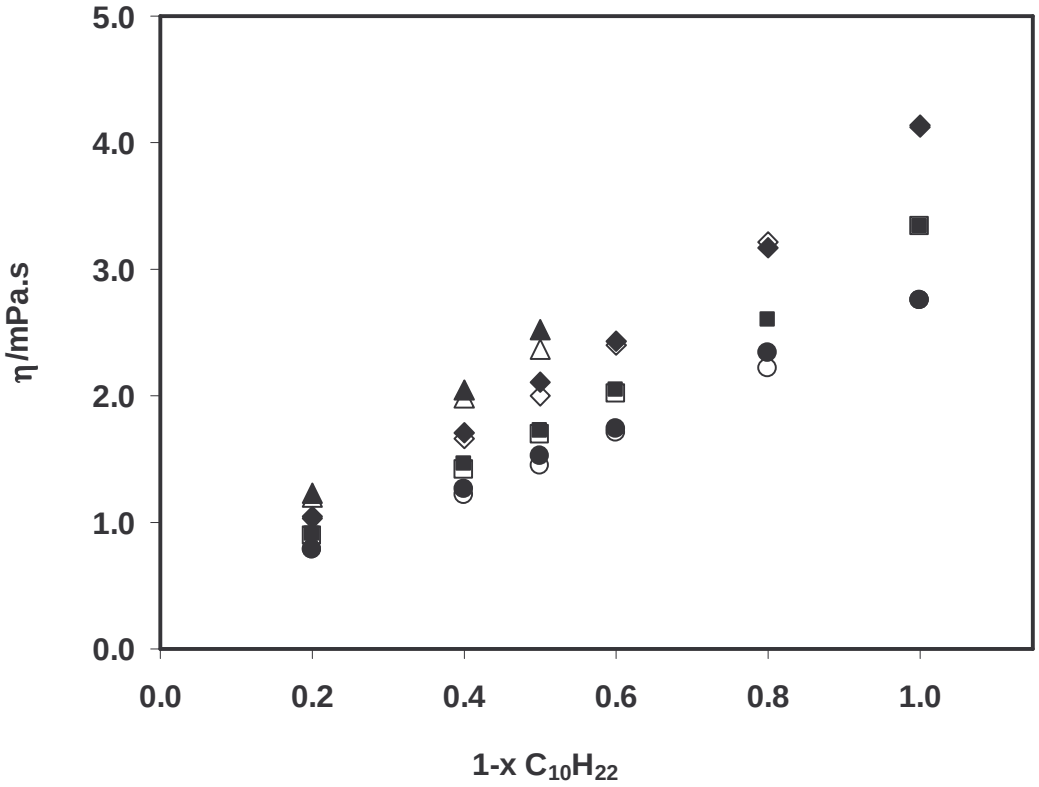

Figure I. 12: **Viscosity of n-$C_{10}H_{22}$ + n-$C_{22}H_{46}$ (filled symbols) and n-$C_{10}H_{22}$ + n-$C_{20}H_{42}$ + n-$C_{24}H_{50}$.(open symbols). Circles, 343.15 K; squares, 333.15 K, triangles 323.15 K, lozenges, 313.15 K.**

The viscosities of the petroleum distillation cuts selected for this thesis are presented in Table I. 9. The characterization of these fractions can be found at section I.2.4.

Table I. 9: Viscosity of the petroleum distillation cuts

Distillation cut	η/mPa·s					
	293.2 K	303.1 K	313.2 K	323.2 K	333.2 K	343.2 K
Sahara	5.81	4.05	3.39	2.71	2.08	1.74
Duc	7.48	5.37	4.04	3.17	2.71	2.22
Troll	6.45	4.72	3.61	2.85	2.31	1.93
Brent	5.96	4.15	3.23	2.60	2.12	1.77
Oso	5.00	3.80	3.18	2.56	2.11	1.67

I.2.3. Liquid Density

Liquid density was determined in an *Anton PAAR DMA 58* unit, based on the vibrating U-tube method. This equipment measures the oscillating period of an U-tube filled with sample that is automatically converted to liquid density after proper calibration. Two density standards have to be selected for calibration, at each temperature. In this work, air and distilled water were used as calibrating fluids. This instrument can operate from 263.15 K up to 343.15 K, and it uses approximately 0.7 cm^3 of sample, injected with a syringe. The temperature is kept constant with a built-in Peltier element that can control temperature in the cell within ± 0.005 K. The temperature is displayed with an accuracy of ± 0.01 K and density values within ± 10^{-2} $Kg \cdot m^{-3}$ (Anton Paar, 1990).

Figure I. 13: ***Anton Paar DMA 58*** **densimeter**

Following each measurement, the U-tube was carefully cleaned with toluene and ethanol. In the end it was dried with compressed air.

The same pure components and mixtures used for the viscosity measurements as reported in I.2.3 were used for determining the liquid densities.

In Table I. 10 a comparison of the measured densities with literature pure component data (DIPPR, 1998; Doutour *et al.*, 2001b; Vargaftik, 1975; Doolittle *et al.*, 1951; Cooper *et al.*, 1991; Aralaguppi *et al.*, 1999) is presented. As can be seen, liquid density average absolute deviations (Eq. I.7) are below 0.2 %, and the average of all deviations is 0.1 %.

In Figure I. 14, n-decane liquid densities are compared with other literature results. As can be observed, very good agreement with literature was obtained.

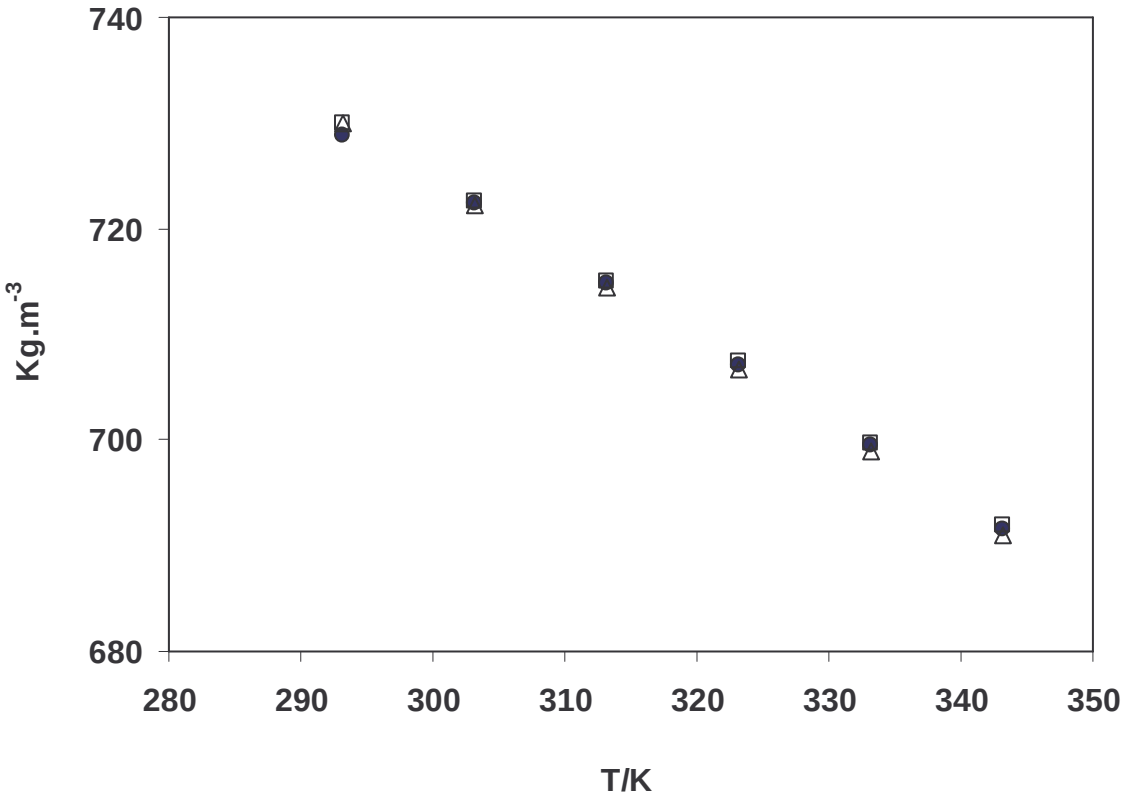

Figure I. 14: Liquid density of n-$C_{10}H_{22}$: ● this work, □ DIPPR, 1998; Δ, Vargaftik, 1975.

Mixture results are reported on Tables I.11 and I.12. No literature data were found for any of the reported mixture points.

Again, as for the interfacial tensions and the viscosities, liquid densities of the ternaries n-$C_{10}H_{22}$ + n-$C_{20}H_{42}$ + n-$C_{24}H_{50}$ and n-C_7H_{16} + n-$C_{20}H_{42}$ + n-$C_{24}H_{50}$ and those of the corresponding binaries (in terms of average chain length of the heavier components), n-$C_{10}H_{22}$ + n-$C_{22}H_{46}$ and n-C_7H_{16} + n-$C_{22}H_{46}$, can be compared (Figures I.15 and I.16).

Table I. 10: Pure n-alkane liquid density and comparison with literature

n-alkane	T/K	ρ/Kg·m^{-3}							
		this work	DIPPR, 1998 [1]	Dutour *et al.*, 2001b	Vargaftik, 1975	Doolittle *et al.*, 1951	Cooper *et al.*, 1991	Aralaguppi *et al.*, 1999	% AAD[2]
n-C_7H_{16}	293.15	683.59	683.76						
	303.15	675.35	675.26						
	313.15	666.74	666.73						0.02
	323.15	657.97	658.00			658.2			
	333.15	649.11	648.90						
	343.13	640.16	639.91						
n-$C_{10}H_{22}$	293.15	728.82	729.99		729.9		729.95		
	303.15	722.37	722.52		722.2			722.5	
	313.15	714.88	714.93		714.5				0.07
	323.15	707.12	707.47		706.7				
	333.15	699.41	699.77		698.9				
	343.13	691.61	691.87		691.0				
n-$C_{16}H_{34}$	293.15	773.33	773.55						
	303.15	766.40	766.44						
	313.15	759.48	759.51						
	323.15	752.58	752.81						0.03
	333.15	745.62	746.11						
	343.13	738.80	739.31						

n-alkane	T/K	ρ/Kg·m^{-3}							
		this work	**DIPPR, 1998** [1]	**Dutour *et al*., 2001b**	**Vargaftik, 1975**	**Doolittle *et al*., 1951**	**Cooper *et al*., 1991**	**Aralaguppi *et al*., 1999**	**% AAD**[2]
n-$C_{20}H_{42}$	313.15	775.13	775.89		775.6				0.10
	323.15	768.33	769.17		769.0				
	333.15	761.72	762.49		762.4				
	343.13	755.07	755.98		755.8				
n-$C_{22}H_{46}$	323.15	774.25	774.63						0.10
	333.15	767.67	768.45						
	343.13	761.12	762.24						
n-$C_{24}H_{50}$	333.15	772.72	772.81	773.77					0.05
	343.13	766.24	766.25	766.66					

[1] average of reported experimental values.

[2] Eq. I.7.

Table I. 11: Liquid density of binary n-alkane mixtures

System	*x* (1)	*x* (2)	ρ/Kg·m^{-3}					
			293.15 K	**303.15 K**	**313.15 K**	**323.15 K**	**333.15 K**	**343.13 K**
n-C_7H_{16} (1)– n-$C_{20}H_{42}$ (2)	0.800	0.200	724.94	717.44	709.73	701.91	694.09	686.30
	0.600	0.400		742.70	735.49	728.35	721.13	713.92
	0.502	0.498		752.39	745.65	738.70	731.65	724.75
	0.403	0.597			755.55	748.85	741.84	735.36
	0.204	0.796			765.22	758.65	751.95	745.29
n-C_7H_{16} (1)– n-$C_{22}H_{46}$ (2)	0.800	0.200		722.13	713.83	706.92	699.53	691.82
	0.600	0.400			741.03	734.90	727.95	720.67
	0.521	0.479			749.62	743.30	736.42	729.69
	0.404	0.596				753.11	746.47	739.81
	0.202	0.798				764.79	758.12	751.66
n-C_7H_{16} (1)– n-$C_{24}H_{50}$ (2)	0.802	0.198			718.81	711.25	703.69	696.16
	0.602	0.398				740.90	734.09	726.89
	0.503	0.497				752.08	745.74	739.08
	0.404	0.596				757.72	750.93	744.17
	0.204	0.796					763.75	757.20
n-$C_{10}H_{22}$ (1) + n-$C_{20}H_{42}$ (2)	0.800	0.200	748.59	741.43	734.23	726.82	719.47	712.13
	0.602	0.398		755.39	748.34	741.28	734.19	726.89
	0.500	0.500		761.50	754.51	747.44	740.49	733.52
	0.400	0.600			759.42	752.46	745.48	738.69
	0.201	0.799			768.00	761.15	754.34	747.66

System	***x* (1)**	***x* (2)**	**ρ/Kg·m^{-3}**					
			293.15 K	**303.15 K**	**313.15 K**	**323.15 K**	**333.15 K**	**343.13 K**
n-$C_{10}H_{22}$ (1) + n-$C_{22}H_{46}$ (2)	0.799	0.201		744.68	737.51	730.24	722.95	715.69
	0.600	0.400			753.74	747.42	739.83	732.81
	0.500	0.500			759.50	752.95	746.11	739.29
	0.400	0.600			765.03	758.09	751.29	744.17
	0.200	0.800				767.13	760.49	753.93
n-$C_{10}H_{22}$ (1) + n-$C_{24}H_{50}$ (2)	0.800	0.200			740.97	733.76	726.59	720.06
	0.601	0.399				750.41	742.73	735.89
	0.501	0.499				757.19	750.04	742.22
	0.400	0.600				763.04	756.39	749.61
	0.203	0.797				772.16	765.65	759.08
n-$C_{16}H_{34}$ (1) + n-$C_{20}H_{42}$ (2)	0.800	0.200	776.80	769.93	763.12	756.18	749.33	742.50
	0.600	0.400		773.33	766.20	759.69	752.88	746.12
	0.500	0.500		774.66	768.03	761.14	754.37	747.64
	0.401	0.599		776.21	769.54	762.66	755.89	749.17
	0.200	0.800			772.61	765.84	759.16	752.38

Table I. 12: Liquid density of ternary n-alkane mixtures

System	*x* (1)	*x* (2)	*x* (3)	ρ/Kg·m^{-3}				
				303.15 K	**313.15 K**	**323.15 K**	**333.15 K**	**343.13 K**
n-C_7H_{16} (1) + n-$C_{20}H_{42}$ (2) + n-$C_{24}H_{50}$ (3)	0.800	0.100	0.100	719.28	714.64	706.87	699.24	691.51
	0.600	0.200	0.200		741.76	733.78	727.13	720.62
	0.502	0.249	0.249		751.10	744.08	737.24	730.33
	0.400	0.300	0.300		759.26	752.22	745.16	738.30
	0.206	0.397	0.397			764.52	757.68	751.09
	0.000	0.500	0.500			774.31	767.69	760.43
n-$C_{10}H_{22}$ (1) + n-$C_{20}H_{42}$ (2) + n-$C_{24}H_{50}$ (3)	0.801	0.100	0.099	744.60	737.37	730.11	722.87	715.55
	0.600	0.200	0.200		753.40	746.44	739.30	732.32
	0.504	0.248	0.248		759.36	752.29	745.40	738.08
	0.401	0.300	0.299		764.90	758.10	751.60	744.40
	0.201	0.400	0.399			766.45	759.88	751.37
	0.000	0.500	0.500			774.31	767.69	760.43

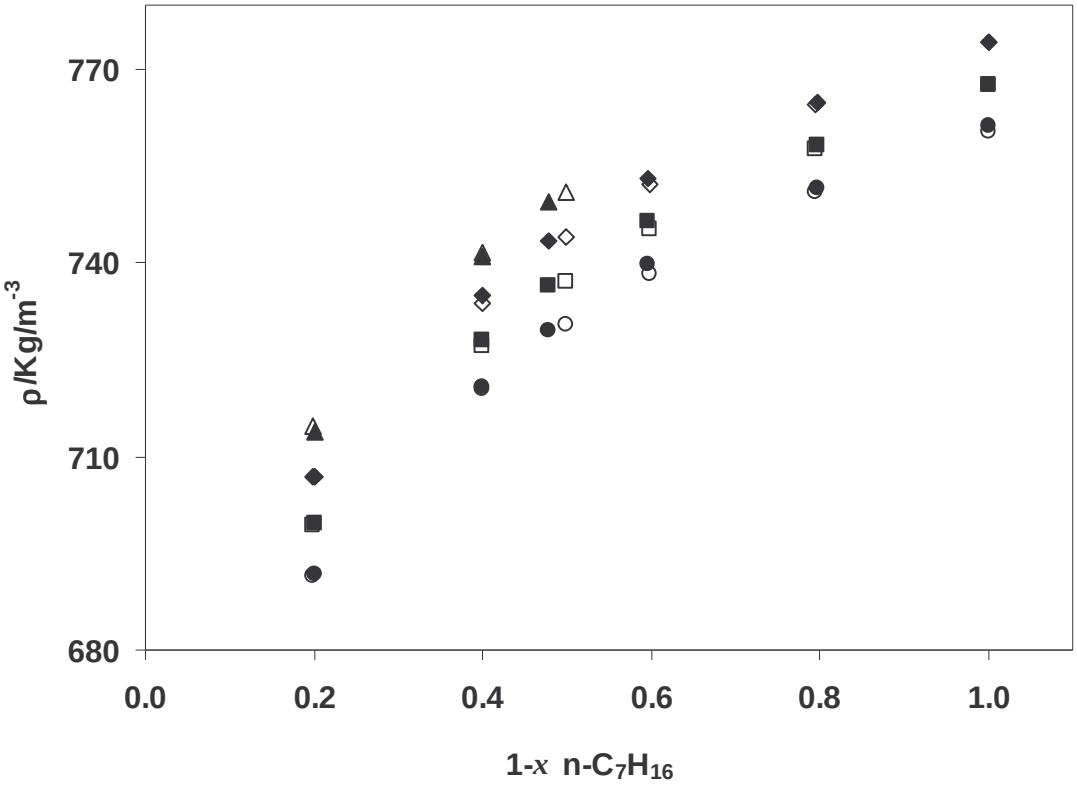

Figure I. 15: **Comparison of the binary n-C_7H_{16} + n-$C_{22}H_{46}$ (filled symbols) and ternary n-C_7H_{16} + n-$C_{20}H_{42}$ + n-$C_{24}H_{50}$ (open symbols) liquid density results. Circles, 343.13 K; squares, 333.15 K, lozenges, 323.15 K; triangles, 313.15 K.**

Binary liquid densities showed a tendency to be slightly higher, although these differences are quite small, with percent deviations very close to zero.

Finally, liquid densities of the petroleum distillation cuts are presented on Table I. 13.

A characterization of these cuts is presented on the next section, including n-alkane composition, molecular weights and solid-liquid transition temperatures.

Table I. 13: Liquid density of the petroleum distillation cuts

Distillation cut	ρ/Kg·m^{-3}					
	293.15 K	**303.15 K**	**313.15 K**	**323.15 K**	**333.15 K**	**343.13 K**
Sahara	836.40	829.54	822.75	815.90	809.05	802.21
Duc	879.12	872.28	865.49	858.66	851.17	844.96
Troll	866.11	859.30	852.44	845.59	838.71	831.88
Brent	847.29	841.12	834.29	827.43	820.53	813.35
Oso	844.56	837.57	830.76	823.87	816.96	810.08

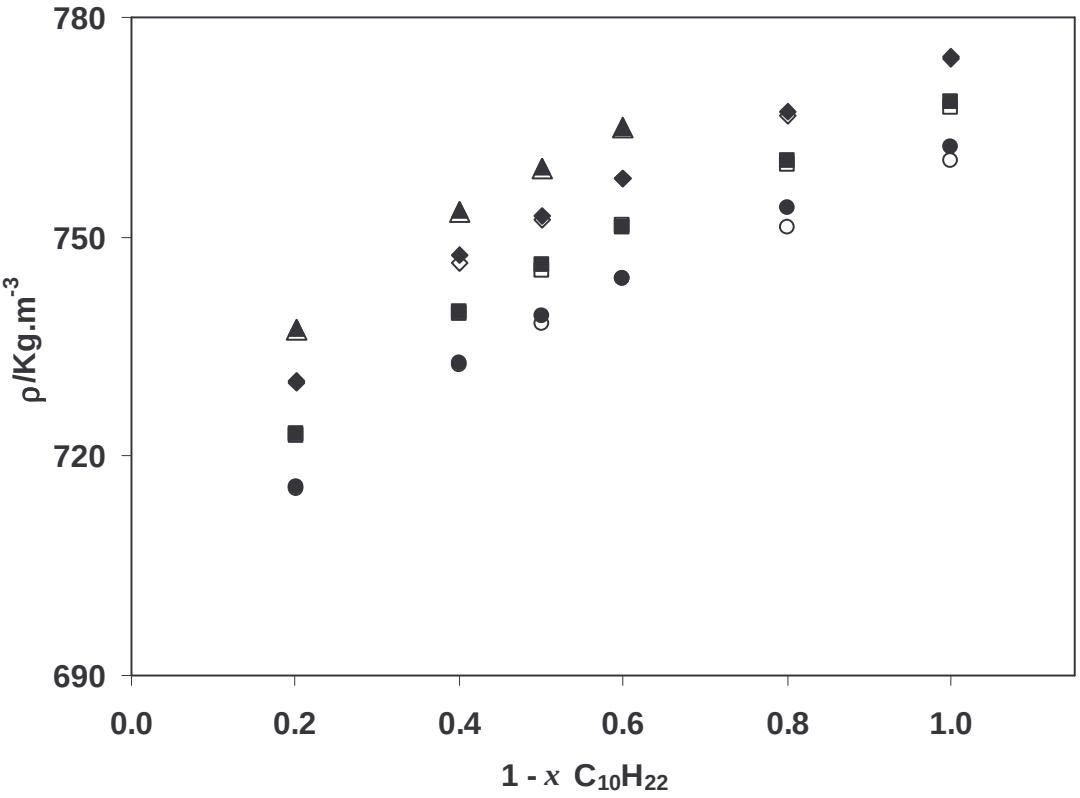

Figure I. 16: **Comparison of the binary n-$C_{10}H_{22}$ + n-$C_{22}H_{46}$ (filled symbols) and ternary n-$C_{10}H_{22}$ + n-$C_{20}H_{42}$ + n-$C_{24}H_{50}$ (open symbols) liquid density results. Circles, 343.13 K; squares, 333.15 K, lozenges, 323.15 K; triangles, 313.15 K.**

I.2.4. Characterization of the Distillation Cuts

This section deals with the characterization of five distillation cuts (503 K-648 K) from crudes of different sources (North Sea, Africa and Middle East) obtained from the Petrogal refinery. They were chosen because they are the basis for the diesels produced at the refinery and cover the range of n-alkane contents typically found there (3 to 30 wt%). Precipitation curves for these cuts, showing the temperature dependence of the solid fraction, were measured by *Differential Scanning Calorimetry* (DSC) according to a method proposed before (Coutinho *et al*., 1997 and 2000). n-alkane compositions were kindly determined at the *Université de Pau et de Pays de L'Adour*, France, by gas chromatography (GC), and the average molecular weight was estimated by freezing point depression. No attempt to obtain any further compositional information was done since, as will be discussed later (section III.5), the non n-alkane compounds do not play a relevant role in the low temperature behavior of these fluids.

To measure the composition of the samples a *Hewlett Packard 6890* chromatograph equipped with a hydrogen flame ionization detector was used. The column employed is composed by a pre-column of 1 m (ID = 530 μm); two 30 m columns, the first an HP 5 MS (ID = 320 μm and film thickness 0.5 μm) and the second a HP 5 (ID = 320 μm and film thickness 0.25 μm), and a final empty column of about 30 cm. The injection is performed on-column. On this chromatograph both the temperature and the carrier gas flow rate are programmable. To obtain a better separation of the heavy n-alkanes, the gas flow rate is kept at 2 cm^3/min during the first 100 minutes and then increased to 3 cm^3/min. The heating starts at 333 K, goes at 2.5 K/min up to 578 K, and then at 2 K/min up to 593 K. Under these conditions n-alkanes between n-decane (n-$C_{10}H_{22}$) and n-triacontane (n-$C_{30}H_{62}$) can be quantified. n-nonane (n-C_9H_{20}) (Aldrich, >99%) was used as reference and CS_2 as solvent. A chromatogram for Oso condensate is shown in Figure I. 17. The compositions obtained are presented in Table I. 14.

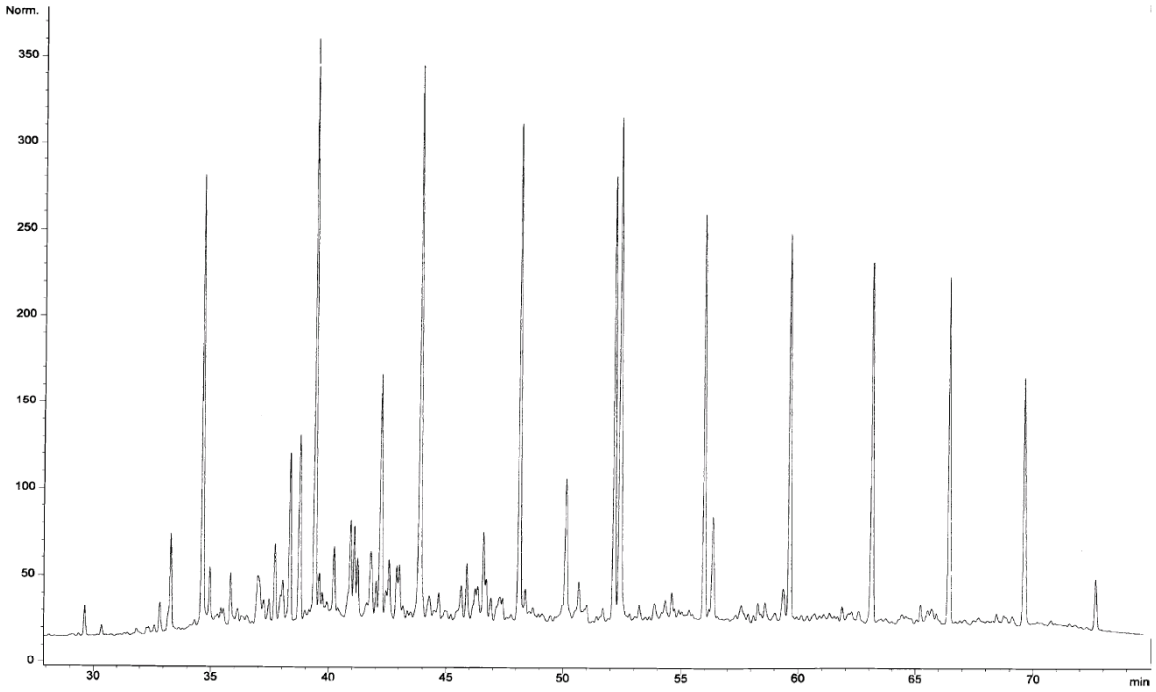

Figure I. 17: **Gas chromatography analysis of the distillation cut obtained from Oso condensate. The higher peaks are the n-alkanes.**

The calorimetric measurements were performed on a *Setaram DSC 141* differential scanning calorimeter. The sample was initially cooled to 130 K, kept at that temperature for 15 minutes to stabilize, and then heated up to 593 K at 3 K/min. This heating rate was chosen since it provides a good compromise between a good signal and to be close to equilibrium conditions. The wax appearance temperatures presented in Table I. 15 were measured under these conditions and may thus be slightly over estimated. The thermograms are presented in Figure I. 18. They are similar to other DSC measurements for fuels and crudes previously reported in the literature (Coutinho *et al*., 2000b; Létoffé *et al*., 1995; Bosselet *et al*., 1983).

Table I. 14: n-alkane composition (wt %) and average molecular weight (g/mol) of the distillation cuts studied

Distillation cut	$C_{10}H_{22}$	$C_{11}H_{24}$	$C_{12}H_{26}$	$C_{13}H_{26}$	$C_{14}H_{30}$	$C_{15}H_{32}$	$C_{16}H_{34}$	$C_{17}H_{36}$	$C_{18}H_{40}$	$C_{19}H_{40}$	$C_{20}H_{42}$	$C_{21}H_{44}$	$C_{22}H_{46}$	$C_{23}H_{48}$	$C_{24}H_{50}$	Total	MW
Brent	0.04	0.06	0.36	10.65	13.42	14.43	11.86	9.72	8.3	7.97	8.25	6.97	6.52	1.42		19.6	222.8
Oso	0.05	0.11	0.56	10.11	12.77	13.61	11.15	9.88	9.01	8.94	8.46	8.04	6.02	1.22	0.04	32.0	226.8
Troll	0.07	0.09	0.28	9.65	14.05	16.36	12.15	9.40	8.63	8.09	8.03	6.32	5.53	1.36		9.79	231.7
DUC			0.07	5.50	13.66	17.30	9.97	7.22	9.52	9.81	11.42	6.19	7.21	2.14		2.79	220.3
Sahara Blend	0.03	0.09	0.53	13.22	14.79	14.94	11.39	10.41	9.07	7.78	7.38	5.54	4.06	0.75	0.02	21.2	235.8
Average distribution	0.05	0.09	0.36	9.83	13.74	15.33	11.30	9.33	8.91	8.52	8.71	6.61	5.87	1.38	0.03		

Table I. 15: measured wax appearance temperatures (WAT)

Distillation cut	Measured WAT/K
Brent	273.8
Oso Condensate	278.9
Troll	265.6
DUC	256.2
Sahara Blend	271.2

After a glass transition at around 190 K, there was an exothermic peak due to the crystallization of species that did not crystallize on cooling. It was followed by a broad endotherm due to the dissolution of the paraffinic crystals in the liquid matrix. The major problem in the treatment of the DSC results for these fluids is the definition of a base line. As proposed by Bosselet *et al*. (1983) and Claudy *et al*. (1995) a polynomial line fitted to the liquid region and the basis of the exotherm, where the dissolution of the paraffins began, is used as base line. Since there is no way to assess the 'true' base line for these fluids this is a fair approach to it. Nevertheless, one must be aware that some uncertainty was introduced in the calculations by its adoption. Using this base line the fraction of solids dissolved is obtained using an approach proposed before (Coutinho *et al.*, 1997 and 2000) were the fraction of melted n-alkanes was identified with the fraction of total energy required to completely melt the n-alkanes obtained from the integration of the energy using the adjusted base line.

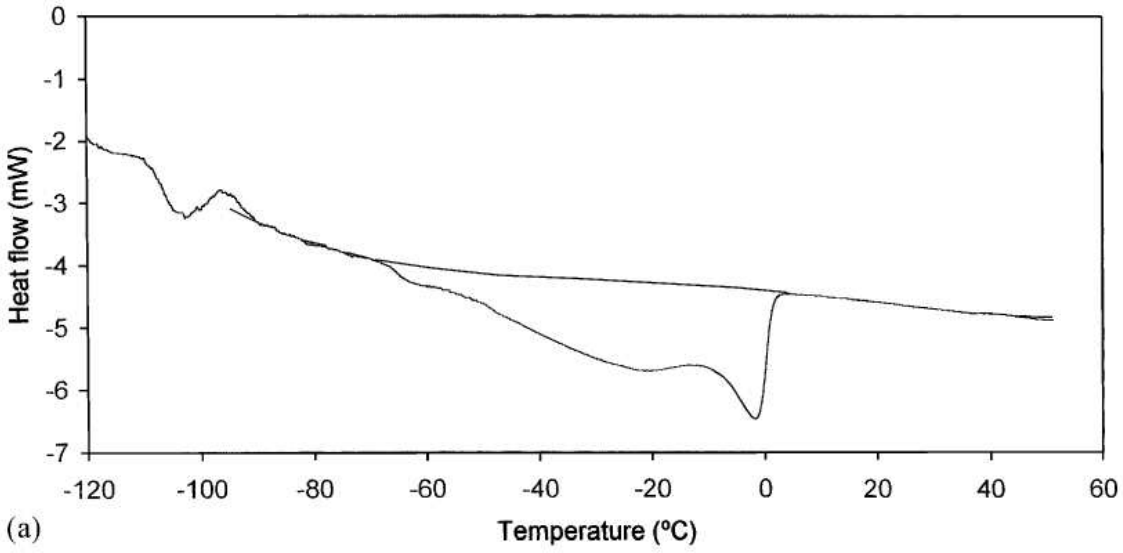

Figure I. 18: **DSC measurements for distillation cuts from Brent a), Oso Condensate b), Troll c), DUC d), and Sahara Blend e).**

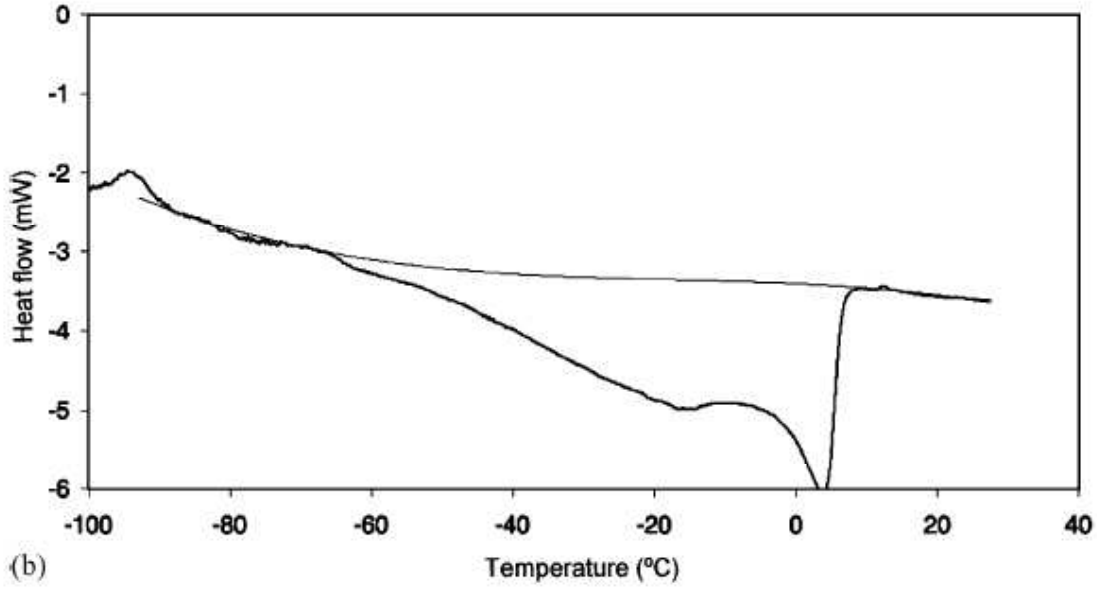

(b)

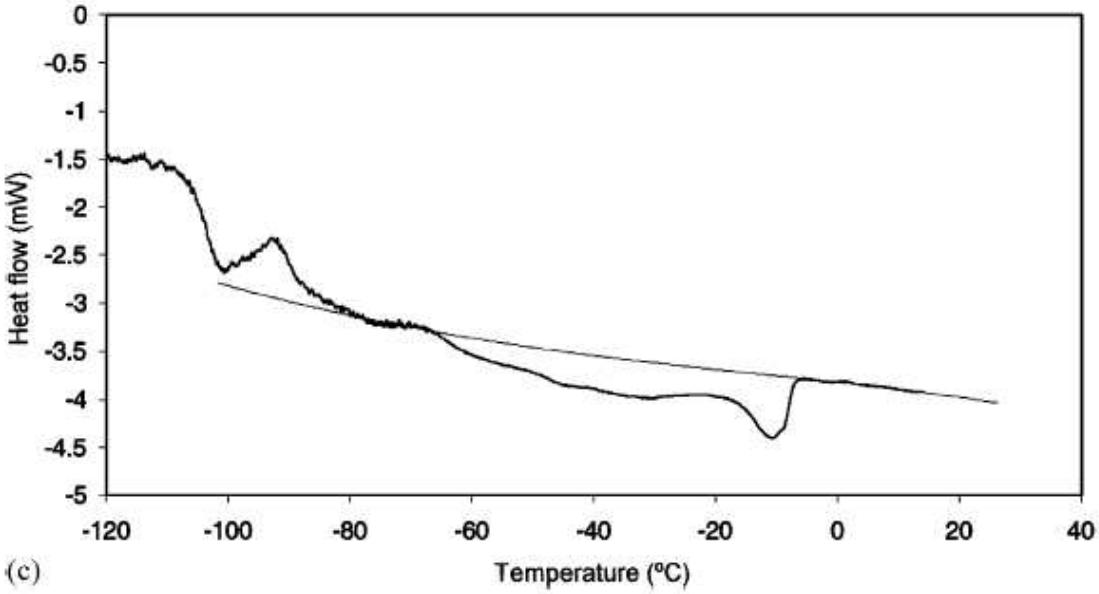

(c)

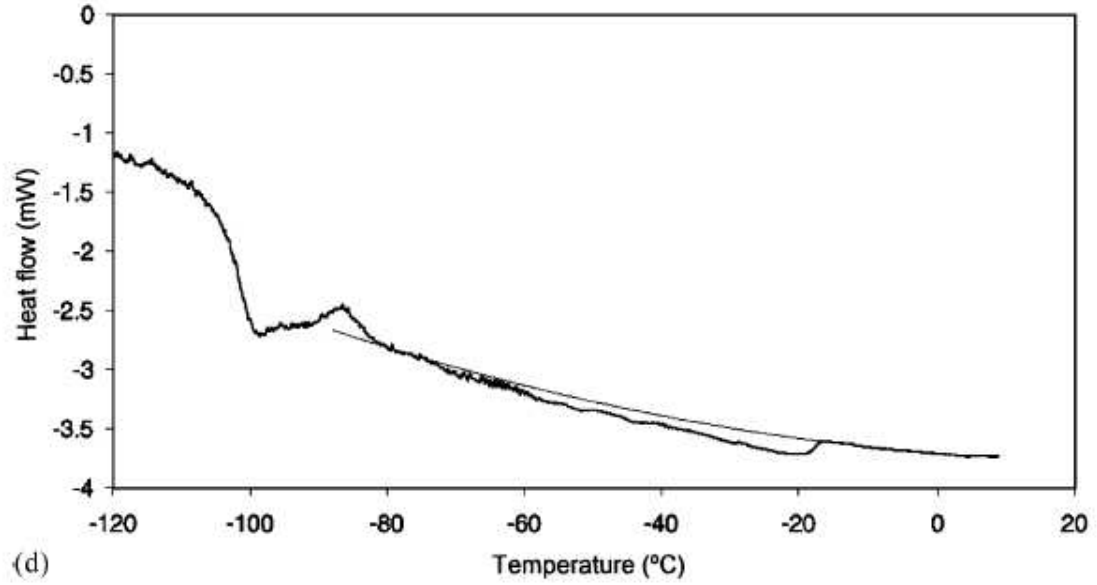

(d)

Figure I.18: (Continued).

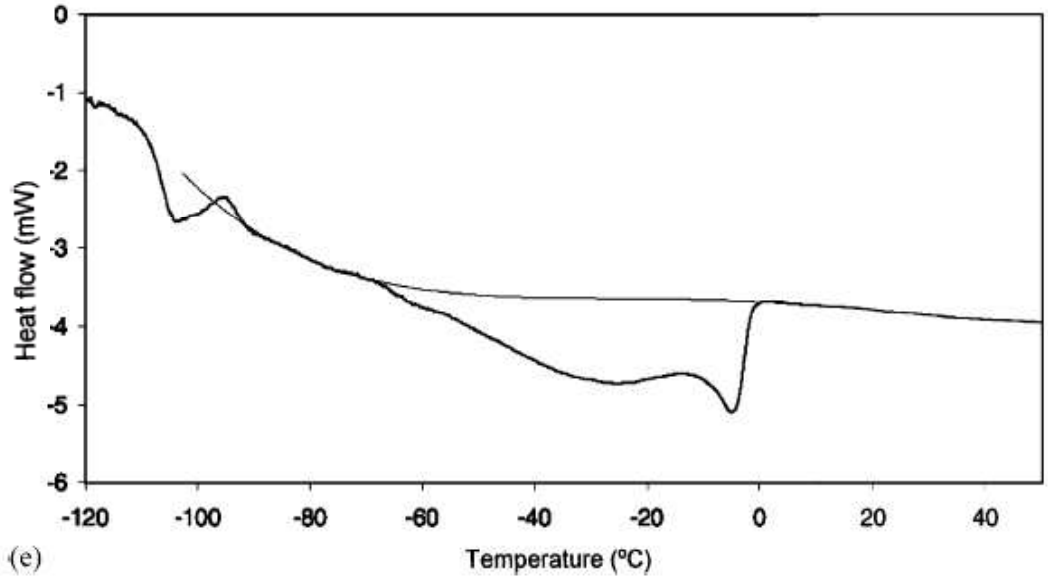

Figure I.18: (Continued).

Results from these calculations will be presented and compared with model results in section III.5.

I.3. Conclusions

Several experimental measurements were reported on vapor-liquid and liquid-liquid interfacial tensions, liquid densities and viscosities. Differential scanning calorimetry and gas chromatography were also used to characterize some petroleum distillation cuts which were selected to represent real hydrocarbon fluids containing heavier n-alkanes.

Pure component data was used to evaluate the performance of the equipment. Special care was given to tensiometry, since the *NIMA DST 9005* tensiometer was used for the first time during these measurements. For that, additional binary mixtures were considered in order to better check its accuracy. As shown during this chapter, vapor-liquid interfacial tension agreed with literature within 1.2 %, water-n-alkane interfacial tension within 0.3 %, viscosity within 2.1 % and liquid density within 0.1 %. It can thus be concluded that the measurements were accurate, giving also some confidence about the results on new systems.

Mixtures were selected in order to extend the available literature database. Particularly for those containing heavier n-alkanes and small chain length homologues (asymmetric mixtures) data were scarce. Seven binary and two ternary mixtures were thus selected for this purpose. Binary results were presented in the full composition range and at a set of temperatures starting from 273.15 K and ending at 343.15 K, the upper working limit of the employed densimeter.

The measured properties of the ternary mixtures, n-C_7H_{16} (or n-$C_{10}H_{22}$) + n-$C_{20}H_{42}$ + n-$C_{24}H_{50}$, were compared with those from the equivalent binaries, n-C_7H_{16} or (n-$C_{10}H_{22}$) + n-$C_{22}H_{46}$ using equimolar n-$C_{20}H_{42}$ and n-$C_{24}H_{50}$ in the preparation of the ternary mixtures. Results confirmed that although the corresponding liquid densities can be considered equal, viscosities and surface tensions of the ternaries tend to be lower than those from the binaries.

Surface freezing, a phenomenon that has been found to occur in some heavier n-alkanes and n-alcohols and that can be followed from tensiometry (Wu *et al*., 1993) was observed from the interfacial tension measurements. Thus, from this work it can be concluded that the *Nima* tensiometer may also be used to investigate this phase transition.

From the measurements reported in this chapter a considerable amount of data is now available for asymmetric n-alkane mixtures. These results were used to develop correlations and evaluate models for their estimation, as will be shown in Part II and Part III.

PART II: DATA CORRELATION

“Astronomers say the universe is finite, which is a comforting thought for those people who can't remember where they leave things"

Woody Allen (1935-), writer and film director.

"There are 1×10^{11} *stars in the galaxy. That used to be a huge number. But it's only a hundred billion. It's less than the national deficit! We used to call them astronomical numbers. Now we should call them economical numbers."*

Richard P. Feynmann (1918 – 1988), physicist.

II.1 Introduction

In this chapter a review of the available experimental critical properties and Pitzer acentric factors, as well as an assessment of correlations for their estimation will be presented and discussed, since these are especially important for modeling purposes, particularly for corresponding states models, as will be later shown during Part III.

In section II.3 surface tension and viscosity data are used to evaluate a linear relation between the natural logarithm of the surface tension and the reciprocal viscosity, first proposed by Pelofsky (1966). The interest in these relations follows from the possibility of obtaining one of these properties from measurements on the other, thus overcoming data deficiency. These relations can also be used to test the validity of measured data, since deviations can be ascribed to experimental errors.

It will be shown that this relation holds for both pure and mixed n-alkanes. Since most of the available data is from the lowest members of the series, results will be mostly focused on the heavier members and some of their mixtures with lighter components (asymmetric mixtures). Results on petroleum distillation cuts, representative of real systems will also be discussed.

"...man will occasionally stumble over the truth, but usually manages to pick himself up, walk over or around it, and carry on."

Winston Churchill (1874-1965), Politician

In this section, a literature review on the available experimental critical temperatures pressures and volumes and the Pitzer acentric factors for n-alkanes is presented and discussed.

Given the lack of data for the heavier components, correlations for their estimation will be assessed and selected, since critical properties are required for the correct modelling of these molecules.

II.2 Critical Properties and Acentric Factors

Critical properties such as critical temperatures, critical pressures and critical volumes and Pitzer acentric factors are frequently required as input data for many models. For example, corresponding states models and equations of state rely on these pure component properties for their accurate modelling results. In this section, an overview of the available experimental data for n-alkanes and an evaluation of some correlations for their prediction are presented.

A good selection of correlations is particularly important for the heavier n-alkanes for which no experimental information is available.

Several works on literature reported critical properties for the n-alkane series (Teja *et al.*, 1990; Tsonopoulos, 1987; Anselme, 1990; Magoulas *et al.*, 1990; Ambrose *et al.*, 1995; Nikitin *et al.*, 1987). Ambrose *et al*. (1995) performed a literature review and presented values for all the n-alkanes ranging from methane up to n-tetracosane (n-$C_{24}H_{50}$). Above n-$C_{24}H_{50}$, Nikitin (1997) reported values for n-$C_{26}H_{54}$, n-$C_{28}H_{58}$, n-$C_{30}H_{62}$ and n-$C_{36}H_{74}$.

These values, reported by Ambrose (1995) and Nikitin (1997), are presented in Table II. 1 and were used to assess the available correlations for the estimation of long chain n-alkanes.

For the acentric factors, Magoulas *et al*. (1990) presented values from methane up to n-eicosane. These are also reported in Table II. 1.

Table II. 1: n-alkane selected experimental critical properties and acentric factors

n-*alkane*	T_c/K	P_c/MPa	V_c/cm^3.mol^{-1}	ω
n-CH_4	190.564	4.599	98.60	0.011
n-C_2H_6	305.32	4.872	145.50	0.099
n-C_3H_8	369.83	4.248	200.00	0.152
n-C_4H_{10}	425.12	3.796	255.00	0.199
n-C_5H_{12}	469.7	3.370	311.00	0.251
n-C_6H_{14}	507.6	3.025	368.00	0.299
n-C_7H_{16}	540.2	2.74	428.00	0.350
n-C_8H_{18}	568.7	2.49	492.00	0.397
n-C_9H_{20}	594.6	2.29	555.00	0.443
n-$C_{10}H_{22}$	617.7	2.11	624.00	0.490
n-$C_{11}H_{24}$	639	1.98	689.00	0.533
n-$C_{12}H_{26}$	658	1.82	754.00	0.573
n-$C_{13}H_{28}$	675	1.68	823.00	0.618
n-$C_{14}H_{30}$	693	1.57	894.00	0.654
n-$C_{15}H_{32}$	708	1.48	966.00	0.696
n-$C_{16}H_{34}$	723	1.40	1034.00	0.737
n-$C_{17}H_{36}$	736	1.34	1103.00	0.772
n-$C_{18}H_{38}$	747	1.29	1189.00	0.812
n-$C_{19}H_{40}$	755	1.16		0.844
n-$C_{20}H_{42}$	768	1.07		0.891
n-$C_{21}H_{44}$	778	1.03		
n-$C_{22}H_{46}$	786	0.98		
n-$C_{23}H_{48}$	790	0.92		
n-$C_{24}H_{50}$	800	0.87		
n-$C_{26}H_{54}$	816	0.795		
n-$C_{28}H_{58}$	824	0.744		
n-$C_{30}H_{62}$	843	0.636		
n-$C_{36}H_{74}$	872	0.475		

To estimate the critical temperatures of heavier n-alkanes, correlations were collected from different sources (Kontogeorgis *et al*., 1997; Marano *et al*., 1997a and 1997b; Teja *et al.*, 1990; Tsonopoulos, 1987; Marrero-Morejón *et al.*, 1999; Hu *et al*., 1993; Lydersen, 1955; Ambrose, 1978 and 1979; Joback *et al*., 1987; Constantinou *et al*., 1994; Robinson, 1987; Nakanishi *et al.*, 1960 and Nikitin *et al.*, 1997).

From all the selected correlations, that from Tsonopoulos (1987), to be used above n-C_3H_8, was found to be the best for describing the experimental critical temperatures (up to n-$C_{36}H_{74}$), although it was derived when only data up to n-$C_{18}H_{38}$ was available:

$$ln(959.98 - T_c) = 6.81536 - 0.211145 \times n^{2/3} \qquad \text{(II. 1)}$$

where T_c is the critical temperature (K) and n is the n-alkane chain length, n-C_nH_{2n+2}.

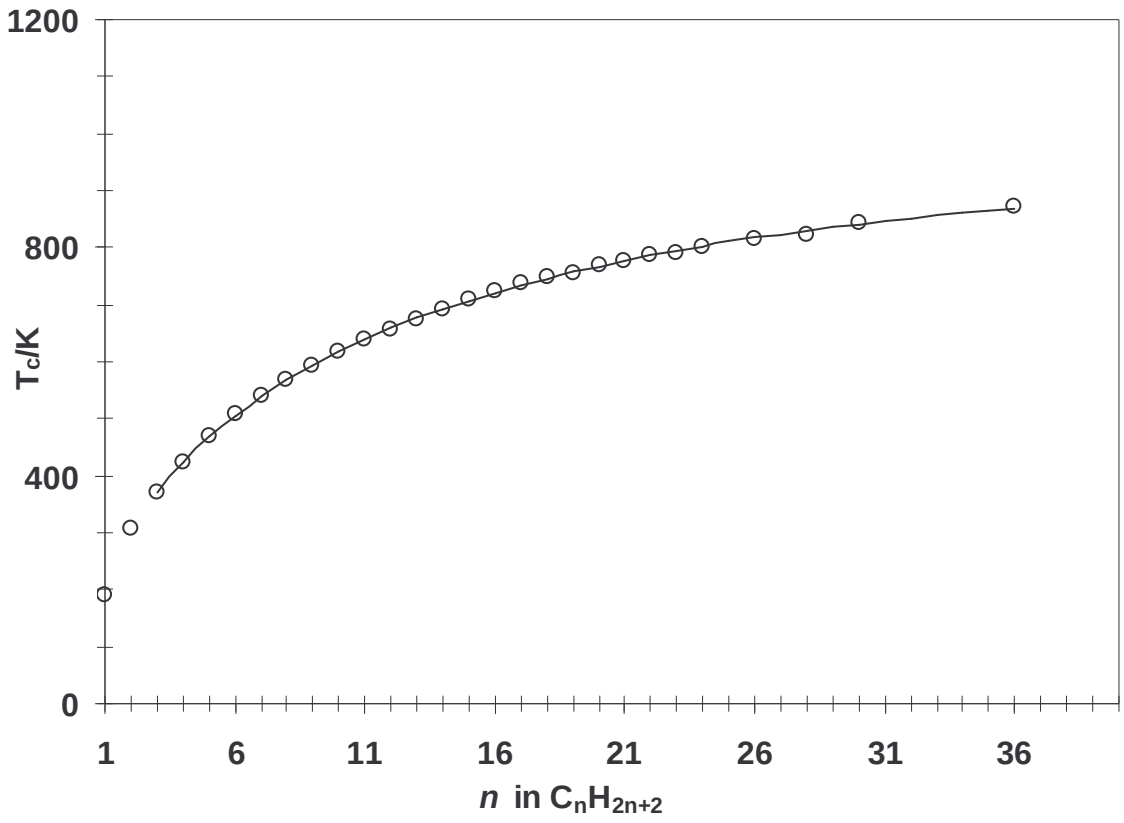

Figure II. 1: **n-alkane critical temperatures. Experimental and correlation results with the Tsonopoulos (1987) correlation.**

For the estimation of critical pressures, correlations were collected from Kontogeorgis *et al.*, 1997; Marano *et al.*, 1997a and 1997b; Teja *et al.*, 1990; Tsonopoulos, 1987; Marrero-Morejón *et al.*, 1999; Hu *et al.*, 1993; Lydersen, 1955; Ambrose, 1978 and 1979; Joback *et al.*, 1987; Constantinou *et al.*, 1994; Robinson, 1987; Nakanishi *et al.*, 1960; Nikitin *et al.*, 1997; Magoulas *et al.*, 1990 and Morgan *et al.*, 1991.

This time, the correlation from Magoulas *et al.* (1990), showed the better results for the available heavier component data, while maintaining also a good description for the lighter n-alkanes (Figure II. 2):

$$ln\, P_c = 4.3398 - 0.3155 \times n^{0.6032} \qquad \text{(II. 2)}$$

where P_c is the critical pressure (bar) ad n is again the n-alkane chain length.

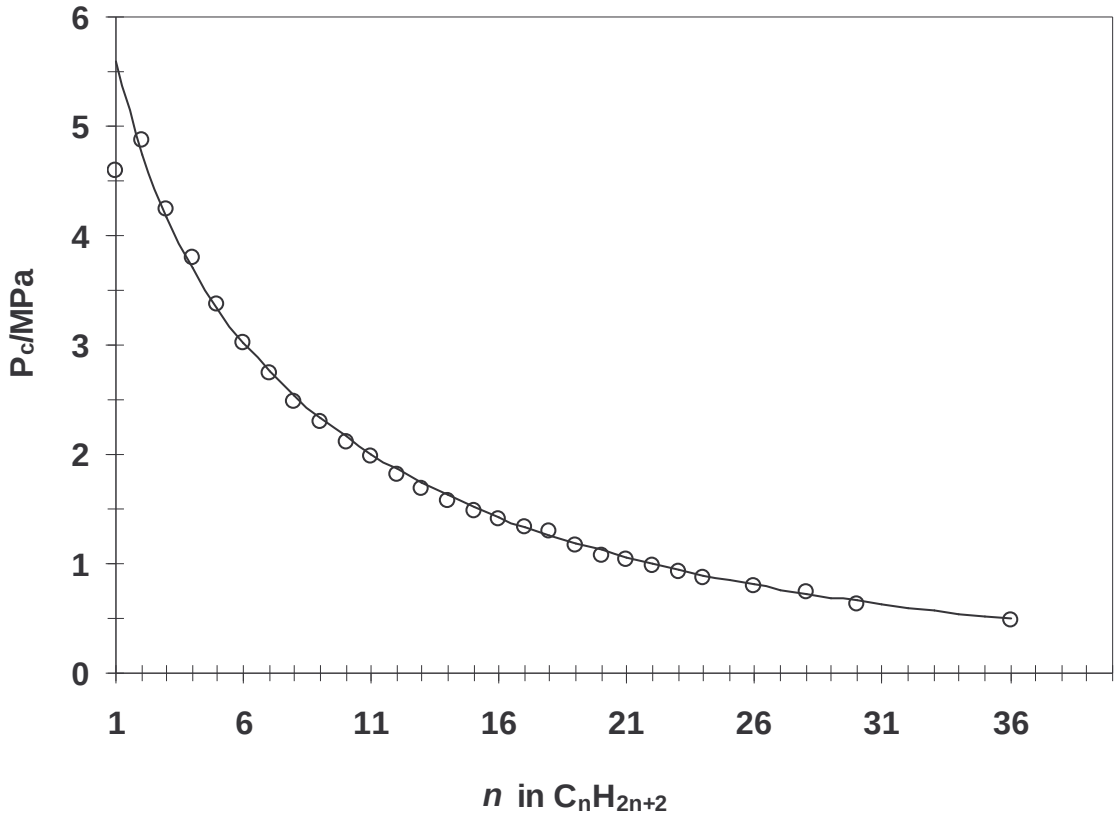

Figure II. 2 **n-alkane critical pressure. Experimental and correlation results with the Magoulas *et al.* (1990) correlation.**

Critical volumes are difficult to measure with precision and so their experimental information are also scarce, as can be seen from Table II. 1, where the heaviest n-alkane for which there is available data is n-$C_{18}H_{38}$.

Correlations for the estimation of critical volumes have been proposed by several researchers (Marano *et al.*, 1997a; Teja *et al.*, 1990; Tsonopoulos, 1987; Marrero-Morejón *et al.*, 1999; Anselme *et al.*, 1990; Lydersen, 1955; Ambrose, 1979; Joback *et al.*, 1987; Constantinou *et al.*, 1994). A good review of some of these correlations can be found in literature (Kontogeorgis *et al.*,1995). In that paper, the variation of the critical density with the molecular weight was also discussed based on the available sets of experimental data and some calculations using the Rackett equation (Rackett, 1970). Kontogeorgis *et al.*(1995) concluded that the critical density of an homologous series should decrease with the molecular weight, after passing through a maximum at low molecular weights. A plot of the experimental n-alkane critical densities as a function of molecular weight is presented in Figure II. 3.

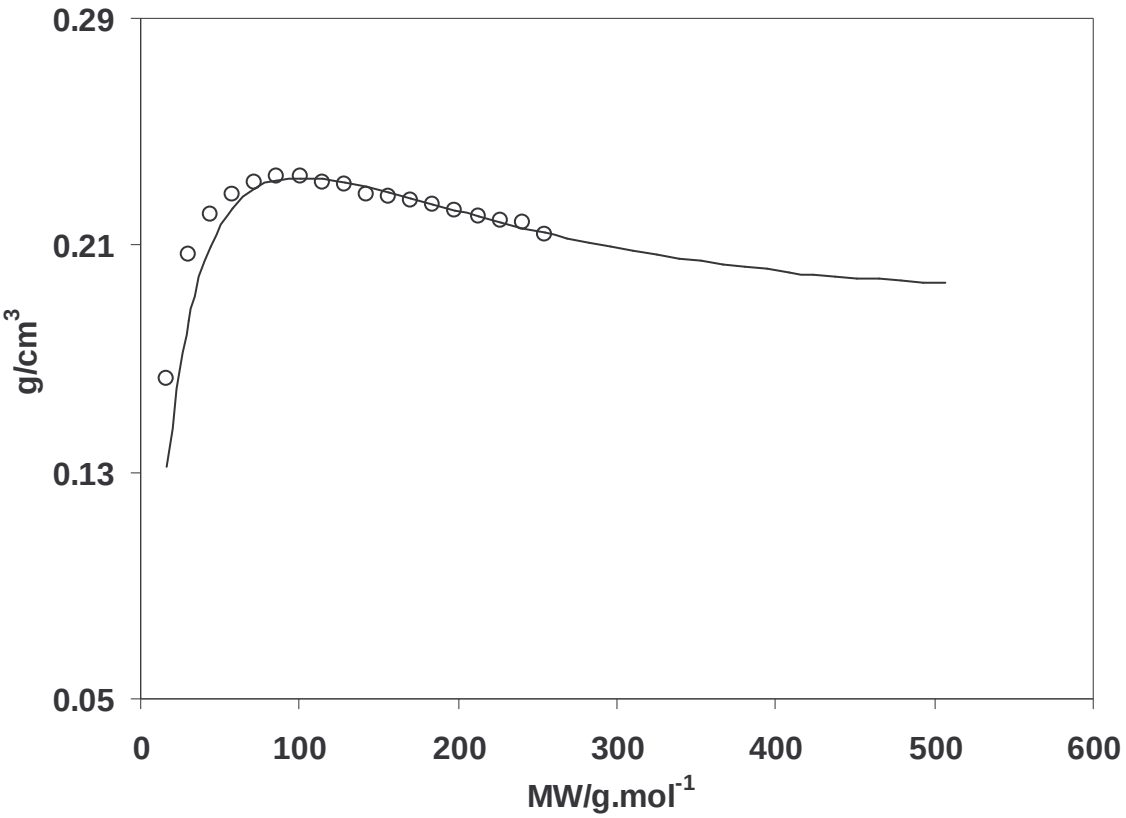

Figure II. 3 **n-alkane critical density. Experimental and correlation results with the Marano *et al* (1997a) correlation.**

To correlate this property, the Marano *et al.* (1997a), the Anselme *et al* (1990) and the Teja *et al.* (1990) correlations presented very similar performance. For the purposes of this work, the Marano *et al.* (1997a) correlation was selected, since it described better the heavier n-alkane critical densities:

$$V_c = \left(2.38 \times (n + 53.5) - 218.7 \times exp\left\{-1.14 \times 10^{-4} \times (n + 53.5)^{2.19}\right\}\right)^{3/2} \qquad \text{(II. 3)}$$

where V_c is the critical volume ($cm^3.mol^{-1}$) and n is the chain length of the n-alkane, n-C_nH_{2n+2}.

Pitzer acentric factors (Pitzer *et al.*, 1955), defined by Eq. II.4, where P stands for pressure, T_r for reduced temperature (T/T_c) and subscript c for critical property can be calculated by several correlations (Han *et al.*, 1993; Marano *et al.*, 1997a; Magoulas *et al.*, 1990; Morgan *et al.*, 1991; Constantinou *et al.*, 1994; Kontogeorgis *et al.*, 1997, Hoshino *et al.*, 1982).

$$\omega = -log_{10}\left(\frac{P_{Tr=0.7}}{P_c}\right) - 1.0 \qquad \text{(II. 4)}$$

From these, the group-contribution correlation presented by Han *et al*. (1993) gave the lowest deviations. For the n-alkanes this equation reduces to II.5:

$$\omega = 0.004423 \times ln(3.3063 + n \times 3.4381)^{3.651} \qquad \text{(II. 5)}$$

where again n stands for the n-alkane chain length.

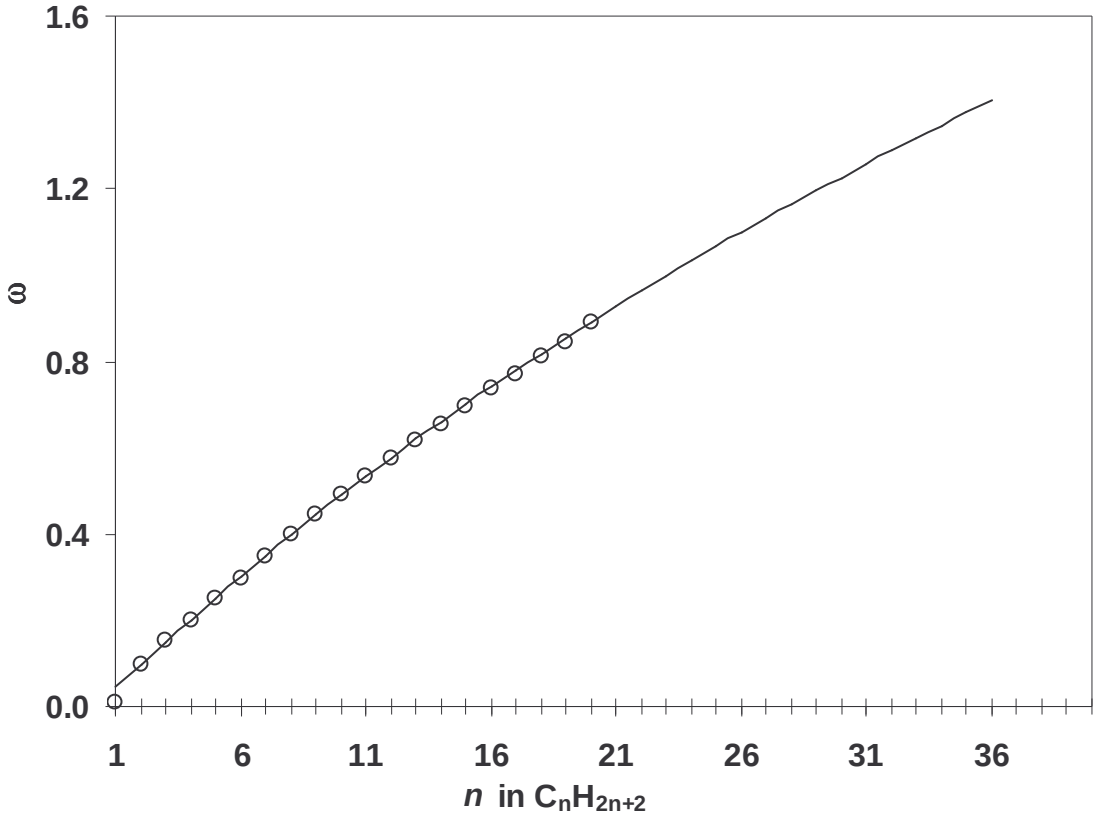

Figure II. 4 **n-alkane acentric factors. Experimental and correlation results with the Han *et al.* (1993) correlation.**

The experimental values reported in Table II. 1 and the selected correlations for the critical temperature, critical pressure, critical volume and the Pitzer acentric factor presented in this section will be used during Part III for modeling purposes. Particularly for corresponding states models, as will be shown in section III.2, the right description of these properties is especially important.

"If we knew what it was we were doing, it would not be called research, would it ?"

Albert Einstein (1879-1955), Physicist

Plots of different data sets verify that the natural logarithm of the surface tension is linear with the reciprocal viscosity, with slope dependent on the molecular weight and constant intercept for average chain lengths greater than n-$C_{10}H_{22}$. For these, the value of the intercept can be related to the surface tension at the temperature of homogeneous nucleation, where the reciprocal viscosity tends to zero.

With this relation only a viscosity (or surface tension) value is required to calculate a surface tension (or viscosity) point.

The presented results show how bulk transport and equilibrium surface properties can be interrelated.

II.3 Surface Tension - Viscosity Relations

Following several attempts to relate surface tension with viscosity, Pelofsky (1966) presented a linear relation between these two thermophysical properties:

$$\ln \sigma = \ln A + \frac{B}{\eta} \qquad \text{(II. 6)}$$

where A and B are constants, σ is the surface tension, and η the viscosity. According to Pelofsky (1966), this empirical relation can be applied for both organic and inorganic phases of pure and mixed components. Several fluids were shown to follow these relations: n-alkanes in the range n-C_2H_6 - n-C_6H_{14}, benzene, toluene, xylenes, phenol and other aromatics, n-alcohols in the range CH_3OH – n-C_4H_9OH, ketones, water and some aqueous solutions.

Latter, Schonhorn (1967) introduced a correction in the second term of the right-hand side of Eq. II.6 to fulfill the requirement that at the critical point surface tension goes to zero, while viscosity tends to a small, but constant value:

$$\ln \sigma = \ln A + \frac{B}{\eta_l - \eta_v} \qquad \text{(II. 7)}$$

where subscripts l and v stand for the liquid and vapor phase property, respectively. This relation was successfully applied for pure metals like sodium and potassium, salts such as KBr, NaBr and NaCl, n-decane, argon, benzene, water, CCl_4 and polyethylene.

In his work, Schonhorn (1967) related *ln A* with σ_N, the surface tension at T_N, the temperature of homogeneous nucleation, that is, the temperature were clusters start to form spontaneously. At this temperature, the reciprocal viscosity tends to zero and thus, $\sigma = A$. Both in the works from Pelofsky (1966) and Shonhorn (1967) no physical meaning has been given to the slope, B, although Pelofsky has used a functional of the molecular weight to correlate this constant for members of the same family.

The data reported on Part I together with other pure component data (DIPPR, 1998; Vargaftik, 1975) will be used for the purposes of this work. Since the literature information for surface tension is considerably smaller than that available for viscosity, surface tension will limit the temperature range of this study. For the same reason, no pressure effect will be considered at this point.

Following the work from Pelofsky (1966), later re-evaluated by Schonhorn (1967) and Pedersen *et al* (1989), several pure and mixed n-alkanes were assessed. Since most of the available data has been taken far from the critical point, where the vapor phase viscosity is

small compared to that of the liquid phase, we can drop the correction introduced in Eq. II.7 and use Pelofsky's approach (Eq. II.6). With this approach, although an incorrect description of the surface tension is obtained close to the critical point, no need for information on the vapor phase viscosity is required, and the formalism of Eq. II.6 can be kept very simple and accurate, far from the critical point, while using a minimum amount of experimental data.

Pure components

In Figure II. 5, the linear relation is verified for some of the studied n-alkanes, n-C_6H_{14} up to n-$C_{20}H_{42}$. The same trend below n-hexane was also verified in this work and has already been shown by Pelofsky (1966). In these plots, only two points in 163 happened to be outside the linear relation, but these were also found to be outliers in the surface tension or viscosity plots as a function of temperature. Thus, if a set of values is found to be away from the linear plot, that may indicate incorrect viscosity or surface tension measurements.

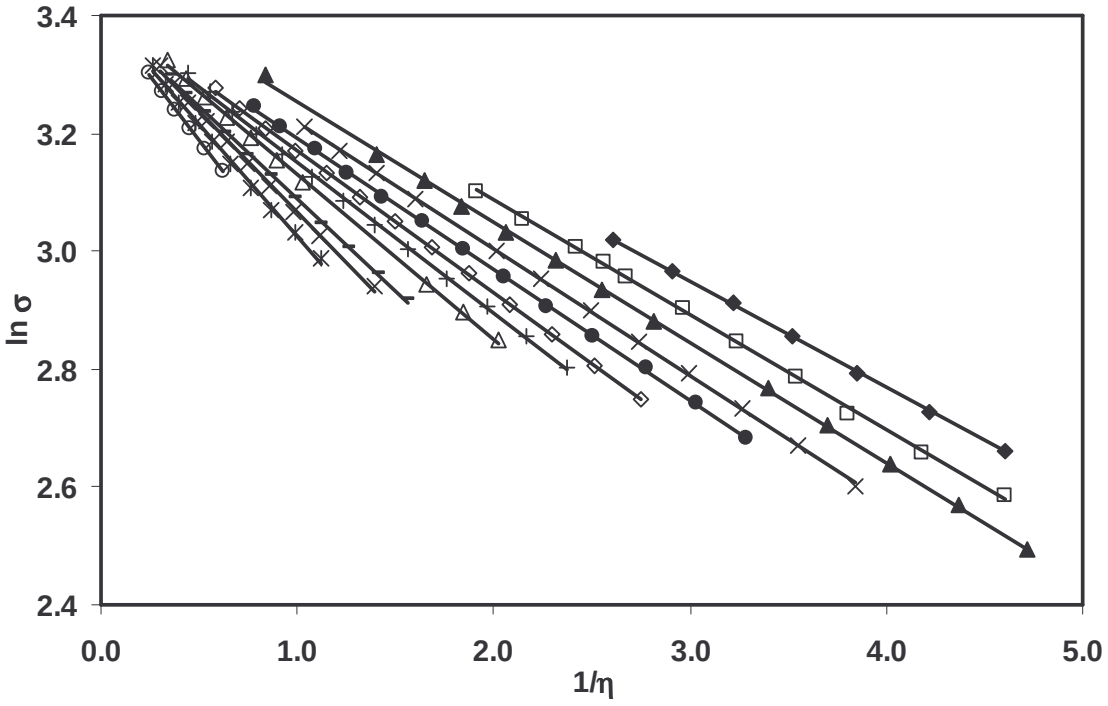

Figure II. 5: **Plots of ln σ as a function of reciprocal viscosity, 1/η for several pure n-alkanes: ◆, n-C_6H_{14}, □, n-C_7H_{16}, ▲ n-C_8H_{18}, x, n-C_9H_{20}, ●, n-$C_{10}H_{22}$, ◊, n-$C_{11}H_{24}$, +, n-$C_{12}H_{26}$, Δ, n-$C_{13}H_{28}$, -, n-$C_{15}H_{32}$, x, n-$C_{16}H_{34}$, *, n-$C_{18}H_{38}$, ○, n-$C_{20}H_{42}$.**

Table II. 2: **Least squares fit for n-alkanes, and corresponding σ_N and T_N values.**

n-alkane	*B*	ln A	σ_N/mN.m^{-1}	calc. T_N/K	T range/K
CH_4	-0.0922	3.35			93.15-163.15
C_2H_6	-0.138	3.60			133.15-193.15
C_3H_8	-0.162	3.55			203.15-263.15
n-C_4H_{10}	-0.174	3.54	34.5	124.8	233.15-293.15
n-C_5H_{12}	-0.166	3.52	33.8	148.3	233.15-293.15
n-C_6H_{14}	-0.180	3.49	32.8	164.0	273.15-333.15
n-C_7H_{16}	-0.194	3.48	32.3	181.0	273.15-363.15
n-C_8H_{18}	-0.204	3.46	31.7	198.5	243.15-393.15
n-C_9H_{20}	-0.215	3.43	31.0	213.5	273.15-393.15
n-$C_{10}H_{22}$	-0.222	3.41	30.4	227.3	273.15-393.15
n-$C_{11}H_{24}$	-0.241	3.41	30.3	234.5	273.15-393.15
n-$C_{12}H_{26}$	-0.256	3.41	30.1	242.8	273.15-393.15
n-$C_{13}H_{28}$	-0.279	3.41	30.2	247.1	273.15-393.15
n-$C_{14}H_{30}$	-0.297	3.41	30.1	255.0	283.15-393.15
n-$C_{15}H_{32}$	-0.312	3.40	30.0	262.0	293.15-393.15
n-$C_{16}H_{34}$	-0.341	3.41	30.2	266.1	293.15-393.15
n-$C_{17}H_{36}$	-0.363	3.41	30.2	270.1	293.15-393.15
n-$C_{18}H_{38}$	-0.380	3.41	30.1	274.1	303.15-393.15
n-$C_{19}H_{40}$	-0.388	3.39	29.8	280.1	313.15-393.15
n-$C_{20}H_{42}$	-0.447	3.41	30.3	278.8	313.15-393.15

As can be seen from Figure II. 5 and Table II. 2, *ln A* tends to a value close to 3.41 as the chain length of the n-alkane increases. This corresponds, in Figure II. 6, to a value of σ_N = A of 30.2 mN.m^{-1}, which agrees quite closely with 31.6 mN.m^{-1}, reported by Shonhorn (1967) for polyethylene. Below n-decane the values of ln *A* (and σ_N) seem to vary linearly with the chain length. The exception is methane, which although following the linear trend, present values that significantly deviate from linearity. For the other n-alkanes, up to n-C_9H_{20}, the following correlations can be used to obtain the value of *ln A*:

$$\ln A = 3.6314 - 0.0224 \times n \qquad \text{(II. 8)}$$

where *n* is the chain length of the n-alkane, C_nH_{2n+2}. If, instead, the molecular weight (MW/g.mol^{-1}) is used in the correlation, the following relation results:

$$\ln A = 3.6314 - 1.558 \times 10^{-3} \times MW \qquad \text{(II. 9)}$$

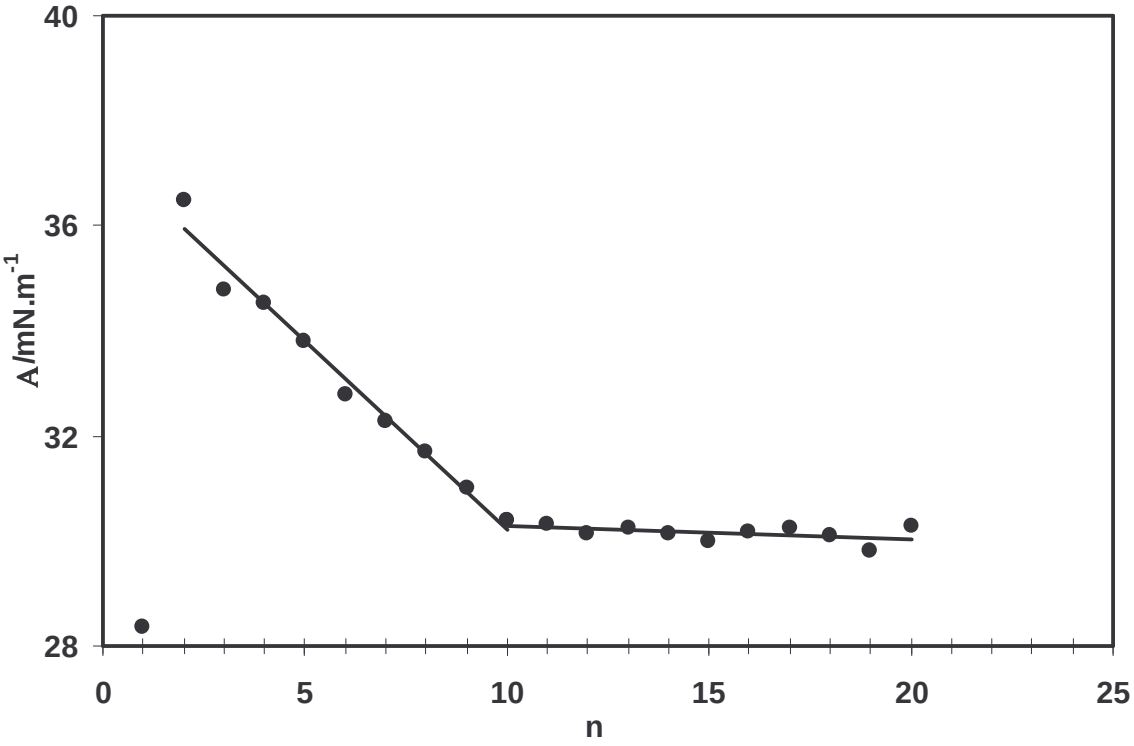

Figure II. 6: **Plots of A as a function of chain length of the n-alkane.**

From the intercept values reported in Table II. 2, and considering that for n-alkanes with chain length above n-C_4H_{10} the viscosity term (B/η) in Eq.II.6 can be neglected close to the formation of the solid phase, temperatures corresponding to these surface tensions were calculated using correlations of experimental data. These temperatures are reported on Table II. 2 under the *calc*. T_N column. If compared with literature melting points (Dirand *et al.*, 2002) it can be recognized that these values fall systematically below the melting temperatures, with values of reduced undercooling, $\Delta T_r = (T_{fus} - T_N)/T_{fus}$ that agree with those known for the n-alkanes (Herhold *et al.*, 1999). It can thus be concluded, following Schonhorn (1967), that the value of *A* corresponds to the surface tension of the fluid at the temperature of homogeneous nucleation (T_N), and that this is constant for chain lengths higher than n-$C_{10}H_{22}$.

For the slopes the same separation seems appropriate, as can be seen from Figure II. 7. Below n-decane one linear trend can be assumed, where methane is again not included, Eqs. II.10 - II.11. Above n-decane another linear trend can be considered, Eqs. II.12 - II.13.

n<10, $$B = -0.1253 - 9.798\times10^{-3}\times n \quad \text{(II. 10)}$$

$$B = -0.1253 - 6.826\times10^{-3}\times MW \quad \text{(II. 11)}$$

n≥10 $$B = -2.135\times10^{-2}\times n \quad \text{(II. 12)}$$

$$B = -1.508\times10^{-3}\times MW \quad \text{(II. 13)}$$

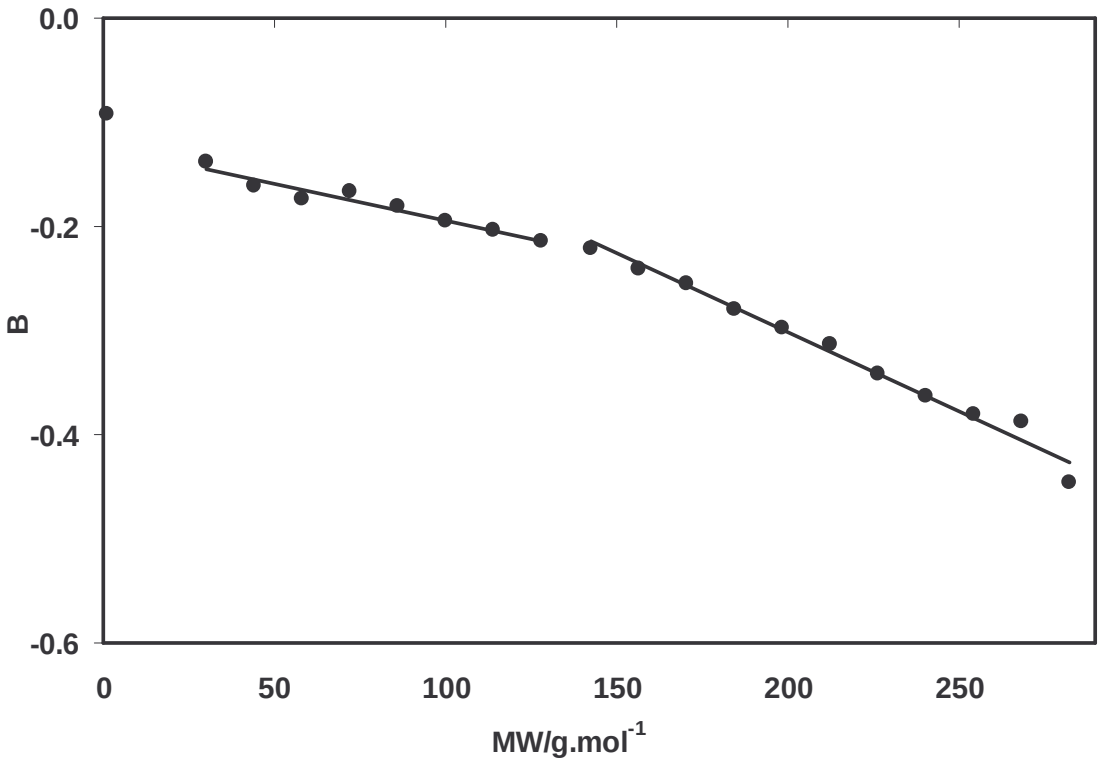

Figure II. 7: Plots of B as a function of MW.

In his work, Pelofsky (1966) proposed to correlate the value of *B*, as a function of the molecular weight and thermal conductivity. Since that would introduce an additional variable in these relations, reducing its predictive ability, in this work, only the molecular

weight of the n-alkane is used to correlate this parameter. The interest in using the molecular weight as a correlating variable, follows from the possibility of applying this relation to more complex systems, for which compositional analysis are difficult to obtain and properties other than the molecular weight, boiling point or specific gravity, may be inaccessible as is the case for most of the petroleum fluids.

Synthetic mixtures

Following the results presented in the previous section, Eq. II.6 was also evaluated for mixtures, namely the asymmetric mixtures containing two or three n-alkanes reported in Part I. In Figure II. 8 plots of ln σ as a function of 1/η for the mixture n-$C_{10}H_{22}$ + n-$C_{20}H_{42}$ are presented at five different compositions. The linear trend is clearly evident, and again, the value of the intercept seems to converge.

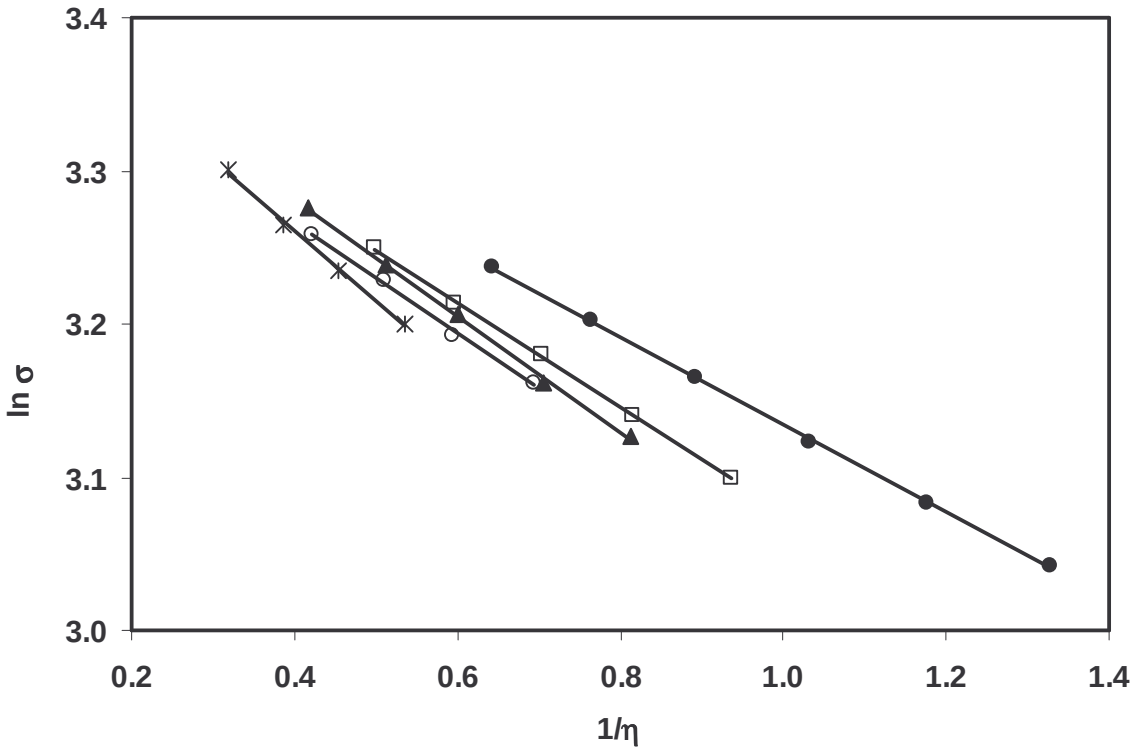

Figure II. 8: **ln σ as a function of 1/η for n-$C_{10}H_{22}$ (1) + n-$C_{20}H_{42}$ (2): ●, x(2)=0.2, □, x(2)=0.4, ▲, x(2)=0.5, ○, x(2)=0.6, *, x(2)=0.8.**

Results of least-squares fits for systems of n-decane (n-$C_{10}H_{22}$) and n-hexadecane (n-$C_{16}H_{34}$) mixed with n-eicosane (n-$C_{20}H_{42}$), n-docosane (n-$C_{22}H_{46}$) and n-tetracosane (n-$C_{24}H_{50}$) are presented on Table II. 3.

Table II. 3: **Least-squares fit for some n-alkane mixtures**

Mixture	*x*(1)	*x*(2)	ln A	B	T range/K
n-$C_{10}H_{22}$(1)+n-$C_{20}H_{42}$(2)	0.80	0.20	3.42	-0.285	293.15-343.15
	0.60	0.40	3.42	-0.340	303.15-343.15
	0.50	0.50	3.43	-0.375	303.15-343.15
	0.40	0.60	3.42	-0.380	313.15-343.15
	0.20	0.80	3.44	-0.458	313.15-343.15
n-$C_{10}H_{22}$(1)+n-$C_{22}H_{46}$(2)	0.60	0.40	3.39	-0.338	313.15-343.15
	0.40	0.60	3.43	-0.452	313.15-343.15
	0.20	0.80	3.39	-0.349	323.15-343.15
n-$C_{10}H_{22}$(1)+n-$C_{24}H_{50}$(2)	0.80	0.20	3.40	-0.325	313.15-343.15
	0.60	0.40	3.40	-0.402	323.15-343.15
	0.50	0.50	3.41	-0.451	323.15-343.15
n-$C_{10}H_{22}$(1)+n-$C_{20}H_{42}$(2)+n-$C_{24}H_{50}$(3)	0.80	0.10	3.38	-0.264	313.15-343.15
	0.60	0.20	3.38	-0.337	313.15-343.15
	0.50	0.25	3.37	-0.329	313.15-343.15
n-$C_{20}H_{42}$(1)+n-$C_{24}H_{50}$(2)	0.50	0.50	3.42	-0.490	323.15-343.15
n-$C_{16}H_{34}$(1)+n-$C_{20}H_{42}$(2)	0.80	0.20	3.43	-0.377	303.15-343.15
	0.60	0.40	3.43	-0.399	303.15-343.15
	0.50	0.50	3.42	-0.374	313.15-343.15
	0.40	0.60	3.43	-0.418	313.15-343.15
	0.20	0.80	3.43	-0.431	313.15-343.15

All these mixtures have average chain lengths, ($n = \sum x_i \times n_i$) above 10, so from the previous conclusions for the pure components, they may have the same intercept. In fact, from Table II. 3 one can check that the values of *ln A* fall within a very short interval [3.38-3.43], with an average of 3.41, the same established previously for the pure components. Thus, in terms of intercept, a constant value of 3.41 applies also for mixtures with n ≥ 10. This can be confirmed in Figure II. 9 for the mixtures reported on Table II. 3, were *A* is plotted as a function of the average chain length.

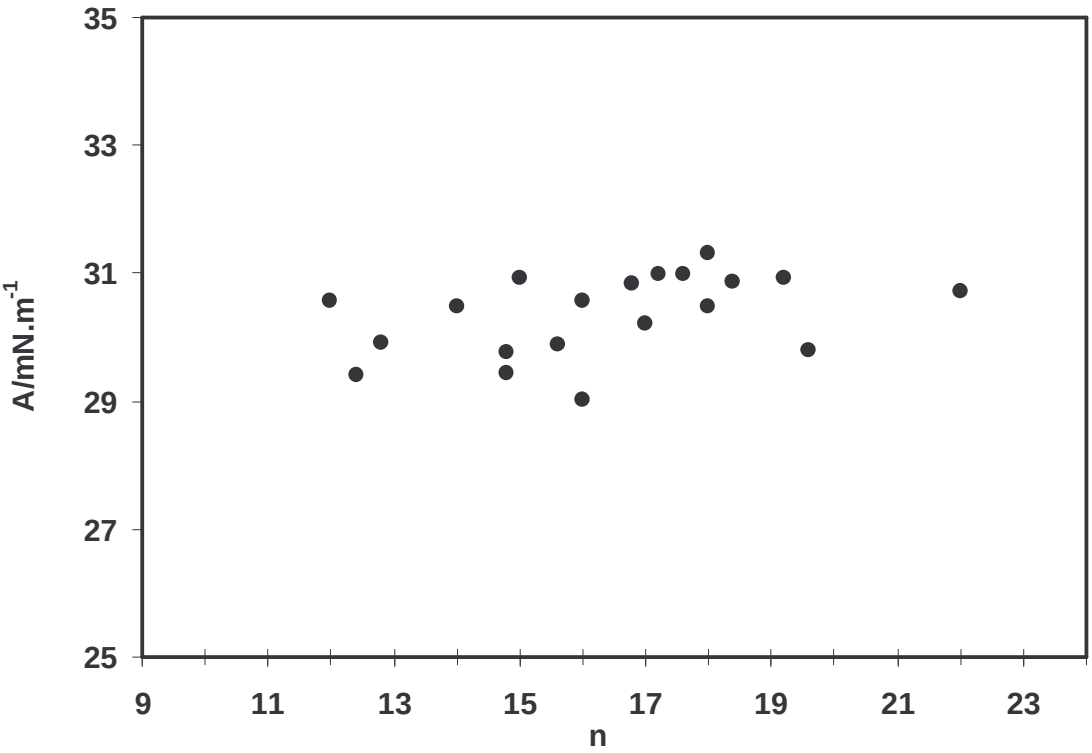

Figure II. 9: **Plots of A for n-alkane mixtures as a function of average chain length.**

To verify that the slopes can also be calculated using the same equations as for the pure fluids, Figure II. 10 was plotted using the *B* values reported on Table II. 3. A least-squares fit for the best linear equation gave a slope of -1.629×10^{-3}, which agrees within 6.6 % with -1.508×10^{-3}, reported on Eq. II.8. Considering the dispersion of values on Figure II. 10, Eq. II.8 was considered to be also valid for mixtures. To check this assumption, Eq. II.8 together with ln A= 3.41 were used to estimate surface tensions from

viscosities and viscosities from surface tensions for mixtures of n-alkanes. Results are reported on Table II. 4.

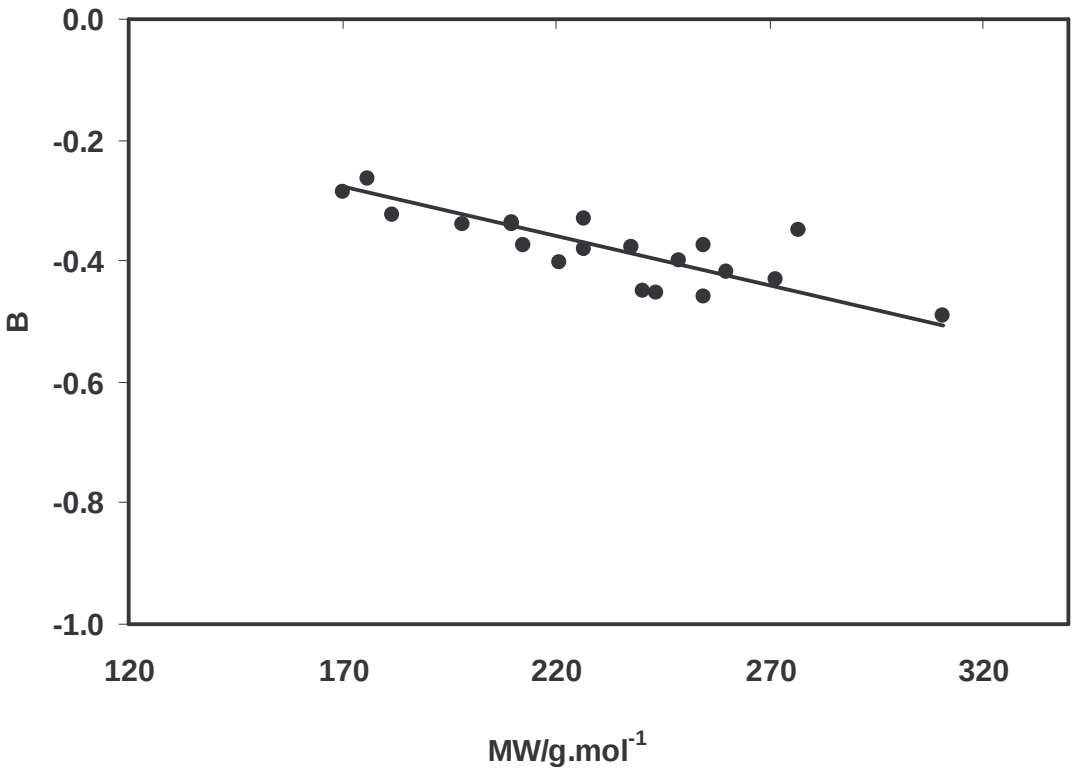

Figure II. 10: Plots of B for n-alkane mixtures as a function of average molecular weight.

As can be seen from Table II. 4, very good surface tension estimation is obtained using Eqs. II.1 and II.8, with the maximum average deviations found for the most asymmetric mixtures. The same trend was found for the estimated viscosities, but higher deviations are observed, ranging from 5 % up to 29 % with an average of 13 %. It can thus be concluded that for the studied asymmetric n-alkane mixtures, Eq. II.6 returns better estimates of surface tension from viscosity, than viscosity estimates from surface tension.

The results obtained for the surface tension open an opportunity to estimate this property at high pressure, for which the available experimental data are scarce and measurements more difficult to perform.

Table II. 4: Estimation of mixture surface tension or viscosity from Eq. 1 using *ln A*=3.41 and Eq. 8 for *B*.

Mixture	Surf. tension, % AAD[a]	Viscosity, % AAD[a]
n-$C_{10}H_{22}$+n-$C_{20}H_{42}$	1.2	5.2
n-$C_{10}H_{22}$+n-$C_{22}H_{46}$	1.8	8.4
n-$C_{10}H_{22}$+n-$C_{24}H_{50}$	3.8	16.6
n-$C_{10}H_{22}$+n-$C_{20}H_{42}$+n-$C_{24}H_{50}$	2.7	11.6
n-$C_{7}H_{16}$+n-$C_{20}H_{42}$	7.8	26.2
n-$C_{7}H_{16}$+n-$C_{22}H_{46}$	8.5	29.2
n-$C_{7}H_{16}$+n-$C_{20}H_{42}$+n-$C_{24}H_{50}$	7.3	22.6
n-$C_{16}H_{34}$+n-$C_{20}H_{42}$	1.4	10.5
Average	3.2	13.1

[a] Eq. I.7

Real Systems

In order to check the extension of this simple model to real fluids, three petroleum distillation cuts of different origins were selected for evaluation (section I.2.4). Plots of ln σ as a function of $1/\eta$ are shown on Figure II. 11, and least-squares constants reported on Table II. 5. It can be confirmed that Eq. II.6 continues to be valid, even for multicomponent fluids containing components from different families, as already demonstrated in a previous work by Pedersen *et al*. (1989).

Table II. 5: **Least-squares fit for petroleum distillation cuts**

***Distillation* cut**	**MW/g.mol^{-1}**	**% n-alkanes**	**ln A**	**B**
Troll	231.7	9.79	3.48	-0.438
Brent	222.8	19.55	3.45	-0.408
Sahara Blend	235.8	21.17	3.44	-0.404

Molecular weight and n-alkane content, are also included on Table II. 5. This time, both the intercept and slope are dependent on composition, and thus, the approach used before for pure and mixed n-alkanes cannot be implemented without the use of mixing rules.

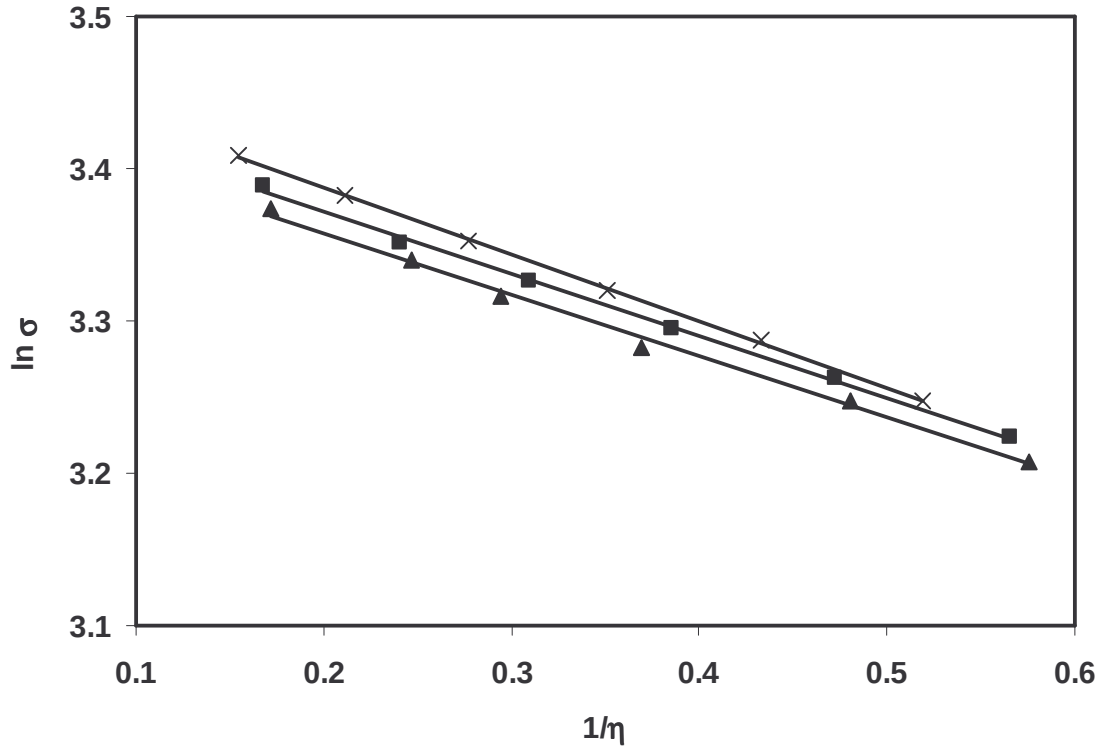

Figure II. 11: **ln σ as a function of 1/η for petroleum distillation cuts: ×, Troll, ■, Brent, ▲, Sahara Blend.**

Pedersen *et al.* (1989) proposed a mixing rule to use these relations for petroleum fluids. Composition in terms of a PNA (*Paraffins-Naphtenes-Aromatics*) distribution is required. Unfortunately, for the distillation cuts presented in this work, no PNA distribution was determined, and thus, the evaluation of this model for the reported distillation cuts is not possible.

II.4. Conclusions

A review on the available experimental critical properties and Pitzer acentric factors was presented. For components above n-$C_{36}H_{74}$ no literature data was found, while for the critical volumes, experimental values have only be reported up to n-$C_{18}H_{38}$.

Correlations for the estimation of the heavier n-alkane properties are thus important, since they are required for the correct modeling of thermophysical properties. Several correlations were assessed and the Tsonopoulos (1987), Magoulas *et al.* (1990), Marano *et al.* (1997a) and the Han *et al.* correlations were found to be the most accurate at describing, respectively, critical temperatures, critical pressures, critical volumes and acentric factors.

A linear relation between the natural logarithm of the surface tension and the reciprocal viscosity was found to be valid for pure n-alkanes, some of their binary and ternary mixtures and for petroleum distillation cuts of different n-alkane content.

The intercept can be linked with the surface tension at the temperature of homogeneous nucleation, where the reciprocal viscosity approaches zero. For n-alkanes with chain length higher than n-$C_{10}H_{22}$ this value is constant. Below n-$C_{10}H_{22}$, a linear correlation can be used for the calculation.

For the slope, two correlations where proposed: one for fluids with chain length higher than n-$C_{10}H_{22}$, and other for fluids with chain length smaller than n-$C_{10}H_{22}$.

Methane is not included in all of the proposed correlations, since its behavior falls outside that observed for the other n-alkanes.

Some heavier and asymmetric n-alkane mixtures reported in the previous chapter of this thesis were evaluated for the extension of the proposed relation. Linearity was again observed, and interestingly, intercepts equal to those of the same chain length pure components were found. The same happened with the slopes that could be calculated from an equation obtained for the pure components. Using the equivalent pure component slopes and intercepts, very good surface tension estimates where obtained from viscosity data. If viscosity is to be obtained from surface tension larger errors shall be expected.

Finally, some petroleum distillation cuts of different origins where shown to follow the presented linear relation, but, as expected, the correlating equations presented before where not applicable, since these contain components other than n-alkanes.

PART III: MODELING

"It would appear that we have reached the limits of what it is possible to achieve with computer technology, although one should be careful with such statements, as they tend to sound pretty silly in 5 years."

John Von Neumann (1903 - 1957), Mathematician and Computer scientist

"Nothing in life is to be feared, it is only to be understood."

Marie Curie (1867 – 1934), physical chemist.

III.1 Introduction

Accurate values of thermophysical properties are essential for the correct process and product design. Frequently, the desired properties at the required temperature, pressure and composition conditions may not yet have been determined experimentally, and so, either an experimental determination must be carried out or an adequate model should be selected. Regularly, models are used, as experimental measurements are expensive and time consuming, and the desired accuracies for the required properties may not be very restrictive.

There is a considerable number of models for the estimation of each thermophysical property (Poling *et al.*, 2000). These models can be classified as theoretical, empirical or semi-empirical. The first are usually the more general and can be applied for new systems, but they often present large deviations and can only be used for qualitative purposes. Empirical models can be highly accurate, since some of its parameters are regressed from experimental data, but these are less theoretically sound and extrapolations for new systems and regions outside the fitted "area" must be done with caution. Semi-empirical models are usually the best solution, since they combine a theoretical formalism with some parameter estimation from available experimental data. In any case, it is very important to perform a model evaluation against a small set of experimental data for similar systems, before we select that model for our particular purposes. In this chapter, with the new data from section I.2, model evaluation will be carried out in order to check their application for these new heavier and asymmetric n-alkane mixtures.

Some of the most accurate models, although mathematically simple and using a small amount of experimental information, are those based on the corresponding states principle. One of the advantages of corresponding states models is that the same formalism can be used for different properties, where the only changes are the definition of the reduced property and the equation used for the reference fluid(s) or the reference fluid(s) itself. Since these models do not use any experimental data of the estimating property of the target fluid, they are also predictive. The only experimental information required from the target fluid are the critical properties and the Pitzer acentric factor. The coupling between the strong theoretical basis behind corresponding states principle and the accuracy of the empirical equations used to describe the reference fluid(s) justify the effort in developing such models.

Corresponding states models have been successfully used for the estimation of properties of pure components and mixtures of small molecules, mainly for nonpolar systems, although some effort has also been made at extending them to polar fluids and their mixtures (Marrucho, 1996). This chapter presents the extension of these models for the evaluation of thermophysical properties of long chain molecules in a broad temperature range, based on information from lower members of the same homologous series. A new model is presented and evaluated for the prediction of the liquid densities, viscosities and vapor-liquid interfacial tensions presented in Part I. It will also be shown that this model may be used for the estimation of other properties such as vapor pressures, thermal conductivities and speeds of sound. Using the same framework, this model can be used to predict all these properties in a broad temperature range and for both lighter and heavier n-alkanes and their mixtures.

No attempt to extensively evaluate literature models for the systems presented on this thesis will be made, as some general reviews can be found on literature (Poling *et al*., 2000) and this would, most certainly, lead to the selection of different models for each thermophysical property. Instead, the focus was on the selection of generalized models that could be simultaneously used for more than one property: corresponding states, as mentioned before, and equations of state based models such as the friction theory for viscosity and liquid density and the gradient theory of fluid interfaces than can be used to simultaneously model phase equilibrium, interfacial tensions and density profiles.

The gradient theory of fluid interfaces and the friction theory are state-of-the-art models, with the most interesting developments reported in the last five years (Cornelisse, 1997; Cornelisse *et al.*, 1996; Kahl *et al.*, 2000 and 2002; Miqueu, 2001; Miqueu *et al.*, 2003 and 2004; Quinõnes-Cisneros *et al.*, 2000, 2001a and 2001b; Zéberg-Mikkelsen *et al.*, 2001 and 2002; Zuo *et al.*, 1996, 1997b and 1998). Some results from these models will be presented and discussed during sections III.3 and II.4, respectively.

Aiming at describe the water-hydrocarbon liquid-liquid interfaces the gradient theory was coupled with the Cubic-Plus-Association (CPA) equation of sate, a thermodynamic model that has shown to be able to describe vapor-liquid and liquid-liquid equilibria of mixtures containing water, alkanes and alcohols (Kontogeorgis *et al.*, 1996, 1999; Yakoumis *et al.*, 1998; Derawi, 2002; Voutsas, 2000; Wu and Prausnitz, 1998). Particularly for water-alkane systems CPA is actually the only model that provides acceptable results for both the solubility of water in the hydrocarbon-phase and the hydrocarbon solubility in the aqueous phase, thus presenting a great potential for the correct modelling of water-hydrocarbon liquid-liquid interfaces.

Finally, during section III.5 solid-liquid equilibria will be considered, as heavier n-alkanes are solid at ambient conditions. Accurate modelling of this kind of mixtures has already been reported (Coutinho, 1995), so in this chapter, data from the petroleum distillation cuts presented in chapter I will be used for checking model performance for real systems. The measured precipitation curves are compared with the predictions using the compositional analysis presented before. The model, which only requires the n-alkane composition, agrees well with the experimental data indicating that it can be an adequate tool to predict the low temperature behaviour of hydrocarbon mixtures. No need for other mixture information, as usually required with other models is necessary.

"As three laws were good enough for Newton, I have modestly decided to stop there"

Arthur C. Clarke (1917 -), writer.

Using the new measurements reported on Part I, along with the critical properties and acentric factors selected on Part II and other data collected from the literature, a new corresponding states model was assessed. It is shown that using a new generalized combining rule for the critical temperature, mixture data can be described with deviations within the experimental uncertainty of the measurements.

III.2. The Corresponding States Principle

III.2.1. Pure Fluids

The application of corresponding states models extends from equilibrium properties such as vapour pressure (Morgan *et al.*, 1994; Pitzer *et al*., 1955; Poling *et al.*, 2000; Teja *et al.*, 1981b; Xiang, 2002), liquid density (Muñoz *et al*., 1983; Poling *et al.*, 2000; Teja *et al*., 1981b; Teja, 1980) or surface tension (Poling *et al*., 2000; Queimada *et al*., 2001; Rice *et al*., 1982; Zuo *et al*., 1997) to transport properties such as viscosity (Ely *et al.*, 1981; Klein *et al.*, 1997; Lee *et al.*, 1993; Poling *et al*., 2000; Teja *et al.*, 1981a;) and thermal conductivity (Poling *et al.*, 2000). In spite of this versatility, the small amount of experimental information required and its mathematical simplicity, corresponding states models can produce very accurate estimates of thermophysical properties, in broad temperature and pressure conditions. If we still add the strong theoretical basis behind the

corresponding states principle we can justify any effort in studying and developing such models.

The corresponding states principle was initially proposed by van der Walls who observed that the reduced version of his equation of state could be written for several fluids. Although the establishment of this principle was originally made only on an empirical basis, following studies in statistical mechanics and kinetic theory have confirmed its theoretical foundations (Ely *et al.*, 2000; Guggenheim, 1945; Leland *et al.*, 1968; Pitzer, 1939; Reed *et al.*,1973; Rowlinson *et al.*, 1982). Today, many generalized equations of state are examples of applications of this principle.

The basic concept of corresponding states principle is to apply dimensional analysis to the configurational portion of the statistical mechanical partition function. The end result of this analysis is the expression of residual thermodynamic properties in terms of dimensionless groups.

In its original form, the corresponding states principle, as proposed by van der Waals, expressed the reduced compressibility factor (Z_r) in terms of a universal function of two parameters, the dimensionless temperature (T_r) and molar volume (V_r) (or pressure, P_r):

$$Z_{rj}(T_r, V_r) = Z_{r0}(T_r, V_r) \qquad \text{(III. 1)}$$

$$T_r = \frac{T}{T_c}, \quad V_r = \frac{V}{V_c}, \qquad P_r = \frac{P}{P_c} \qquad \text{(III. 2)}$$

Where Z is the compressibility factor, PV/RT, and the subscripts r and c stand for reduced and critical property and j and 0 for target and spherical reference fluid, respectively.

Experimental evidence has, however, shown that this two-parameter *corresponding states* approach was limited to the noble gases and nearly spherical molecules such as nitrogen, oxygen and methane. To extend this theory to a broader range of fluids, additional characterization parameters have been introduced to account for the non-conformalities. Two main approaches have been applied in this parameterization: the first

performs a multi-parameter Taylor's series expansion of the property of interest about the parameters; the second approach is to extend the simple two-parameter corresponding states principle at its molecular origin. This is accomplished by making the intermolecular potential parameters functions of the additional characterization parameters and the thermodynamic state, e.g. the temperature. The end result is a corresponding states model that has the same mathematical form as the simple two-parameter model, but the definitions of the dimensionless volume and temperature are more complex, involving the so-called *shape factors* (Ely *et al.*, 2000).

An additional third parameter, the *Pitzer acentric factor*, ω, was introduced (Pitzer *et al.*, 1955) to generalize the scope of the corresponding states principle to include fluids whose force fields slightly depart from those of the original spherical symmetry. Reduced pressure was used instead of reduced volume due to the uncertainty usually ascribed to the measurement of critical volumes. A Taylor series expansion of the property of interest is performed about this third parameter, with the series being usually truncated beyond the first derivative.

$$Z_{r\,j}(T_r, P_r, \omega) = Z_{r0}(T_r, P_r) + \omega\, Z_r(T_r, P_r) \qquad \text{(III. 3)}$$

where Z_{ro} has the same meaning as in Eq. III.1 and Z_r is a function that represents the departure from the spherical symmetry. In a Taylor series expansion this function represents the derivative $\partial Z / \partial \omega$. In spite of the analytic formalism of Eq. III.3, values for the functions Z_{r0} and Z_r were only presented in tabular form by Pitzer and co-workers.

With the advent of cheaper and faster computers, Lee *et al.* (1975) suggested replacing the derivative in the Taylor series with its finite difference:

$$Z_{r\,j}(T_r, P_r, \omega) = Z_{r\,0}(T_r, P_r) + \frac{\omega_{\,j}}{\omega_{\,1}}\left[\, Z_{r\,1}(T_r, P_r) - Z_{r\,0}(T_r, P_r) \,\right] \qquad \text{(III. 4)}$$

Subscript *1* represents a non-spherical reference fluid ($\omega > 0$).

Although this new formalism contained a correction for the departure from the spherical symmetry, some problems arose in the description of polar or asymmetric systems. Since Eq. III.4 still contains a spherical reference fluid, ($\omega = 0$), large interpolations/extrapolations were frequent in the description of real systems. Another problem was related with the widespread use of methane as the spherical reference fluid. Since methane has a triple point relatively high compared with the majority of the hydrocarbons, some low temperature calculations would result in the extrapolation of the methane equation of state introducing considerable errors in the predicted data.

Following Teja and coworkers (Plöcker *et al.*, 1978; Rice *et al.*, 1982; Teja *et al.*, 1981a and 1981b; Teja, 1980; Wong *et al.*, 1983; Zuo *et al.*, 1997) the spherical reference in Eq. III.4 was abandoned. Therefore, both reference fluids could be similar to the evaluating fluid, reducing the errors due to large interpolations/extrapolations. Several thermophysical properties were estimated according to this new framework with very good predictive results:

$$X_r = X_{r1} + \frac{\omega - \omega_1}{\omega_2 - \omega_1}(X_{r2} - X_{r1}) \qquad \text{(III. 5)}$$

where X_r stands for the reduced property to be evaluated and subscripts 1 and 2 for the two reference fluid properties at the same reduced conditions as those of the target fluid. In all cases, good agreement with experimental data was obtained in the range of fluids covered by the two references. However, considerable deviations can be found if the reference fluids are far apart in the series from the target fluid, either interpolating or extrapolating (Figs. III.1-III.6). In an attempt to correct for these deviations, and based on the dependence of the desired properties with ω (or chain length) presented on Figs. III.1 - III.6, the Taylor series expansion of the reduced property was carried out to the second-order term:

$$X_r = X_{r_1} + D_1(\omega - \omega_1) + D_2(\omega - \omega_1)(\omega - \omega_2) \qquad \text{(III. 6)}$$

$$D_1 = \frac{X_{r_2} - X_{r_1}}{\omega_2 - \omega_1} \quad D_2 = \frac{\frac{X_{r_3} - X_{r_1}}{\omega_3 - \omega_1} - \frac{X_{r_2} - X_{r_1}}{\omega_2 - \omega_1}}{\omega_3 - \omega_2} \qquad \text{(III. 7)}$$

A third reference fluid is introduced with the advantage that no change in the reference system has to be done if one wants to study a large range of fluids or an asymmetric system. If instead, the Teja approach is adopted for asymmetric systems with a single reference system, considerable deviations resulting from the interpolations/extrapolations may be found as will be shown below.

A quadratic dependence on the acentric factor for heavy alkanes (up to n-$C_{28}H_{58}$) was previously used with success by Morgan and Kobayashi (1994) to correlate vapour pressures and heats of vaporization.

The linear Teja approach (Eq.III.5) and the new 2nd order perturbation model (Eq.III.4) were evaluated for liquid density, liquid-vapor interfacial tensions and viscosities of pure n-alkanes from methane up to n-hexatriacontane, and some of their mixtures. Some results will also be presented for reduced vapor pressures, thermal conductivies and speeds of sound of the n-alkane series, to show how this model can be used to improve the prediction of other thermophysical properties (Figs. III.1 – III.6).

Special care has been taken regarding the selection of the surface tension data since the values very often differ considerably from author to author (Katz and Saltman, 1939; Leadbetter *et al.*, 1964; Mass and Wright, 1921; Calado *et al.*, 1978; Jasper and Kring, 1955; Grigoryev *et al.*, 1992; Jasper, 1972; Jasper *et al.* 1953; McLure *et al.*, 1982; Hunten *et al.*, 1929; Wu, 1999). The data reported by Jasper *et al.* (1955, 1972, 1953) and by Grigoryev *et al* (1992) were used preferentially. The latter article covers all the liquid region of n-alkanes between n-C_5H_{12} and n-C_8H_{18}. Eq.III.8 was used to correlate the experimental liquid-vapor interfacial tensions of the reference fluids, thus yielding two parameters per each fluid:

$$\gamma = A \times (1 - T_r)^B \qquad \text{(III. 8)}$$

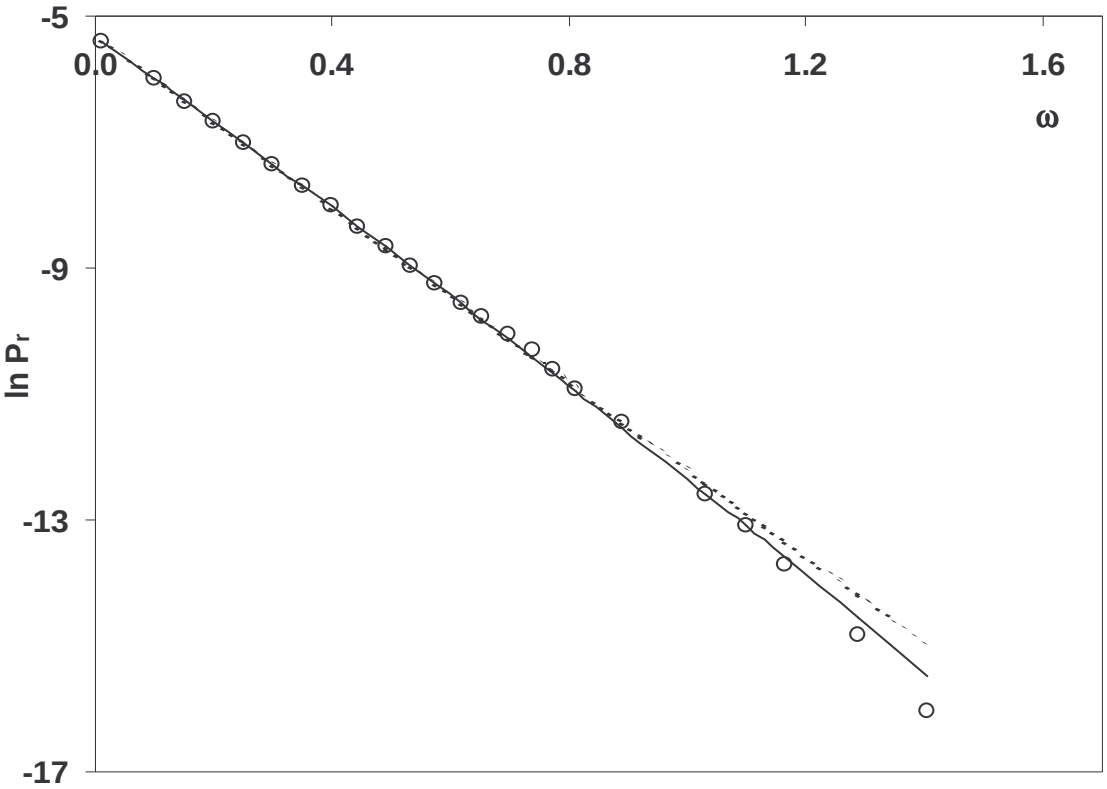

Figure III. 1: **Reduced vapor pressure (P_r) as a function of the acentric factor (ω) at Tr = 0.5. ○, experimental, (–) Eq. III.6, (--), Eq. III.5.**

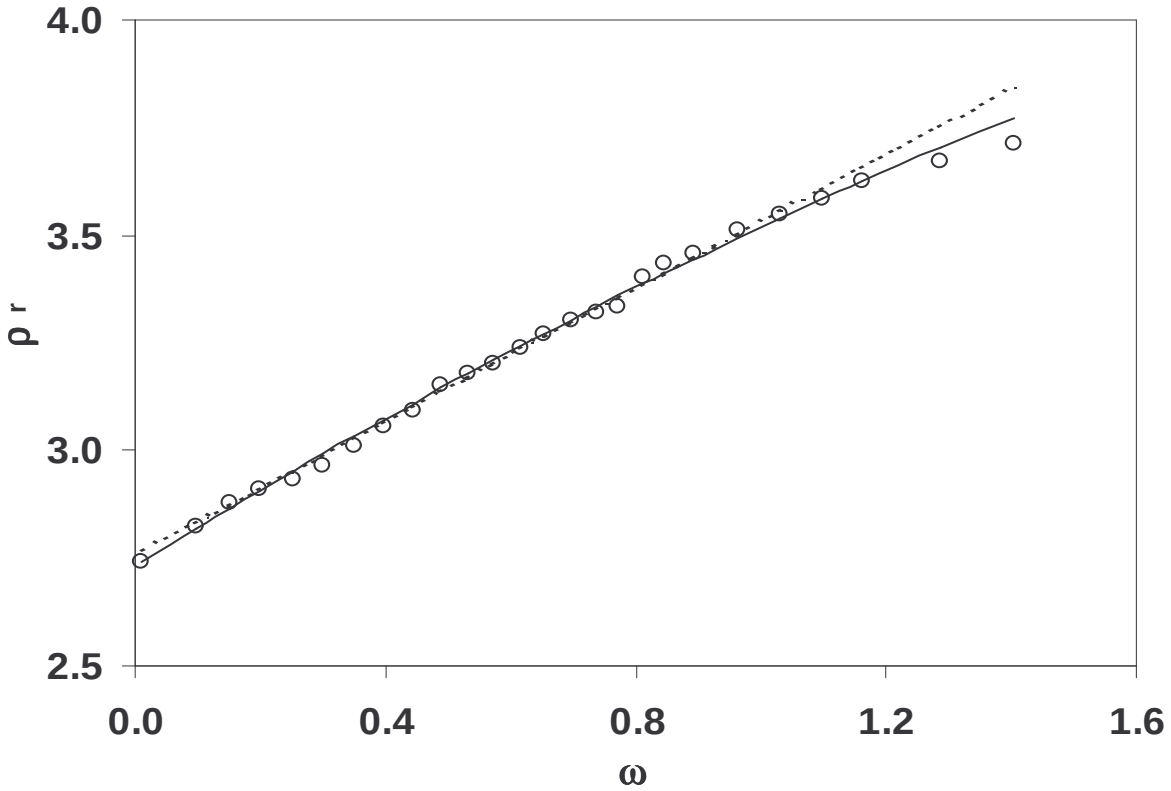

Figure III. 2: **Reduced liquid density (ρ_r) as a function of the acentric factor (ω) at T_r=0.5. ○, experimental, (–) Eq. III.6, (--), Eq. III.5.**

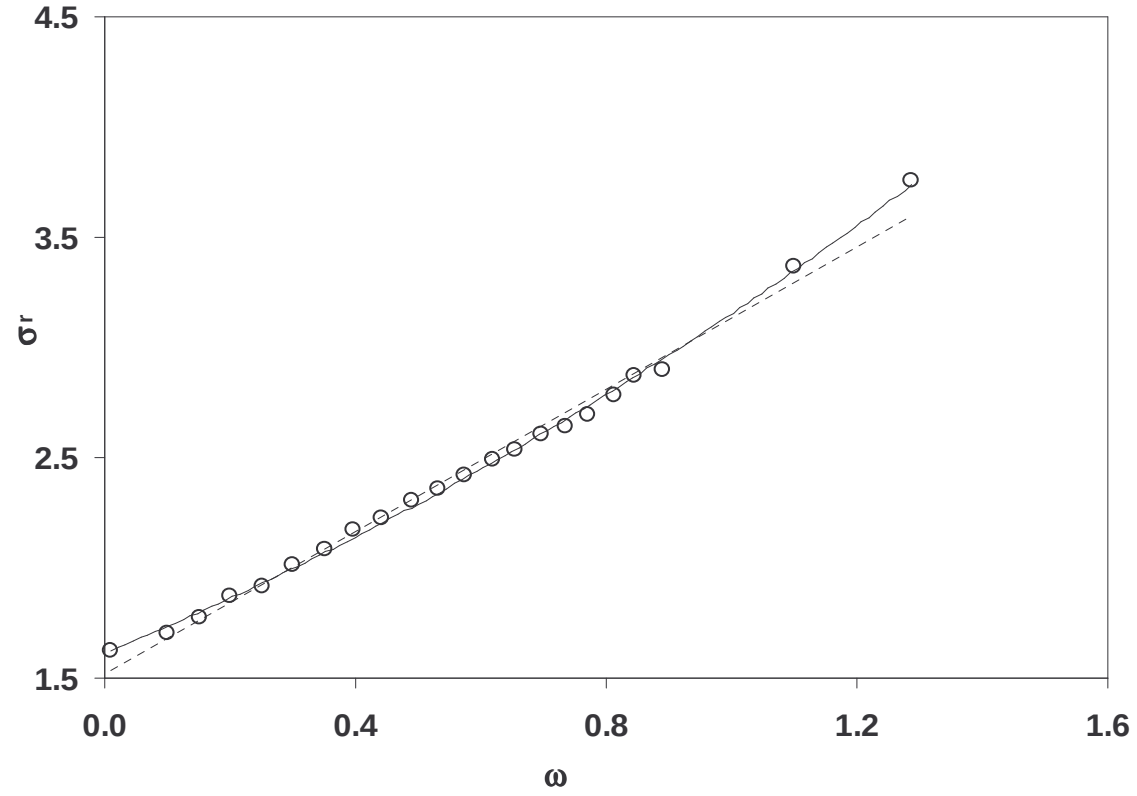

Figure III. 3: **Reduced surface tension for n-alkanes as a function of acentric factor at Tr=0.5. ○, experimental, (–) Eq. III.6, (--), Eq. III.5.**

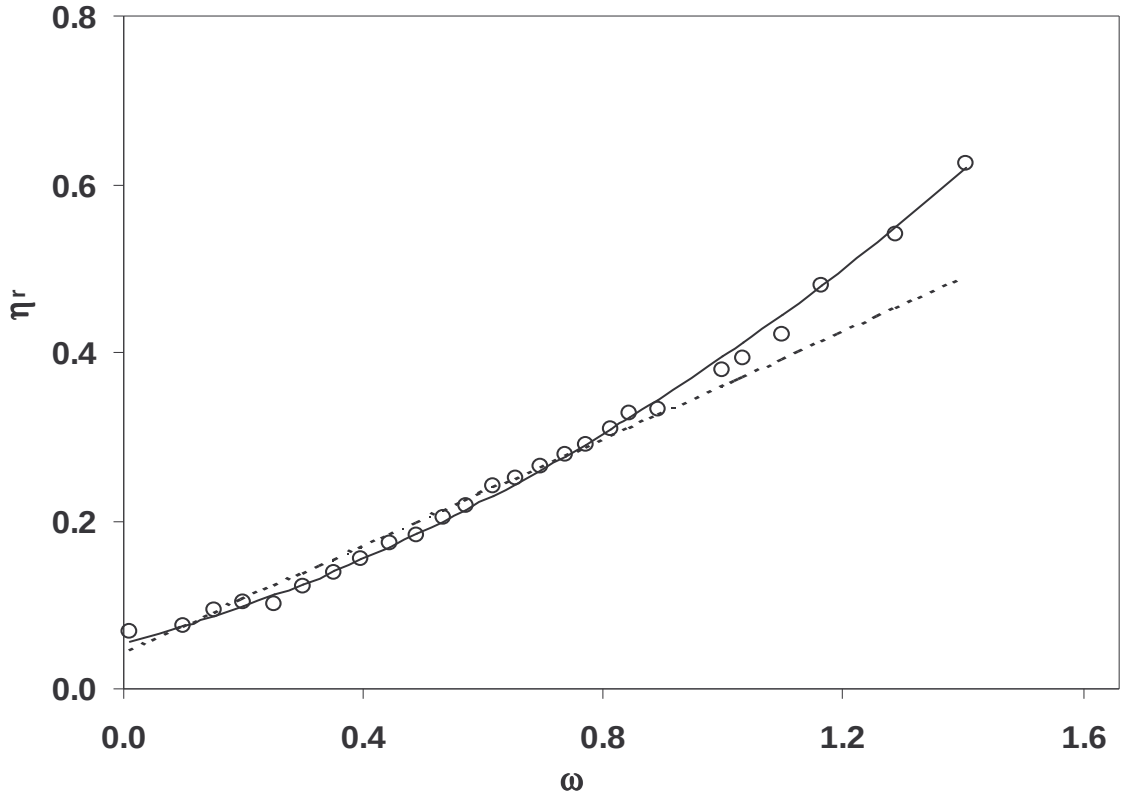

Figure III. 4: **Reduced viscosity (η_r) as a function of the acentric factor (ω) at T_r=0.5. ○, experimental, (–) Eq. III.6, (--), Eq. III.5.**

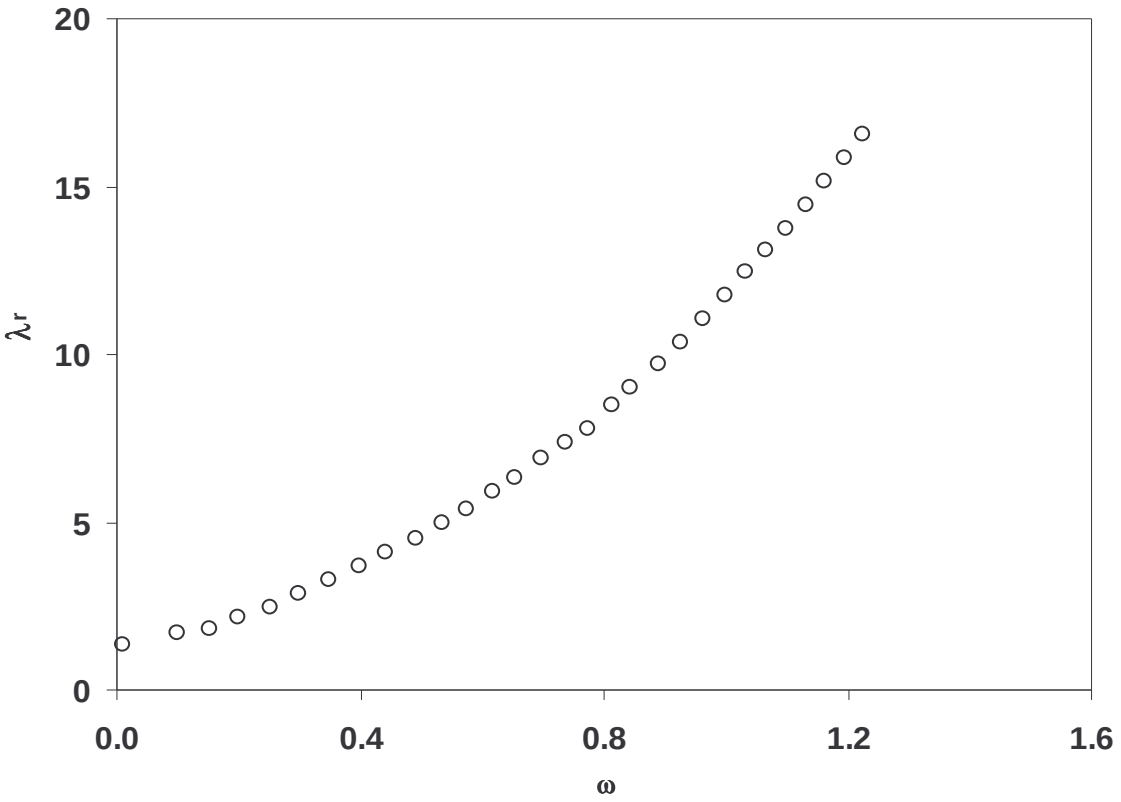

Figure III. 5: Reduced thermal conductivity as a function of the acentric factor (ω) at T_r=0.5.

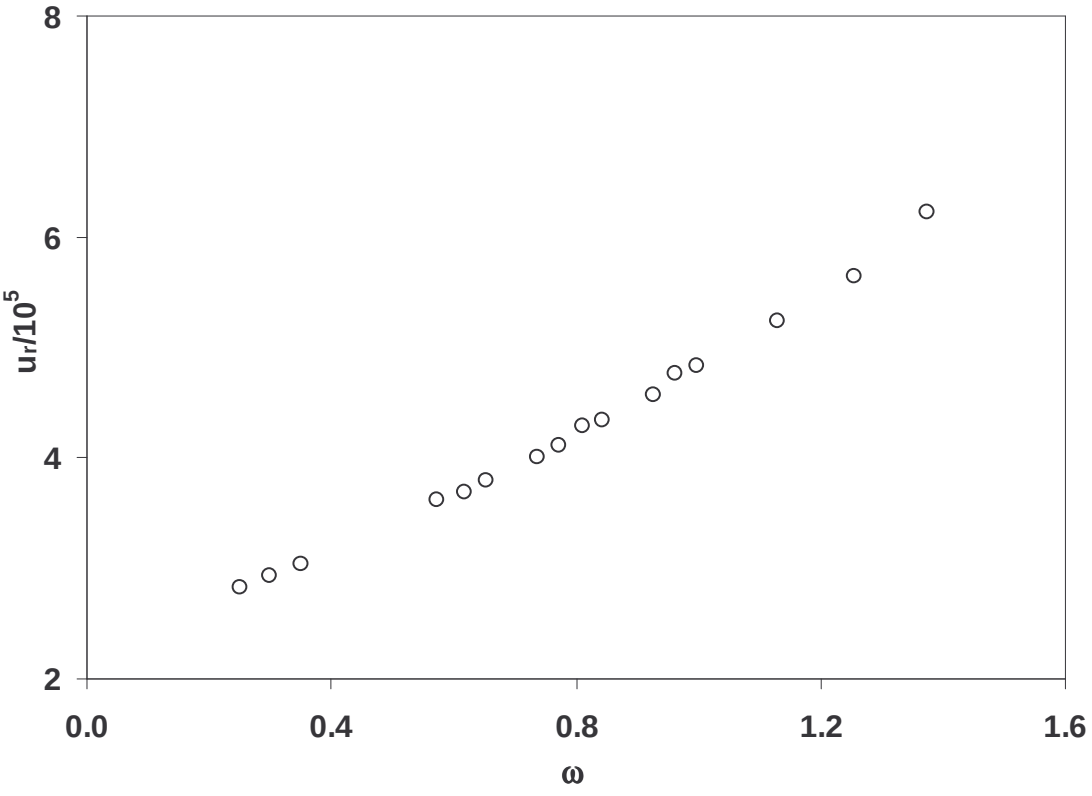

Figure III. 6: Reduced speed of sound as a function of the acentric factor (ω) at T_r=0.5.

For vapor pressures, viscosities, thermal conductivities and liquid densities the experimental information presented on the DIPPR database (1998) was selected. The reported correlations were used when reliable and enough experimental information was available. For some of the components, the correlating parameters were refitted to assure a good data description in the full range of temperatures used in this study, using the following equations, the same as those considered on the DIPPR database (1998):

$$P/bar = \exp\left(A + B/T + C \times \ln T + D \times T^{E}\right) \times 1.0 \times 10^{-5} \quad \text{(III. 9)}$$

$$\eta/mPa.s = \exp\left(A + B/T + C \times \ln T + D \times T^{E}\right) \times 10^{3} \quad \text{(III. 10)}$$

$$\rho/mol.cm^{-3} = \frac{A}{10^{3} \times B^{\left[1+\left(1-T/C\right)^{D}\right]}} \quad \text{(III. 11)}$$

$$\lambda/W.m^{-1}.K^{-1} = A + B \times T + C \times T^{2} \quad \text{(III. 12)}$$

Speeds of sound used to plot Figure III. 6 were obtained from Dutour (2000), who presented a considerable amount of data in broad temperature and pressure ranges for n-alkanes between n-C_6H_{14} and n-$C_{36}H_{74}$,. The correlating equations used to estimate the data were the following, where the pressure was set to 1 MPa while plotting Figure III. 6:

$$u/m.s^{-1} = \sqrt{\frac{E + F \times P}{A + B \times P + C \times P^{2} + D \times P^{3}}}$$

$$E = 1 + E_1 \times T$$

$$A = A_0 + A_1 \times T + A_2 \times T^{2} + A_3 \times T^{3} \quad \text{(III. 13)}$$

where T is the absolute temperature (K), P is the pressure (MPa) and A-F are correlating parameters.

In the following of this section, results will be concentrated on liquid densities and viscosities, and liquid-vapor interfacial tensions. Table III. 1 presents the studied n-alkanes for each property.

A collection of reduced temperatures covering a broad range of the liquid region was selected for evaluation, starting at T_r=0.45, close to the triple point of methane, and ending at T_r=0.75. The higher limit for the reduced temperature was established to avoid the extrapolation to higher temperatures of the correlating equations.

Table III. 1: Studied n-alkanes

Property	**n in C_nH_{2n+2}**
Vapor pressure	1:18, 20, 24, 26, 28, 32, 36
Liquid density	1:20, 22, 24, 26, 28, 32, 36
Surface tension	1:10, 12:14, 16:20, 26,32
Viscosity	1:20, 23, 24, 26, 28, 32, 36

Liquid density (ρ/mol.m^{-3}), viscosity (η/mPa.s) and surface tension (γ/mN.m^{-1}) are reduced using the following equations:

$$\rho_r = V_c \times \rho \qquad \text{(III. 14)}$$

$$\eta_r = \frac{\eta \times V_c^{2/3}}{MW^{1/2} \times T_c^{1/2}} \qquad \text{(III. 15)}$$

$$\gamma_r = \gamma \times \frac{V_c^{2/3}}{T_c} \qquad \text{(III. 16)}$$

where T_c ,V_c and MW are the critical temperature, K, critical volume, cm^3·mol^{-1}, and molecular weight, g·mol^{-1}. Another reducing equation for viscosity, involving the critical pressure instead of the critical volume, can also be used (Ely *et al*., 1981; Lee *et al*., 1993), but our studies showed that it did not improve the results. The literature also displays diverse ways to reduce interfacial tension: Rice *et al.* (1982) used the critical volume and

critical temperature (as in Eq. III.16), while Zuo *et al*. (1996) and Brock *et al.* (1955) used the critical pressure and critical temperature, respectively Eqs. III.17 and III.18.

$$\gamma_r = \ln\left(\frac{\gamma}{P_c^{2/3}T_c^{1/3}} + 1\right) \qquad \text{(III. 17)}$$

$$\gamma_r = \frac{\gamma}{P_c^{2/3}T_c^{1/3}} \qquad \text{(III. 18)}$$

Both equations were plotted as a function of the acentric factor for the n-alkane series with similar results to those presented in Figure III. 3.

Pressure is reduced using the following equation:

$$P_r = \frac{P}{P_c} \qquad \text{(III. 19)}$$

and the natural logarithm of P_r was taken as X_r in Eqs. III.5-III.7.

Experimental critical properties were collected from the literature, when available (Ambrose *et al.*, 1995). Correlations were considered for those n-alkanes for which there were no experimental information. Critical temperature was calculated from the correlation of Tsonopoulos (1987), critical pressure from that of Magoulas *et al.* (1990), critical volume from Marano *et al.* (1997a) and the Pitzer acentric factor from Han *et al.* (1993), as discussed during Part II.

Although it would be theoretically possible to choose the same reference system to evaluate all properties, a small error in one or more of the reference fluids could mislead the results. Because of that, and in order to compare Eqs. III.5 and III.6, reference systems were selected for each property and model, so the smallest overall deviation was obtained.

These reference systems are presented in Table III. 2 and the corresponding correlating coefficients to be used with Eqs. III.8-III.11 are reported in Table III. 3.

Table III. 2: **Selected reference systems**

Property	**Reference system**	
	Linear model	**2nd order perturbation**
Vapor pressure	n-C_4H_{10} / n-$C_{12}H_{26}$	n-CH_4 / n-C_9H_{20} / n-$C_{26}H_{54}$
Liquid density	n-C_4H_{10} / n-$C_{12}H_{26}$	n-CH_4 / n-$C_{15}H_{32}$ / n-$C_{26}H_{54}$
Surface tension	n-C_2H_6/ n-$C_{12}H_{26}$	n-C_6H_6 / n-$C_{14}H_{30}$ / n-$C_{26}H_{54}$
Viscosity	n-C_2H_6 / n-$C_{15}H_{32}$	n-C_2H_6 / n-C_8H_{18} / n-$C_{18}H_{38}$

Table III. 3 Correlating coefficients of the reference fluids to be used with Eqs. III.8- III.11

n-*alkane*	**Property**	**Correlation coefficients**				
		A	**B**	**C**	**D**	**E**
CH_4	Liq. density	2.9214	0.28976	190.56	0.28881	
	Vap. pressure	39.205	-1324.40	-3.4366	3.102×10^{-5}	2.0
n-C_2H_6	Viscosity	-7.0046	276.380	-0.6087	3.111×10^{-18}	7.0
	Surface tension	49.957	1.22351			
n-C_4H_{10}	Liq. density	1.0677	0.27188	425.12	0.28688	
	Vap. pressure	66.343	-4363.20	-7.0460	9.451×10^{-6}	2.0
n-C_8H_{18}	Viscosity	-7.7310	979.376	-0.5460		
n-$C_{12}H_{26}$	Liq. density	0.3554	0.25551	658.00	0.29368	
	Vap. pressure	137.47	-11976.0	-16.698	8.091×10^{-6}	2.0
	Surface tension	55.459	1.32596			
n-$C_{14}H_{30}$	Surface tension	56.494	1.36894			
n-$C_{15}H_{32}$	Liq. density	0.2844	0.25269	708.00	0.30786	
	Vap. pressure	135.57	-13478.0	-16.022	5.614×10^{-6}	2.0
	Viscosity	-2.9196	1196.57	-1.2470		
n-$C_{18}H_{38}$	Viscosity	-2.3884	1280.02	-1.3112		
n-$C_{26}H_{54}$	Liq. density	0.1624	0.24689	819.00	0.34102	
	Vap. pressure	155.64	-20116.0	-17.616	2.673×10^{-18}	6.0
	Surface tension	56.273	1.38709			

It should be noted that with the 2nd order perturbation model (Eq. III.6) methane can be used as the first reference fluid while the choice of a heavier member is required for the

Teja approach (Eq. III.5). Basically, the 2nd order perturbation uses a lighter, an intermediate and a heavier member to represent the entire series.

Figures III.1-III.4, showing the reduced properties as a function of the acentric factor at a reduced temperature of 0.5, clearly evidence that a linear perturbation cannot describe the behavior of the heavier n-alkanes. The introduction of a second order perturbation is required for an adequate description of the properties of heavy n-alkanes.

Results are presented in Table III. 4 as a function of reduced temperature only. No pressure effects were considered. This table shows how the introduction of the second order term of the Taylor series expansion improves the prediction of the reduced properties at all the studied reduced temperatures. The average improvements over the linear approach are 32% for liquid density, 33% for vapour pressure and 56% for viscosity. Surface tension results are not presented in this table, since for most of the n-alkanes for which there are experimental data, only a narrow temperature range was available. Above n-$C_{16}H_{34}$, data was only found up to $T_r = 0.55$.

Table III. 4: Percent average absolute deviation of the linear and 2nd order models as a function of reduced temperature

T_r	% AAD of the reduced property					
	Liquid density		Vapor pressure		Viscosity	
	linear	2nd order	linear	2nd order	linear	2nd order
0.45	0.66	0.50	1.29	0.87	11.19	4.47
0.50	0.63	0.47	1.01	0.59	8.18	3.69
0.55	0.62	0.44	0.82	0.42	6.63	3.11
0.60	0.63	0.42	0.67	0.36	5.97	2.34
0.65	0.65	0.39	0.56	0.42	5.86	2.09
0.70	0.68	0.40	0.52	0.44	6.12	2.54
0.75	0.71	0.45	0.57	0.55	6.62	3.79
Average	0.65	0.44	0.78	0.52	7.22	3.15

Some trends in the deviations with reduced temperature reported in Table III. 4 can be ascribed to uncertainties propagating from the experimental measurements to the reference fluid correlating equations. Measurements at higher temperatures are typically more

uncertain, and properties such as vapour pressure and viscosity often present greater uncertainty at low temperatures due to the difficulties in measuring smaller vapour pressures and the sharp increase of viscosity with the proximity of the melting point.

Figures III.7 – III.12 illustrate the percent average deviation of the estimated reduced properties as a function of the chain length of the n-alkane. It can be seen that the linear approach proposed by Teja and co-workers has some limitations for the heavier n-alkanes and that the average deviation decreases considerably around the reference fluid, confirming that this model is not able to predict the trend in the reduced property, as shown before on Figures III.1 – III.4.

In both models the highest deviations are found for the lowest and highest reduced temperatures, except for viscosity where the highest deviations are mainly from the lowest reduced temperature. As mentioned before, this should be the result of the higher uncertainties in the corresponding experimental measurements, coupled with the smaller amount of data usually found in these regions that can make the correlating equations less accurate in these zones.

The 2nd order perturbation model shows a more random distribution of the deviations. Some higher values can be observed for liquid density and vapour pressure for the heavier members of the series, but still the deviations are smaller than those from the linear approach.

From Figures III.1 – III.12 and Table III. 4 it can thus be concluded that if the evaluation of all the series of the n-alkanes using the linear perturbation model is required we should use, at least, two sets of reference systems. Using the new 2nd order perturbation just one reference system is enough.

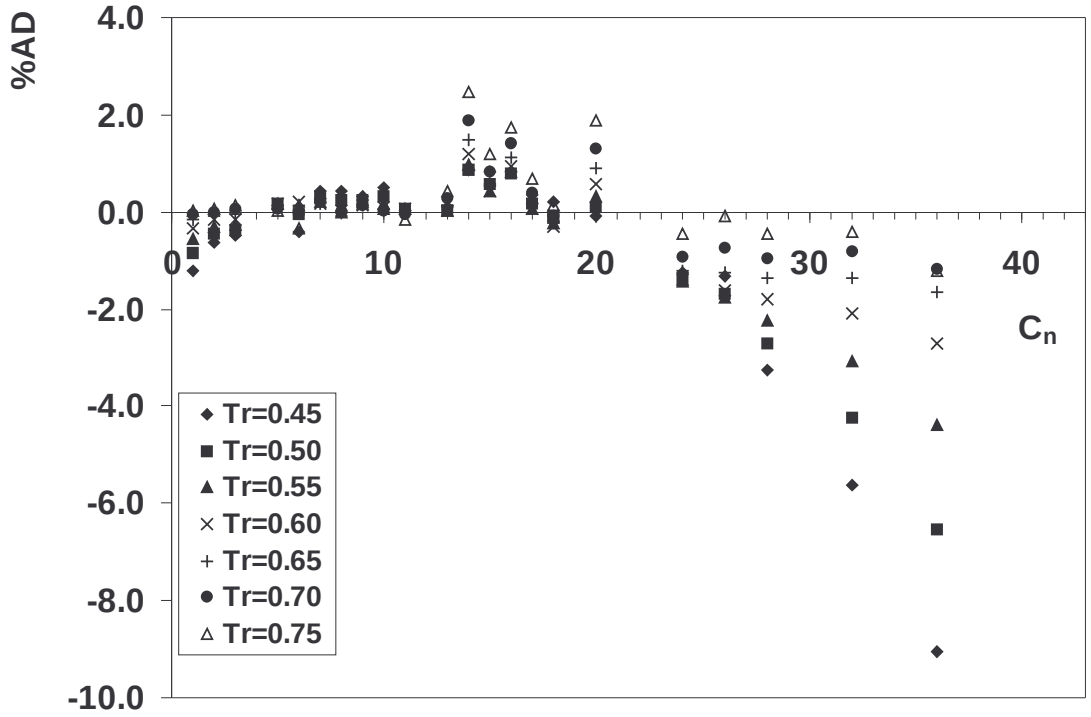

Figure III. 7: **Average deviation of the reduced vapor pressure predicted with the linear perturbation model as a function of the chain length of the n-alkane.**

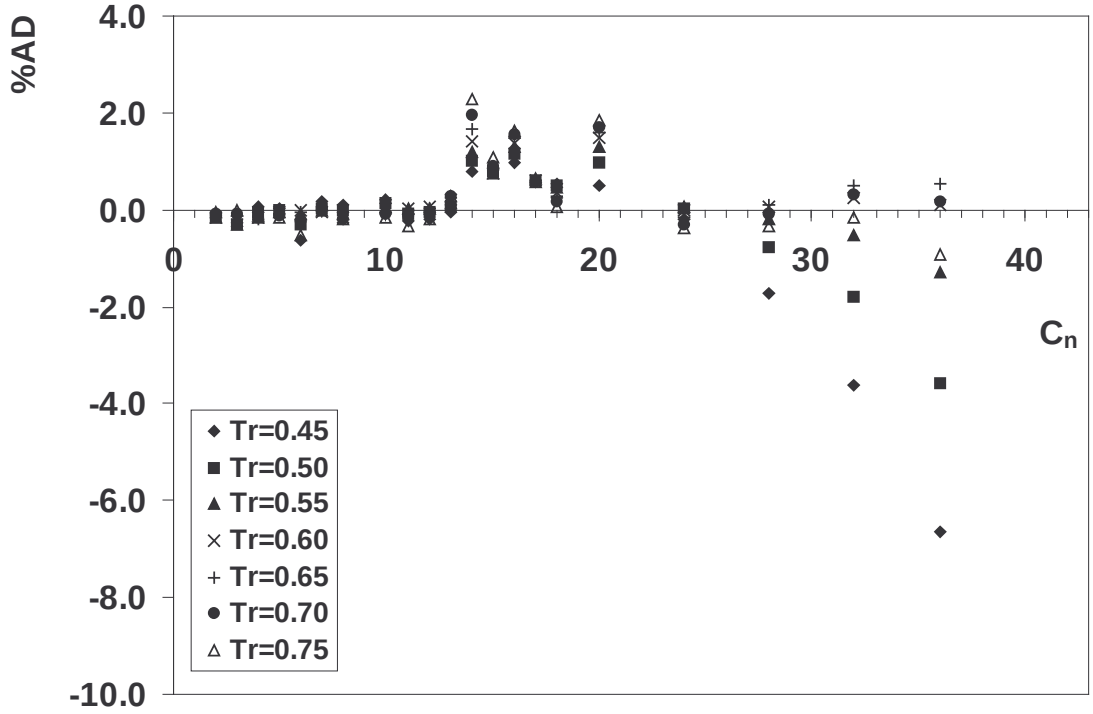

Figure III. 8: **Average deviation of the reduced vapor pressure predicted with the 2nd order perturbation model as a function of the chain length of the n-alkane.**

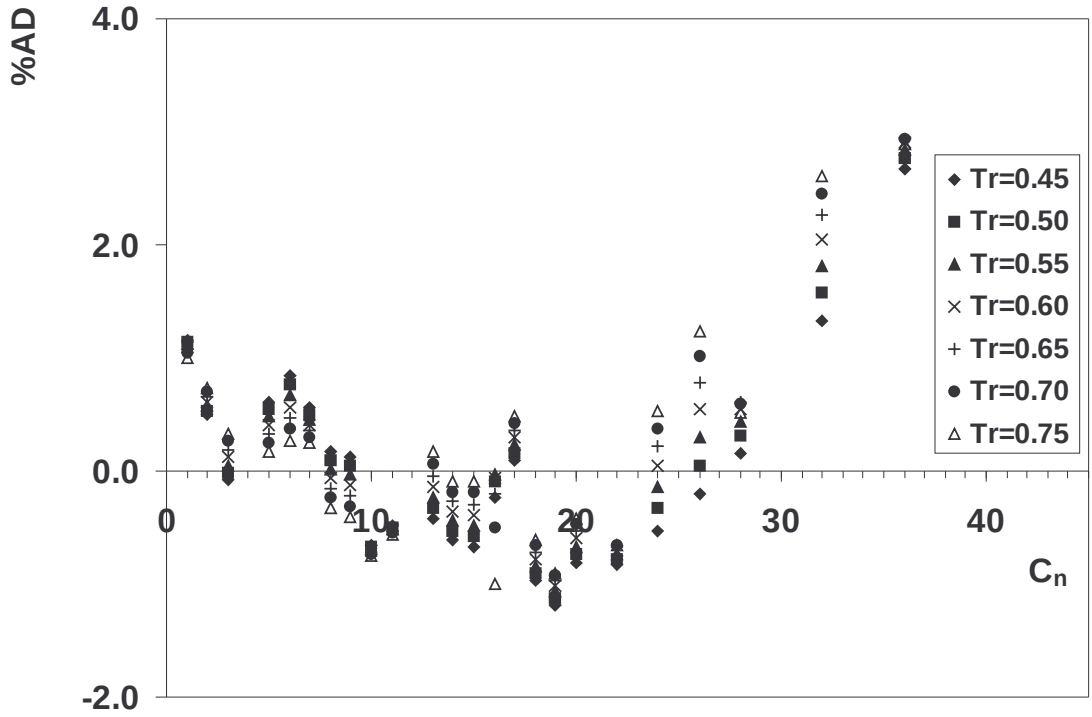

Figure III. 9: **Average deviation of the reduced liquid density predicted with the linear perturbation model as a function of the chain length of the n-alkane.**

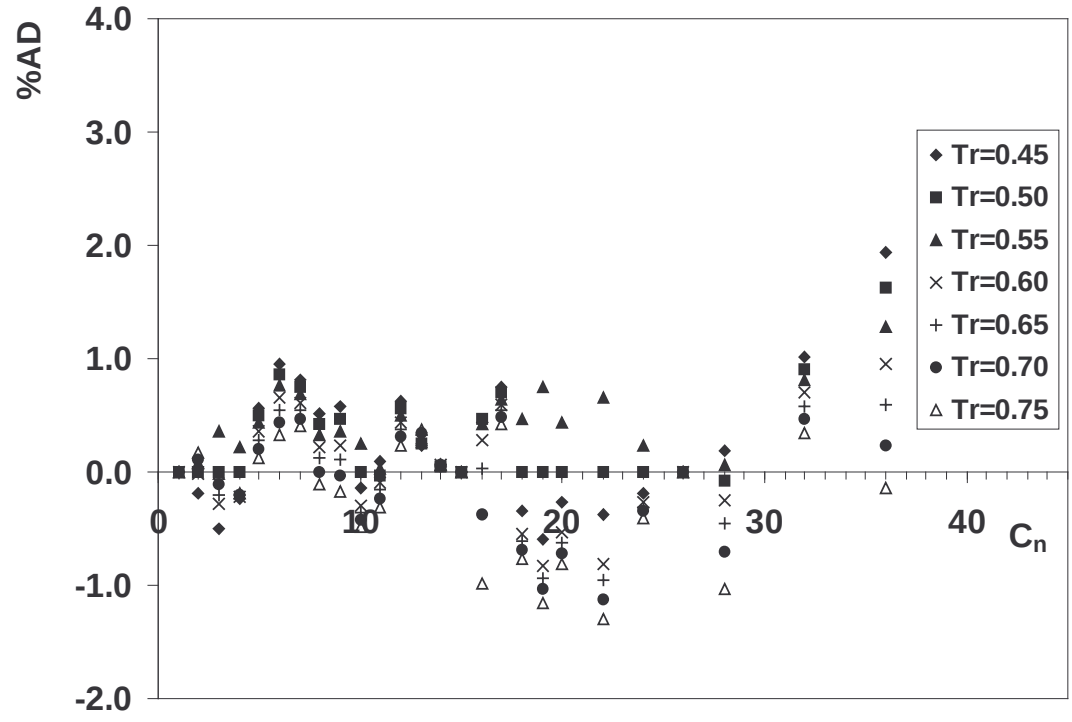

Figure III. 10: **Average deviation of the reduced liquid density predicted with the second-order perturbation model as a function of the chain length of the n-alkane.**

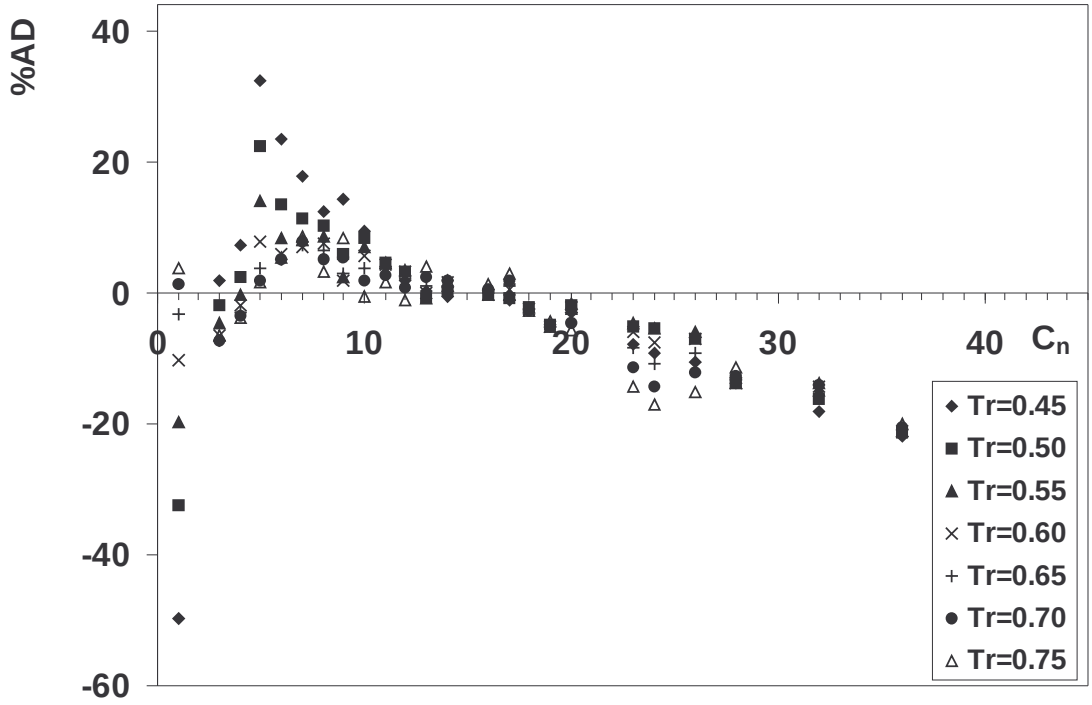

Figure III. 11: **Average deviation of the reduced viscosity predicted with the linear perturbation model as a function of the chain length of the n-alkane.**

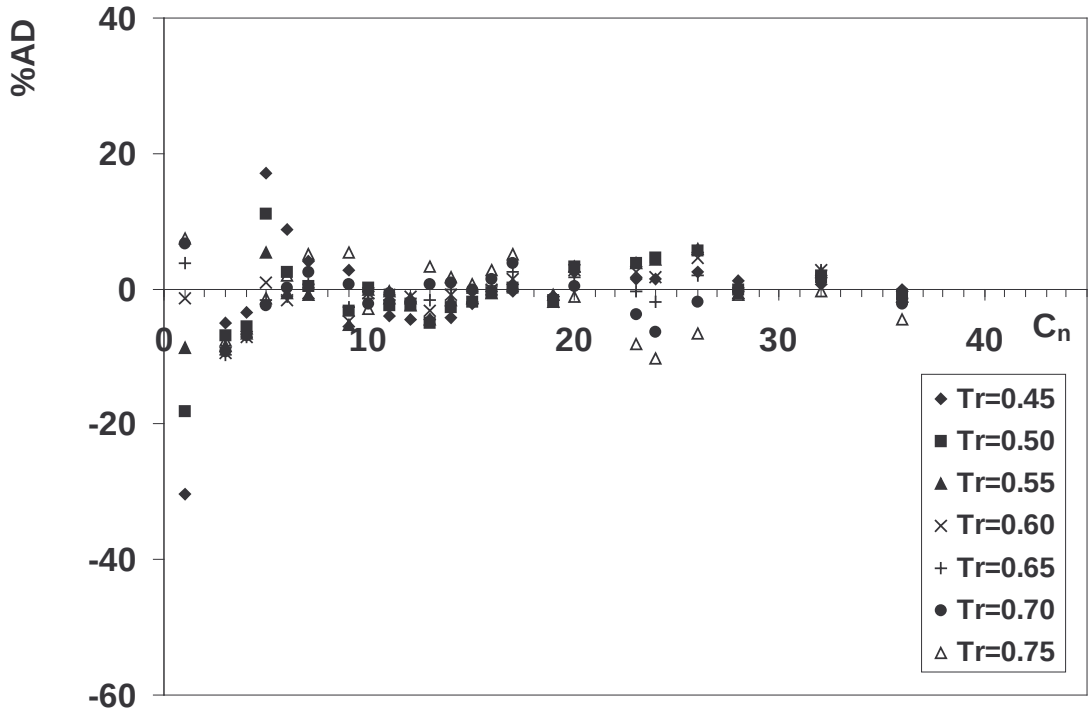

Figure III. 12: **Average deviation of the reduced viscosity predicted with the 2nd order perturbation model as a function of the chain length of the n-alkane.**

The proposed model, Eq.III.6, was tested for 320 surface tension values for the n-alkanes and resulted in an average absolute deviation (AAD) of 1.14% (Table III. 5 and Figure III. 13). It can clearly been seen that this new model is able to describe both lighter and heavier n-alkanes in a broad temperature range.

Table III. 5: Evaluation of the 2º order perturbation model for surface tension

n-*alkane*	**AAD (%)**	**nº of points**	**T range/K**
n-C_2H_6	0.96	23	129.2-273.50
n-C_3H_6	2.94	22	202.15-312.6
n-C_4H_{10}	4.60	20	238.0-318.5
n-C_5H_{12}	1.47	18	144.8-407.25
n-C_7H_{16}	0.53	26	183.21-459.18
n-C_8H_{18}	1.53	20	218.51-501.27
n-C_9H_{20}	0.31	13	273.15-393.15
n-$C_{10}H_{22}$	0.33	13	273.15-393.15
n-$C_{12}H_{26}$	0.22	13	273.15-393.15
n-$C_{13}H_{28}$	0.23	13	273.15-393.15
n-$C_{14}H_{30}$	0.20	12	283.15-393.15
n-$C_{16}H_{34}$	0.98	11	293.15-393.15
n-$C_{17}H_{36}$	0.76	10	303.15-393.15
n-$C_{18}H_{38}$	0.21	10	303.15-393.15
n-$C_{19}H_{40}$	1.24	11	293.15-393.15
n-$C_{20}H_{42}$	0.19	11	293.15-393.15
n-$C_{26}H_{54}$	2.73	11	343.15-453.15
n-$C_{32}H_{66}$	2.26	11	346.35-422.45
n-$C_{60}H_{122}$	5.48	7	383.15-453.15

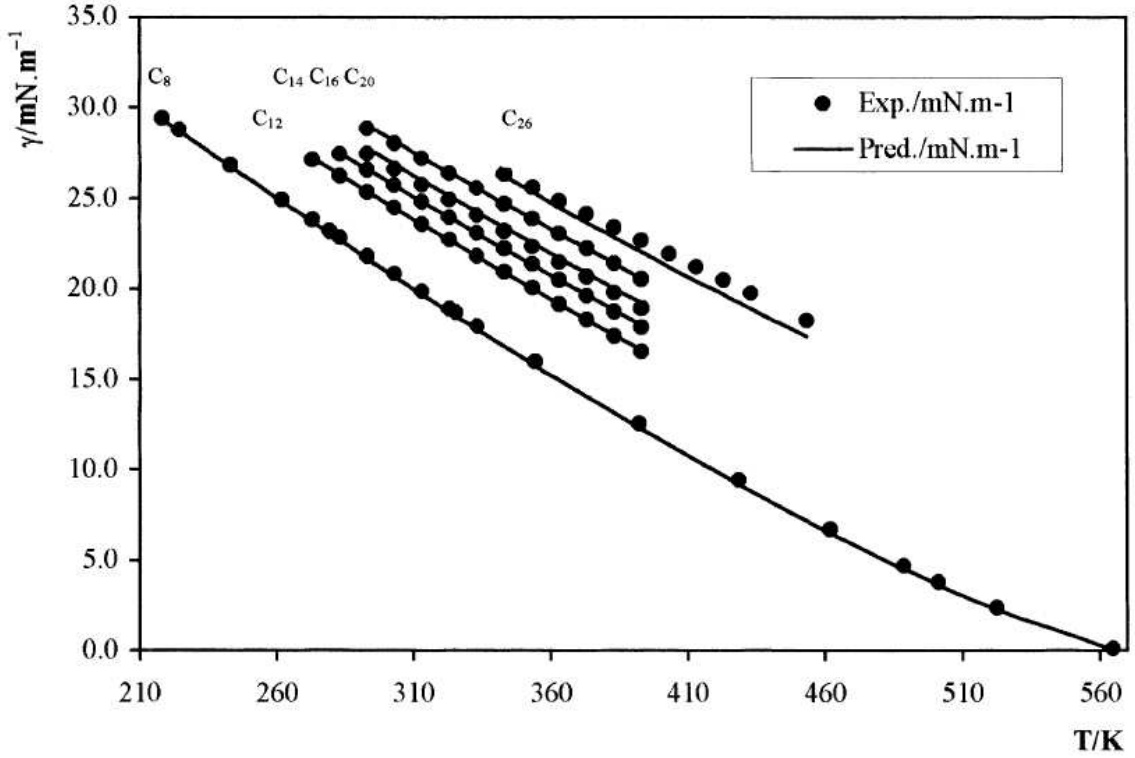

Figure III. 13: Comparison of experimental and predicted surface tension for n-alkanes-2nd order perturbation model.

As mentioned before, to extend the corresponding states theory to a broader range of fluids, additional characterization parameters need to be introduced. Two main approaches have been applied in this parameterization: the first performs a multi-parameter Taylor's series expansion of the property of interest about the parameters, as has been seen above; the second approach is to extend the simple two-parameter corresponding states principle at its molecular origin. This is accomplished by making the intermolecular potential parameters functions of the additional characterization parameters and the thermodynamic state, e.g. the temperature, with the end result being a corresponding states model that has the same mathematical form as the simple two-parameter model, but with more complex definitions of the dimensionless volume and temperature, involving the so-called *shape factors*. This is usually called the *Extended Corresponding States Theory* (Ely *et al.*, 2000). In the remaining of this section, this approach will be evaluated for liquid-vapor interfacial tensions.

In the extended corresponding states theory, the surface tension of the target fluid is calculated from a single reference fluid using the following equation:

$$\gamma_j = \frac{f_j}{h_j^{2/3}} \times \gamma_0(T_{rj} / \theta) \qquad \text{(III. 20)}$$

where h_j and f_j are the equivalent substance reducing ratios and θ and ϕ the energy and volume shape factors, respectively. The relationship between these quantities is given by:

$$V = V_0\ h_j = V_0 \frac{V_{jc}}{V_{0c}} \phi \qquad T = T_0\ f_j = T_0 \frac{T_{jc}}{T_{0c}} \theta \qquad \text{(III. 21)}$$

The shape factors are weak functions of the reduced temperature and, in principle, of the reduced density. They are evaluated by solving simultaneously any two equations relating the thermophysical property of the target and the reference fluid. Normally the compressibility factor and the Helmholtz energy are used. Several review papers have been published focusing on this approach and the most extensive are those of Leland and Chappelear (1968), Rowlinson *et al.* (1969) and Mentzer *et al*. (1980).

In order to apply this theory to evaluate surface tension, Murad (1983) calculated shape factors by the simultaneous solution of the reduced compressibility factors and the reduced surface tensions. The values of these shape factors were then fitted to functions of the temperature and density, using the formulae proposed by Leach *et al*. (1968).

This procedure has the disadvantage of yielding shape factors that are not the same of those obtained by solving the compressibility factor and the Helmholtz energy. Since, theoretically, these shape factors should be the same, recalculation of these shape factors showed that this difference is essentially due to the lack of accuracy of the reference fluid data available at the time. Another weak point of the model proposed by Murad is the fixed reference fluid, methane, which does not allow an accurate mapping for heavy n-alkanes.

Following Cullick *et al.* (1982), Marrucho *et al.* (1998) proposed a new predictive method for the determination of the shape factors along the saturation boundary. Using the Frost-Kalkwarf-Thodos equation to describe the saturation pressure and the Rackett equation (Rackett, 1970) for the saturated liquid density, the expressions for the shape factors are:

$$\theta = \frac{1 - C_{r0} + 2\left(1 - T_{rj}\right)^{2/7} \ln\left(Z_{cj} / Z_{c0}\right) - \Delta B_r + \Delta C_r \ln T_{rj} + B_{rj} / T_{rj}}{1 - C_{r0} + B_{r0} / T_{rj}} \qquad \text{(III. 22)}$$

$$\phi = \frac{\left(Z_{cj}\right)^{\left(1-T_{rj}\right)^{2/7}}}{\left(Z_{c0}\right)^{\left(1-T_{rj}/\theta\right)^{2/7}}} \qquad \text{(III. 23)}$$

where:

$$B_r = -6.207612 - 15.37641\,\omega - 0.574946 \times 10^{-\omega} \qquad \text{(III. 24)}$$

$$C_r = 8/3 + 9B_r / (5 \ln 10) \qquad \text{(III. 25)}$$

$$\Delta B_r = B_{rj} - B_{r0} \qquad \text{(III. 26)}$$

$$\Delta Cr = C_{rj} - C_{r0} \qquad \text{(III. 27)}$$

This is a predictive approach if vapor pressure and liquid density data are available, but Z_c and the exponent in the Rackett equation can be treated as adjustable parameters, and B_r and C_r can be found by a correlation scheme.

The surface tension values calculated using the shape factors from Eqs. III.22 and III.23, for several n-alkanes, C_2H_6-$C_{20}H_{42}$, $C_{26}H_{54}$ and $C_{32}H_{66}$ are compared with experimental results in Table III. 6 and Figure III. 14. An average absolute deviation of 3.7% was obtained. The selected reference fluids were n-pentane for the range C_2H_6-C_7H_{16}, n-decane for C_8H_{18}-$C_{12}H_{26}$ and $C_{15}H_{32}$ for those n-alkanes with more than 12 carbon atoms. Surface tension for n-hexacontane was not predicted due to the lack of a

suitable reference fluid. Some deviations were found for the first elements of the series, but it should be kept in mind that experimental data for some fluids, like propane and n-butane, presents scatter.

When using this approach, special care should also be presented in the choice of the reference fluid. The ideal reference fluid should be structurally similar to the target fluid and have a broad temperature range of surface tension experimental values.

Table III. 6: Evaluation of the new predictive ECST model for surface tension

Substance	AAD(%)	nº of points	T range/K
n-C_2H_6	5.9	23	129.2-273.50
n-C_3H_8	6.7	22	202.15-312.6
n-C_4H_{10}	9.0	20	238.0-318.5
n-C_5H_{12}	1.7	21	175.12-447.13
n-C_6H_{14}	3.5	26	183.21-459.18
n-C_8H_{18}	3.8	20	218.51-501.27
n-C_9H_{20}	0.6	13	273.15-393.15
n-$C_{10}H_{22}$	0.5	13	273.15-393.15
n-$C_{12}H_{26}$	2.6	13	273.15-393.15
n-$C_{13}H_{28}$	1.5	13	273.15-393.15
n-$C_{14}H_{30}$	0.3	12	283.15-393.15
n-$C_{16}H_{34}$	1.7	11	293.15-393.15
n-$C_{17}H_{36}$	1.4	10	303.15-393.15
n-$C_{18}H_{38}$	1.0	10	303.15-393.15
n-$C_{19}H_{40}$	1.7	11	293.15-393.15
n-$C_{20}H_{42}$	5.7	11	293.15-393.15
n-$C_{26}H_{54}$	6.6	11	343.15-453.15
n-$C_{32}H_{66}$	13.0	11	346.35-422.45

The two proposed models, the Taylor series expansion (Eq. III.6) and the shape factor model (Eq. III.20), are compared with each other for n-heptane in Figure III. 15. It can be observed that first yields better predictions than the shape factors model. This fact is mainly due to the larger number of reference fluids used in the first model.

The extended corresponding states model is particularly useful when not more than one reference fluid is available, but if the reference fluid is not similar to the evaluating fluid, larger deviations can occur.

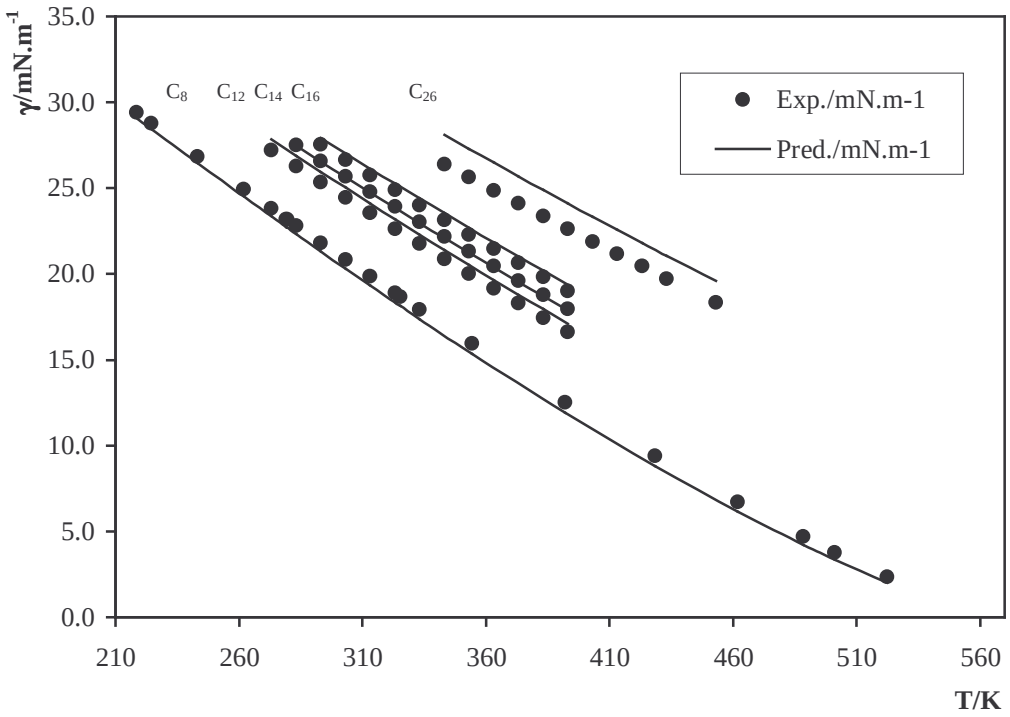

Figure III. 14: **Comparison of experimental and predicted surface tension for n-alkanes- ECST model.**

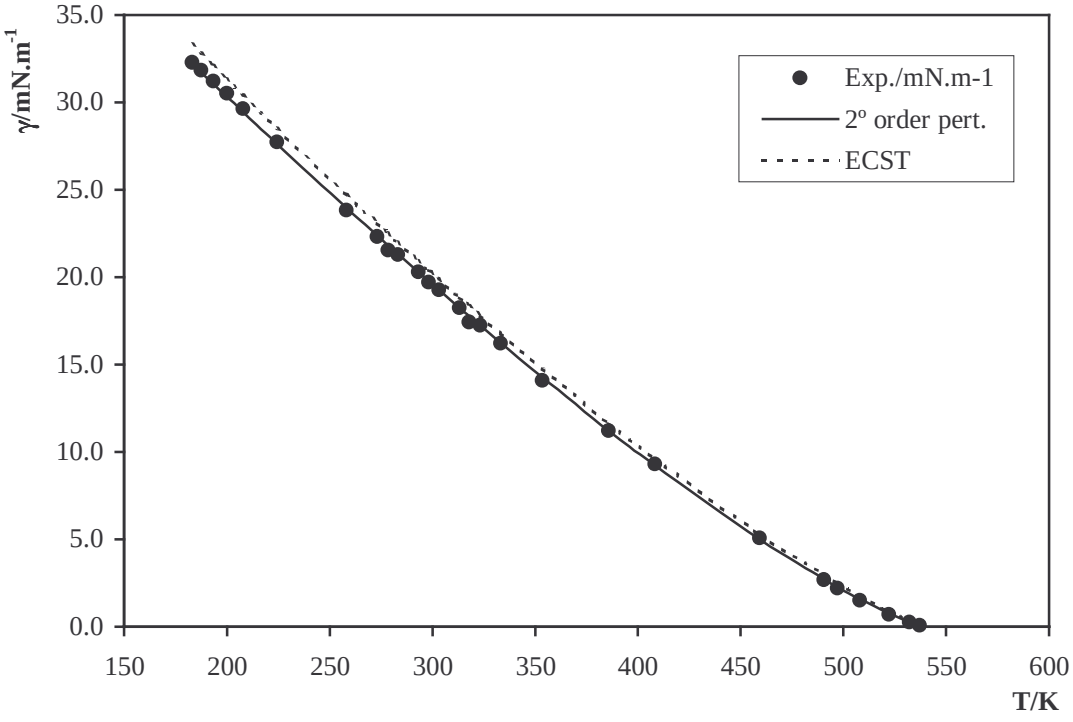

Figure III. 15: **Graphical presentation of experimental and predicted values of surface tension of n-heptane using the new predictions.**

III.2.2. Simple Mixtures

Mixtures were evaluated with the second order perturbation model (Eq. III.6) using the *one-fluid theory* with the following mixing and combining rules for the pseudocritical parameters:

$$\omega_m = \sum_i x_i \omega_i \qquad \text{(III. 28)}$$

$$V_{cm} = \sum_i \sum_k x_i x_k V_{cik} \qquad \text{(III. 29)}$$

$$T_{cm} V_{cm} = \sum_i \sum_k x_i x_k T_{cik} V_{cik} \qquad \text{(III. 30)}$$

$$V_{cik} = \frac{1}{8}\left(V_{ci}^{\frac{1}{3}} + V_{ck}^{\frac{1}{3}}\right)^3 \qquad \text{(III. 31)}$$

$$T_{cik} = \sqrt{T_{ci} T_{ck}} \left(\frac{\sqrt{V_{ci} V_{ck}}}{V_{cik}} \right)^{\left(\frac{n}{3}\right)-1} \qquad \text{(III. 32)}$$

In the above equations indexes *i* and *k* represent pure components and *x* mole fraction. For the use with Eqs. III.28 - III.32, experimental critical properties were collected from the literature, when available and correlations were considered for those n-alkanes for which there were no experimental information, as presented in section II.2.

Following Coutinho *et al.* (2000) a more general combining rule for the cross-critical temperature, T_{cik}, was adopted (Eq. III.32). It was shown that for phase equilibrium calculations, this combining rule progressively deteriorates with component asymmetry, with the value of *n* approaching 3 for extremely asymmetric systems, such as those involving some polymer solutions.

Other combining rules can be derived from this expression setting different values of the parameter *n*. Setting *n* = 3, one obtains the geometric combining rule. Plocker *et al.* (1978) used n = 3.75 for calculating vapor-liquid equilibria of asymmetric systems. Other

values of *n* between 3 and 7.5 can also be found (Coutinho *et al.*, 2000). The *n* parameter can thus be fitted or used as variable with the system asymmetry, and thus no binary interaction parameters are required while using this approach.

The optimum values of *n* to be used with Eq. III.32 were estimated from the data measured in this work and data from literature for binary systems

The following objective function was used within a least-squares fit:

$$Fobj = \left\{ \left(X_{m,\exp} - \sum_i x_i \times X_{i,\exp} \right) - \left(X_{m,\mathrm{mod}\,el} - \sum_i x_i \times X_{i,\mathrm{mod}\,el} \right) \right\} \qquad \text{(III. 33)}$$

where subscript *m* denotes mixture and *exp* experimental value.

While using this objective function, we consider that our model returns the correct values for the pure components and that only the curvature of the property *vs.* composition has to be corrected.

For surface tension an *n* value of 4.6 was obtained from this overall fit.

To show how this model can represent mixture data using a small amount of experimental information, n-heptane, n-decane and n-eicosane were selected as reference fluids, and only the measurements reported in I.2.1, taken in a small reduced temperature range, were selected. For each reference fluid, surface tension was fitted to a two-parameter equation (Eq. III.8).

Deviations presented by this model for the surface tension of 18 binary and 2 ternary n-alkane mixtures are compared on Table III. 7 using n = 4.6 and n = 6.0 in Eq. III.32. As can be seen, for low asymmetries the best choice is to use n = 6.0, while for the most asymmetric mixtures, deviations can be reduced to half of its value if we select n = 4.6.

A comparison between the model using n = 4.6 and experimental data reported in this work is shown on Figs. III.16 – III.21. An average absolute deviation of 1.1 % was found against the mixture data points. Using n = 6 in Eq. III.32, an average absolute deviation about 80 % higher is obtained.

With respect to the comparison between the binary n-heptane + n-docosane and the ternary n-heptane + n-eicosane + n-tetracosane, very small deviations are observed using this model, in agreement with the experimental results. Binary data calculated from the model are, in average, 0.3 % higher than that of the ternary mixture. Similar results can be obtained from the experimental values, as was noted in I.2.1.

Results show that using only 4 to 8 pure component surface tension values from each reference fluid, one is able to estimate all the corresponding mixture data with a very small deviation. These results clearly show that the proposed model is adequate to the liquid-vapor surface tension modeling of hydrocarbon mixtures.

Table III. 7: Estimation of the surface tension of n-alkane mixtures for different values of n (Eq. III.32) with the corresponding states model

Mixture	Reference	*% AAD*	
		***n* = 6.0**	***n* = 4.6**
$n\text{-}C_6H_{14} + n\text{-}C_8H_{18}$	a	1.49	1.57
$n\text{-}C_7H_{16} + n\text{-}C_{10}H_{22}$	b	0.73	0.57
$n\text{-}C_6H_{14} + n\text{-}C_{10}H_{22}$	c	0.80	1.28
$n\text{-}C_{16}H_{34} + n\text{-}C_{20}H_{42}$	b	0.52	0.52
$n\text{-}C_{16}H_{34} + n\text{-}C_{20}H_{42}$	d	1.36	1.44
$n\text{-}C_{16}H_{34} + n\text{-}C_{22}H_{46}$	d	0.80	0.92
$n\text{-}C_8H_{18} + n\text{-}C_{14}H_{30}$	a	2.52	2.93
$n\text{-}C_{10}H_{22} + n\text{-}C_{16}H_{34}$	b	0.50	0.48
$n\text{-}C_{10}H_{22} + n\text{-}C_{16}H_{34}$	c	0.82	1.19
$n\text{-}C_6H_{14} + n\text{-}C_{14}H_{30}$	a	3.43	4.48
$n\text{-}C_7H_{16} + n\text{-}C_{16}H_{34}$	b	0.65	0.82
$n\text{-}C_7H_{16} + n\text{-}C_{16}H_{34}$	e	1.33	2.12
Average		1.25	1.53
	Asymmetric systems		
$n\text{-}C_7H_{16} + n\text{-}C_{20}H_{42}$	*this work*	0.86	0.82
$n\text{-}C_7H_{16} + n\text{-}C_{22}H_{46}$	*this work*	1.78	1.01
$n\text{-}C_7H_{16} + n\text{-}C_{24}H_{50}$	*this work*	2.95	1.50
$n\text{-}C_7H_{16} + n\text{-}C_{20}H_{42} + n\text{-}C_{24}H_{50}$	*this work*	2.11	1.07
$n\text{-}C_{10}H_{22} + n\text{-}C_{20}H_{42}$	*this work*	1.22	0.57
$n\text{-}C_{10}H_{22} + n\text{-}C_{22}H_{46}$	*this work*	2.15	1.38
$n\text{-}C_{10}H_{22} + n\text{-}C_{24}H_{50}$	*this work*	2.86	1.70
$n\text{-}C_{10}H_{22} + n\text{-}C_{20}H_{42} + n\text{-}C_{24}H_{50}$	*this work*	1.45	0.59
Average (asymmetric systems)		1.92	1.08

a – Pugachevich *et al.*, 1980 b – Rolo *et al.*, 2002 c – Pandey *et al.*, 1982

d – Águila-Hernandez, 1987 e – Koefoed *et al.*, 1958

In Table III. 8 and Figure III. 21 it is shown how this simple model can return liquid density estimates that deviate from the experimental data as much as different sets of data deviate between themselves. The previously suggested reference system n-CH_4+n-$C_{15}H_{32}$+n-$C_{26}H_{54}$ was selected to obtain the reported results, using n=6 in Eq. III.32. As can be seen from the results, no need for further model refinement is required, and the model can be kept predictive. For the viscosity modelling of the reported asymmetric systems, an optimised n value is essential to reduce the absolute percent deviations below 10 %, but no need for system dependent n-values was found. Using n= -1.5, very good viscosity estimates were obtained, as reported on Table III. 8 and Figure III. 22, for the binary n-$C_{10}H_{22}$ + n-$C_{20}H_{42}$. Although typical n-values are in the range 3-7.5 (Coutinho *et al.*, 2000), viscosity modeling using corresponding states theory with the one-fluid concept presents several simplifications, particularly for asymmetric mixtures, as discussed by Ely *et al.* (1981). Therefore, the optimized value of n=-1.5 accounts for these simplifications, and should thus be considered as a fitting parameter. Only binary mixture data was used for the optimization. The previously suggested viscosity reference system, n-C_2H_6+n-C_8H_{18}+n-$C_{18}H_{38}$ was selected to obtain the reported results.

Table III. 8: Modeling results with the new CS model

System	**%AAD**		
	Liquid density	**viscosity**	**surface tension**
n-C_7H_{16} + n- $C_{20}H_{42}$	1.0	3.3	0.8
n-C_7H_{16} + n- $C_{22}H_{46}$	1.5	6.3	1.0
n-C_7H_{16} + n- $C_{24}H_{50}$	1.2	6.5	1.5
n-C_7H_{16} + n-$C_{20}H_{42}$ + n-$C_{24}H_{50}$	1.2	5.0	1.1
n-$C_{10}H_{22}$ + n- $C_{20}H_{42}$	0.1	2.3	0.6
n-$C_{10}H_{22}$ + n- $C_{22}H_{46}$	0.2	3.3	1.4
n-$C_{10}H_{22}$ + n- $C_{24}H_{50}$	0.2	7.9	1.7
n-$C_{10}H_{22}$ + n-$C_{20}H_{42}$ + n- $C_{24}H_{50}$	0.2	2.7	0.6
Average	0.7	4.7	1.1

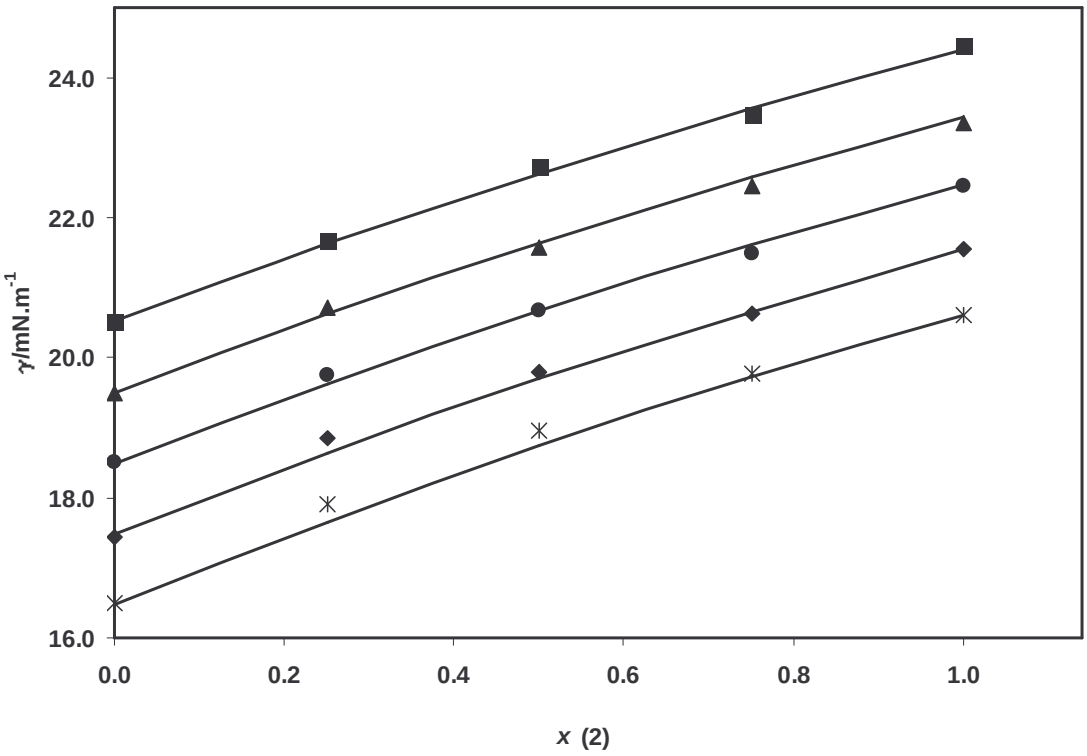

Figure III. 16: **Surface tension of n-C_7H_{16} (1) + n-$C_{10}H_{22}$ (2). ■, 293.15 K; ▲, 303.15 K; ●, 313.15 K; u , 323.15 K; *, 333.15 K; –, model.**

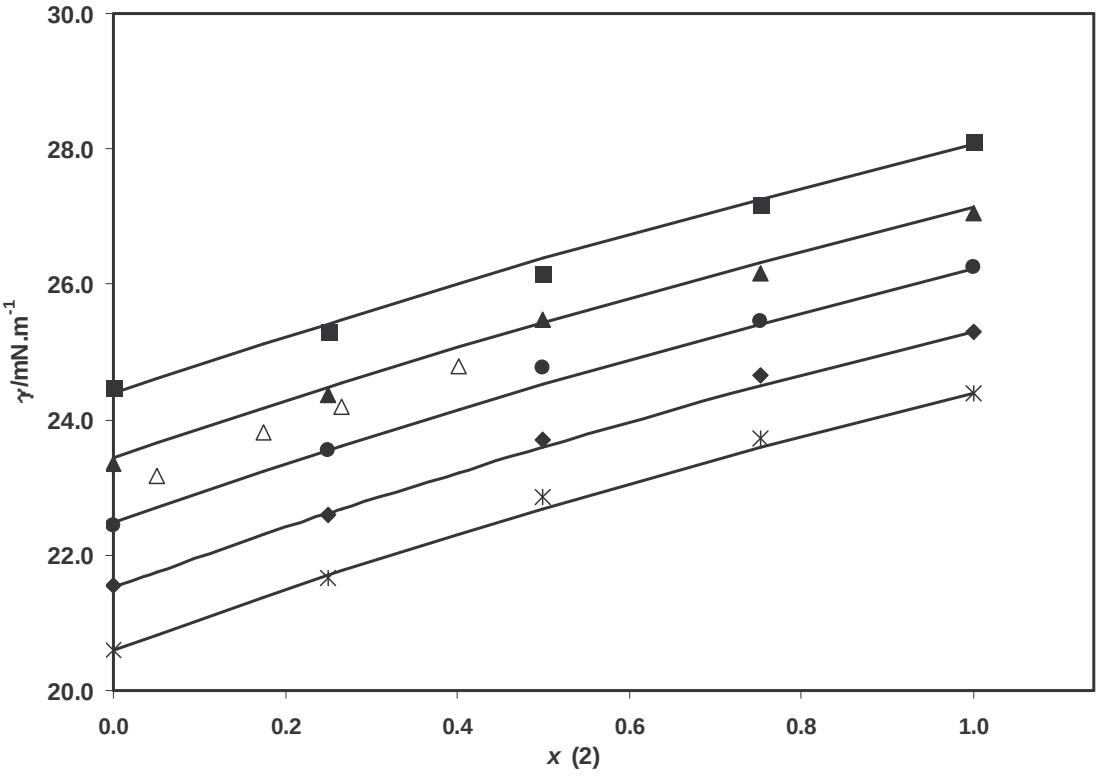

Figure III. 17: **Surface tension of n- $C_{10}H_{22}$ (1) + n-$C_{16}H_{34}$ (2). ■, 293.15 K; ▲, 303.15 K; ●, 313.15 K; u , 323.15 K; *, 333.15 K; Δ, Pandey *et al.*, 1982, 303.16 K; –, model.**

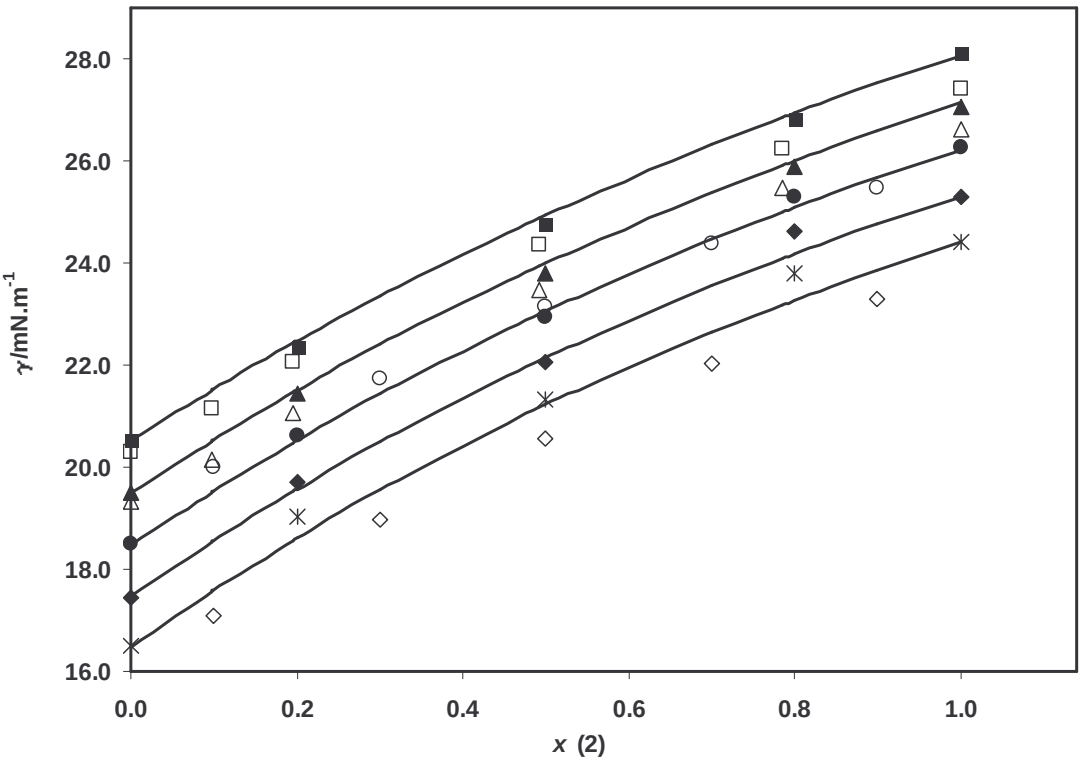

Figure III. 18: **Surface tension of n- C_7H_{16} (1) + n-$C_{16}H_{34}$ (2). ■, 293.15 K; ▲, 303.15 K; ●, 313.15 K; ∪ , 323.15 K; *, 333.15 K; □, 293.15 K - Koefoed *et al.*, 1958; Δ, 303.15 K - Koefoed *et al.*, 1958; ○, 303.15 K - Pugachevich *et al.*, 1979; ◊, 333.15 K - Pugachevich *et al.*, 1979; –, model.**

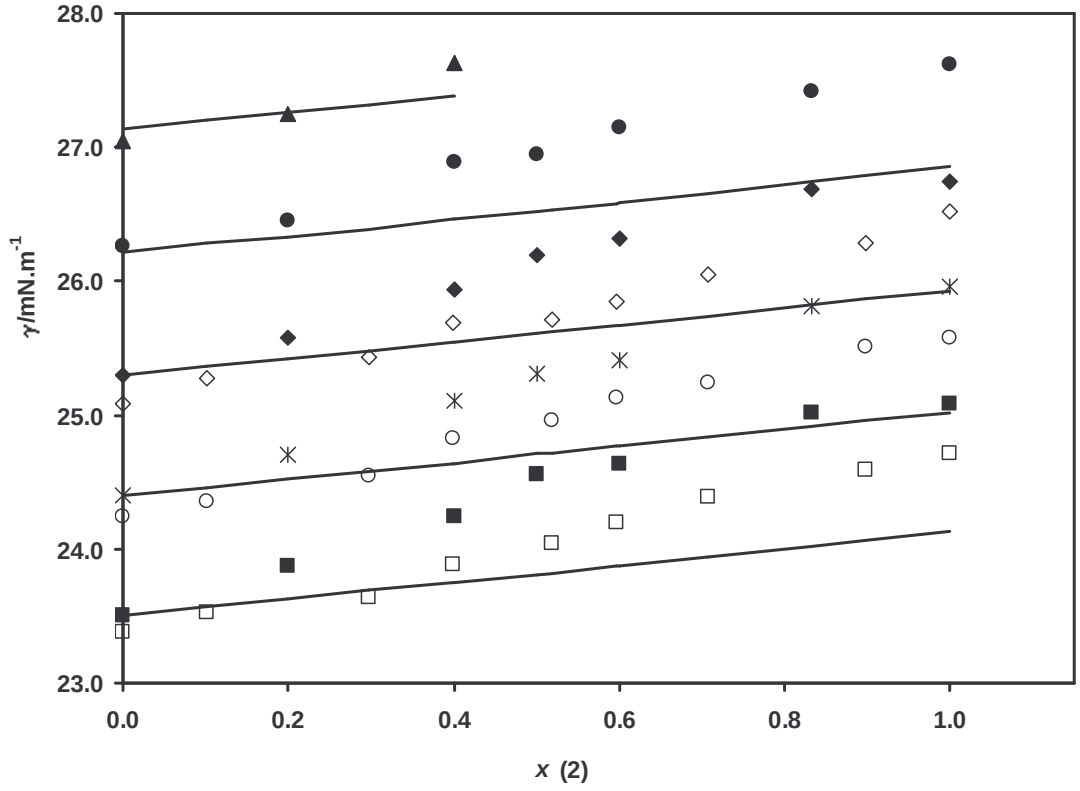

Figure III. 19: **Surface tension of n- $C_{16}H_{34}$ (1) + n-$C_{20}H_{42}$ (2). ▲, 303.15 K; ●, 313.15 K; ∪ , 323.15 K; *, 333.15 K; ■, 343.15 K; ◊, 323.15 K – Águila-Hernandez, 1987; ○, 333.15 K - Águila-Hernandez, 1987; □, 343.15 K - Águila-Hernandez, 1987; –, model.**

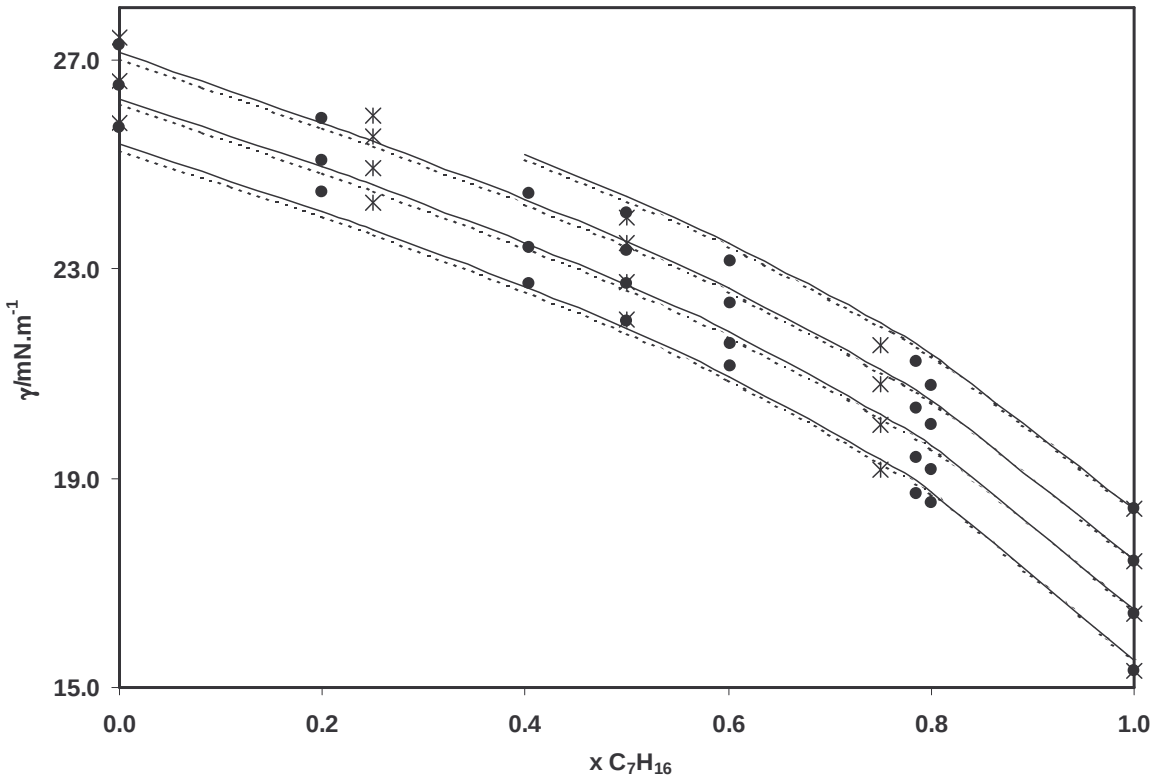

Figure III. 20: **Surface tension of (*), n- C_7H_{16} (1) + n-$C_{24}H_{50}$ (2), (o), n- C_7H_{16} (1) + n-$C_{20}H_{42}$ (2) + n-$C_{24}H_{50}$ (3). –, model.**

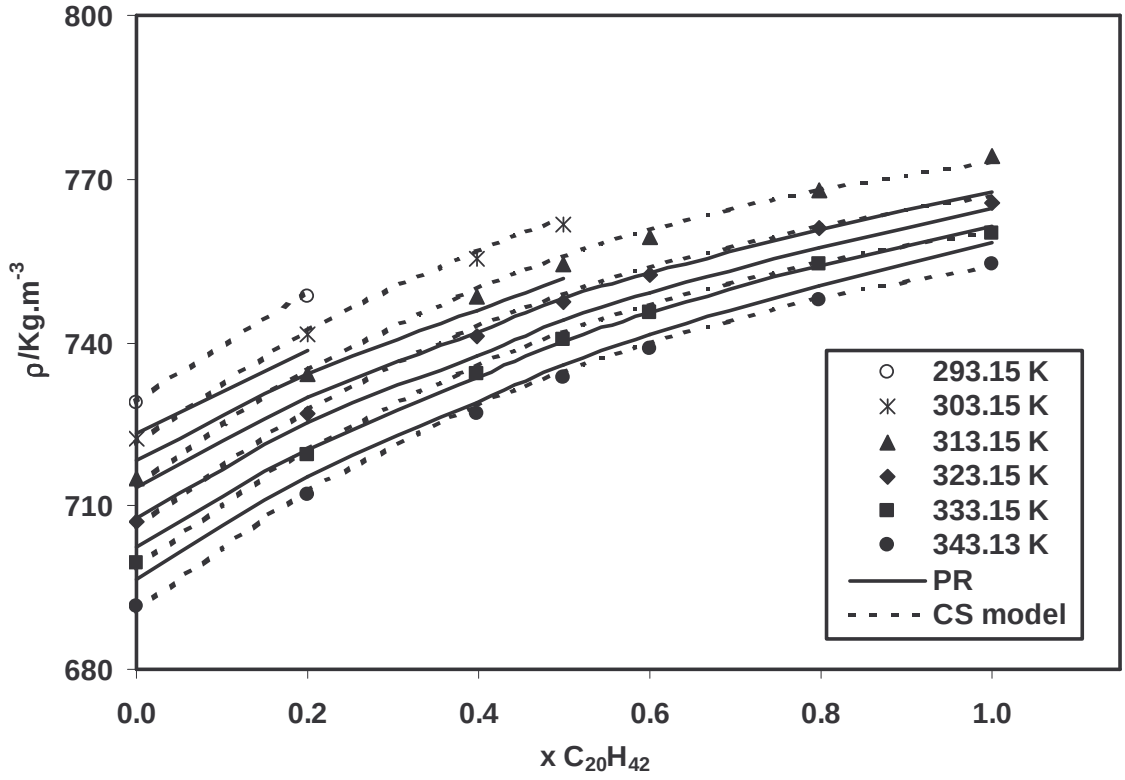

Figure III. 21: **Liquid density of the binary mixture n-$C_{10}H_{22}$ + n-$C_{20}H_{42}$. Experimental results and model predictions.**

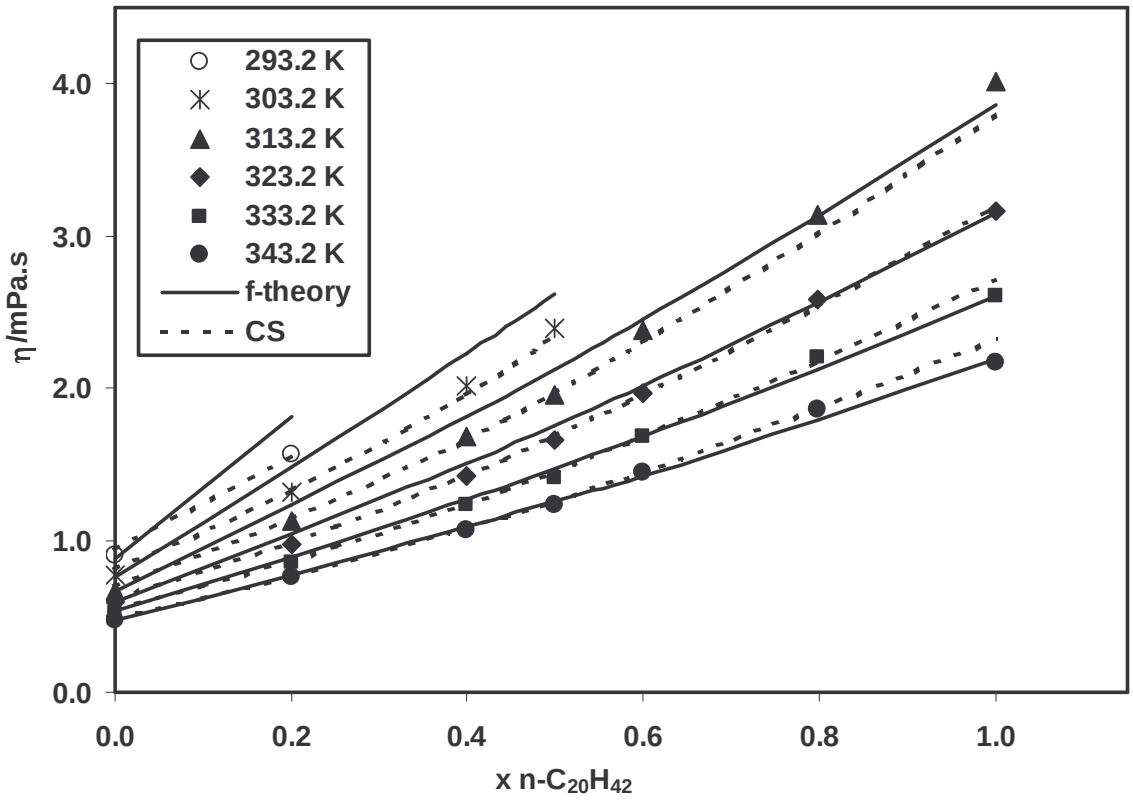

Figure III. 22: **Viscosity of the binary mixture n-$C_{10}H_{22}$ + n-$C_{20}H_{42}$. Experimental results and model predictions.**

"God does not care about our mathematical difficulties. He integrates empirically."

Albert Einstein (1879-1955), Physicist

The gradient theory of fluid interfaces was combined with the Cubic-Plus-Association equation of state (CPA), taking advantage of the correct representation of interfacial tensions provided by the gradient theory and the excellent phase equilibrium of water and hydrocarbons obtained from CPA.

Studies involving the vapor-liquid interfacial tensions of some selected associating and non-associating pure components (water, ethanol, n-butane, n-pentane, n-hexane, n-heptane) are presented and discussed.

A correlation for the influence parameter is presented from which surface tensions can be obtained in a broad temperature range with average errors smaller than 1%.

III.3. Gradient Theory of Fluid Interfaces

Although very powerful for the description of interfacial tensions and density profiles across the interface, the gradient theory has not been widely used. Most of the proposed applications are limited to the liquid-vapor interface of some polar and non-polar fluids and simple mixtures (Miqueu, 2001; Zuo *et al.*, 1997, 1998; Cornelisse *et al*., 1996; Miqueu *et al*. 2003, 2004; Kahl *et al.*, 2000, 2002). Few authors (Zuo *et al.*, 1998; Kahl *et al.*, 2000, 2002) have attempted to model liquid-liquid interfaces and only recently (Kahl *et al.*, 2002) an associating EOS was used for addressing liquid-liquid systems containing associating components.

Since the gradient theory is based on the knowledge of the equilibrium phase densities and the Helmholtz free energy density calculated from an equation of state, an association state-of-the-art thermodynamic model, the CPA-EOS, which combines a physical contribution from a cubic EOS with an association contribution derived from Wertheim theory, will be used. This EOS has already shown to be an accurate model to describe the VLE and LLE of mixtures containing water, alkanes and alcohols (Kontogeorgis *et al*., 1996, 1999; Yakoumis *et al*., 1998; Derawi, 2002; Voutsas, 2000; Wu and Prausnitz, 1998). Particularly for water-alkane systems CPA is actually the only model that provides acceptable results for both the solubility of water in the hydrocarbon-phase and the hydrocarbon solubility in the aqueous phase (Yakoumis *et al*., 1998; Voutsas *et al*., 2000).

For the non-associating components chosen for evaluation, two cubic equations of state (EOS), the Soave-Redlich-Kwong (SRK) (Soave,1972) and the Peng-Robinson (PR) (Peng and Robinson, 1974) were selected for comparison with the CPA equation of state.

Gradient theory

The gradient theory of fluid interfaces originated from the work of van der Waals, but only after Cahn and Hilliard (1958) found widespread use. Since 1958 it has been applied for the modeling of the liquid-vapor and liquid-liquid interfacial tension of different systems such as polar and non-polar fluids and some polymers. Recently, Miqueu generalized the gradient theory for multicomponent mixtures (Miqueu, 2001; Miqueu *et al*., 2004):

$$\sigma = \int_{\rho_N^{vap}}^{\rho_N^{liq}} \sqrt{2\Delta\Omega(\rho)\sum_i \sum_j c_{ij} \frac{d\rho_i}{d\rho_N}\frac{d\rho_j}{d\rho_N}}\, d\rho_N \qquad \text{(III. 34)}$$

$$\Delta\Omega(\rho) = \Omega(\rho) - p \qquad \text{(III. 35)}$$

where p is the equilibrium pressure (Pa), σ is the surface tension (N.m^{-1}), ρ^{liq} and ρ^{vap} are the liquid and vapor phase densities (mol.m^{-3}), subscript N stands for the mixture

reference component and c is the so-called influence parameter ($J.m^5.mol^{-2}$). Ω (ρ) is the grand thermodynamic potential defined as follows:

$$\Omega(\rho) = f_0(\rho) - \sum_i \rho_i \mu_i \qquad \text{(III. 36)}$$

where $f_o(\rho)$ is the Helmholtz free energy density of the homogeneous fluid, at local composition ρ, and μ_i are the pure-component chemical potentials.

The pure-component influence parameter, c_{ii}, has a theoretical definition, that can hardly be implemented. For practical purposes, the influence parameter is adjusted from surface tension data (Miqueu, 2001; Zuo *et al.*, 1997, 1998; Cornelisse *et al*., 1996; Miqueu *et al*. 2003, 2004; Kahl *et al.*, 2000, 2002):

$$c_{ii} = \frac{1}{2}\left[\frac{\sigma_{exp}}{\int_{\rho^{vap}}^{\rho^{liq}} \sqrt{\Delta\Omega(\rho)}\, d\rho}\right]^2 \qquad \text{(III. 37)}$$

The influence parameter should diverge close to the critical point, where surface tension vanishes.

For mixtures, cross influence parameters, c_{ij}, are calculated from the pure component influence parameters using a geometric mean rule:

$$c_{ij} = \sqrt{c_{ii} c_{jj}} \qquad \text{(III. 38)}$$

CPA equation of state

Before using the gradient theory, it is necessary to determine the equilibrium densities of the coexisting phases, the chemical potentials and the Helmholtz free energy from an

adequate model. In this work, the Cubic Plus Association (CPA) equation of state was used for these purposes. CPA is an equation of state that combines a physical contribution accounting for physical forces and an association contribution accounting for hydrogen bonding and other chemical forces (Kontogeorgis *et al*., 1996, 1999; Yakoumis *et al*., 1998; Derawi, 2002; Voutsas, 2000; Wu and Prausnitz, 1998). Written in terms of the compressibility factor:

$$Z = Z^{phys.} + Z^{assoc.} \qquad \text{(III. 39)}$$

For the physical term the Soave-Redlich-Kwong (SRK) EOS is employed (Kontogeorgis *et al*., 1996, 1999; Yakoumis *et al*., 1998; Derawi, 2002; Voutsas, 2000):

$$Z^{phys} = Z^{SRK} = \frac{V}{V-b} - \frac{a}{RT(V+b)} \qquad \text{(III. 40)}$$

The energy parameter, *a*, can be calculated as a function of temperature (Eq. III.41), where a_0 and c_1, fitted from vapor pressures and liquid densities, are used instead of the critical constants, allowing for better liquid density estimates and thus, no further need for a volume correction. The co-volume, b, is simultaneously optimized with a_0 and c_1.

$$a = a_0 \left[1 + c_1 \times (1 - \sqrt{T_r}) \right]^2 \qquad \text{(III. 41)}$$

The association contribution in CPA is similar with that used in SAFT, written below using the Michelsen-Hendriks (2001) formalism:

$$Z^{assoc.} = -\frac{1}{2}\left(1 + \rho \frac{\partial \ln g}{\partial \rho}\right) \sum_i x_i \sum_{A_i} \left(1 - X_{A_i}\right) \qquad \text{(III. 42)}$$

where ρ is the density, g the radial distribution function, x_i the i[th] component mole fraction and X_{Ai} the mole fraction of component *i* not bonded at site A. For non-associating fluids, such as hydrocarbons, the association term disappears and CPA reduces to SRK.

A simplified version of the hard-sphere radial distribution function, proposed by Kontogeorgis *et al.* (1999) was employed:

$$g(\rho) = \frac{1}{1-1.9\eta}, \eta = \frac{1}{4}b\rho \qquad \text{(III. 43)}$$

and X_{Ai} was found by simultaneously solving the following set of equations, where *A* and *B* represent the different associating sites and subscripts *i* and *j* the different components:

$$X_{Ai} = \frac{1}{1+\rho\sum_j x_j \sum_{B_j} X_{B_j} \Delta^{A_i B_j}} \qquad \text{(III. 44)}$$

For water, the 4C association scheme was selected, in which it is consider that hydrogen bonding occurs between the two hydrogen atoms and the two lone pairs of electrons in the oxygen of the water molecules.

For the pure component, this results in the following X_A expression :

$$X_A = X_B = X_C = X_D = \frac{-1+\sqrt{1+8\rho\Delta^{AC}}}{4\rho\Delta^{AC}} \qquad \text{(III. 45)}$$

$$\Delta^{AA} = \Delta^{AB} = \Delta^{BB} = \Delta^{CC} = \Delta^{CD} = \Delta^{DD} = 0$$

$$\Delta^{AC} = \Delta^{AD} = \Delta^{BC} = \Delta^{BD} \neq 0 \qquad \text{(III. 46)}$$

where Δ^{AC} is the association strength between sites A and C on the associating molecule (self-association), given by the expression:

$$\Delta^{AC} = g(\rho)\left[\exp\left(\frac{\varepsilon^{AC}}{RT}\right)-1\right] b\beta^{AC} \qquad \text{(III. 47)}$$

ε^{AC} and β^{AC} are, respectively, the association energy and volume between sites A and C, and must be calculated together with the parameters of the physical part from experimental vapor pressures and liquid density data.

For ethanol, the 2B association scheme applies, where hydrogen bonding is considered between the hydroxyl hydrogen and one of the lone pairs of electrons from the oxygen atom in another alcohol molecule:

$$X_A = X_B = \frac{-1+\sqrt{1+4\rho\Delta^{AB}}}{2\rho\Delta^{AB}} \qquad \text{(III. 48)}$$

$$\Delta^{AA} = \Delta^{BB} = 0,\ \Delta^{AB} \neq 0 \qquad \text{(III. 49)}$$

Classical mixing rules are used in the physical contribution, while no mixing rules are required in the association term. Only combining rules are needed in the case of cross-associating systems.

To evaluate the performance of the combination of the gradient theory with the CPA EOS, a study was carried for some n-alkanes, an alcohol (ethanol) and water. For the n-alkanes, CPA is reduced to the physical contribution, thus allowing us to compare the results obtained from the physical term of CPA, where fitted *a* and *b* parameters are used (Table III. 9), with the results where the *a* and *b* expressions from SRK and PR are used. The required critical properties and acentric factors were collected from Ambrose (1995) and Magoulas and Tassios (1990) and are presented in Table II. 1.

Table III. 9: **CPA parameters for the pure components selected for this work (SI units)**

fluid	a_0	c_1	$b\times10^5$	ε	β
n-C_4H_{10}	1.3143	0.7077	7.21	-	-
n-C_5H_{12}	1.8198	0.7986	9.10	-	-
n-C_6H_{14}	2.3678	0.8308	10.79	-	-
n-C_7H_{16}	2.9178	0.9137	12.54	-	-
H_20	0.12277	0.6736	1.45	16655	0.0692
C_2H_5OH	0.86716	0.7369	4.91	21532	0.0080

Highly accurate data from the *NIST Chemistry WebBook* (http://www.webbookk.nist.gov/fluid) was selected to obtain the n-alkane data on vapor pressure, saturation liquid and vapor phase densities and surface tension along the saturation curve.

As can be seen from Table III. 10 and Figs III.23-III.24 very good vapor pressure and vapor density results are obtained from CPA for the selected n-alkanes. Higher deviations are obtained close to the critical point, as expected from a classical EOS (Voutsas *et al*., 2000). Still, results are better or similar to those obtained from the SRK or the PR EOS, as the equation of state parameters were fitted to the experimental liquid densities and vapor pressures. Considerable improvements can be found with CPA on the equilibrium liquid phase densities, as can be seen in Figure III. 24.

Limitations on the use of classical cubic EOS for the estimation of liquid phase densities are known, and a regular procedure to overcome this problem is to include a volume translation as suggested by Peneloux *et al*. (1982). This procedure was already used (Miqueu 2001; Miqueu *et al*., 2003, 2004) to obtain the correct liquid densities to use within the gradient theory. As shown in Table III. 10 and Figures III.23 – III.24, the use of fitted parameters to correlate a and b on the physical term of CPA allows the reproduction of both liquid and vapor phase properties with a good accuracy with no need for a volume translation.

For the associating components water and ethanol data was collected from the NIST Chemistry WebBook (water) and from the correlations presented by Dillon *et al.* (2003) and from the DIPPR database (ethanol). As can be seen from Figs III.25 – III.28 and Table III. 10, very good vapor pressure and equilibrium vapor and liquid phase densities are obtained both for water and ethanol.

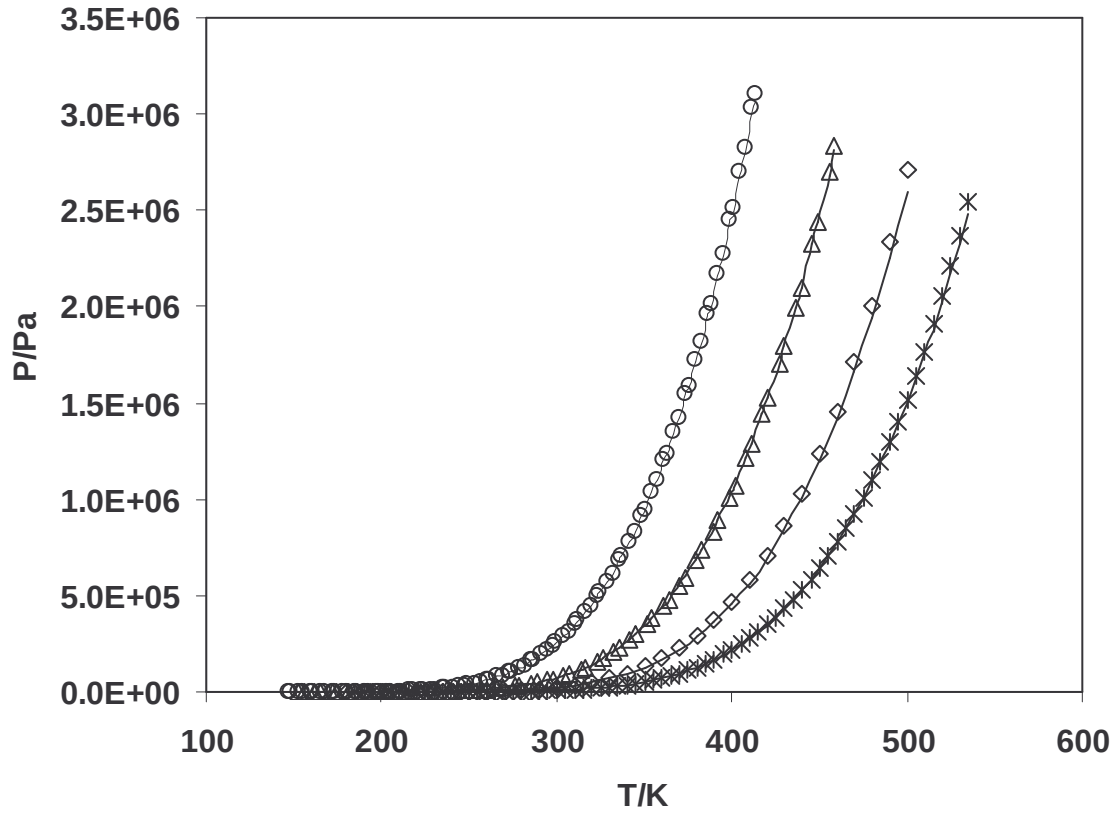

Figure III. 23: **n-alkane vapor pressures. Experimental (o, n-C_4H_{10}, Δ, n-C_5H_{12}, ◊, n-C_6H_{14}, x, n-C_7H_{16}) and CPA results (—).**

Table III. 10: Modeling results in the reduced pressure range $0.45 < T_r < 0.80$

Fluid	EOS	%AAD[a]			
		P	$\rho_{liq.}$	$\rho_{vap.}$	σ
C_4H_{10}	CPA	0.44	4.56	1.42	0.06
	SRK	1.82	7.20	2.00	0.14
	PR	1.27	4.84	1.40	0.16
C_5H_{12}	CPA	0.46	0.77	1.26	0.08
	SRK	1.87	9.15	2.09	0.20
	PR	1.69	2.59	1.91	1.21
C_6H_{14}	CPA	2.25	0.75	3.15	0.21
	SRK	1.46	10.9	1.77	0.31
	PR	2.25	0.81	2.48	0.20
C_7H_{16}	CPA	1.61	0.51	2.53	0.22
	SRK	1.49	12.3	1.92	0.20
	PR	2.50	1.03	2.84	0.29
H_2O	CPA	0.73	0.82	1.72	0.27
C_2H_5OH	CPA	1.39	0.43	1.10	0.24

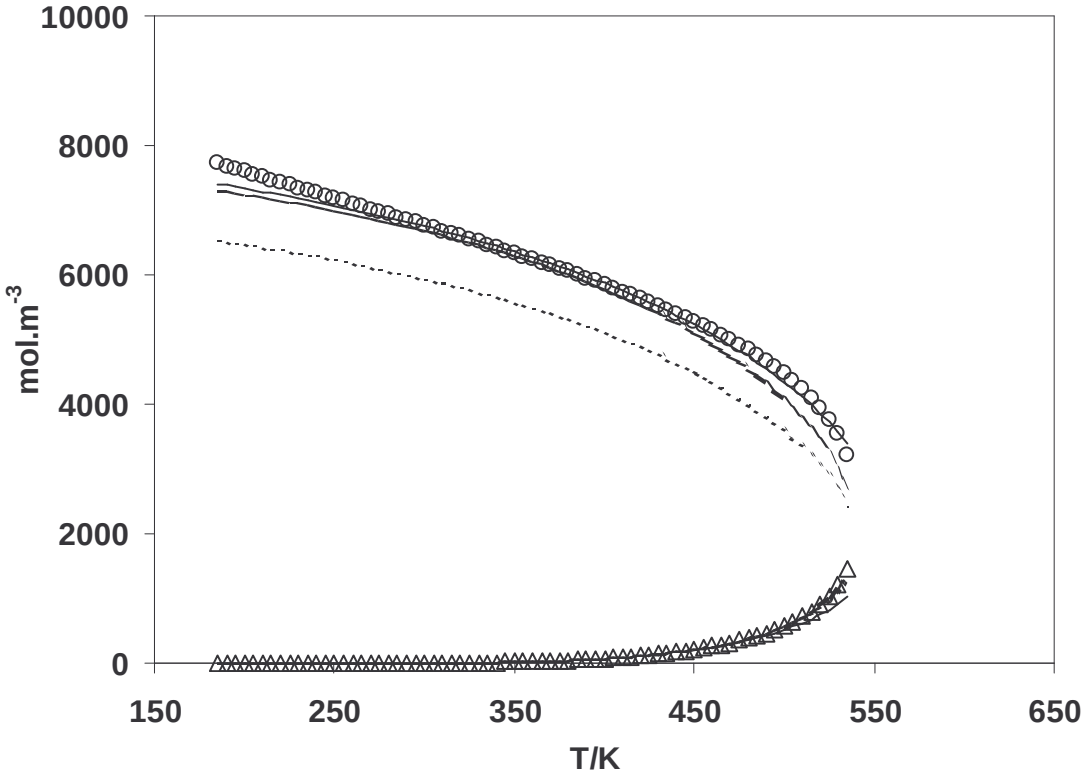

Figure III. 24: **n-heptane saturation densities. Experimental (o, liquid, Δ, vapor), CPA (—), SRK (--) and PR (– —) estimates.**

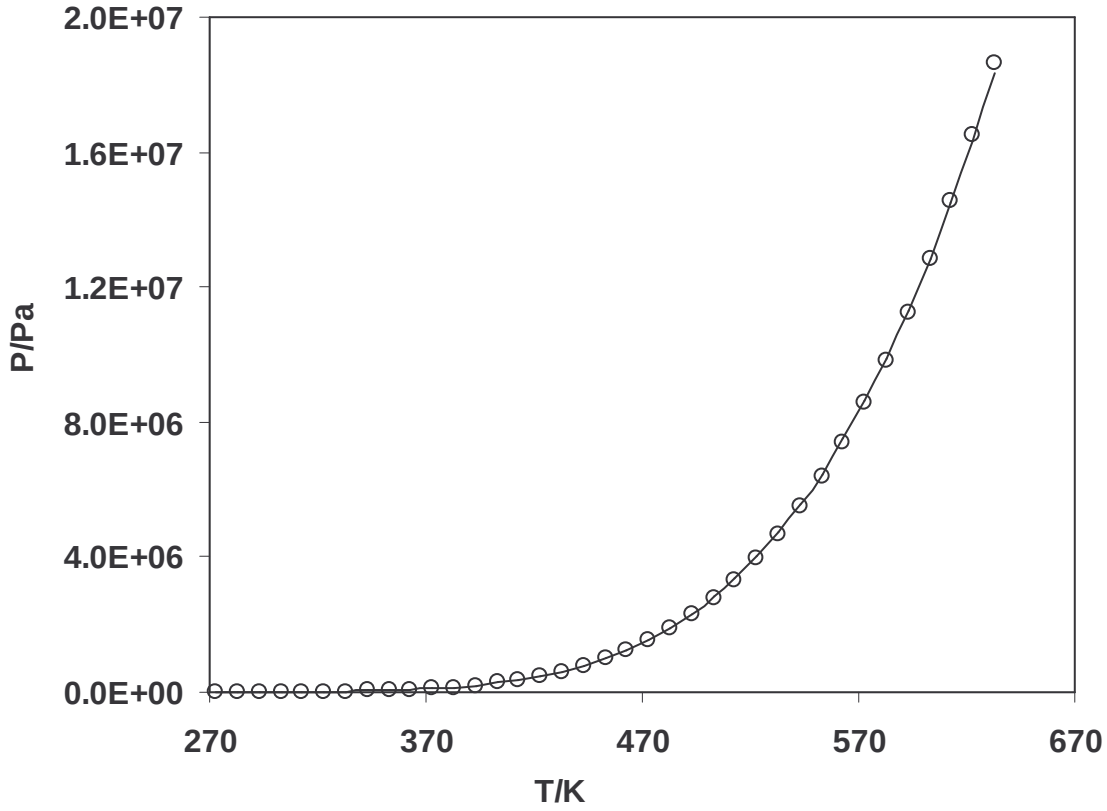

Figure III. 25: **Water vapor pressure: experimental (o) and CPA results (—).**

Using Eq. III.37 the pure component influence parameters can be computed. These are plotted as $c/ab^{2/3}$ for n-heptane, water and ethanol, as a function of $1-T/T_c$, in Figures III.29 – III.31. As shown for n-heptane in Figure III. 29, the three EOS present the same behavior in the 1-T_r range above 0.2, but for CPA the behavior close to the critical point is exactly the opposite of that found for SRK or PR. This qualitative trend is not in agreement with the theoretical definition of the influence parameter and the scaling laws near the critical point (Miqueu, 2001), and should be the consequence of considering during the fitting of the influence parameter, two different critical temperatures: one given by the CPA EOS and a second one implicit on the experimental surface tension data used for the fitting (that is, when σ =0).

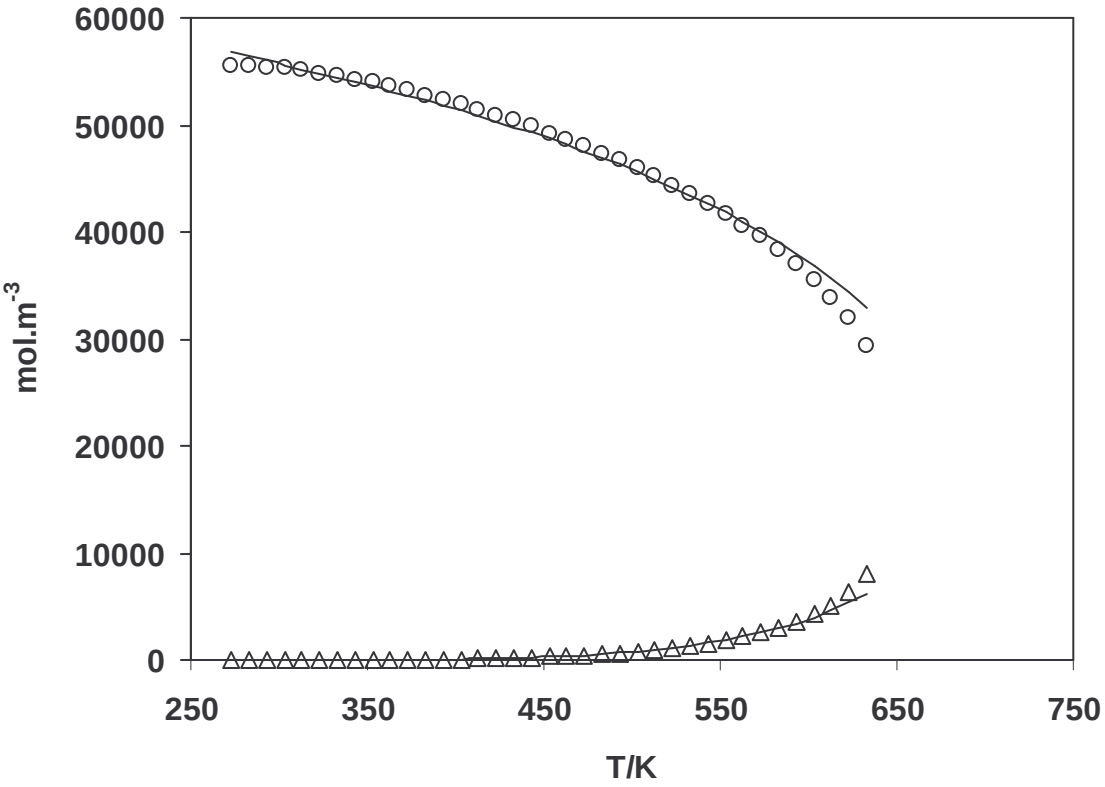

Figure III. 26: Water density. Experimental (o, liquid, Δ, vapor) and CPA (—) estimates.

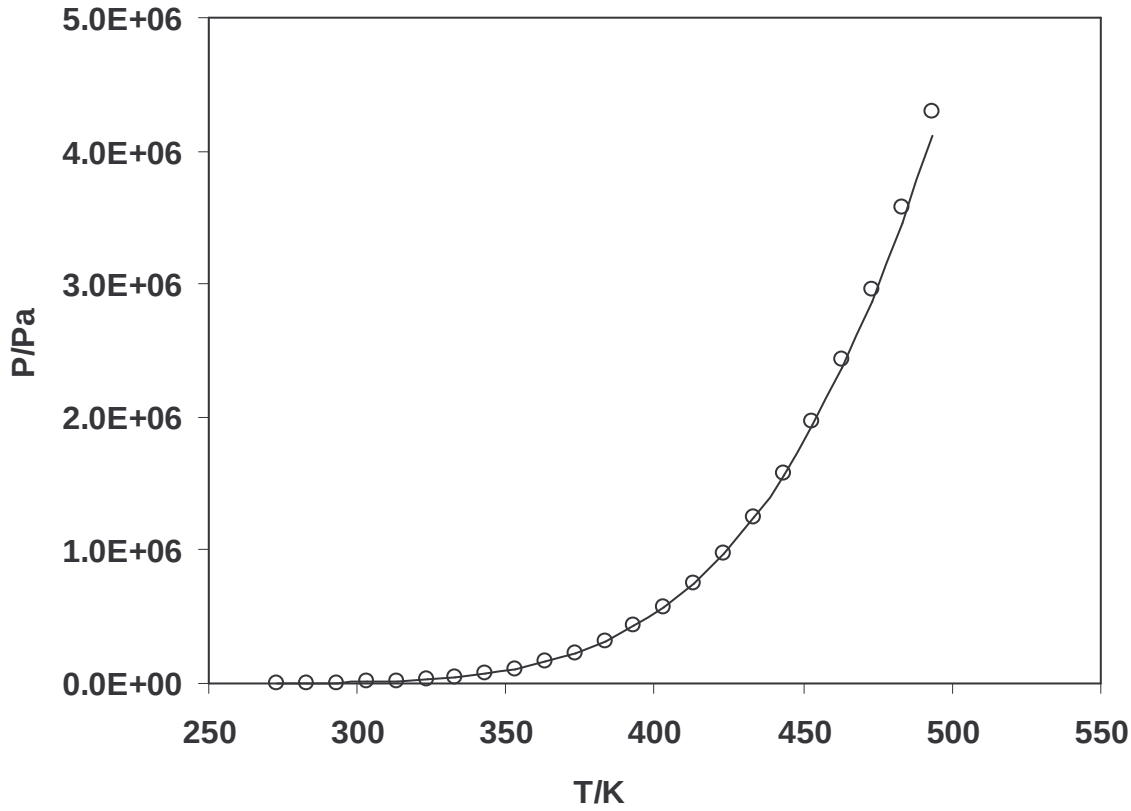

Figure III. 27: **Ethanol vapor pressure. experimental (o) and CPA results (—).**

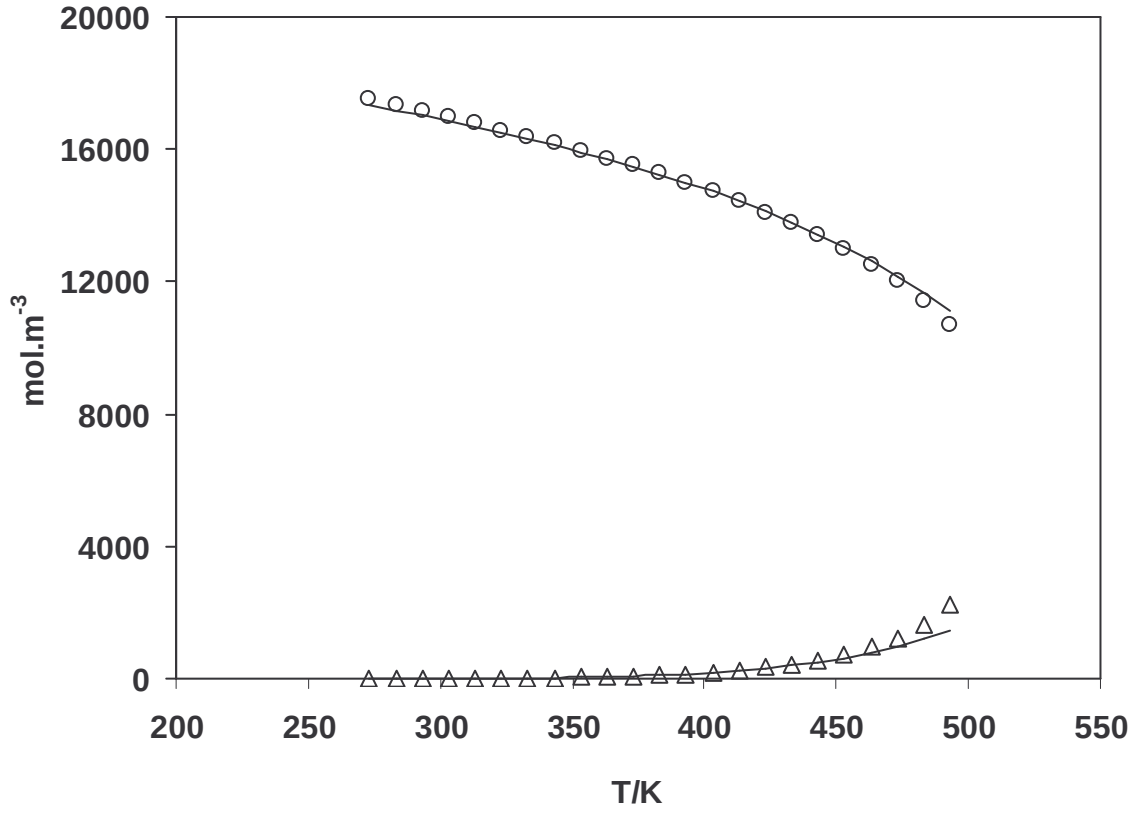

Figure III. 28: **Ethanol density. Experimental (o, liquid, Δ, vapor) and CPA (—) estimates.**

Since it is known that SRK, PR and CPA cannot adequately represent the critical region and since for most of the practical purposes, the temperature range of interest will be in the 1-T_r range above 0.2, a polynomial correlation can be used for the CPA influence parameter in order to obtain a fast estimate of the interfacial tension. As proposed before (Miqueu, 2001, Miqueu *et al*., 2003, 2004) a linear correlation for $c/ab^{2/3}$ as a function of 1-T_r is sufficient for the modeling of interfacial tensions when using a cubic EOS, but as can be observed from Figs III.29 – III.31, a quadratic correlation seems more appropriate while using CPA, especially for water:

$$\frac{c}{ab^{2/3}} = D + E \times (1 - T_r) + F \times (1 - T_r)^2 \qquad \text{(III. 50)}$$

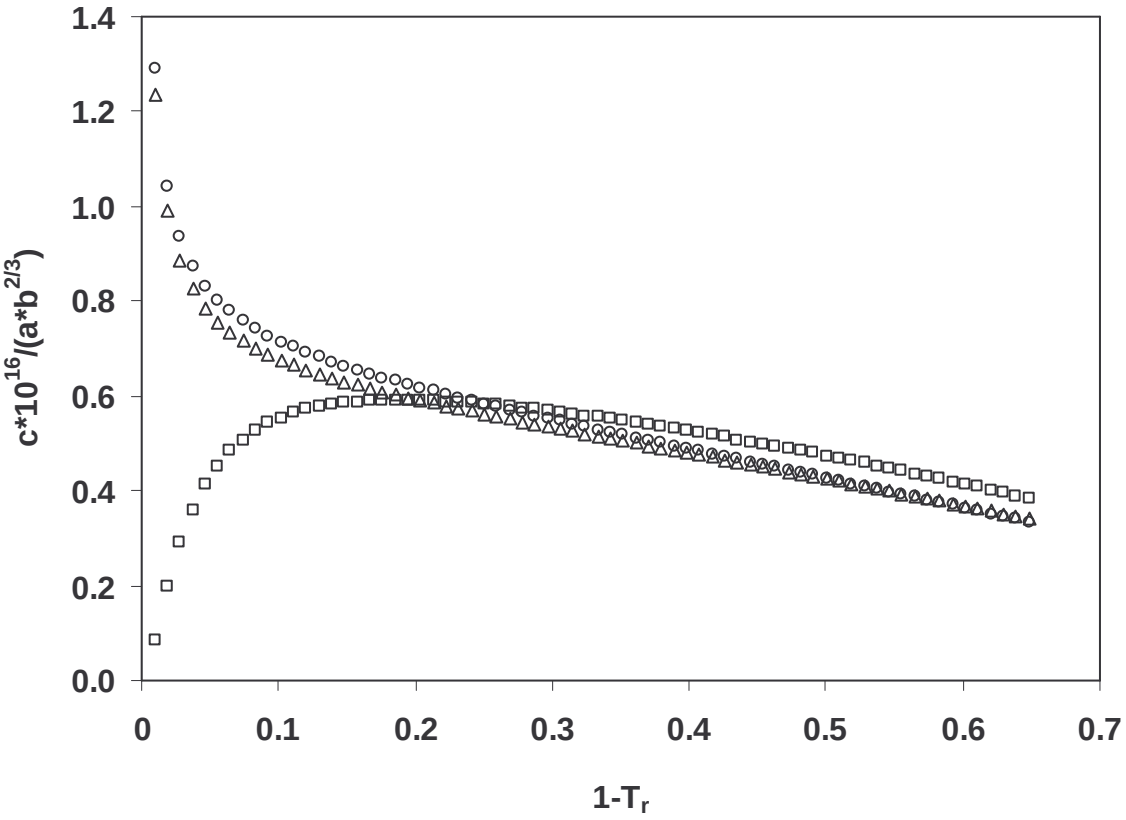

Figure III. 29: n-heptane influence parameters. CPA (□), SRK (o) and PR (Δ) estimates.

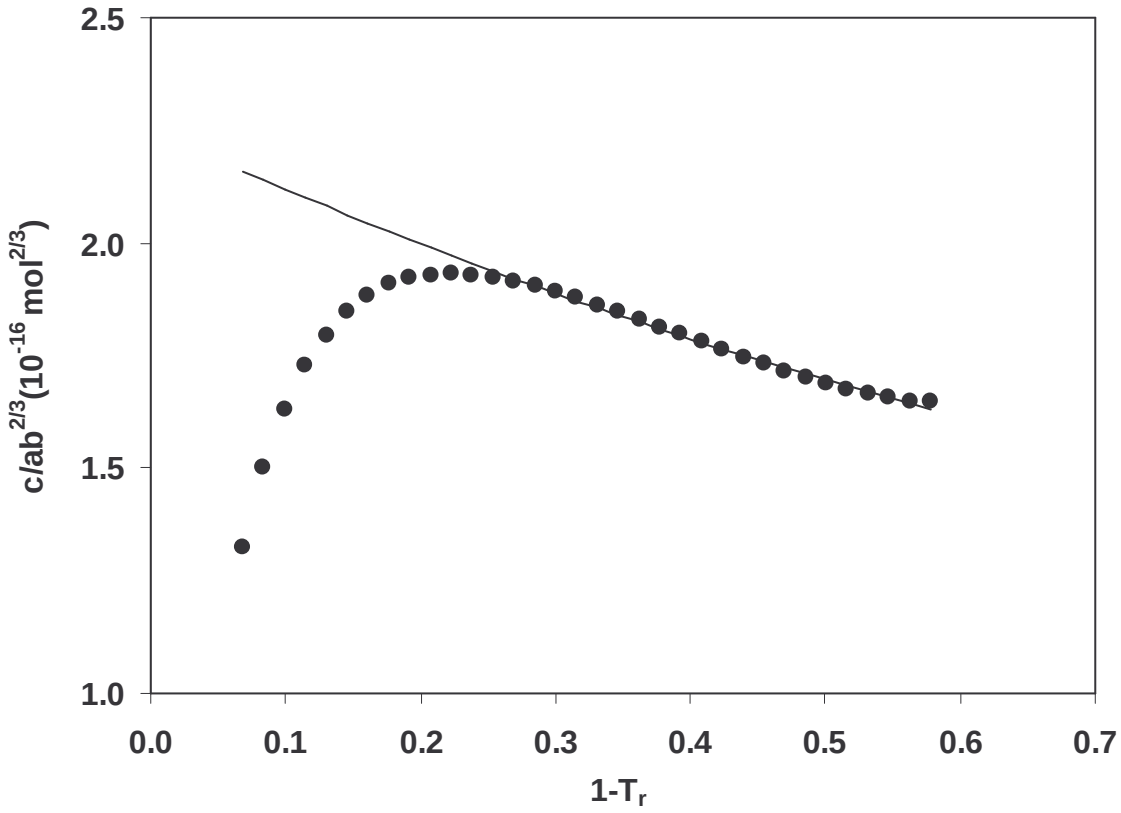

Figure III. 30: **Water influence parameters. CPA estimates (•) and correlation (—).**

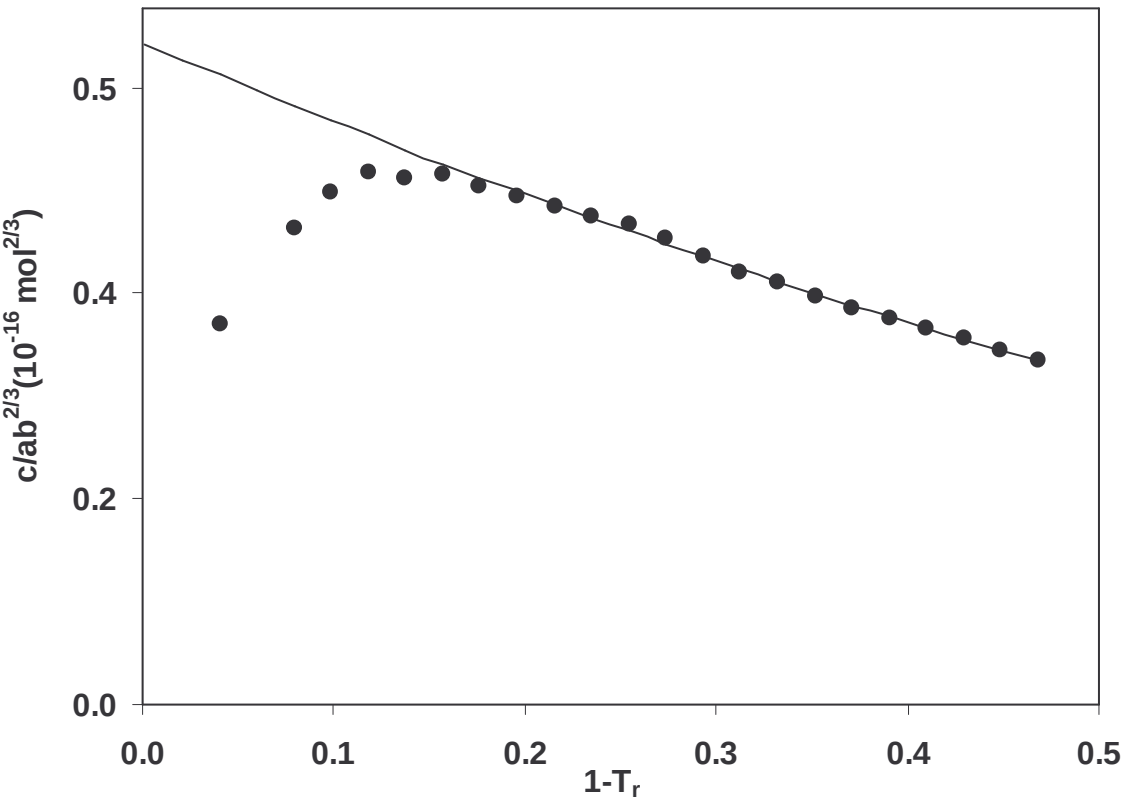

Figure III. 31: **Ethanol influence parameters. CPA estimates (•) and correlation (—).**

D, E and F parameters for the fluids selected for this work are presented on Table III. 11.

Table III. 11: **Correlation coefficients for calculating the influence parameters (Eq. III.60)**

Fluid	D	E	F
C_4H_{10}	0.7081	-0.0102	-0.5626
C_5H_{12}	0.7847	-0.3962	-0.3256
C_6H_{14}	0.6010	0.1349	-0.6887
C_7H_{16}	0.6266	-0.0539	-0.4986
H_2O	2.2505	-1.3646	0.5113
C_2H_5OH	0.5703	-0.7017	0.2471

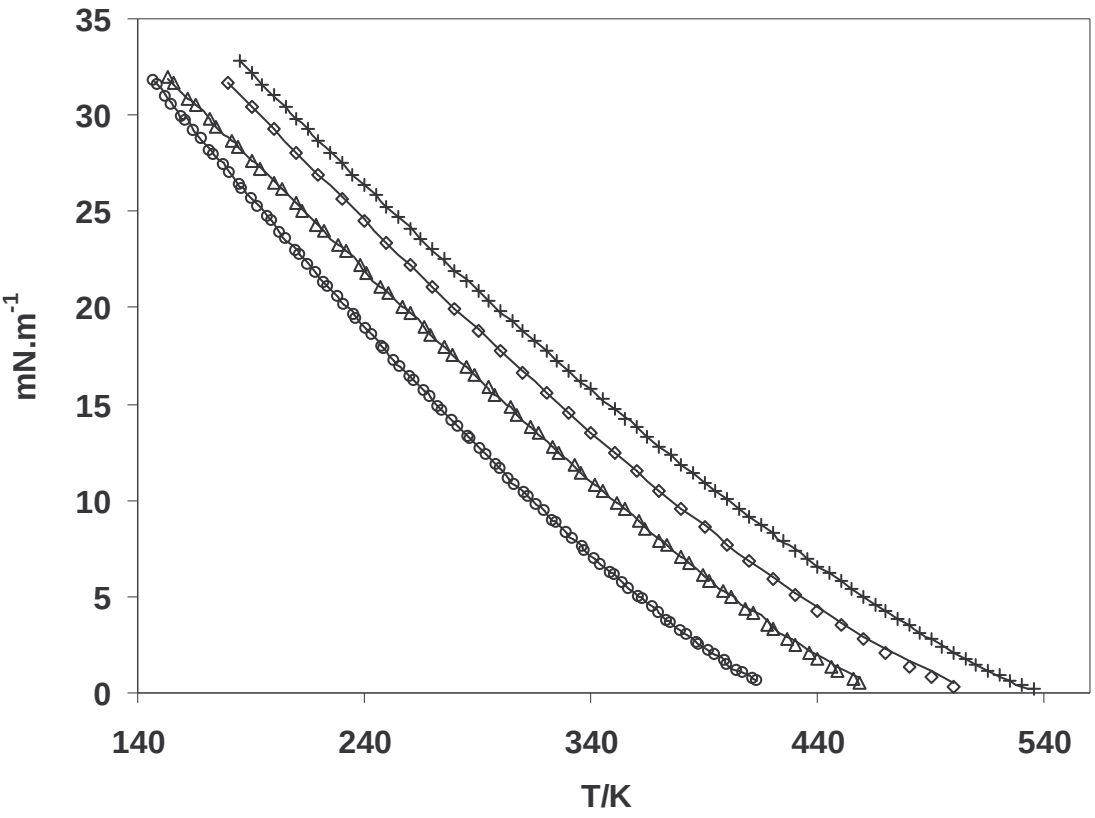

Figure III. 32: **n-alkane surface tension. Experimental (o, n-C_4H_{10}, Δ, n-C_5H_{12}, ◊, n-C_6H_{14}, +, n-C_7H_{16}) and gradient theory results (—).**

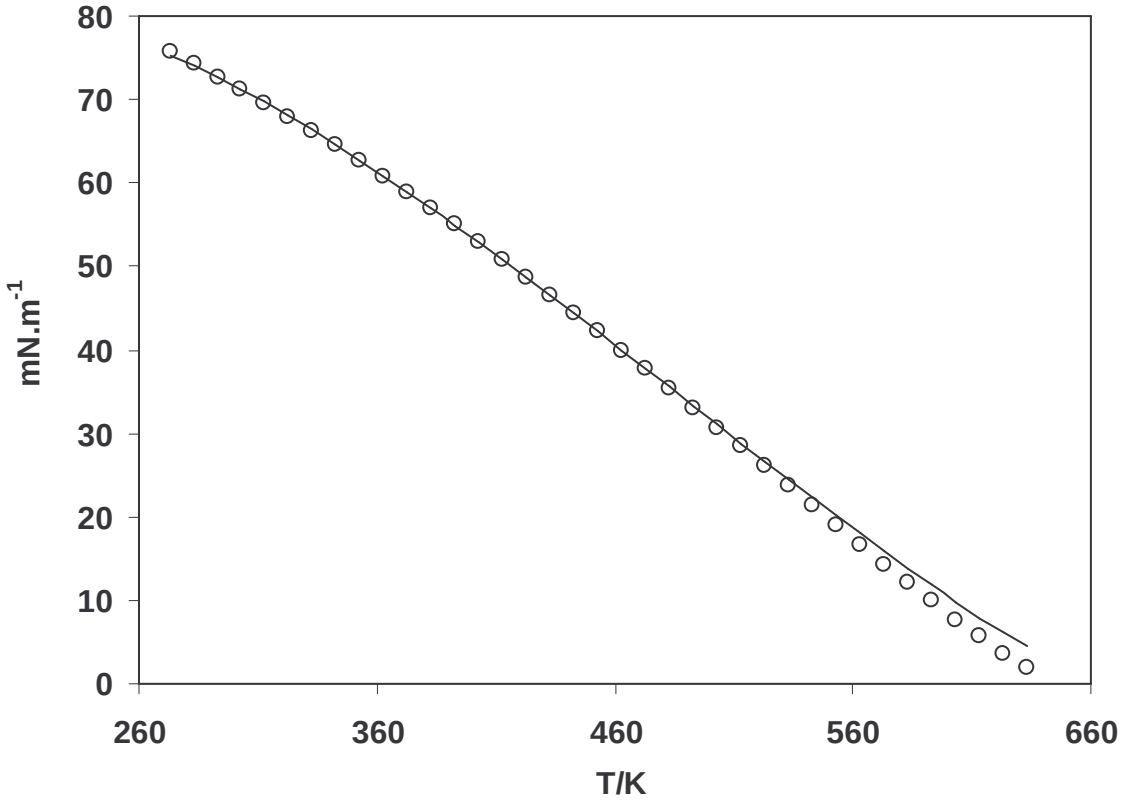

Figure III. 33: Water surface tension. Experimental (o) and gradient theory results (—).

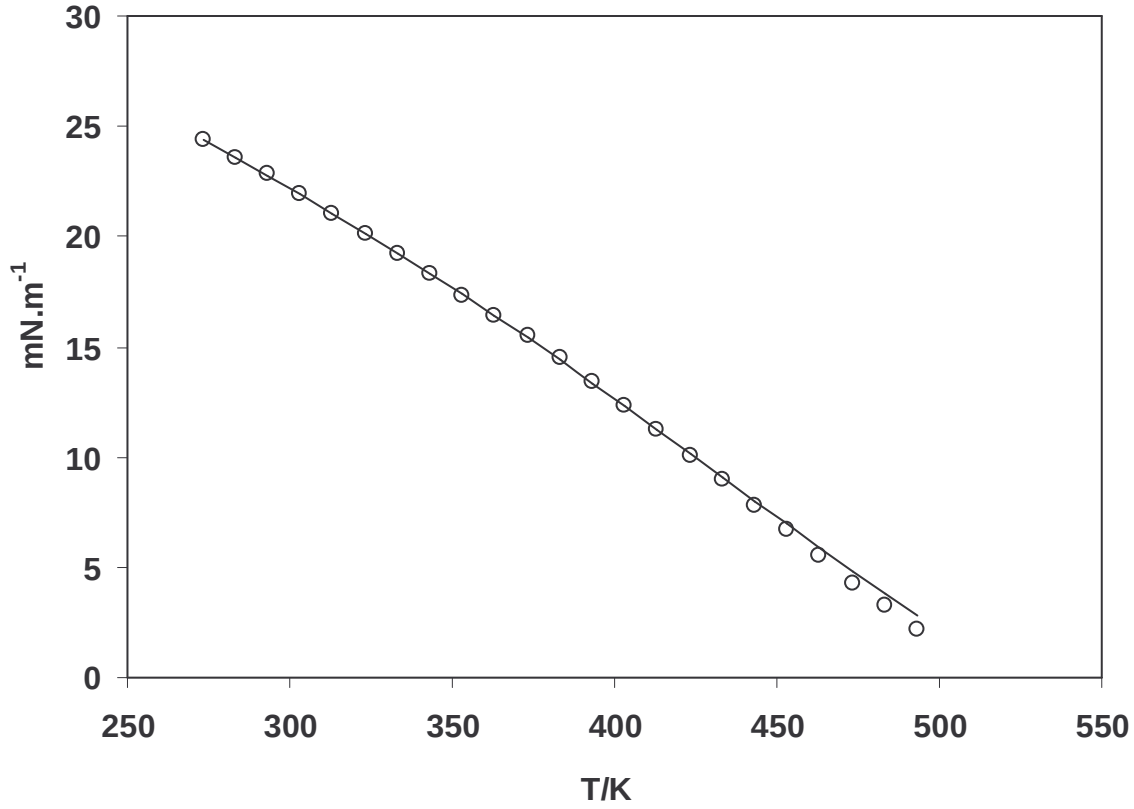

Figure III. 34: Ethanol surface tension. Experimental (o) and gradient theory results (—).

Surface tension was calculated using these coefficients in Equation III.50. Results are presented on Table III. 10 in the reduced temperature range $0.45 < T_r < 0.8$ and Figs III.32 - III.34. Very good results are obtained, as presented in Table III. 10 with average percent deviations below 1.2 %. At higher temperatures, closer to the critical point, deviations are higher as already expected from the simplifications introduced with Eq. III.65, but as can be seen from Figs III.32 – III.34 the correct qualitative trend is present along all the presented results.

Based on these results, future developments will include extension of the theory to heavier n-alkanes, some aromatics and other associating components. Then, multicomponent mixtures and real fluids with a vapor-liquid or with a vapor-liquid and a liquid-liquid interface may be considered.

"It's not that I'm so smart, it's just that I stay with problems longer."

Albert Einstein (1879-1955), Physicist

The friction theory, a state-of-the art model for the estimation of viscosities based on the attractive and repulsive pressure terms given by an equation of state, is used in this section to model the viscosities reported in I.2.2. The Peng-Robinson equation of state was used for these purposes and the liquid densities reported in I.2.3 will also be compared with those resulting from this cubic equation of state.

III.4. Friction Theory

The recently proposed *friction theory* (Quiñones-Cisneros *et al,* 2000, 2001a, 2001b; Zéberg-Mikkelsen et al, 2001, 2002) was used for the viscosity modeling. This general model has been applied successfully for viscosity predictions of several different mixtures, such as those involving hydrocarbons (Quiñones-Cisneros *et al.*, 2000, 2001a), crude oil systems (Quiñones-Cisneros *et al*, 2001b), light gases (Zéberg-Mikkelsen *et al.*, 2001), and carbon dioxide + hydrocarbon mixtures (Zéberg-Mikkelsen *et al.*, 2002) over a broad temperature and pressure range.

In this work, the simplest form of the *friction theory* (or *f-theory*) as described in Quiñones-Cisneros *et al.,* (2001a) was used. The viscosity is modeled from a mechanical viewpoint, considering two contributions: one arising from the dilute gas and the other from the friction between layers, respectively, η_0 and η_f :

$$\eta = \eta_0 + \eta_f \tag{III. 51}$$

where η represents the viscosity, in mPa·s.

The dilute gas viscosity is calculated as a function of temperature, T/K, using the critical volume, v_c /m^3·mol^{-1}, the critical temperature, T_c/K, the molecular weight, MW/Kg·mol^{-1}, and the acentric factor, ω (Chung *et al.*, 1988; Quiñones-Cisneros et al., 2001a):

$$\eta_0 = 0.12897 \frac{\sqrt{MW\,T}}{v_c^{\,2/3}\Omega^*} F_c \tag{III. 52}$$

$$\Omega^* = \frac{1.16145}{T^{*0.14874}} + \frac{0.52487}{\exp\left(0.77320T^*\right)} + \frac{2.16178}{\exp\left(2.43787T^*\right)} - 6.435\times10^{-4}\,T^{*0.14874}\sin\left(18.0323T^{*-0.76830} - 7.27371\right) \tag{III. 53}$$

$$T^* = \frac{1.2593T}{T_c} \tag{III. 54}$$

$$F_c = 1 - 0.2756\omega \tag{III. 55}$$

The additional term, originally present in Eq. III.52 accounting for hydrogen bonding and polarity, was dropped due to the non-polar nature of the systems reported in this work.

The pure component friction contribution is related to a van der Waals type of equation of state repulsive and attractive pressures by means of temperature-dependent friction coefficients, $\hat{\kappa}$.

$$\eta_f = \left[\hat{\kappa}_r \times \frac{p_r}{p_c} + \hat{\kappa}_{rr} \times \left(\frac{p_r}{p_c}\right)^2 + \hat{\kappa}_a \times \frac{p_a}{p_c}\right] \times \eta_c \tag{III. 56}$$

where p stands for the pressure (Pa), both subscripts *r* and *rr* represent repulsive, and *c* and *a* critical and attractive, respectively. η_c is a pure component characteristic critical viscosity for which the following equation was used (Quiñones-Cisneros *et al*., 2001):

$$\eta_c = 3.8136\times10^{-8}\, p_c\, MW^{0.601652} \qquad \text{(III. 57)}$$

In this work, the Peng-Robinson (PR) equation of state (Peng and Robinson, 1974) was combined with the PR f-theory one-parameter general model (Quiñones-Cisneros *et al*., 2001a).

The extension to mixtures follows from the properties of the pure components:

$$\eta_{mx} = \eta_{0\,mx} + \eta_{f\,mx} \qquad \text{(III. 58)}$$

$$\eta_{0\,mx} = exp\left[\sum_{i=1}^{n} x_i\, ln\left(\eta_{0\,i}\right)\right] \qquad \text{(III. 59)}$$

$$\eta_{f\,mx} = \kappa_{r\,mx}\, p_r + \kappa_{rr\,mx}\, p_r^{\,2} + \kappa_{a\,mx}\, p_a \qquad \text{(III. 60)}$$

$$\kappa_{r\ \ mx} = \sum_{i=1}^{n} z_i \frac{\eta_{c\,i}\, \hat{\kappa}_{r\,i}}{p_{c\,i}} \qquad \text{(III. 61)}$$

$$\kappa_{rr\ \ mx} = \sum_{i=1}^{n} z_i \frac{\eta_{c\,i}\, \hat{\kappa}_{rr\,i}}{p^{\,2}{}_{c\,i}} \qquad \text{(III. 62)}$$

$$\kappa_{a\,mx} = \sum_{i=1}^{n} z_i \frac{\eta_{c\,i}\, \hat{\kappa}_{a\,i}}{p_{c\,i}} \qquad \text{(III. 63)}$$

$$z_i = \frac{x_i}{MW_i^{\,0.3} \sum_{i=1}^{n} \frac{x_i}{MW_i^{\,0.3}}} \qquad \text{(III. 64)}$$

where mx stands for a mixture property, n is the number of components, and x_i is the mole fraction of the i^{th} component.

Modelling results, both for liquid density and viscosity, are reported on Table III. 12 and Figs. III.35 - III.44. Preliminary results, showed that the Peng-Robinson equation of state is unable to produce accurate predictions of the liquid densities of heavy n-alkanes, with errors propagating to the viscosities, leading to poor viscosity results. It is known that cubic equations of state cannot provide accurate liquid density estimates of heavy hydrocarbons (Penéloux, 1982). Following the approach used before with the friction theory, critical parameters were fitted to the liquid densities in order to better describe both the liquid densities and viscosities, since a good EOS pressure description is required within the f-theory. The fitted critical parameters are reported in Table III. 13. Table III. 12 and Figs. III.40 – III.44 show how the Peng-Robinson EOS can now adequately represent liquid densities.

Good viscosity predictions are obtained with the friction theory, as can be seen from Figs. III.35-III.39 with the largest deviations found for the ternary systems and the most asymmetric mixtures containing n-heptane. No mixture information was used in either the EOS or in the f-theory. The heavier but less asymmetric mixture, n-$C_{16}H_{34}$ + n-$C_{20}H_{42}$ shows that this viscosity model can give reliable results for heavy components, thus supporting the idea that the larger deviations in the mixtures containing n-heptane arise from their asymmetry.

Within the same mixture, major deviations were found for both models at the lowest temperatures, where viscosity measurements are harder to perform, and thus more uncertain. At these temperatures, the PR EOS also showed the largest liquid density deviations, from which larger viscosity deviations may be expected from the f-theory.

Table III. 12: Modeling results with pure component properties for the f-theory and the PR EOS reported on table III.10.

Mixture	*average absolute deviation (AAD) (%)*	
	f-theory	*PR EOS*
n-C_7H_{16} – n-$C_{20}H_{42}$	7.1	0.8
n-C_7H_{16} – n-$C_{22}H_{46}$	7.5	0.6
n-C_7H_{16} – n-$C_{24}H_{50}$	8.0	0.7
n-$C_{10}H_{22}$ – n-$C_{20}H_{42}$	4.2	0.52
n-$C_{10}H_{22}$ – n-$C_{22}H_{46}$	4.2	0.43
n-$C_{10}H_{22}$ – n-$C_{24}H_{50}$	3.8	0.37
n-$C_{16}H_{34}$ – n-$C_{20}H_{42}$	2.0	0.6
n-C_7H_{16} – n-$C_{20}H_{42}$ – n-$C_{24}H_{50}$	9.1	0.7
n-$C_{10}H_{22}$ – n-$C_{20}H_{42}$ – n-$C_{24}H_{50}$	9.2	0.55
Average (all data points)	6.0	0.6

Table III. 13: Pure component properties used within the f-theory and the PR EOS.

n-*alkane*	**T_c (K)**	**P_c (Pa x 10^{-5})**	**V_c ($m^3 \cdot mol^{-1}$ x 10^3)**	**ω**	**MW ($Kg \cdot mol^{-1}$ x 10^3)**
n-C_7H_{16}	540.20	27.40	0.42800	0.350	100.204
n-$C_{10}H_{22}$	614.6	22.49	0.57326	0.49	142.285
n-$C_{16}H_{34}$	736.44	17.18	0.83516	0.718	226.446
n-$C_{20}H_{42}$	751.14	14.10	0.99043	0.865	282.554
n-$C_{22}H_{46}$	763.76	13.07	1.0624	0.963	310.607
n-$C_{24}H_{50}$	783.98	12.29	1.1334	1.032	338.661

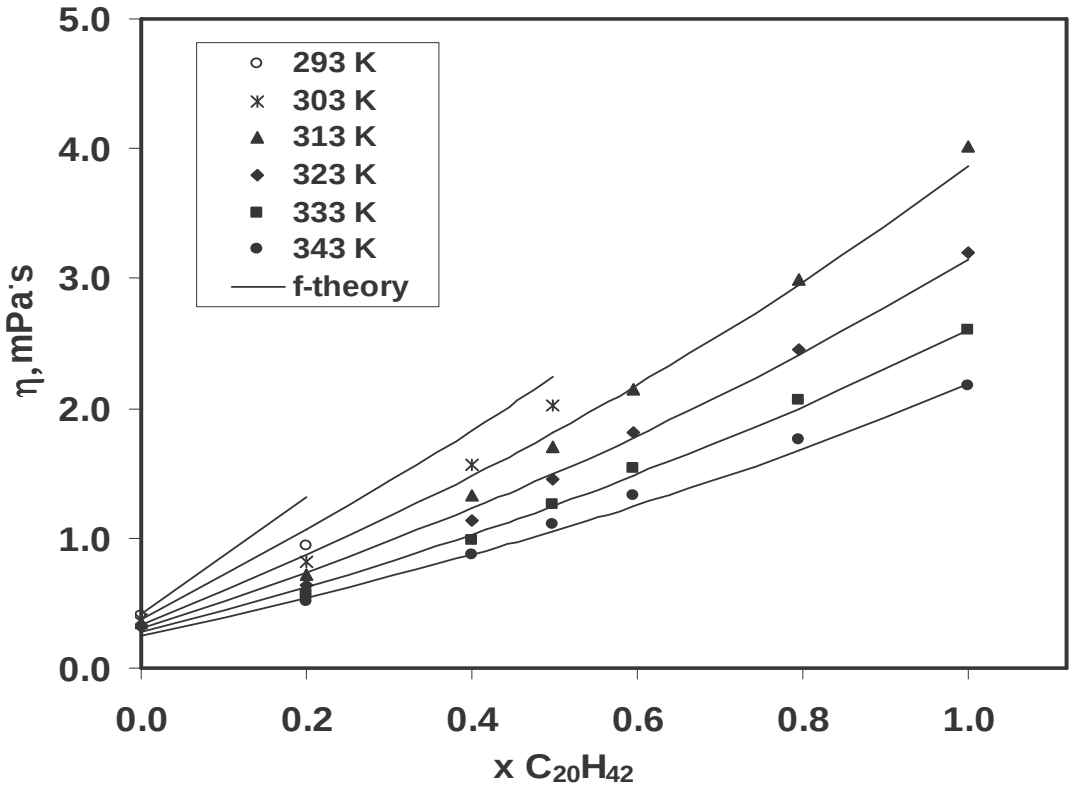

Figure III. 35: **Viscosity of the binary mixture n-C_7H_{16} + n-$C_{20}H_{42}$; experimental results and model predictions.**

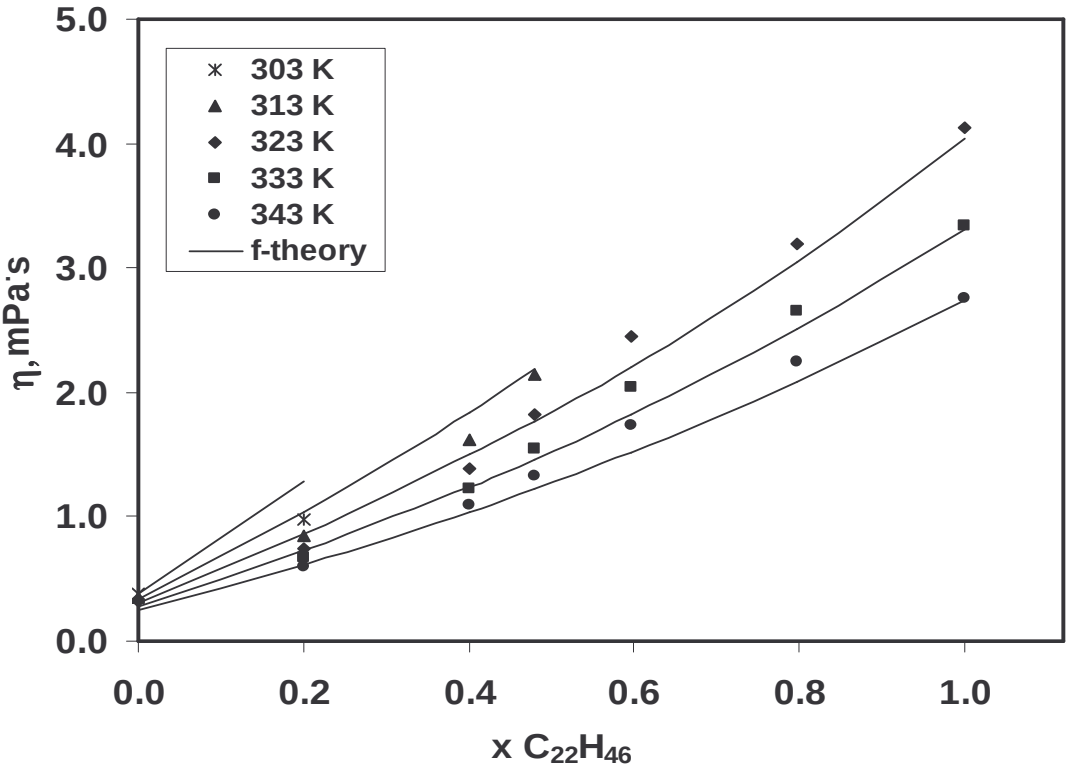

Figure III. 36: **Viscosity of the binary mixture n-C_7H_{16} + n-$C_{22}H_{46}$; experimental results and model predictions.**

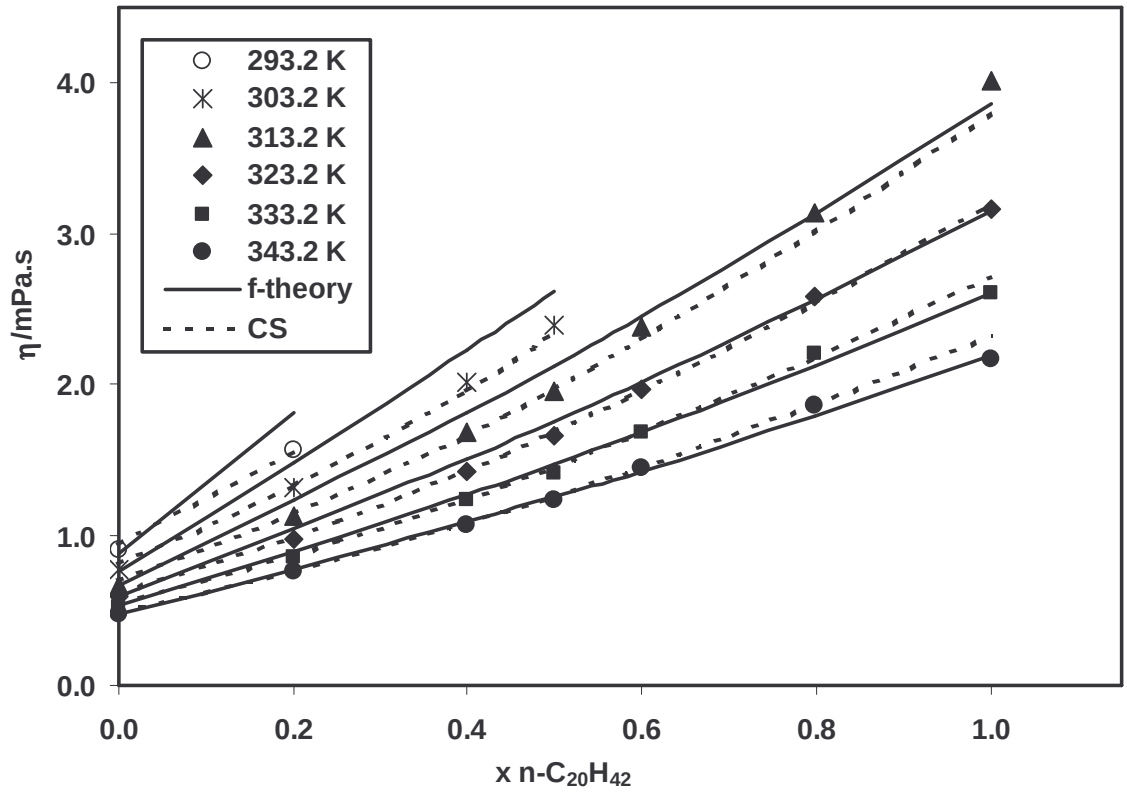

Figure III. 37: **Viscosity of the binary mixture n-$C_{10}H_{22}$ + n-$C_{20}H_{42}$. Experimental results and model predictions.**

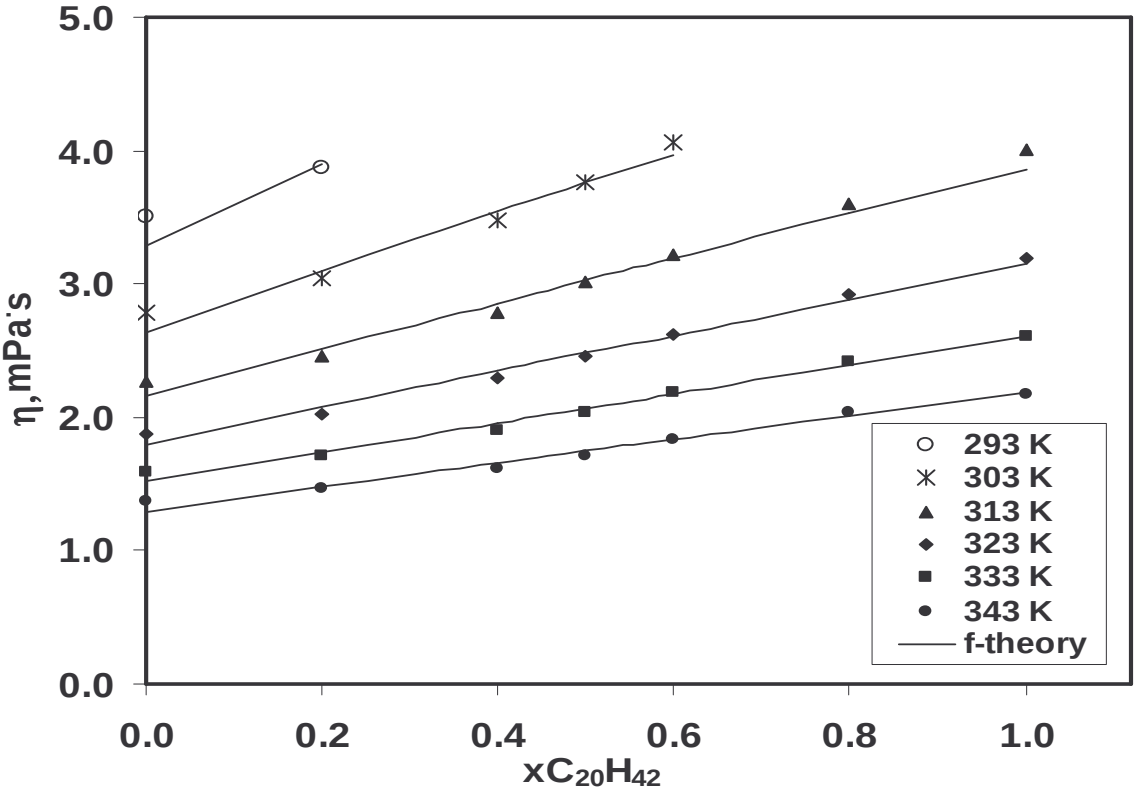

Figure III. 38: **Viscosity of the binary mixture n-$C_{16}H_{34}$ + n-$C_{20}H_{42}$; experimental results and model predictions.**

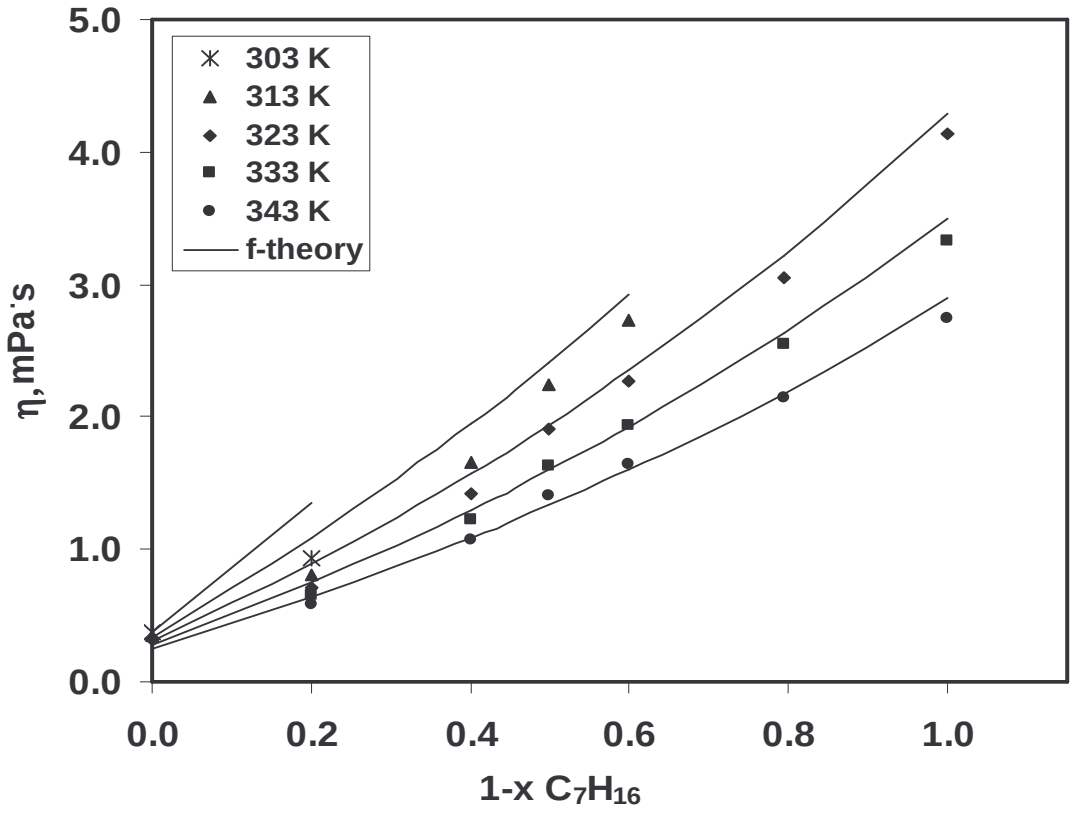

Figure III. 39: **Viscosity of the ternary mixture n-C_7H_{16} + n-$C_{20}H_{42}$ + n-$C_{24}H_{50}$; experimental results and model predictions.**

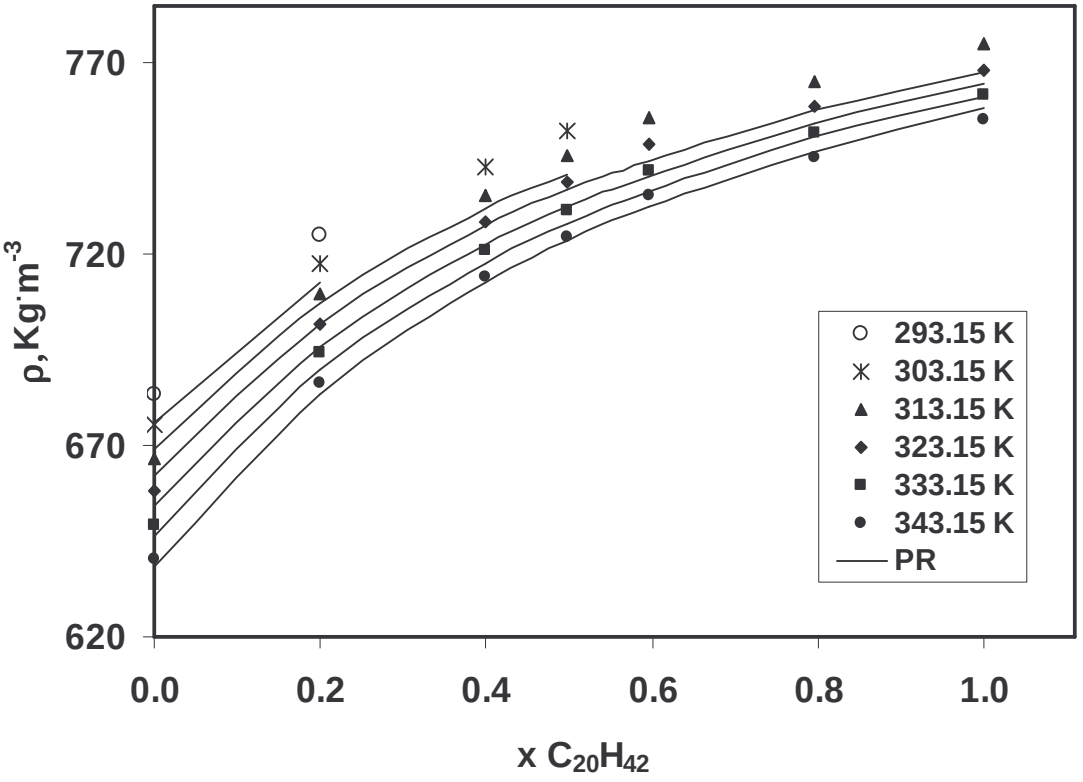

Figure III. 40: **Liquid density of the binary mixture n-C_7H_{16} + n-$C_{20}H_{42}$; experimental results and model predictions.**

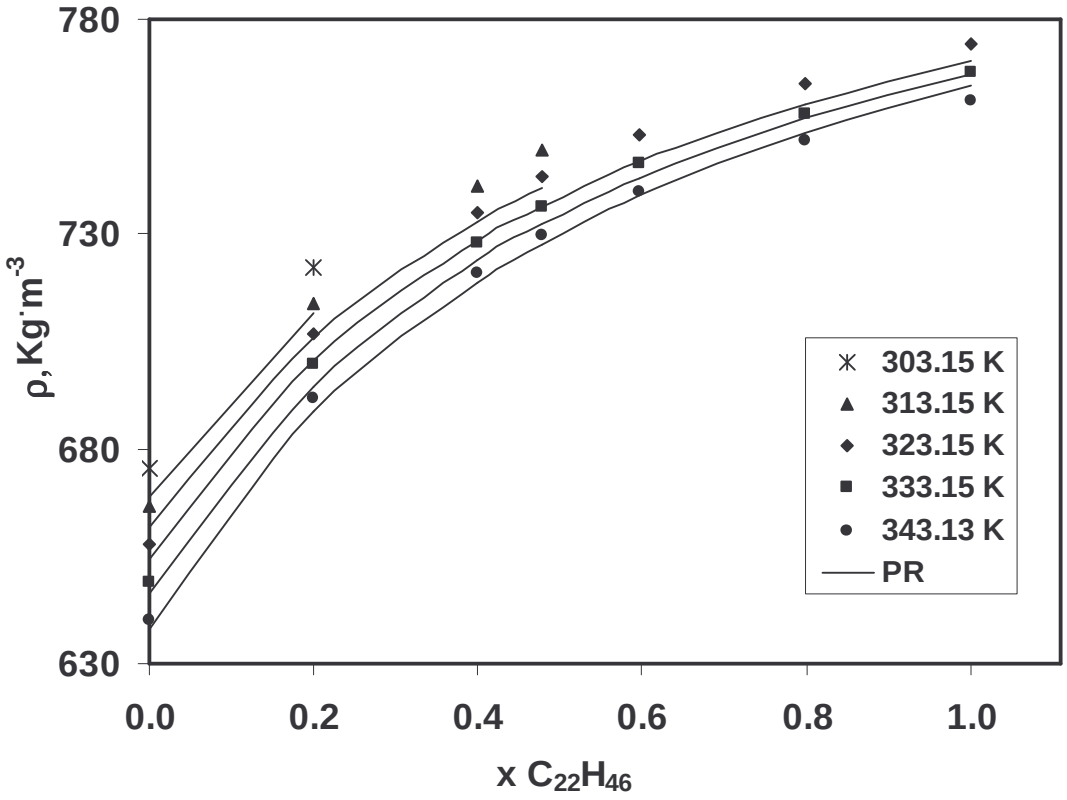

Figure III. 41: **Liquid density of the binary mixture n-C_7H_{16} + n-$C_{22}H_{46}$; experimental results and model predictions.**

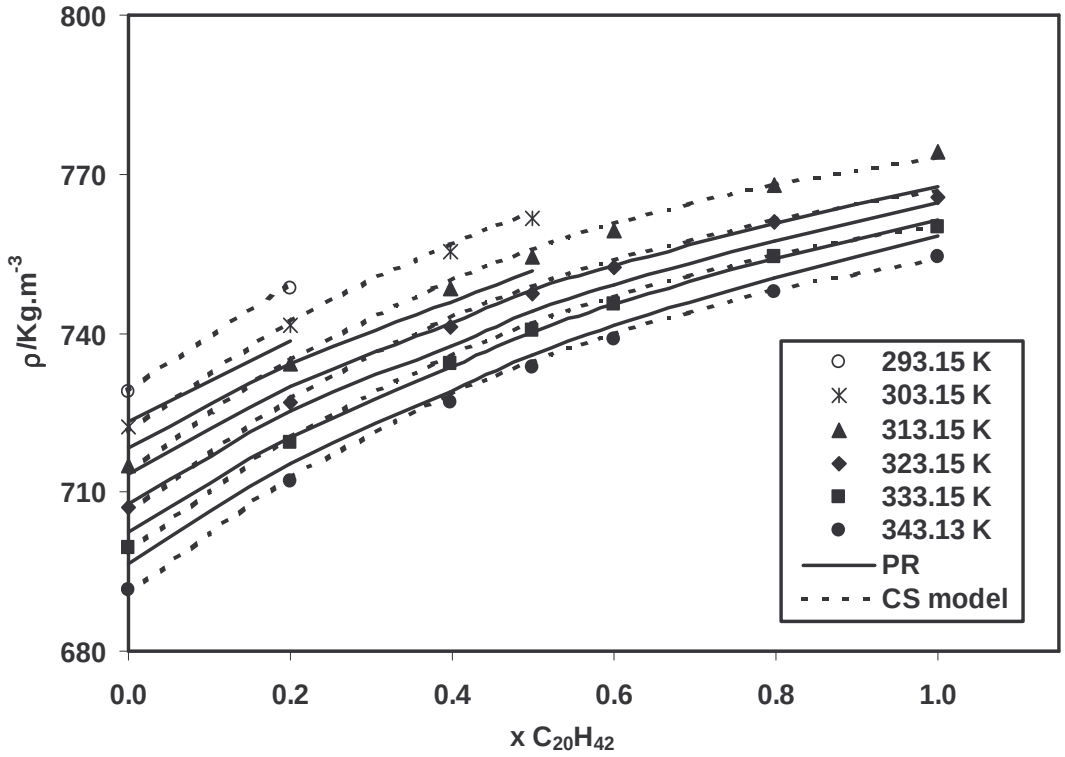

Figure III. 42: Liquid density of the binary mixture n-$C_{10}H_{22}$ + n-$C_{20}H_{42}$. Experimental results and model predictions.

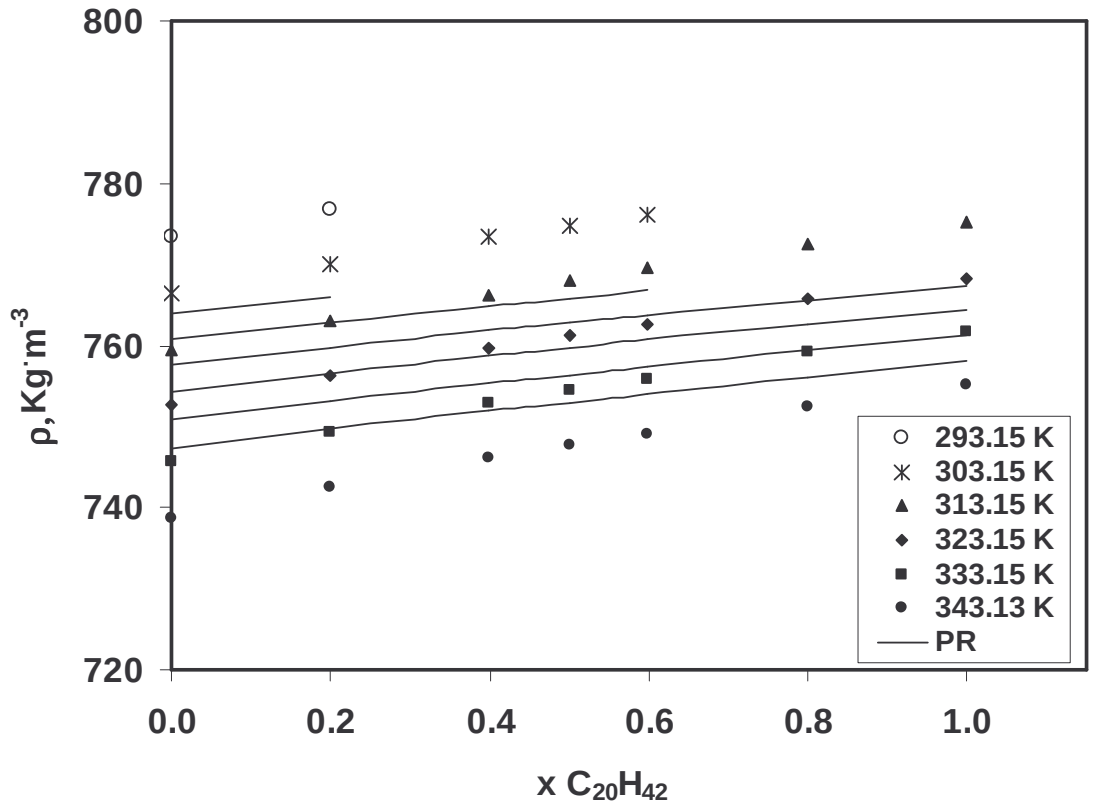

Figure III. 43: **Liquid density of the binary mixture n-$C_{16}H_{34}$ + n-$C_{20}H_{42}$; experimental results and model predictions.**

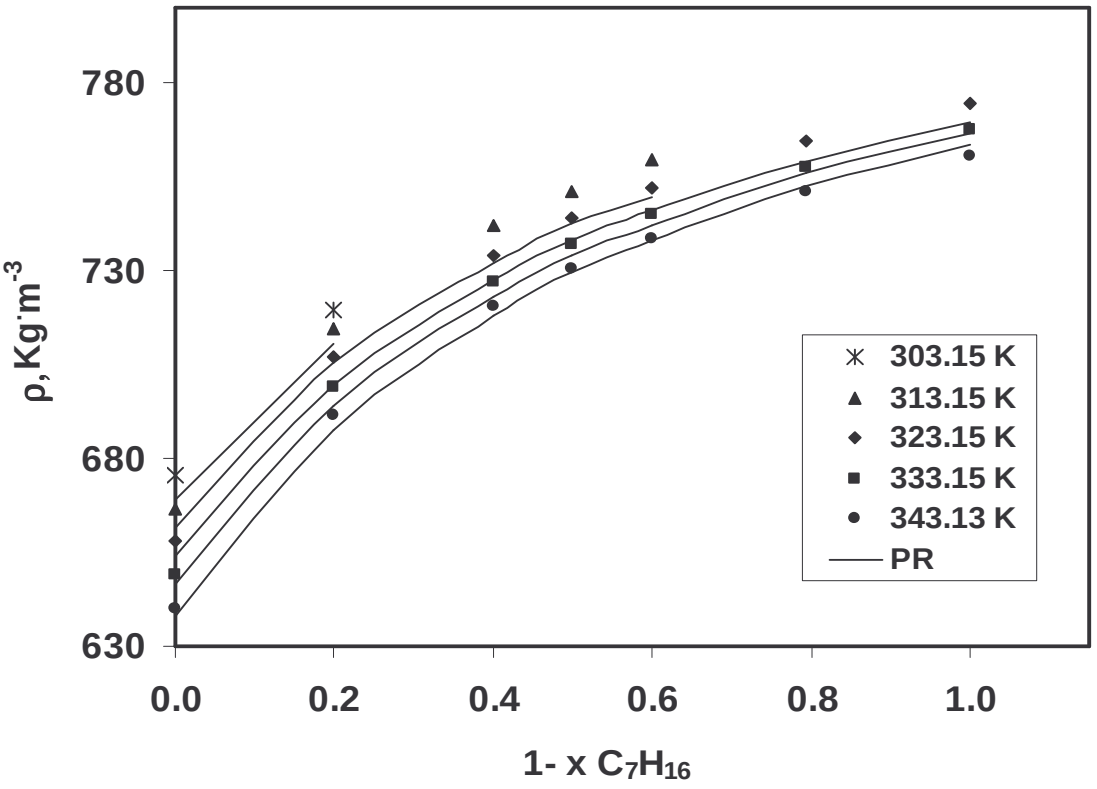

Figure III. 44: **Liquid density of the ternary mixture n-C_7H_{16} + n-$C_{20}H_{42}$ + n-$C_{24}H_{50}$; experimental results and model predictions.**

III.5. Solid – Liquid Equilibrium in Hydrocarbon Fluids

The new European standards for automotive fuels, issued under the Auto-Oil program (1996), are changing the way fuels are produced. There is a clear trend towards more paraffinic fuels (Neale, 1997; Mota, 1998), with better combustion habits, and thus more environmentally friendly, but that will have a worst behaviour at low temperatures presenting higher cloud and pour points.

The solubility of the long n-alkanes strongly decreases with temperature and, for diesels, below 280 K, the exact liquid-solid transition temperatures depend on the n-alkane content and its distribution. Below this temperature, crystals of n-alkanes start precipitating, plugging pipes and fuel filters.

The production of fuels that simultaneously conform to the new European standards and the low temperature behaviour restrictions will demand either an increasing use of additives, such as pour point depressants, or the redesign of the distillation to reduce the concentration of n-alkanes to an acceptable level. For this purpose it is important to be able to relate the n-alkane crystallisation with the composition of the fluid. This will help to adequately design the production and blend of fuels, and to select the most adequate additives (Wang *et al*., 1999).

The solid formation was described in this section as a solid-liquid equilibrium of n-alkanes. The general solid-liquid equilibrium equation relating the compositions with the non-ideality of the phases and the pure component thermophysical properties is used (Prausnitz *et al*., 1999):

$$\left(\ln \frac{s\ \gamma^{s}}{x\ \gamma^{l}} = \frac{\Delta h_m}{RT_m}\left(\frac{T_m}{T}-1\right) + \frac{\Delta h_{tr}}{RT_{tr}}\left(\frac{T_{tr}}{T}-1\right) - \frac{\Delta_s^l Cp_m}{R}\left(\ln\frac{T}{T_m}+\frac{T_m}{T}-1\right)\right)_i \qquad \text{(III. 65)}$$

In previous works the liquid phase was assumed as non-ideal and modelled using the Flory-free volume equation (Coutinho *et al*., 1995). The use of this model for the liquid phase would require a more detailed knowledge of its composition such as a PIONA analysis or equivalent. However, the non-ideality of the liquid phase is not very significant (Erikson *et al*, 1983) and as discussed in a previous work (Coutinho *et al*., ano?) to consider the solvent composed of 25% of aromatics or being fully paraffinic does not change the low temperature behaviour of a solution. To simplify the approach, both in calculation and experimental requirements, an ideal liquid phase will be adopted in this work.

The solid phase non-ideality will be described by the Predictive UNIQUAC model (Coutinho *et al*., 1996; Coutinho, 1998). This is a version of the original UNIQUAC where:

$$\frac{g^E}{RT} = \sum_{i=1}^{n} x_i \ln\left(\frac{\Phi_i}{x_i}\right) + \frac{Z}{2}\sum_{i=1}^{n} q_i x_i \ln\frac{\theta_i}{\Phi_i} - \sum_{i=1}^{n} x_i q_i \ln\left[\sum_{j=1}^{n}\theta_j \exp\left(-\frac{\lambda_{ij}-\lambda_{ii}}{q_i RT}\right)\right] \qquad \text{(III. 66)}$$

with

$$\Phi_i = \frac{x_i r_i}{\sum_j x_j r_j} \quad \text{and} \quad \theta_i = \frac{x_i q_i}{\sum_j x_j q_j} \qquad \text{(III. 67)}$$

using a new definition for the structural parameters *r* and *q* (Coutinho, 1998).

The predictive local composition concept (Coutinho and Stenby, 1996) allowed an estimation of the interaction energies, λ_{ij}, used by these models. The pair interaction energies between two identical molecules are estimated from the heat of sublimation of the pure n-alkane taking the solid phase as an orthorhombic crystal,

$$\lambda_{ii} = -\frac{2}{Z}\left(\Delta h_{sblm\ i} - RT\right) \qquad \text{(III. 68)}$$

Here Z is the coordination number and has a value of Z=6 for orthorhombic crystals. The heats of sublimation, $h_{sblm}=h_{vap}+h_m+h_{tr}$, are calculated at the melting temperature of the pure component. The heat of vaporisation h_{vap} is assessed using the PERT2 correlation by Morgan and Kobayashi (1994).

The pair interaction energy between two non-identical molecules is given by

$$\lambda_{ij} = \lambda_{jj} \qquad \text{(III. 69)}$$

where *j* is the n-alkane with the shorter chain of the pair *ij*.

This solid-liquid equilibrium model is thus a *purely predictive* model that uses in the calculation of the phase behaviour nothing but pure component properties.

An example of the use of this model for a simple mixture involving n-$C_{10}H_{22}$, n-$C_{24}H_{50}$, n-$C_{25}H_{52}$ and n-$C_{26}H_{54}$ is presented in Figure III. 45.

The n-alkane composition was experimentally obtained from the GC analysis and is presented in Table I. 14. No other information is required about the composition of the fluid.

As discussed above, an ideal liquid phase will be assumed and thus no differentiation will be done between aliphatic and aromatic compounds in the liquid phase. A single pseudo-compound will be used to describe the liquid phase. Its concentration is given by the concentration of non n-alkanes obtained from the GC analysis. The choice of the

pseudo-compound is done by matching the average molecular weight of the pseudo-solution used in the calculation with the measured average molecular weight.

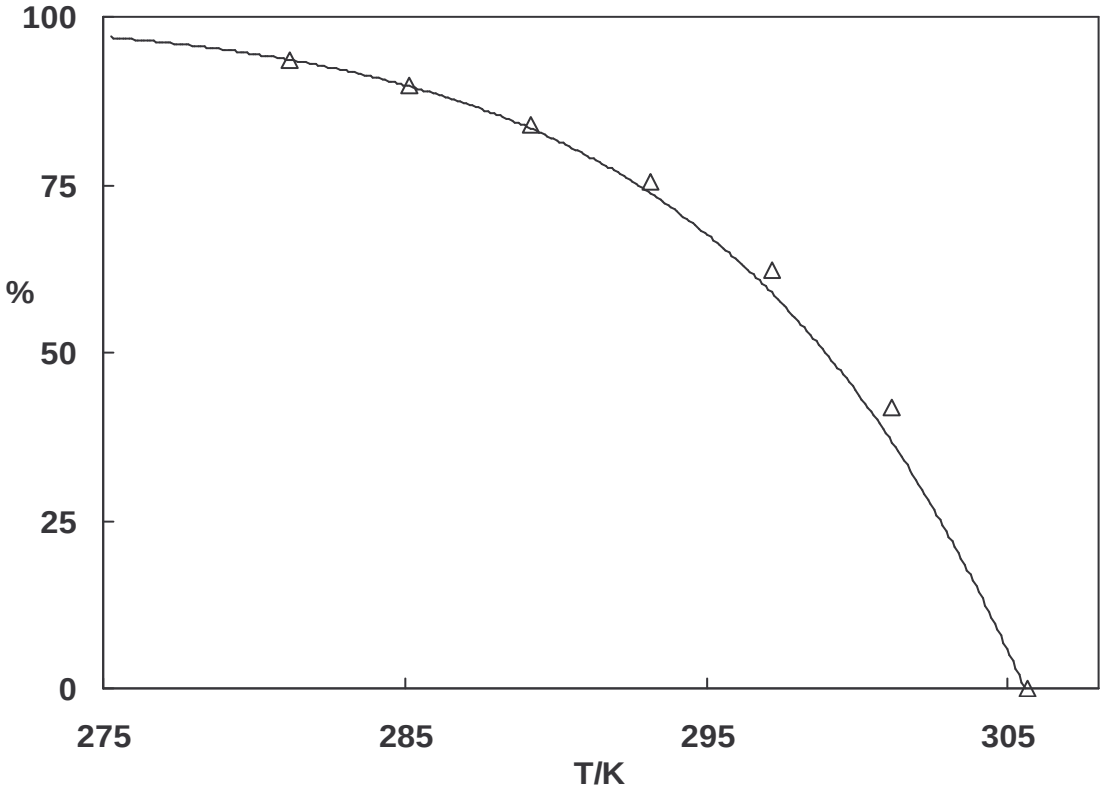

Figure III. 45: **Comparison between the experimental and calculated percentage of crystallized paraffins in a n-$C_{10}H_{22}$+n-$C_{24}H_{50}$+n-$C_{25}H_{52}$+n-$C_{26}H_{54}$ mixture (mol%, respectively, 80%, 7.71% 6.62% and 5.67%) (Pauly *et al.*, 2004)**

Table III. 14: Comparison between measured and predicted wax appearance temperature (WAT)

Distillation cut	**Measured WAT/K**	**Predicted WAT/K**	**Deviation/K**
Brent	273.8	272.7	1.1
Oso Condensate	278.9	277.5	1.4
Troll	265.6	265.3	0.3
DUC	256.2	256.6	0.4
Sahara Blend	271.2	271.1	0.1
Average deviation			*0.66*

The experimental and model precipitation curves obtained are presented in Figure III. 46. The curves present similar shapes only shifted in temperature with differences that are related to the to the total n-alkane content. For the samples studied in this work the WAT's nicely correlate with the total n-alkane content as shown in Figure III. 47. Unfortunately, as has been shown before (Reddy, 1986; Rossmyr, 1979; Mirante *et al*., 2001), this sort of correlation cannot be generalised to fluids with n-alkane distributions different than those used in the development of the correlation, as the WAT is highly dependent on the n-alkane distribution besides the total content.

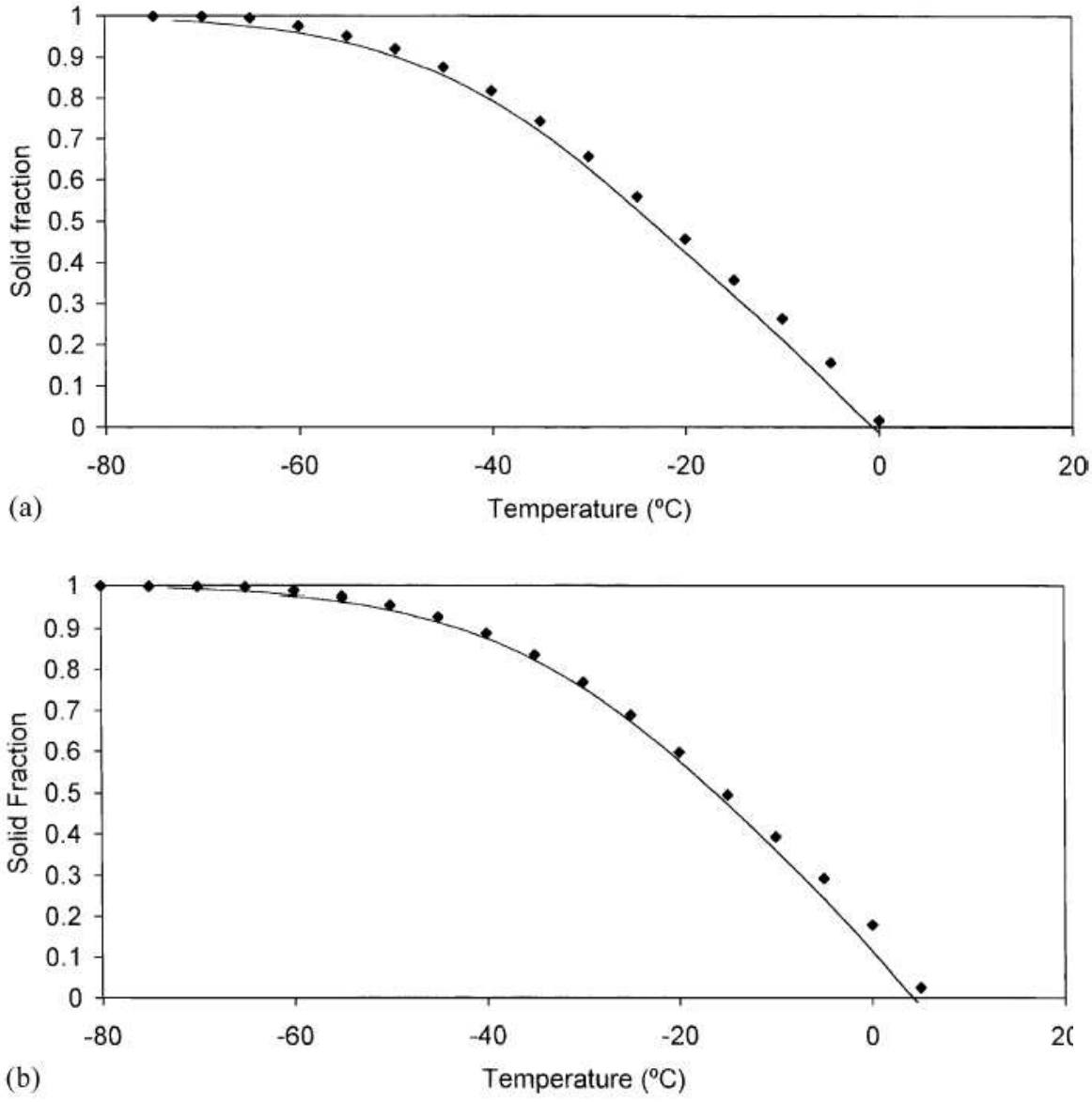

Figure III. 46: **Measured and predicted precipitation curves for distillation cuts from Brent a), Oso Condensate b), Troll c), DUC d), and Sahara Blend e).**

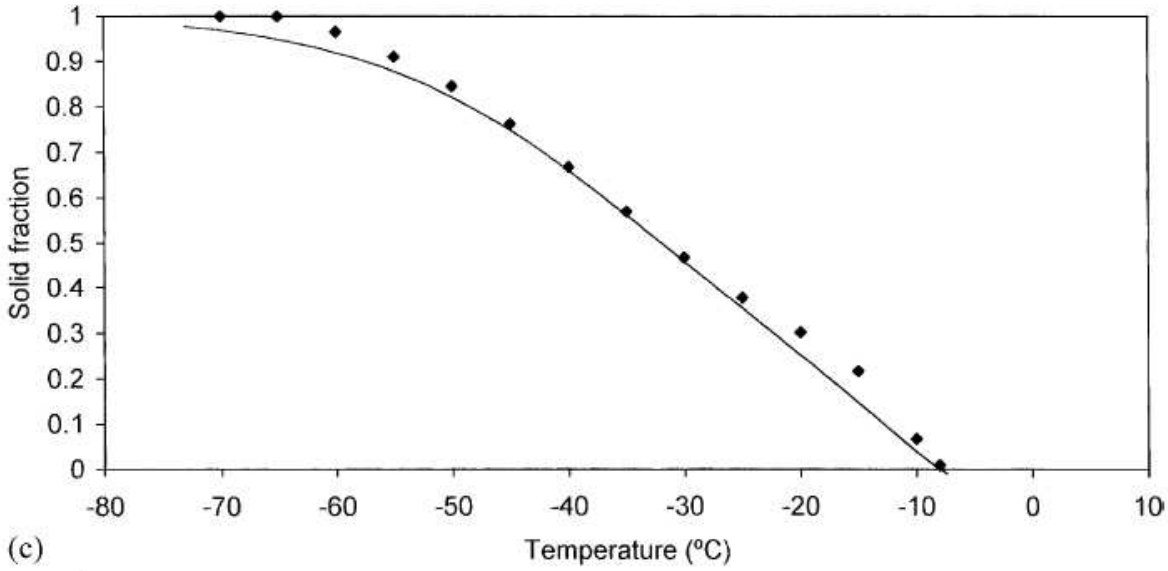

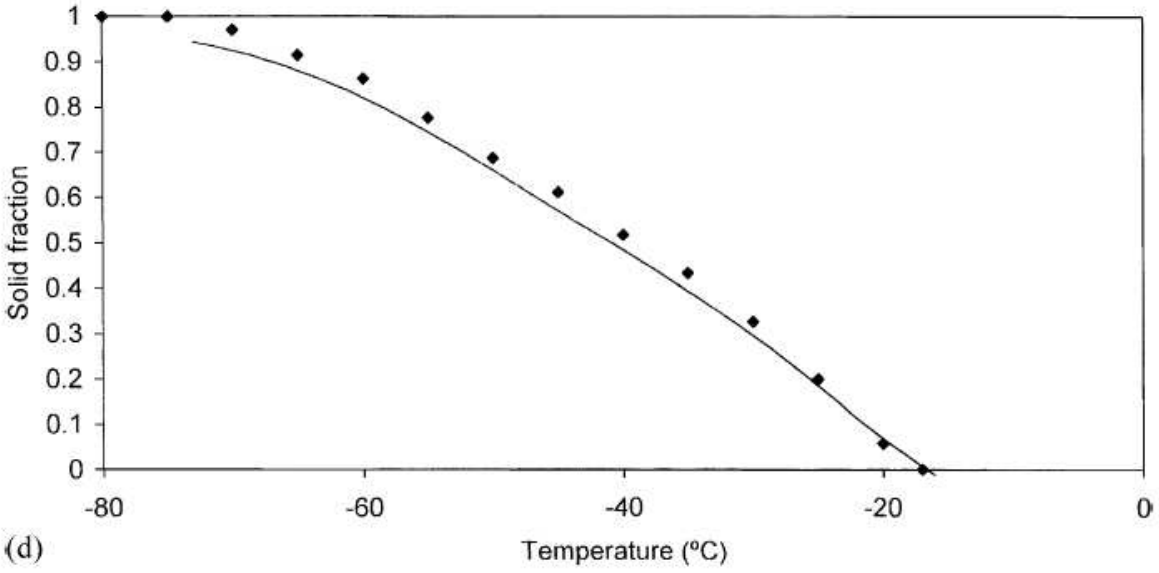

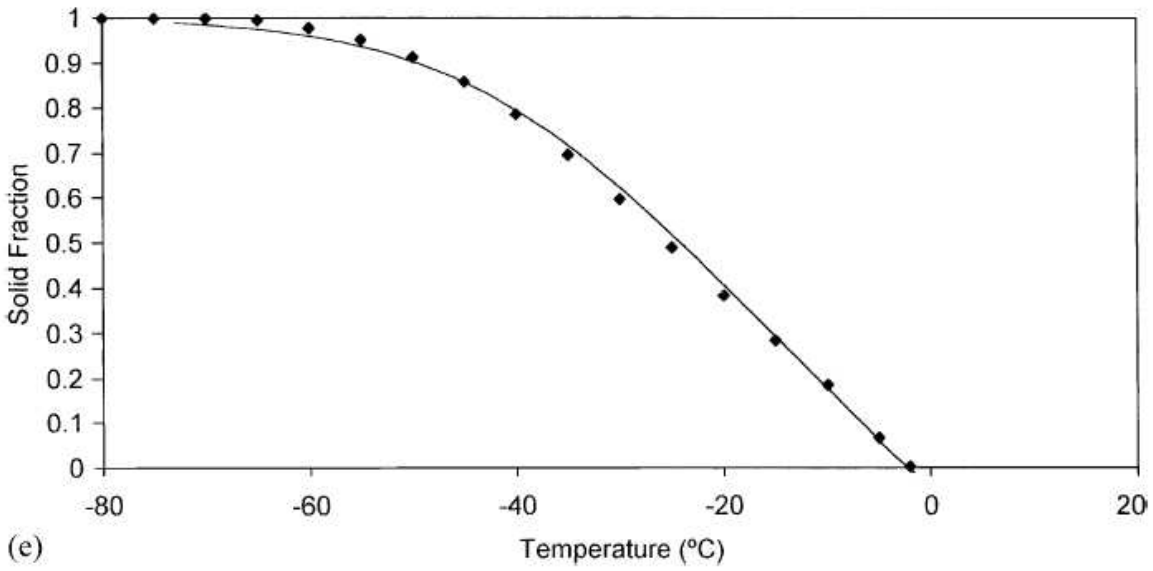

Figure III.46: (continued)

Some recent results for crudes (Ronningsen *et al*., 1991; Delmas *et al*., 2000) show that the total n-alkane content in waxy crudes is related to the average molecular weight of the fluid. For the distillation cuts studied and other fuels from literature (Coutinho *et al*., 2000; Reddy, 1986) it was found that such relation does not exist. The data in Table I. 14 clearly illustrates this.

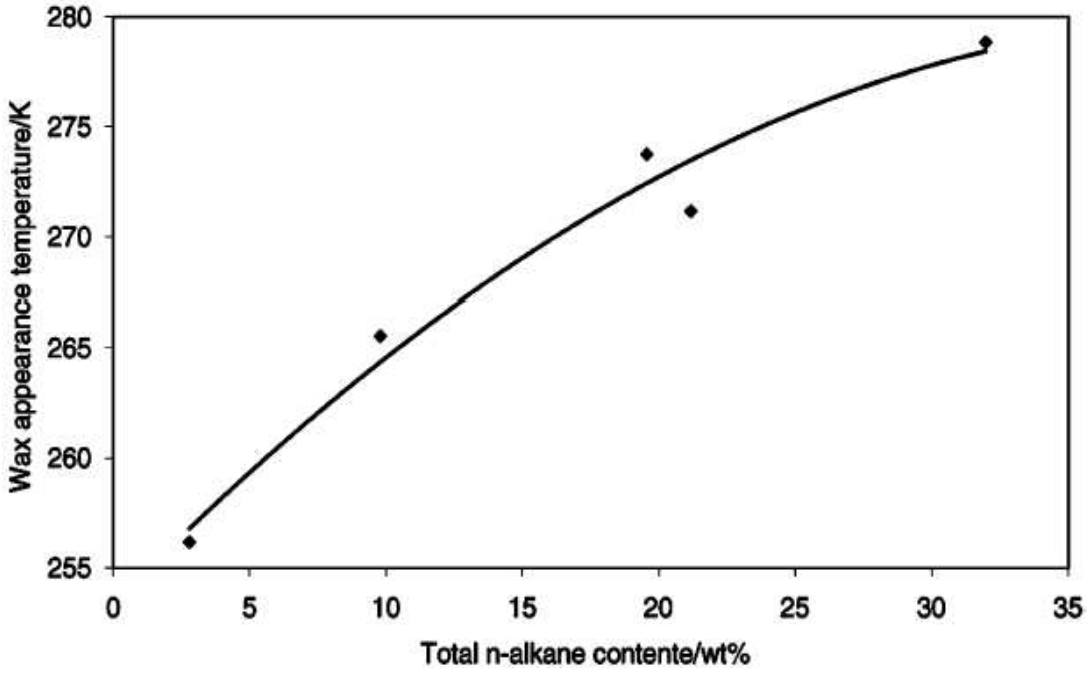

Figure III. 47: Relation between total n-alkane content and wax appearance temperatures for the studied cuts.

As can be seen, the model predictions agree very well with the experimental precipitation curves. Even for very low total n-alkane contents as for the cut from DUC oil, which contains only 2.8 wt% of n-alkanes, and a WAT of 256 K, an excellent description of the experimental data is obtained. Due to the feeble n-alkane content the DSC measurement for this fluid is particularly difficult due to the low intensity of the energy measured and thus a larger experimental error is associated to this measurement. Generally, it seems that the model slightly underestimates the measured precipitation curves. Since the DSC measurements are performed with a heating rate, that does not assure that the equilibrium is attained in the sample, the temperatures measured are slightly overestimated and this may explain the deviations between the experimental data and the model predictions. Other reason may reside in the inadequacies of the baseline chosen.

Model limitations would also be another obvious explanation given the huge simplifications made in what concerns the sample composition. Nevertheless, and taking into account all the simplifications used and assumptions done, the model predictions and the experimental data present a surprisingly good agreement. The proposed model, using only the information from a GC analysis, can thus provide a quick and reliable estimate of the low temperature behaviour of the fuel and could easily be used to plan fuel blends to meet some given low temperature specifications.

As suggested before, for the distillation cuts studied it would be possible to develop a correlation to predict WAT's from the total n-alkane content. Given the similarity of the n-alkane distributions among the studied samples, that appears to be completely independent of the total n-alkane content, it would also be possible, from the results presented, to propose an average n-alkane distribution for 230-375 ºC distillation cuts. Such a distribution was previously presented in Table I. 14. By using the average distribution, only a measurement of the total n-alkane content would be required to apply the model to obtain a reliable estimate of the low temperature behaviour of the fuel.

III.6. Conclusions

A new corresponding states model was proposed for the estimation of vapour pressures, liquid densities vapor-liquid interfacial tensions and viscosities of the series of the n-alkanes. This model is predictive and only uses experimental information from the reference fluids and the critical properties of the target fluid.

The inclusion of the second order term in the Taylor series expansion of the reduced property about the Pitzer acentric factor has proved to improve the predicting abilities of the corresponding states principle for the entire n-alkane series, particularly for the heavier components.

A list of reference systems was proposed for each property. Using this new 2^{nd} order perturbation framework only one reference system should be enough to predict the entire n-alkane series. Since this model is mathematically able to represent the reduced property as function of the acentric factor, it is expected to interpolate/extrapolate better than the linear approach presented before.

The extended corresponding states theory was also suggested for the determination of liquid-vapor interfacial tension, this time with the possibility of selecting an adequate reference fluid and given a minimum amount of information: critical temperature, critical volume, critical compressibility factor and acentric factor of the reference and the target fluid as well as some surface tension data of the reference fluid. Although this last approach has shown notable deviation, it is much simpler to use and involves less information.

Very good liquid density results were obtained from the corresponding states model. Viscosity and surface tension estimation using this model require the optimization of the cross-critical temperature combining rule, but using a system independent n parameter, very good results are obtained.

The friction theory, a general and recently proposed model for viscosity, that has already shown to be able to model several fluid mixtures over a broad temperature and pressure range, was used to describe the measured viscosity and liquid density data. In combination with the Peng–Robinson equation of state and after fitting the pure component

critical properties to improve the description of the liquid densities, a good representation of the viscosities resulted from the f-theory.

The correct volumetric and phase behaviour resulting from the CPA EOS was presented and discussed in order to evaluate the use of this equation of state in the framework of the gradient theory of fluid interfaces. Using correlations to obtain the cubic and associative term pure component parameters, it was found that the saturated liquid phase densities could be obtained with a high accuracy with no need to perform any volume correction as usually needed while using cubic EOS with energy and co-volume parameters calculated from critical properties.

Highly accurate data on pure water, n-butane, n-pentane, n-hexane, n-heptane and ethanol were selected to calculate the pure component gradient theory influence parameters and from these a quadratic correlation was proposed from which surface tension can be obtained in the reduced temperature range below 0.8 with average errors of less than 1.5%. Although this correlation was presented for a limited range of reduced temperatures, it was found that qualitative results could be obtained in the full liquid range for the selected components evaluated on this work. Future developments will focus on mixtures.

Distillation cuts from five crude oils commonly used to fuel production, had their low temperature behaviour studied. Precipitation curves were predicted by a thermodynamic model assuming ideal liquid phase and a solid phase whose non-ideality is described by the Predictive UNIQUAC model. It was shown that the model provides an accurate description of the experimental data and can thus be used for a quick estimate of the low temperature behaviour of a fuel or to plan fuel blends to meet existing regulations.

Final Conclusions

Several experimental measurements were presented on properties such as vapor-liquid and liquid-liquid interfacial tensions, liquid densities and viscosities. Measurements were performed in six pure n-alkanes: n-C_7H_{16}, n-$C_{10}H_{22}$, n-$C_{16}H_{34}$, n-$C_{20}H_{42}$, n-$C_{22}H_{46}$ and n-$C_{24}H_{50}$, 7 binary mixtures (n-C_7H_{16}+n-$C_{20}H_{42}$, n-C_7H_{16}+n-$C_{22}H_{46}$, n-C_7H_{16}+n-$C_{24}H_{50}$, n-$C_{10}H_{22}$+n-$C_{20}H_{42}$, n-$C_{10}H_{22}$+n-$C_{22}H_{46}$, n-$C_{10}H_{22}$+n-$C_{24}H_{50}$, n-$C_{16}H_{34}$+n-$C_{20}H_{42}$), and two ternary mixtures (n-C_7H_{16} + n-$C_{20}H_{42}$ + n-$C_{24}H_{50}$, n-$C_{10}H_{22}$ + n-$C_{20}H_{42}$ + n-$C_{24}H_{50}$). Additionally, to check the performance of the new *Nima DST9005* tensiometer the mixtures n-C_7H_{16}+n-$C_{10}H_{22}$, n-C_7H_{16}+n-$C_{16}H_{34}$, and n-$C_{10}H_{22}$+n-$C_{16}H_{34}$, were also considered. As shown during *Part I* the selected equipment presented deviations with respect to literature data of 1 % for interfacial tension, 2% for viscosity and 0.1% for liquid density, thus showing its ability to measure with accuracy.

Measurements were also performed on five petroleum distillation cuts in order to have some representative data of real systems. These fractions were also characterized in terms of their molecular weights, n-alkane composition and solid-liquid equilibria.

Binary and ternary data were compared to check if, in a mixture, a single component, n-$C_{22}H_{46}$ is different from an equimolar mixture of other two, n-$C_{20}H_{42}$+n-$C_{24}H_{50}$. For all the properties it was found that the binaries presented higher values of the thermophysical property than the equivalent ternaries, although for liquid densities the difference was very small.

During Part II correlations were considered. Since for correct modeling, accurate pure component properties, namely, critical temperature, critical pressure, critical volume and Pitzer acentric factor are required, it was first reviewed the available literature data and afterwards assessed some of the correlations to extend the data for n-alkanes for which no experimental information exists. It was found that the Tsonopoulos (1987) correlation presented the best agreement with critical temperatures, the Magoulas *et al*. (1990) correlation with the critical pressures, the Marano *et al*. (1997a) correlation with the critical pressures and the Han *et al*. (1993) correlation with the acentric factors.

Later in this chapter, a relation between liquid-vapor surface tension and viscosity was presented and discussed. Some interesting conclusions came out from this relation, as some chain length effects, the applicability of pure component parameters for mixtures and the possibility of correlating the parameters as a function of chain length or the molecular weight. Very good estimates of liquid-vapor interfacial tensions were obtained from viscosities, while viscosities obtained from interfacial tensions presented higher deviations.

In Part III it was shown how the corresponding states principle can be used to model several thermophysical properties of the entire n-alkane series based on three reference fluids. Plots of the reduced property as a function of the acentric factor were presented to show that the trend is not linear, and that results are considerably improved if we add the second order term of the Taylor series expansion. The application of this model to mixtures is straightforward, via adequate mixing rules. To obtain the best results for asymmetric systems, an adjustable parameter, theoretically valid, was introduced in the combining rule for the critical temperature.

Viscosities and liquid densities were also modeled using the friction theory, a state-of-the-the-art viscosity model, based on the repulsive and attractive contributions for pressure as given by a cubic equation of state. For the application of this theory to the mixtures reported in Part I, it was found necessary to tune the critical temperature and pressure of the heavier components, so that both good density and viscosity results were obtained. It this way, critical temperature and critical pressure no longer have any physical meaning and should considered as fitting parameters.

Based on the good performance of the gradient theory of fluid interfaces at describing interfacial tensions, and that of the CPA equation of sate for water-n-alkane phase equilibria, in section III.4 a combination of these models was evaluated for the estimation of equilibrium pressures and densities and vapor-liquid interfacial tensions of non-associating (n-alkanes) and associating (water and ethanol) components. Preliminary results are encouraging, but a considerable body of modeling work remains to be done.

A model to predict the solid-liquid equilibria in paraffinic systems presented by Coutinho (1998) was used to describe the solid deposition curves measured for the petroluem cuts in Part I. Very good agreement was obtained, although the only compositional analysis used by this model is that of the n.-allkanes.

Regarding the presented results, it is now considered that enough experimental and modeling work is available to describe systems containing both pure heavier n-alkanes or their mixtures with lighter components.

The most exciting phrase to hear in science, the one that heralds new discoveries, is not "Eureka!" (I've found it), but "That's funny..."

Isaac Asimov (1920-1992), writer.

Perspectives for Future Work

Although a considerable amount of data was presented on this thesis, a surface tension-viscosity relation was proposed, and some new and state-of-the-art models have been evaluated for thermophysical properties and solid-liquid equilibria of mixtures containing heavier n-alkanes, some questions remain to study or came up during this work that deserve to be mentioned as objects for further study.

With respect to the experimental measurements, there is still a large amount of systems for which experimental evidence remains unavailable. For interfacial tensions the existing data is considerably reduced: only a narrow range of temperature dependent data are found for each system and pressure dependency are still more limited. For modelling purposes data are particularly important, since only a few measurements may not be sufficient for an adequate model tuning.

Liquid-liquid interfaces have a great potential as a research subject. Not only they are involved in industrial products such as coatings, paints, detergents and others as well as they are determining properties in some environmental processes, such as in an oil spill. The effect of the nature and concentration of electrolytes in the interfacial tension is an interesting topic since this may help us understand some phenomena happening in real systems.

With regard to other properties, while some new data have been added to literature on heavier n-alkanes and their mixtures, interest in heavier components, as for example the industrial interest in paraffin wax for the design of phase change materials for energy storage, may require additional measurements on thermal conductivities for n-alkanes, even some heavier than those reported on this thesis. With this new data, it will also be possible to verify the extension of the proposed models for larger molecules, and thus fill the gap between short length molecules and polymers.

In Part II a relation between liquid-vapor interfacial tension and viscosity was presented for pure n-alkanes, their mixtures and some petroleum distillation cuts. Although this relation may be used to estimate liquid-vapor interfacial tensions from viscosities, as made by *Pedersen et al.*(1989), it also presented very interesting chain length effects as well as some information about the solid phase of those systems. Not only it was found that it is possible to relate a bulk phase (viscosity) property with an equilibrium surface (interfacial tension) property, but also that some information about the solid phase can be taken from these. To my point of view, although this relation is still on the correlations domain, it deserves some further attention.

Viscosities, liquid densities and liquid-vapor interfacial tensions were successfully modeled using an improved corresponding states model. Some results for vapor pressures, thermal conductivities and speeds of sound showed that this model may be easily extended to other properties. This is a point which remains to be issued. The extension to other families of fluids is another research subject which may lead to the generalization of the corresponding states model presented on this thesis. Ultimately, this shall be applied to real systems, such as the studied petroleum distillation cuts, but for these a more detailed compositional analysis (such as a PIONA) is required, since the measured properties are not only determined by the n-alkanes.

Finally, the combination of the gradient theory of fluid interfaces with an association equation of state, such as CPA, has a great potential for the estimation of both vapor-liquid and liquid-liquid interfaces, phase equilibrium and density profiles across the interface. The work presented in section III.4 is only the beginning of this subject, and the final objectives are, of course, to be able to model real systems such as some petroleum fluids, that may contain heavier components or be mixed with a gas such as CO_2, but also some

other “non-classical” systems such as those containing aqueous mixtures of electrolytes or alcohols involved in liquid-liquid interfaces.

References

Águila-Hernandez, J. (1987), *Tensión Superficial de n-alcanos y de Cíclicos-Alcanos.*, B. Sc. Thesis, Universidad Autónoma de Puebla, Mexico.

Ali, S. M. F. (2003), *Heavy Oil – Evermore Mobile*, J. Pet. Sci. Tech., 37:5-9.

Ambrose, D. (1978), *Correlation and Estimation of Vapor-Liquid Critical Properties. I. Critical Temperatures of Organic Compounds*, National Physical Laboratory, Teddington, NPL Rep. Chem. 92.

Ambrose, D. (1979), *Correlation and Estimation of Vapor-Liquid Critical Properties. I. Critical Temperatures of Organic Compounds*, National Physical Laboratory, Teddington, NPL Rep. Chem. 98.

Ambrose, D.and Tsonopoulos, C. (1995), *Vapor-Liquid Critical Properties of Elements and Compounds.2.Normal Alkanes*, J. Chem. Eng. Data, 40: 531-546.

Aminabhavi, T. M., Patil, V. B., Aralaguppi, M. I. and Phayde, H. T. S. (1996), *Density, Viscosity, and Refractive Index of the Binary Mixtures of Cyclohexane, Heptane, Octane Nonane, and Decane at (298.15, 303.15, and 308.15 K)*, J. Chem. Eng. Data 41: 521 – 525.

Anton Paar KG (1989), *AMV –200 Automated Microviscometer*, Anton Paar KG, Austria.

Anton Paar KG (1990), *Density Meter DMA 58 Manual*, Anton Paar KG, Austria.

Anselme, MJ, Gude, M. and Teja, A. S. (1990) *The Critical Temperatures and Densities of the normal alkanes from Pentane to Octadecane*, Fluid Phase Equilibr., 57(3): 317-326.

Aralaguppi, M. I., Jadar, C. V. and Aminabhavi, T. M. (1999), *Density, Refractive Index, Viscosity, and Speed of Sound in Binary Mixtures of Cyclohexanone with Hexane, Heptane, Octane, Nonane, Decane, Dodecane, and 2,2,4-trimethylpentane*, J. Chem. Eng. Data 44: 435 – 440.

Assael, M. J., Oliveira, C. P., Papadaki, M. and Wakeham, W. A. (1992), *Vibrating-Wire Viscometers for Liquids at High Pressures*, Int. J. Thermophys. 13: 593 – 615.

Auto Oil Programme (1996), Doc: COM(96)248, European Commission, Brussels.

Babadagli, T., (2003), *Evaluation of EOR Methods for Heavy-oil Recovery in Naturally Fractured Reservoirs*, J. Pet. Sci. Tech., 37: 25-37.

Bosselet, F., Létoffé, J.M., Claudy, P. and Valentin, P. (1983), *Study on the Thermal Behavior of n-alkanes in Complex Hydrocarbon Media by Differential Calorimetric Analysis.2. Determination of the Level of n-alkanes Contained in a Gas Oil. Determination of the Cloud Point*, Therm. Acta, 70(1-3): 19-34.

Brock, J. R. and Bird, R. B. (1955), *Surface Tension and the Principle of Corresponding States*, AIChE. J., 1: 174-177.

Cahn, J. W. and Hilliard, J. E. (1958), *Free Energy of a Nonuniform System. 1. Interfacial Free Energy*, J. Chem. Phys., 28(2): 258-267.

Calado, J., McLure, I. and Soares, V. (1978), *Surface tension for Octafluorocyclobutane, n-butane and Their Mixtures from 233 K to 254 K, and Vapour Pressure, Excess Gibbs Function and Excess Volume for the Mixtures at 233 K*, Fluid Phase Equilibr., 2: 199-213.

Constantinou, L. and Gani, R. (1994), *New Group Contribution Method for Estimating Properties of Pure Compounds*, AIChE J., 40(10):1697-1710.

Cooper, E. F. and Asfour, A. (1991), *Densities and Kinematic Viscosities of Some C6-C16 n-alkane Binary Liquid Systems at 293.15 K*, J. Chem. Eng. Data 36: 285 - 288.

Cornelisse, P.M.W., Peters, C.J. and Arons, J.D. (1996), *Non-Classical Interfacial Tension and Fluid Phase Behavior*, Fluid Phase Equilib., 117 (1-2): 312-319.

Cornelisse, P.M.W. (1997), *The Gradient Theory Applied: Simultaneous Modeling of Interfacial Tension and Phase Behavior*, PhD. Thesis, Delft Technical University, Delft, Netherlands.

Coutinho, J. A. P. (1995), *Phase Equilibria in Petroleum Fluids: Multiphase Regions and Wax Formation*, PhD. Thesis, Technical University of Denmark, Lyngby, Denmark.

Coutinho, J. A. P., Vlamos, P. M. and Kontogeorgis, G. M. (2000a), *General Form of the Cross-Energy Parameter of Equations of State*, Ind. Eng. Chem. Res., 39: 3076-3082.

Coutinho, J. A. P, Dauphin, C. and Daridon, J.L. (2000b), *Measurements and Modelling of Wax Formation in Diesel Fuels*, Fuel, 79: 607-616.

Coutinho, J. A. P. (1998), *A New Model for the Description of Multiphase Solid-Liquid Equilibria in Complex Hydrocarbon Mixtures*, Ind. Eng. Chem Res. 37: 4870-4875.

Coutinho, J. A. P. and Daridon, J. L. (2001), *Low Pressure Modelling of Wax Formation in Crude Oils*, Energy and Fuels, 15 (6):1454-1460.

Coutinho, J.A.P. and Stenby, E.H. (1996), *Predictive Local Composition Models for Solid/Liquid Equilibrium in n-alkane Systems: Wilson Equation for Multicomponent Systems*, Ind. Eng. Chem. Res. 35: 918-925.

Coutinho, J. A. P., Andersen, S.I. and Stenby, E.H. (1995), *Evaluation of Activity-Coefficient Models in Prediction of Alkane Solid-Liquid Equilibria*, Fluid Phase Equilibria, 103: 23-39.

Coutinho, J. A. P., Calange, S.and Ruffier-Meray, V. (1997), *Measuring the Amount of Crystallinity in Solutions using DSC*, Can. J. Chem. Eng. 75(6): 1075-1079.

Coutinho, J. A. P., Mirante, F., Ribeiro, J. C., Sansot, J. M. Daridon, J. L. (2002), *Cloud and Pour Points in Fuel Blends*, Fuel, 81: 963-967.

Cullick, A. S. and Ely, J. F. (1982), *Densities of Vinyl-Chloride from 5 to 65-degrees-C and Saturation Pressure to 4.2 MPa*, J. Chem. Eng. Data, 27: 276-281.

Chung, T. H., Ajlan, M., Lee, L. L. and Starling, K. E. (1988), *Generalized Multiparameter Correlation for Nonpolar and Polar Fluid Transport Properties*, *Ind. Eng. Chem. Res.* 27(4): 671-679.

Dandekar, A. Y., Andersen, S. I. and Stenby, E. H. (1998), *Measurement of Viscosity of Hydrocarbon Liquids Using a Microviscometer*, J. Chem. Eng. Data 43: 551 – 554.

Daridon, J. L., Pauly, J., Coutinho, J. A. P. And Montel, F. (2001), *Solid-Liquid-Vapor Phase Boundary of a North Sea Waxy Crude: Measurement and Modeling*, Energy & Fuels 15:730-735.

Dauphin, C., Daridon, J. L., Coutinho, J. A. P., Baylère, P. and Potin-Gautier, M. (1999), *Wax Content Measurements in Partially Frozen Paraffinic Systems*, Fluid Phase Equilib. 161:135-151.

Delmas, K., Ruffier- Meray, V., Brucy, F. (2000), *Minimum Oil Analysis for Reliable WAT Modeling*, 2nd Int. Conf. Petroleum Phase Behaviour and Fouling, Copenhagen, Denmark.

Derawi, S. O. (2002), *Modeling of Phase Equilibria Containing Associating Fluids*, PhD. Thesis, Technical University of Denmark, Lyngby, Denmark.

Design Institute for Physical Property Data (1998), *DIPPR Database*, AIChE, New York.

Dillon, H. E. and Pennoncello, S. G. (2003), *A Fundamental Equation for the Calculation of the Thermodynamic Properties of Ethanol*, Fifteenth Symposium on Thermophysical Properties, Boulder (CO), U.S.A.

Dirand, M., Bouroukba, M., Chevallier, V., Petitjean, D., Behar, E., Ruffier-Meray, V. (2002) *Normal Alkanes, Multialkane Synthetic Model Mixtures and Real Petroleum Waxes: Crystallographic Structures, Thermodynamic Properties and Crystallization*, J. Chem. Eng. Data, 47: 115-143.

Doolittle, A. K. and Peterson, R. H. (1951), *Preparation and Physical Properties of a Series of n-alkanes, J. Am. Chem. Soc.* 73: 2145-2151.

Ducoulombier, D., Zhou, H., Boned, C., Peyrelasse, J., Saint-Guirons, H. and Xans, P. (1986), *Pressure (1-1000 bars) and Temperature (20-100ºC) Dependence of the Viscosity of Liquid Hydrocarbons*, J. Phys. Chem., 90: 1692 – 1700.

Dutour, S. (2000), *Vitesse du Son et Propriétés Thermodynamiques Dérivées Dans de Hydrocarbures de Haut Poids Moléculaire Sous Pressions Élevées*, PhD. Thesis, Université de Pau et des Pays de L'Adour, Pau, France.

Dutour, S., Lagourette, B. and Daridon, J. (2001a), *High-Pressure Speed of Sound and Compressibilities in Heavy Normal Hydrocarbons:n-$C_{23}H_{48}$ and n-$C_{24}H_{50}$*, J. Chem. Thermodyn. 33(7): 765-774.

Dutour, S., Lagourette, B. and Daridon, J. L.(2001b), *High-Pressure Speed of Sound and Compressibilities in Heavy Normal Hydrocarbons:n-$C_{28}H_{58}$ and n-$C_{36}H_{74}$*, J. Chem. Thermodyn. 34(4): 475-484.

Earnshaw, J. C. and Hughes, C. J. (1992), *Surface-Induced Phase Transition in Normal Alkane Fluids*, Phys. Rev. A, 46 (8): R4494-R4496

Ely, J. F. and Hanley, H. J. M. (1981), *Prediction of Transport Properties. 1. Viscosity of Fluids and Mixtures*, Ind. Eng. Chem. Fund., 20: 323-332.

Ely, J. F. and Marrucho, I. M. (2000), in Sengers, J. V., Kayser, R. F., Peters, C. J. and White Jr. H. J. (Eds.), *Equations of State for Fluids and Fluid Mixtures*, Part I, Elsevier, Amsterdam, Netherlands.

Erikson, D.D., Niessen, V.G. and Brown, T.S. (1993), *Thermodynamic Measurement and Prediction of Paraffin Precipitation in Crude Oil*, SPE 26604.

Farid, M. M., Khudhair, A. M., Razack, S. A. K. and Al-Hallaj, S. (2004), A Review on Phase Change Energy Storage: Materials and Applications, Ener Conv. Management, 45: 1597-1615.

Freud, B. B. and Freud, H. Z. (1930), *A Theory of the Ring Method for the Determination of Surface Tension*, J. Am. Chem. Soc., 52: 1772-1783.

Gaonkar, A. G. and Neuman, R. D. (1984), *The Effect of Wettability of Wilhelmy Plate and Du Noüy ring on Interfacial Tension Measurements in Solvent Extraction Systems*, J. Coll. Int. Sci., 98(1): 112-119.

Giller, E. and Drickamer, H. (1949), *Viscosity of Normal Paraffins Near the Freezing Point*, Ind. Eng. Chem. 41: 2067-2069.

Goebel, A. And Kunkenheimer, K. (1997), *Interfacial Tension of the Water/n-alkane Interface*, Langmuir, 13: 369-372.

Grigoryev, B., Nemzer, B., Kurumov, D. and Sengers, J. (1992), *Surface tension of Normal Pentane, Hexane, Heptane and Octane*, Int. J. Therm. 13: 453-464.

Guggenheim, E. (1945), *The Principle of Corresponding States*, J. Chem. Phys., 13 (7): 253-261.

Han, B. and Peng, D. (1993), *A Group-Contribution Correlation for Predicting the Acentric Factors of Organic Compounds*, Can. J. Chem. Eng., 71: 332-334.

Harkins, W. D. and Jordan, H. F. (1930), *A Method for the Determination of Surface and Interfacial Tension from the Maximum Pull on a Ring*, J. Am. Chem. Soc., 52: 1751-1772.

Herhold, A., Ertas, D., Levine, A. J. and King, H. E. (1999), *Impurity Mediated Nucleation in Hexadecane-in-Water Emulsions*, Phys. Rev. E, 59(6): 6946-6955.

Hoshino, D, Nagahama, K. and Hirata, M. (1982), *Prediction of Acentric Factor of Alkanes by the Group Contribution Method*, J. Chem. Eng. Japan, 15(2):153-155.

Hu, W., Lovland, J. and Vonka, P. (1993), *Generalized Vapor Pressure Equations for n-alkanes, 1-alkenes and 1-alkanols*, 11th Int. Congress Chem. Eng. Chemical Equipment Design and Automation, CHISA'93, Prague, Check Republick.

Huh, C. and Mason, S. G. (1975), *A Rigorous Theory of Ring Tensiometry*, Coll. Pol. Sci., 253: 566-580.

Hunten, K. and Mass, O. (1929), *Título*, J. Am. Chem. Soc., 51 (1929) 160.

Jasper, J. (1972), *The Surface Tension of Pure Liquid Compounds*, J. Phys. Chem. Ref. Data, 1: 841-984.

Jasper, J. and Kring, E. (1955), *The Isobaric Surface Tension and Thermodynamic Properties of the Surfaces of a Series of n-alkanes, C5 to C18, 1-alkenes, C6 to C16, and of n-decylcyclopentane, n-decylcyclohexane and n-decylbenzene*, J. Phys. Chem., 59: 1019-1021.

Jasper, J., Kerry, E.and Gregorich, F. (1953), *The Orthobaric Surface Tensions and Thermodynamic Properties of the Liquid Surfaces of the n-Alkanes, C5 to C28*, J. Am. Chem. Soc., 75: 5252-5254.

Joback, K. G. (1984), *A Unified Approach to Physical Property Estimation Using Multivariate Statistical Techniques*, S. M. Thesis, Department of Chemical Engineering, Massachussets Institute of Technology, Cambridge MA (USA).

Joback, K. G. and Reid, R. C. (1987), *Estimation of Pure-Component Properties from Group Contributions*, Chem. Eng. Comm. 57(1-6): 233-243.

Kahl, H. and Enders, S. (2000), Calculation of Surface Properties of Pure Fluids Using Density Gradient Theory and SAFT-EOS, Fluid Phase Equilib., 172: 27-42.

Kahl, H. and Enders, S. (2002), Interfacial Properties of Binary Mixtures, Phys. Chem. Chem. Phys., 4: 931-936.

Katz, D. and Saltman, W. (1939), *Surface Tension of Hydrocarbons*, Ind. Eng. Chem., 31: 91-94.

Klein, S. A., McLinden, M. O. and Laesecke, A. (1997), *An Improved Extended Corresponding States Method for Estimation of Viscosity of Pure Refrigerants and Mixtures*, Int. J. Refrig., 20 (3): 208-217.

Knapstad, B., Skjølsvik, P. and Øye, H. (1989), *Viscosity of Pure Hydrocarbons*, J. Chem. Eng. Data 34(1): 37-43.

Koefoed, J. and Villadsen, J. (1958), *Surface Tension of Liquid Mixtures*, Acta Chem. Scand., 12(5): 1124-1135.

Kontogeorgis, G. M., Voutsas, E.C., Yakoumis, I.V. and Tassios, D.P. (1996), *An Equation of State for Associating Fluids*, Ind. Eng. Chem. Res., 35 (11): 4310-4318.

Kontogeorgis, G. M., Yakoumis, I. V., Meijer, H., Hendriks, E. M. and Moorwood, T. (1999), *Multicomponent Phase Equilibrium Calculations for Water-Methanol-Alkane Mixtures*, Fluid Phase Equilib.,158-160: 201-209.

Kontogeorgis, G. M. and Tassios, D. P. (1997), *Critical Constants and Acentric Factors for Long-chain alkanes Suitable for Corresponding States Applicatios. A Critical Review*, Chem. Eng. J., 66:35-49.

Kontogeorgis, G. M., Fredenslund, A. and Tassios, D. P. (1995), *Chain Length Dependence of the Critical Density of Organic Homologous Series*, Fluid Phase Equilibr., 108 (1-2):47-58.

Leach, J. W., Chappelear, P. S. and Leland, T. W. (1968), *Use of Molecular Shape Factors in Vapor-Liquid Equilibrium Calculations With Corresponding States Principle*, A.I.Ch.E. J., 14 (4): 568-576.

Leadbetter, A., Taylor, D. and Vincent, B. (1964), *The Densities and Surface Tensions of Liquid Ethane and Nitrous Oxide,* Can. J. Chem., 42: 2930-2932.

Lee, B. and Kesler, M. (1975), *A Generalized Thermodynamic Correlation Based on Three Parameter Corresponding States*, AIChE J., 21(3): 510-527.

Lee, M. and Wei, M. (1993), *Corresponding-States Model for Viscosity of Liquids and Liquid Mixtures,* J. Chem. Eng. Jpn., 26 (2): 159-165.

Leland, T. W. and Chappelear, P. S. (1968), *The Corresponding States Principle,* Ind. Eng. Chem., 60 (7): 15-43.

Létoffé, J.M., Claudy, P., Garcin, M. and Volle, J.L. (1995), *Evaluation of Crystallized Fractions of Crude Oils by Differenttial Scanning Calorimetry-Correlation with Gas-Chromatography*, Fuel, 74: 92-95.

Lunkenheimer, K. (1989), *The Effect of Contact Angle on Ring Tensiometry*: *An Experimental Study*, J. Coll. Int. Sci., 131(2): 580-583.

Lydersen, A. L. (1955), *Estimation of Critical Properties of Organic Compounds*, Univ. Wisconsin Coll. Eng., Eng. Exp. Stn. Rept. 3, Madison, WI (USA).

Magoulas, K. and Tassios, D. (1990), *Thermophysical Properties of n-Alkanes from C1 to C20 and their Prediction to Higher Ones*, Fluid Phase Equilibria, 56: 119-140.

Marano, J. and Holder, G. (1997a), *General Equation for Correlating the Thermophysical Properties of n-paraffins, n-olefins, and other Homologous Series. 2.Asymptotic Behavior Correlations for PVT Properties,* Ind. Eng. Chem. Res., 36: 1895-1907.

Marano, J. and Holder, G. (1997b), *General Equation for Correlating the Thermophysical Properties of n-paraffins, n-olefins, and other Homologous Series. 1.Formalism for Developing Asymptotic Behavior Correlations,* Ind. Eng. Chem. Res., 36: 1887-1894.

Marrero-Morejón, J. and Fontdevila, P. (1999), *Estimation of Pure Compound Properties Using Group-Interaction Contributions*, AICHE J., 45(3):615-621.

Marrucho, I. M. and Ely, J. F. (1998), *Extended Corresponding States for Pure Polar and Non-polar Fluids: an Improved Method for Shape Factor Prediction*, Fluid Phase Equilibr, 150-151: 215-223.

Marrucho, I. M. (1996) *Extended Corresponding States Theory: Application for Polar Compounds and Their Mixtures*, PhD. Thesis, Universidade Téncica de Lisboa, Lisboa, Portugal.

Martin, P. and Szablewski, M. (1999), *Nima Technology Tensiometers and Langmuir-Blodgett Troughs – Operating Manual, 5th Ed.*, Grunfeld, F. (Ed.), Nima Technology Ltd., Coventry, England.

Mass, O. and Wright, C. (1921), *Some Physical Properties of Hydrocarbons Containing Two and Three Carbon Atoms*, J. Am. Chem. Soc., 43: 1098-1110.

McLure, I., Sipowska, J.and Pegg, I. (1982), *Surface Tensions of (an alkanol+an alkane) 1.Propan-1-ol + heptane.*, J. Chem. Thermodyn., 14: 733-741.

Mentzer, R.A., Young, K.L., Greenkorn, R.A. and Chao, K.C. (1980) Sep. Sci. Technol., 15(9): 1613-1678.

Michelsen, M. L. and Hendriks, E. M. (2001), *Physical Properties from Association Models*, Fluid Phase Equilibr., 180(1-2): 165-174.

Miqueu, C. (2001), *Modélisation à Température et Pression Élevées de la Tension Superficielle de Composants de Fluides Pétroliers et de Leurs Mélanges Synthétiques ou Réels*, PhD thesis, Univ. Pau et des Pays de L'Adour, Pau, France.

Miqueu, C., Mendiboure, B., Graciaa, A. and Lachaise, J. (2003), *Modelling of the Surface Tension of Pure Components with the Gradient Theory of Fluid Interfaces*, Fluid Phase Equilib., 207: 225-246.

Miqueu, C., Mendiboure, B., Graciaa, A. and Lachaise, J. (2004), *Modelling of the Surface Tension of Binary and Ternary Mixtures with the Gradient Theory of Fluid Interfaces*, Fluid. Phase Equilib., 218: 189-203.

Mirante, F. and Coutinho, J.A.P. (2001), *Cloud Point Prediction of Fuels and Fuel Blends*, Fluid Phase Equilib, 180:247-255.

Morgan, D. L. and Kobayashi, R. (1991), *Triple Point Corresponding States in Long-Chain n-Alkanes*, Fluid Phase Equilibr., 94: 51-87.

Morgan, D. L. and Kobayashi, R. (1994), *Extension of Pitzer CSP Model for Vapor Pressures and Heats of Vaporization to Long-Chain Hydrocarbons*, Fluid Phase Equilibr., 94: 51-87.

Mota, J. S. (1998), *Título*, Presented at CHEMPOR'98, Lisbon, September.

Munõz, F. and Reich, R. (1983), *New Parameters for the Lee-Kesler Correlation Improve Liquid Density Predictions*, Fluid Phase Equilibr., 13: 171-178.

Murad, S. (1983), *Generalized Corresponding States Correlation for the Surface Tension of Liquids and Liquid Mixtures*, Chem. Eng. Commun., 24: 353-358.

Nakanishi, K., Kurata, M. and Tamura, M. (1960), *Physical Constants of Orgaic Liquids. A Monograph for Estimating Physical Constants of Normal Paraffins and Isoparaffins*, J. Chem. Eng. Data, 5(2):210-219.

Neale, T. (1997), *Título*, Presented at Euro Sinergy Conference, Brussels.

NIST Chemistry WebBbook, http://webbook.nist.gov/chemistry/fluid/.

Nikitin, E., Pavlov, P. and Popov, A. (1997), *Vapour-liquid Critical Temperatures and Pressures of Normal Alkanes with from 19 to 36 Carbon Atoms, Naphtalene and m-terphenyl Determined by the Pulse-Heating Technique*, Fluid Phase Equilibr., 141: 155 – 164.

Pandey, J., Pant, N. (1982), *Surface Tension of Ternary Polymeric Solutions*, J. Am. Chem. Soc., 104: 3299-3302.

Pauly, J., Daridon, J. L. and Coutinho, J. A. P. (2004), *Solid Deposition as a Function of Temperature in the nC10+(nC24-nC25-nC26) System*, in preparation.

Penfold, J. (2001), *The Structure of the Surface of Pure Liquids*, Rep. Prog. Phys., 64: 777-814.

Pedersen, K. S., Fredenslund, Aa., Thomassen, P. (1989), *Properties of Oils and Natural Gases*, *in* Contributions in Petroleum Engineering, vol. 5, Gulf Publishing Company, Houston, pp. 199-207.

Pelofsky, A. H. (1966), *Surface Tension-Viscosity Relation for Liquids*, J. Chem. Eng. Data, 11: 394-397.

Peneloux, A., Rauzy, E. and Freze, R. (1982), *A Consistent Correction for Redlich-Kwong-Soave Volumes*, Fluid Phase Equilib., 8: 7-23.

Peng, D. Y. and Robinson, D. B. (1974), *A New Two Constant Equation of State*, Ind. Eng. Chem. Fund., 15: 59-64.

Peterson, I. R. (1997), *Design Considerations for an Electrobalance Microforce Sensor*, Rev. Sci. Instr., 68(2):1130-1136.

Pitzer, K. S. (1939), *Corresponding States for Perfect Liquids*, J. Chem. Phys., 7: 583-590.

Pitzer, K. S., Lippmann, D. Z., Curl, R. F., Huggins, C. M. and Petersen, D. E. (1955), *The Volumetric and Thermodynamic Properties of Mixtures. II. Compressibility Factor, Vapor Pressure and Entropy of Vaporization*, J. Am. Chem. Soc., 77: 3433-3440.

Plöcker, U., Knapp, H. and J. Prausnitz, (1978), *Calculation of High-Pressure Vapor-Liquid Equilibria From a Corresponding States Correlation With Emphasis on Asymmetric Mixtures*, Ind. Eng. Chem. Process. Des. Dev., 17(3): 324-332.

Poling, B. E., Prausnitz, J. M. and O'Connell, J. P (2000), *The Properties of Gases and Liquids*, 5th ed., McGraw-Hill, New York.

Prausnitz, J.M.; Lichtenthaler, R.N.; Azevedo, E.G. (1999) *Molecular Thermodynamics of Fluid-Phase Equilibria*; 3rd ed., Prentice-Hall: Englewood Cliffs, NJ.

Pugachevich, P. and Cherkasskaya, A. (1980), *The Surface Properties of Ternary Solutions of Normal Alkanes*, Russ. J. Phys. Chem, 54 (9): 1328-1330.

Pugachevich, P. P., Khovorov, Y. A. and Beglyarov, E. M. (1979), *The Surface Properties of Binary Mixtures of Polymer Homologues. Russ. J. Phys. Chem.*, 53 (2): 235-236.

Queimada, A J., Stenby, E. H., Marrucho, I. M. and Coutinho, J. A. P.(2003a) *A New Corresponding States Model for the Estimation of Thermophysical Properties of Long-Chain n-alkanes*; Fluid Phase Equilibr., 212: 303-314.

Queimada, A. J., Dauphin, C., Marrucho, I. M. and Coutinho, J. A. P. (2001a), Low Temperature Behaviour of Refined Products from DSC Measurements and Their Thermodynamical Modelling, Therm. Acta, 372: 93-101.

Queimada, A. J., Marrucho, I. M., Coutinho, J. A. P. and Stenby, E. H. (2003b), *Viscosity and Liquid Density of Asymmetric n-alkane Mixtures: Measurement and Modeling*, in Proceedings of the 15th Symposium on Thermophysical Properties, NIST, Boulder (USA).

Queimada, A. J., Marrucho, I. M.and Coutinho, J. A. P. (2001b), *Surface tension of pure heavy n-alkanes: a corresponding states approach.* Fluid Phase Equilibr., 183: 229-239.

Queimada, A. J., Quinõnes-Cisneros, S. E., Marrucho, I. M., Coutinho, J. A. P. and Stenby, E. H. (2003c), *Viscosity and Liquid Density of Asymmetric Hydrocarbon Mixtures*, Int. J. Thermophys, 24(5): 1221.

Queimada, A. J., Silva, F. A. E., Caço, A. I., Marrucho, I. M. and Coutinho, J. A. P., (2003d), *Measurement and Modeling of Surface Tensions of Asymmetric Systems: Heptane, Eicosane, Docosane, Tetracosane and Their Mixtures*, Fluid Phase Equilib.,214: 211-221.

Quiñones-Cisneros, S. E., Zéberg-Mikkelsen, C. K. and Stenby, E. H.(2000) *The Friction Theory (f-theory) for Viscosity Modeling*, Fluid Phase Equilibr. 169: 249 - 276.

Quiñones-Cisneros, S. E., Zéberg-Mikkelsen, C. K. and Stenby, E. H. (2001a), *One Parameter Friction Theory Models for Viscosity*, Fluid Phase Equilibr. 178: 1 - 16.

Quiñones-Cisneros, S. E., Zéberg-Mikkelsen, C. K. and Stenby, E. H. (2001b), *The friction theory for viscosity modeling: extension to crude oil systems*,Chem. Eng. Sci. 56: 7007 - 7015.

Rackett, H. G. (1970), *Equation of State for Saturated Liquids*, J. Chem. Eng. Data, 15 (4):514-517.

Reddy, S.R. (1986), *A Thermodynamic Model for Predicting n-paraffinsCrystallization in Diesel Fuels*, Fuel, 65: 1647 - 1652.

Reed, T. M. and Gubbins, K. E. (1973), *Applied Statistical Mechanics*, McGraw-Hill, New York, chap. 11.

Rice, P. and Teja, A. (1982), *A Generalized Corresponding-States Method for the Prediction of Surface Tension of Pure Liquids and Liquid Mixtures*, J. Coll. Int. Sci., 86: 158-163.

Robinson, R. L., Gasem, K. A. M. And Ross, C. H. (1987), *Phase Behavior of Coal Fluids: Data for Correlation Development*, Progress Report DEFG22-83PC60039-11, USA Department of Energy.

Rolo, L. I., Caço, A. I., Queimada, A. J., Marrucho, I. M. and Coutinho, J. A. P.(2002), *Surface Tension of Heptane, Decane, Hexadecane, Eicosane, and Some of Their Binary Mixtures*, J. Chem. Eng. Data, 47: 1442-1445.

Ronningsen, H.P., Bjordal, B., Hansen, A.B. and Pedersen, W.B. (1991), *Wax Precipitation From North Sea Crude Oils: 1. Characterization and Dissolution Temperatures and Newtonian and Non-Newtonian Flow Properties*, Energy & Fuels, 5: 895-908.

Rossmyr, L.I. (1979), Cold Flow Properties and Response to Cold Flow ..., Ind. Eng. Chem. Prod. Res. Dev., 18: 227-230.

Rowlinson, J. S. and Swinton, F. L. (1982), *Liquids and Liquid Mixtures*, Butterworths, London.

Rowlinson, J.S. and Watson, I.D. (1969), *The Prediction of the Thermodynamic Properties of Fluids and Fluid Mixtures- I - The Principle of Corresponding States*, Chem. Eng. Sci., 24: 1565-1574.

Rusanov, A., Prokhorov, V. (1996), *Interfacial Tensiometry*, Mobius, D.and Miller, R. Eds., In *Studies in Interface Science Series*, vol. 3; Elsevier: Amsterdam.

Schonhorn, H. (1967), *Surface Tension-Viscosity Relationship for Liquids*, J. Chem. Eng. Data, 12: 524-525.

Soave, G. (1972), *Equilibrium Constants from a Modified Redlich-Kwong Equation of State*, Chem. Eng. Sci., 27(6): 1197-1203.

Taylor, B. N. And Kuyatt, C. E. (1994), *Guidelines for Evaluating and Expressing the Uncertainty of NIST Measurement Results*, NIST, Gaithersburg (MD) USA.

Taylor, B. N. (1995), *Guide for the Use of the International System of Units*, NIST, Gaithersburg (MD) USA.

Teja, A. S. and Rice, P. (1981a), *The Measurement and Prediction of the Viscosities of Some Binary Liquid Mixtures Containing n-hexane*, Chem. Eng. Sci., 36: 7-10.

Teja, A. S., (1980), *A corresponding States Equation for Saturated Liquid Densities. I-Application to LNG*, AIChE J., 26 (3): 337-341.

Teja, A. S., Sandler, S. I. and Patel, N. C. (1981b), *A Generalization of the Corresponding States Principle Using Two Nonpherical Reference Fluids* Chem. Eng. J., 21: 21-28.

Teja, A., Lee, R., Rosenthal, L. and Anselme, M. (1990), *Correlation of the Critical Properties of Alkanes and Alkanols*, Fluid Phase Equilibr., 56:153 - 169.

Tsonopoulos, C. (1987), *Critical Constants of Normal Alkanes from Methane to Polyethylene*, AIChE. J., 33: 2080-2083.

Vargaftik, N. B. (1975), *Tables on the Thermophysical Properties of Liquids and Gases – in Normal and Dissociated States*, 2nd ed., John Wiley, New York.

Viswanath, D. S. and Natarajan, G. (1989), *Data Book on the Viscosity of Liquids*, Hemisphere, New York.

Voutsas, E. C., Boulougouris, G. C., Economou, I. G. and Tassios, D. P. (2000), *Water/Hydrocarbon Phase Equilibria Using the Thermodynamic Perturbation Theory*, Ind. Eng. Chem. Res., 39: 797-804.

Wakefield, D. L., Marsh, K. N. and Zwolinski, B. J. (1988) Int. J. Thermophys. 9: 47 – .

Wakeham, W. A., Nagashima, A. and Sengers., J. V. (Eds.) (1991), *Measurement of the Transport Properties of Fluids*, in Experimental Thermodynamics III, Blackwell Scientific Publications, Oxford, United Kingdom.

Wang, S.L., Flamberg, A. and Kikabhai, T. (1999)), *Select the Optimum Pour Point Depressant – Wax Modifiers for Crude Oils and Heavy Fuels Improve Transportability*, Hydrocarbon Processing, February78(2): 59 - 63.

Wienaung, F. and Katz, D. L.(1943), *Surface Tensions of Methane-Propane Mixtures*, Ind. Eng. Chem., 35(2): 239-246.

Wong, D. S. H., Sandler, S. I. and Teja, A. S. (1983), *Corresponding States, Complex Mixtures and Mixture Models*, Fluid Phase Equilibr., 14: 79-90.

Wu, J. and Prausnitz, J. M. (1998), *Phase Equilibria for Systems Containing Hydrocarbons, Water and Salt: An Extended Peng-Robinson Equation of State*, Ind. Eng. Chem. Res., 37: 1634-1643.

Wu, S. (1999), *Surface and Interfacial Tensions of Polymers, Oligomers, Plasticizers, and Organic Pigments*, in Branrup, J., Immergut, C. and Grulke, E. (Eds.), *Polymer Handbook*, 4th ed., Wiley Interscience, New York.

Wu, X. Z., Ocko, B. M., Sirota, E. B., Sinha, S. K., Deutsch, M., Cao, B. H. and Kim, M. W. (1993), *Surface Tension Measurements of Surface Freezing in Liquid Normal Alkanes*, Science, 261: 1018-1021.

Xiang, H. W. (2002), *The New Simple Extended Corresponding-States Principle: Vapor Pressure and Second Virial Coefficient*, Chem. Eng. Sci., 57: 1439-1449.

Yakoumis, I.V., Kontogeorgis, G.M., Voutsas, E.C., Hendriks, E.M. and Tassios, D.P. (1998), *Prediction of Phase Equilibria in Binary Aqueous Systems Containing Alkanes, Cycloalkanes and Alkanes with the Cubic-plus-Association Equation of State*, Ind. Eng. Chem.Res., 37 (10): 4175-4182.

Zéberg-Mikkelsen, C. K., Quiñones-Cisneros, S. E. and Stenby, E. H. (2001), *Viscosity Modeling of Light Gases at Supercritical Conditions Using the Friction Theory, Ind. Eng. Chem. Res.*, 40: 3848-3854.

Zéberg-Mikkelsen, C. K., Quiñones-Cisneros, S. E. and Stenby, E. H. (2002), *Viscosity Prediction of Carbon Dioxide + Hydrocarbon Mixtures Using the Friction Theory, Pet. Sci. Technol.* 20(1-2): 27-42.

Zeppieri, S., Rodríguez, J. and López de Ramos, A. L. (2001), *Interfacial Tension of Alkane+Water Systems*, J. Chem. Eng. Data, 46:1086-1088.

Zuo, Y. and Stenby, E. H. (1997a), *Corresponding-States and Parachor Models for the Calculation of Interfacial Tensions*, Can. J. Chem. Eng., 75: 1130-1137.

Zuo, Y. X. and Stenby, E. H. (1996), *A Linear Gradient Theory Model for Calculating Interfacial Tensions of Mixtures*, J. Coll. Int. Sci., 182: 126-132.

Zuo, Y.X. and Stenby, E.H. (1997b), *Calculation of Interfacial Tensions with Gradient Theory*, Fluid Phase Equilib. 132 (1-2): 139-158.

Zuo, Y.X. and Stenby, E.H. (1998) *Calculation of Interfacial Tensions of Hydrocarbon-Water Systems Under Reservoir Conditions*, In Situ, 22 (2): 157-180.

Publication List

Queimada, A. J.; Quiñones-Cisneros, S. E.; Marrucho, I. M.; Coutinho, J. A. P.; Stenby, E. H.; Viscosity and Liquid Density of Asymmetric Hydrocarbon Mixtures; Int. J. Thermophys., 2003, 24(5), 1121-1239.

Queimada, A J.; Stenby, E. H.; Marrucho, I. M.; Coutinho, J. A. P.; A New Corresponding States Model for the Estimation of Thermophysical Properties of Long-Chain n-alkanes; Fluid Phase Equilibr., 2003; 212; 303-314.

Queimada, A. J.; Silva, F. A. E.; Caço, A. I.; Marrucho, I. M.; Coutinho, J. A. P.; Measurement and Modeling of Surface Tensions of Asymmetric Systems: Heptane, Eicosane, Docosane, Tetracosane and their Mixtures, Fluid Phase Equilibr, 2003, 214 (2), 211-221.

Rolo, L. I.; Caço, A. I.; Queimada, A. J.; Marrucho, I. M.; Coutinho, J. A. P.; Surface Tension of Pure and Mixed n-heptane, n-decane and n-hexadecane; J. Chem. Eng. Data; 2002; 47; 1442-1445.

Queimada, A J.; Marrucho, I. M.; Coutinho, J. A. P.; Surface Tension of Pure Heavy n-alkanes: a Corresponding States Approach; Fluid Phase Equilibr.; 2001; 183-184; 229-238.

Queimada, A. J.; Dauphin, C.; Marrucho, I. M.; Coutinho, J. A. P.; Low Temperature Behaviour of Refined Products from DSC Measurements and their Thermodynamical Modelling; Thermochimica Acta; 2001; 372; 93-101.

Queimada, A. J.; Marrucho, I. M.; Coutinho, J. A. P.; Stenby, E. H.; Viscosity and Liquid Density of Asymmetric n-alkane Mixtures: Measurement and Modelling, Submmited to Int. J. Thermophys.

Queimada, A. J.; Marrucho, I. M., Stenby, E. H.; Coutinho, J. A. P.; Generalized Relation Between Surface Tension and Viscosity: a Study on Pure and Mixed n-alkanes, Fluid Phase Equilibria, in press.

Queimada, A. J.; Miqueu, C.; Marrucho, I. M.; Kontogeorgis, G. M.; Coutinho, J. A. P.; Modeling Vapor-Liquid Interfaces with the Gradient Theory in Combination with the CPA Equation of State, Submitted to Fluid Phase Equilibria.

Caço, A. I., Queimada, A. J., Marrucho, I. M. and Coutinho, J.A.P., Surface Tension of Binary and Ternary Mixtures Containing n-decane, n-eicosane, n-docosane and n-tetracosane, *in preparation.*

Queimada, A. J., Costa, C., Marrucho, I. M. and Coutinho, J. A. P, Water - n-alkane (n-C_7H_{16} – n-$C_{24}H_{50}$) Interfacial Tension Measurements, *in preparation.*

Queimada, A. J., Marrucho, I. M. Stenby, E. H. and Coutinho, J. A. P., Measurement and modeling of surface tensions, liquid densities and viscosities of some petroleum distillation cuts, *in preparation.*